

https://dspace.org/

Integrated geophysical investigation of the Karoo Basin, South Africa

Scheiber-Enslin, Stephanie E

2016-05-10
http://hdl.handle.net/10539/20352

Downloaded from a DSpace repository. https://dspace.org/

Stephanie E. Scheiber-Enslin

Integrated Geophysical Investigation of the Karoo Basin, South Africa

A thesis submitted to the Faculty of Science, University of the Witwatersrand, Johannesburg, in fulfilment of the requirements for the degree of Doctor of Philosophy

Johannesburg, August 2015

School of Geosciences, University of the Witwatersrand



Declaration

I declare that this thesis is my own, unaided work. It is being submitted for the Degree of Doctor of Philosophy in the University of the Witwatersrand, Johannesburg. It has not been submitted before for any degree or examination in any other University.

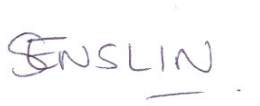

20th day of August 2015

Acknowledgements

To Jörg…thanks for teaching me to talk softer and to not take criticism so personally. Thanks for always being on time and knowing so much. You were the best office partner.

To Sue…for all the interesting chats, whether geophysical or other, you always had interesting ideas.

I couldn't have asked for better supervisors than the two of you.

You left me to my own devises, but always guided me in the right direction.

To Janine and Leonie…thank you for showing me what strong women in Science look like, and that we are still human

To Patrick…thanks for making my PhD what it was with CGS resources

To everyone at CGS…you made my PhD life so much fuller,

even though it was a long drive

To Dad…you came to every Geoscience talk, even when I wasn't giving it…thank you for being proud of me

To my Mom…for always expecting the best from me…and always suggesting…

You both made me believe I could do whatever I wanted

To my Husband…the best field assistant ever (it's an adventure!)…and for never letting me say that I was useless…you put up with a lot of grumpiness and a lot of 'it's almost done'… I thought it first…



Abstract

The possibility of extensive shale gas resources in the main Karoo Basin has resulted in a renewed focus on the basin, and particularly the Whitehill Formation. The main Karoo Basin has been the subject of geological studies since before the 1920s, but geophysical data provides an opportunity to shed new light on the basin architecture and formation. In this thesis, I use regional gravity, magnetic and borehole data over the basin, as well as vintage seismic data in the southern part of the basin. Modern computational capacity allows for more information to be extracted from these seismic data, and for these data to be better integrated with potential field data. The integration of datasets in a three-dimensional model (3D) has allowed for a better understanding of the shape of the basin and its internal structure, in turn shedding light on basin formation.

A new depth map of the basin constructed using this extensive database confirms that the basin deepens from on- to off-craton. The basin is deepest along the northern boundary of the Cape Fold Belt (CFB), with a depth of ~4000 m in the southwestern Karoo and ~5000 m in the southeastern part of the basin. Sediment thickness ranges from ~5500 to 6000 m. The Whitehill Formation along this boundary reaches a depth of ~ 3000 m in the southwest and ~4000 m in the southeast. Despite limited boreholes in this region, the basin appears to broadly deepen to the southeast. These seismic and borehole data also allow for mapping of the Cape Supergroup pinch-out below the Karoo basin (32.6˚S for the Bokkeveld and 32.4˚S for the Table Mountain Group), with the basin reaching a thickness of around 4 km just north of the CFB. The gravity effect of these sediments in the south is not sufficient to account for the low of the Cape Isostatic Anomaly near Willowmore and Steytlerville. This ~45 mGal Bouguer gravity low dominates the central region of the southern Karoo at the northern border of the CFB. The seismic data for the first time show uplift of lower-density shales of the Ecca Group (1800 – 2650 kg/m^3) in this region, and structural and seismic data suggest that these lower density sediments continue to depth of 11 to 12 km along normal and thrust faults in this region. Two-dimensional density models show that

these shallow crustal features, as well as deeper lower crust compared to surrounding regions, account for the anomaly.

These seismic and borehole data also allow for constraints to be placed on the distribution and geometry of the dolerite intrusions that intruded the basin after its formation, and in some cases impacted on the shale layer, to be constrained. The highest concentrations of dolerites are found in the northwest and east of the basin, pointing towards two magma sources. The region of lowest concentration is in the south-central part of the basin. Here the intrusions are confined to the Beaufort Group, ~1000 m shallower than the shale reservoir, suggesting it should be the focus of exploration efforts. These dolerite sills are shown to be between 5 and 30 km wide and are saucer-shaped with ~ 800 m vertical extent, and dips of between 2˚ and 8˚ on the edges. The sheets in the south of the basin extend for over 150 km, dipping at between 3˚ and 13˚, and are imaged down to ~ 5 km. This change in dip of the sheets is linked to deformation within the Cape Fold Belt, with greater dips closer to the belt, although these sheets do not appear to intrude strata dipping at more than 15 to 20˚.

In order to understand the shape of the Karoo basin and construct a 3D model of the basin, an understanding is needed of the underlying basement rocks. The Beattie Magnetic Anomaly (BMA) that stretches across the entire southern part of the basin forms part of the basement Namaqua-Natal Belt. Filtered magnetic data confirm that the Namaqua and Natal Belts are two separate regions with different magnetic characteristics, which is taken into account during modelling. The BMA is shown to be part of a group of linear magnetic anomalies making up the Natal Belt. The anomaly itself will therefore not have an individual effect on basin formation, and the effect of the Natal Belt as a whole will have to be investigated. An in-depth study of outcrops associated with one of these linear magnetic anomalies on the east coast of South Africa suggest the BMA can be attributed to regions of highly magnetic (10 to 100 x 10^{-3} SI) supracrustal rocks in Proterozoic shear zones. Along two-dimensional magnetic models in the southwestern Karoo constrained by seismic data, these magnetic zones are modelled as dipping slabs with horizontal extents of ~20-60 km and vertical extents of ~10-15 km. Body

densities range from 2800- 2940 kg/m^3 and magnetic susceptibilities from 10 to 100 x 10^{-3} SI.

These, as well as other geophysical and geological constraints, are used to construct a 3D model of the basin down to 300 km. Relatively well-constrained crustal structure allows for inversion modelling of lithospheric mantle densities using GOCE satellite gravity data, with results in-line with xenolith data. These results confirm the existence of lower density mantle below the craton (~3270 kg/m^3) that could contribute to the buoyancy of the craton, and an almost 50 kg/m^3 density increase in the lithospheric mantle below the surrounding Proterozoic belts. It is this change in lithospheric density along with changes in Moho depths that isostatically compensate a large portion of South Africa's high topography (<1200 m). The topography higher than 1200 m along the edge of the plateau, along the Great Escarpment, are shown to be accommodated by an asthenospheric buoyancy anomaly with a density contrast of around 40 kg/m^3, while still mimicking the Bouguer gravity field. These findings are in line with recent tomographic studies below Africa suggesting an "African Superplume" or "Large Low Velocity Seismic Province" in the deep mantle.

The basin sediment thickness maps were further used to investigate the formation of the main Karoo Basin. This was accomplished by studying the past flexure of the Whitehill Formation using north-south two-dimensional (2D) profiles. Deepening of the formation from ~3000 m in the southwest to ~4000 m in the southeast is explained using the concept of isostasy, i.e., an infinite elastic beam that is subjected to an increasing load size across the Cape Fold Belt. Load height values increase from 4 km in the southwest to 8 km in the southeast. This larger load is attributed here to "locking" along a subduction zone further to the south. The effective elastic thickness (Te) of the beam also increases from around 50 km over the Namaqua and Natal Belts in the southwest to ≥80 km over the Kaapvaal Craton and Natal Belt in the southeast. The changes in Te values do not correlate with changes in terrane, i.e., a north to south change, as previously though. The large extent and shape of the Karoo basin can therefore, in general, be explained as a flexural basin, with the strength of the basement increasing towards the southeast. Therefore, while factors such as mantle flow could have

contributed towards basin formation, reducing the load size needed, it is no longer necessary in order to account for the large extent of the basin. This flexure model breaks down further to the southeast, most likely due to a very high Te value. This could be the reason for later plate break in this region during Gondwana breakup. It is inferred that this increase in Te is linked to the buoyancy anomaly in the asthenospheric mantle.

Table of Contents

Declaration ii

Acknowledgements iii

Abstract iv

List of Figures xiii

List of Tables xli

List of symbols and nomenclature xliv

1 Introduction 1

1.1 Thesis Objective 2

1.2 Organization of the Thesis 2

1.3 Contribution of Thesis 3

2 Karoo Basin 6

2.1 Abstract 7

2.2 Introduction 8

2.3 The Karoo and Cape Basins 9

2.4 Cape Isostatic Anomaly 18

2.5 Data 19

2.6 Methodology 30

2.7 Results 32

2.7.1 Depth and Thickness Maps 32

2.7.2 Cape Isostatic Anomaly 39
2.8 Discussion 48
2.9 Conclusions 51
2.10 Acknowledgements 52
3 Karoo Dolerites 53
3.1 Abstract 54
3.2 Introduction 55
3.3 The Main Karoo Basin 56
3.4 The Karoo Igneous Province 61
3.5 The Karoo Dolerite Network 62
3.6 Dolerite Geometries 64
3.7 Data 66
3.7.1 Soekor Deep Wells 68
3.7.2 Soekor Seismic Data 72
3.7.3 CGS Aeromagnetic Data 76
3.8 Methodology 78
3.9 Results 79
3.9.1 Northwestern Main Karoo Basin (Fraserburg) 79
3.9.2 Southeastern Main Karoo Basin (Queenstown) 83
3.9.3 Southeastern Karoo (Somerset-East) 86
3.9.4 Southwestern Main Karoo Basin (Graaff-Reinet) 97

3.10 Discussion 99

3.11 Conclusions 105

3.12 Acknowledgements 106

4 Basement 107

4.1 Abstract 108

4.2 Introduction 109

4.3 Geology of the Namaqua-Natal Metamorphic Belt and Cape Fold Belt 112

4.4 Previous Geophysical Studies 116

4.5 Data 118

4.5.1 Regional 118

4.5.2 Petrophysical studies 120

4.6 Magnetic Field Analysis and Forward Modelling 126

4.7 Results 127

4.7.1 Magnetic Linear Anomalies within Mobile Belts 127

4.7.2 Forward Modelling 135

4.8 Discussion 144

4.9 Conclusions 151

4.10 Acknowledgements 152

5 3D Model 153

5.1 Summary 154

5.2 Introduction 155

5.3 Overview of South African Geology 156

5.4 South Africa's High Topography 161

5.5 Crustal Thickness and Mantle Variations Below South Africa 163

5.6 Data 165

5.6.1 Seismic Data 165

5.6.2 Teleseismic Data 168

5.6.3 Lithosphere-Asthenosphere Boundary (LAB) 168

5.6.4 Satellite Gravity and Gradient Fields 169

5.6.5 Gravity Data 169

5.7 Isostatic State and Moho Gravity Effect 174

5.8 3D Model of the Lithosphere 176

5.9 Modelling Results 178

5.10 Test for Loading at the Base of the Model 186

5.11 Isostatic Implications of 3D model 187

5.12 Discussion 194

5.13 Conclusions 195

5.14 Acknowledgments 196

6 Flexure 197

6.1 Abstract 198

6.2 Introduction 199

6.3 The Main Karoo Basin 199

6.4 Basin Formation 201

6.5 Cretaceous Uplift 203

6.6 Data 203

6.6.1 Karoo Depth Maps 203

6.6.2 Teleseismic Data 205

6.7 Two-Dimensional Flexure Profiles 206

6.8 Whitehill Formation Flexure Profiles 209

6.9 Flexural Isostasy by Comparing Topographic Load and Seismic Moho 214

6.10 Discussion 216

6.11 Conclusions 220

6.12 Acknowledgments 220

7 Concluding Remarks 221

7.1 Conclusions 222

7.2 Future Studies 222

8 Reference 224

9 Appendix 242

Appendix 1 – Matlab Best-fit Program for Eastern Flexure Profile 242

List of Figures

Figure 2-1. Topographic map of South Africa showing the tectonic provinces: KVC – Kaapvaal craton, NNB – Namaqua-Natal Belt and CFB – Cape Fold Belt. The divide between the Namaqua (west) and Natal (east) terranes as determined from borehole (Eglington, 2006) and magnetic data (Scheiber-Enslin *et al.*, 2014a) [Chapter 4] is shown (green line). The main Karoo Basin (red outline) covers a large portion of the high inland plateau (Johnson *et al.*, 2006). 9

Figure 2-2. Distribution map of the geological units of the main Karoo Basin across South Africa, and the Cape Basin in the southern part of the country (Stratigraphy), 1980). Major tectonic provinces are outlined (see Figure 2-1 for details). Several cities and towns are indicated include Cape Town (CT); Johannesburg (JHB); East London (EL); Margate (MG) and Port St Johns (PStJ). 12

Figure 2-3. Topographic map of the central portion of the eastern arm of the Cape Fold Belt (Amante and Eakins, 2009). Willowmore (WM), Steytlerville (SV), Mossel Bay (MB) and Cape St Francis (StF) are shown as white circles. The dashed line marks the approximately northern extent of the fold belt. Mapped and inferred faults in the region are indicated (normal – black lines; thrust – black line with black triangles), and labelled (normal faults: CF – Coega, GF – Gamtoos, GRF – Grootrivier, KNF – Kango, KF – Kouga, OQM – Outenique Mountains; thrust faults: BK – Baviaanskloof, JF – Jackalsbos, KWF – Klein Winterhoek, SF- Soutkloof, ZF – Zuurberg)

(Booth *et al.*, 2004, Booth and Shone, 1999, Roby *et al.*, 1995, Toerien, 1991, Toerien and Roby, 1979). The area outlined (red box) is shown on the zoomed in inset map..... 17

Figure 2-4. (a) Free-air, (b) Bouguer, (c) isostatic gravity anomaly and (d) total magnetic intensity maps for South Africa. Major tectonic provinces are outlined (see Figure 2-1 for details). The Cape Isostatic Anomaly extends from Willowmore (WM) through to Steytlerville (ST) and Port Elizabeth (PE) on the east coast (white circles). The Williston (WS), Beattie (BMA) and Mbashe (MB) anomalies are indicated in (d) (Thomas *et al.*, 1992b).... 19

Figure 2-5. Available data used to constrain main Karoo Basin (red line) depth maps. These include deep SOEKOR boreholes (Rowsell and De Swardt, 1976), Council for Geoscience and industry boreholes (D. Cole, pers. comm.) in the southwestern part of the basin (orange triangles), and industry boreholes giving basement depths in the northeastern part of the basin (blue triangles, Rutherford, 2009). Seismic data include reflection seismic (yellow, Lindeque *et al.* (2011) and Loots (2013)), refraction seismic profiles (green, Stankiewicz *et al.* (2007)), offshore seismic lines (blue, Parsiegla *et al.* (2007) and Parsiegla *et al.* (2008)) and Soekor seismic data (black lines). These Soekor data include survey KW in the southeastern Karoo around East London (EL, Fatti, 1970). Moho depth estimates are indicated (black circles, values in kilometres) (Parsiegla *et al.*, 2008, Parsiegla *et al.*, 2007, Muller, 1991, Durrheim, 1987, Graham and Hales, 1965, Nguuri *et al.*, 2001, Lindeque *et al.*, 2011, Harvey *et al.*, 2001). For some sites, due to duplicate studies, multiple estimates are listed. In some cases Cities indicated include

Aliwal North (AN), Beaufort West (BW), Coffee Bay (CB), Fraserburg (FB), Graaff-Reinet (GR), Hertzogville (HV), Mossel Bay (MB), Port Elizabeth (PE), Queenstown (QT), Somerset-East (SE) and Cape St Francis (StF) (white circles). 26

Figure 2-6. Depth maps for a) the base of the main Karoo Basin (base of the Dwyka Group) and b) the top of the Whitehill Formation (relative to the WGS84 ellipsoid). In (a) the northern extent of the Table Mountain Group (yellow line; solid - definite and dashed – approximate location) and Bokkeveld Group (red line; solid - definite and dashed – approximate location) are shown. The outlines of major tectonic provinces are shown (see Figure 2-1 for details). Data used to create the maps are shown (seismic – black lines; boreholes – black triangles). Outcropping strata of the Dwyka Group and Whitehill Formation are shown in (a) and (b) respectively (purple). The Msikaba Formation of the Cape Supergroup outcrops between the towns of Margate (MG) and Port St Johns (PStJ) on the east coast. Several towns are indicated (white circles, see Figure 2-5 for details)..... 34

Figure 2-7. Thickness maps for a) the main Karoo Basin and b) Cape Supergroup (1000 metre contour intervals shown). Outcropping Dwyka and Witteberg Group rocks are shown in (a) and (b) respectively (purple). Several towns are indicated (white circles, see Figure 2-5 for details). The towns of Willowmore (WM) and Steytlerville (SV) are marked (white circles)..... 36

Figure 2-8. Gravity effect of (a) Karoo and (b) Cape Supergroup sediments shown in Figure 2-7a and b respectively. The gravity effects are combined in (c). See Figure 2-7 for details. 39

Figure 2-9. (a) Depth map of the Whitehill Formation (from Figure 2-6b) and (b) corresponding geological map of the region surrounding the town of Willowmore (WM) and Steytlerville (SV) (Stratigraphy), 1980). Faults in the Cape Fold Belt are indicated (normal – black line, thrust – black line with triangles; KWF – Klein Winterhoek thrust fault, see Figure 2-3 for more details) (Booth *et al.*, 2004, Booth and Shone, 1999, Roby *et al.*, 1995, Toerien, 1991, Toerien and Roby, 1979). Soekor seismic profiles (black lines) and boreholes (black triangles) are indicated. The coastal towns of Mossel Bay (MB), Port Elizabeth (PE) and Cape St Francis (StF) are marked (white circles). The location of east-west seismic profile KL04C is indicated in (a) (red line), as well as the north-south profiles BV01 (green line), BV03 (yellow line) and P01 (orange line). Deformation of Karoo and Cape Supergroup sediments is recorded further north on these sections compared to other sections in the surrounding southern Karoo. 40

Figure 2-10. (a) East-west seismic section KL04C (location indicated in Figure 2-9a). (b) Interpreted section with horizons marked: Whitehill Formation (ES, Ecca Shales), top of the Bokkeveld (BV) Group and top of the basement (GG, black dashed line). Interpreted faults and direction of movement are indicated (red lines and black arrows). Displacement along the smaller listric faults is evident in the ES horizon. These faults have been continued down through the BV horizon though displacement is not easily resolved. Depths are given as two-way travel-times and as a non-linear depth scale. Peaks are filled red and troughs blue..... 42

Figure 2-11. (a) Bouguer gravity and (b) isostatic gravity anomaly map of the region surrounding Willowmore (WM) and Steytlerville (SV), showing the low of the Cape Isostatic Anomaly. Faults in the Cape Fold Belt are indicated (normal – black line, thrust – black line with triangles, see Figure 2-3 for more details) (Booth *et al.*, 2004, Booth and Shone, 1999, Roby *et al.*, 1995, Toerien, 1991, Toerien and Roby, 1979). Jurassic sediments of the Uitenhage Group are outlined in red. Two refraction seismic profiles are indicated (solid black line) (Stankiewicz *et al.*, 2007). The approximate northern limit of the Cape Fold Belt is shown (dashed black line), as well as the towns of Mossel Bay (MB), Port Elizabeth and Cape St. Francis (StF) (white circles). 44

Figure 2-12. (a) Geological map and (b) 2D Bouguer gravity profile along the western (left) and eastern (right) seismic refraction profiles shown in (c) (locations shown in Figure 2-11, modified from Stankiewicz *et al.*, 2007). Seismic velocities are in km/s (Stankiewicz *et al.*, 2007). The extent of the Cape Isostatic Anomaly (CIA) is marked on the eastern gravity profile. The Karoo and Cape Supergroups (SG) are labelled. Faults south of the Karoo Basin are labelled (normal faults: Kango (KNF), Coega (CF) and Gamtoos (GF); thrust fault: Klein Winterhoek (KWF)) and direction of movement determined by Stankiewicz *et al.* (2007) are indicated (black arrows). South of the Karoo Basin, along both profiles, Stankiewicz *et al.* (2007) indicates a closely associated normal and thrust fault (c), while on the geological map in (a) only a normal fault (KNF) is evident along the western profile. The possible source of the Beattie Magnetic Anomaly (BMA) is marked. 48

Figure 2-13. Total magnetic intensity map over the Cape Isostatic Anomaly (contours at 20 mGal intervals). The gravity low correlates with a change in direction of the high intensity Beattie Magnetic Anomaly (BMA). 50

Figure 3-1. (a) Map of South Africa with the major tectonic provinces indicated. The Archean Kaapvaal Craton (KVC) is surrounded by the Proterozoic Namaqua-Natal Belt (NNB), and the younger Cape Fold Belt in the south. All of these provinces are overlain by the Late Carboniferous to Early Jurassic main Karoo Basin (thick black line) (Johnson *et al.*, 2006). (b) Simplified structural map of the southern Karoo. The main dyke trends determined from the 1:1,000,000 map are east-west and north-northwest. These trends are associated with an inferred transform fault in the central Karoo linking inferred rifts off the west and east coast (Chevallier *et al.*, 2001). Chevallier *et al.* (2001) divided the dykes into three domains (*D1, D2* and *D3*). The dolerite line defines the southern limit of the outcropping dolerites (thick red line). Deep wells in the Karoo are indicated (black triangles). The northeastern limit of the Whitehill Formation (the source of possible shale gas) is indicated by the towns Hertzogville (HV) and Coffee Bay (CB) (Cole *et al.*, 2011). 60

Figure 3-2. (a) Plot of the dolerite thickness distribution as determined from existing reports (Rowsell and De Swardt, 1976) and unpublished log data. Dolerite thickness are indicated: greater than 150 m (red triangles), less than 150 m (green triangles), and zero dolerite further south of the dolerite line (blue triangles). Soekor seismic lines in the southern part of the basin are marked (black lines). The surveys (and corresponding wells) are divided into

regions, namely the northwestern region around Fraserburg (FB) in the Northern Cape; southwestern region around the town of Graaff-Reinet (GR); and two regions in the southeastern main Karoo Basin close to Somerset-East (SE), and Queenstown (QT) further north. Additional wells exist around Lesotho and the towns of Aliwal North (AN) and East London (EL). Previously interpreted seismic line SWK01 stretches south from Beaufort West (BW) (Fatti and Du Toit, 1970). See Figure 3-1 for details. The dotted line indicates the profile shown in (b). (b) Approximately southwest-northeast profile through the main Karoo Basin, showing the dolerite distribution (horizontal lines) in deep wells QU1/66, AB1/65, KA1/66, VREDE1/66, CR1/68, WE1/66 and SW1/67. Stratigraphic boundaries between wells are marked (dotted lines): BF – Beaufort Group, EC – upper Ecca Group, ES – Ecca shales (lower Ecca shales topped by the Whitehill Formation), DW – Dwyka Group, BV – Bokkeveld Group (red square), TM – Table Mountain Group (orange triangle), GG – Granite-gneiss basement (blue square). The total well depths are indicated with solid black lines. Over 400 m of dolerite occurs in each well in the east/southeast and northwest at all stratigraphic levels, while <150 m of dolerite is found in the southwest wells within the Beaufort Group. 67

Figure 3-3. Time-depth plots for Soekor seismic data. The measured depths (MD) of the Whitehill Formation from wells (Rowsell and De Swardt 1976) and the two-way travel times (TWT) of the first continuous strong reflector (i.e., Whitehill Formation) are plotted (MD_TWT_Wh). Interval velocities determined by Fatti and du Toit (1970) are also plotted, as well as the

sonic velocity log from well WE1/66 (Fatti, 1987). A second-order binomial curve is fit to the data with a y-intercept of zero ($R^2 = 0.99$). 75

Figure 3-4. (a) Location map of seismic profile NW3-9 (black line) and well QU1/65 (black triangle, marked with red arrow) in the northwest Karoo (thick black outline). (b) Geological map of the region north of Fraserburg with the seismic profiles (thick black line) and well QU1/65 marked. The line was shot over Beaufort Group sediments (green), a Karoo dolerite sill (pink, marked with red arrows) and dykes (thin black lines). (c) The profile is correlated with a north-south magnetic profile. The magnetic data have been high-pass filtered to remove the regional field. The edges of the sill are clearly visible on the filtered magnetic data (red arrows). (d) The seismic profile NW3-9 is shown (red = peaks and blue = troughs) with the vertical axis displayed as two-way travel time in seconds and depth in metres (non-linear). Formation tops recorded down well QU1/65 are marked (blue dashes). Expected strong reflectors at depth should correlate with the Whitehill Formation (ES, Ecca shales) and granite-gneiss basement (GG) as constrained by wells data, but none are visible. This is due to strong shallower reflectors interpreted as dolerite sills (D) from well intersections. Other strong shallow reflectors that do not correlate with dolerites in the well are interpreted as multiples (yellow arrows, although the lack of correlation could be due to an inaccurate velocity curve because of the large number of dolerites). The shallow sill visible in outcrop (red arrows in b) is not resolvable on the seismic data, and neither are vertical structures such as dykes. (e) Temperature (˚C x 100) versus depth (km) curve calculated

for the dolerite sills in well QU1/65 ten years after emplacement (Cawthorn and Walraven, 1998). The location of the Whitehill Formation is marked (green line, Wh). The temperature curve (red line), solidus curve (blue line) and liquidus curve (pink line) are indicated relative to the original emplacement temperature (1200˚C). The temperature after 10 years of cooling is still approximately 700-800˚C within the Whitehill Formation due to dolerite emplacement. 82

Figure 3-5. (a) Location map for seismic profile BV12W (west) and BV14 (east) in the eastern Karoo (in the region of Queenstown). The proximity of these lines to the well-studied Golden Valley Sill (GVS) complex is shown on the geological map in (b). Outcropping sills clearly seen on the seismic profiles (c) are marked on the geological map with red arrows. The depth extent of these shallow sills is around 800 m, while the inclined sheets dip at between 2 to 8˚ (dashed black lines below sheets). The base of the Morning Sun Sill (MSS), which forms part of the complex, is visible of the seismic data (dashed black line below sill) although the inclined sheets that outcrop are not. The reflector representing the Whitehill Formation (ES) is marked (constrained from nearby seismic lines), with shallower reflectors representing other sills or multiples. (d) Focusing in on the GVS complex, a magnetic (TMI) profile (e) over the centre of the GVS complex shows that the shallower GVS has a strong signal, while the deeper MSS and thin Golden Valley Dyke (GVD) have signals close to the resolution of the data (blue arrows). The signal over the GVS is more complex than expected for a simple sill, implying additional dolerite structures at depth.

A topographic profile (Topo) shows the high relief of the GVS. See Figure 3-4 for additional details. 86

Figure 3-6. Geological map of the region in the southeastern Karoo close to the town of Somerset-East. This region is covered by five seismic profiles: part of BV02, BV05, BV06, BV07 and part of BV12. Extensive dolerite sheets can be mapped in outcrop from profile to profile (green, red and blue arrows). 87

Figure 3-7. (a) Location plot of seismic profile BV07 in the southeastern Karoo, west of the town of Somerset-East. On the geological map (b) it can be seen that BV07 intersects two dolerites sheets close together (red arrow) and lies close to well CR1/68. (c) Seismic profile BV07 with the deep reflectors of the Whitehill Formation (ES), Bokkeveld (BV), Table Mountain (TM) Groups and basement (GG) marked, as constrained by well data (CR1/68) and nearby seismic lines. An interpreted inclined sheet (DS) is marked. A black box marks the region focused on and interpreted in (d, green horizons). It appears that a deeper sill is connected by this inclined sheet to a shallower sill that outcrops (red arrows). The interpreted northern limb of the shallow sill (blue arrow) does not outcrop. See Figure 3-4 for additional details. 90

Figure 3-8. (a) Location map for seismic profile BV06 in the southeastern Karoo, east of the town of Somerset-East. The profile (thick black line) passes over three dolerites sheets (red arrows) that show up clearly on the (b) geological map and (c) gridded magnetic data. (d) Seismic profile BV06 with the deep reflectors of the Whitehill Formation (ES) and basement (GG)

constrained by surrounding seismic lines (reflectors are labelled from below). Shallower reflectors represent dolerite sheets (DS) that connect to sills at depth and cut through the Beaufort sediments to the surface. One such sheet appears to have intruded close to the Whitehill Formation (ES). Multiples have been interpreted between these sills. (e) A south-north magnetic model coincident with the profile (dotted line in (c) and black box in (d)). This model shows how these interpreted sheets/sills on the seismic profile (green horizons) can be easily modelled using a susceptibility value of 0.15 SI (Maré, 2012) and remanent magnetism close to the present-day field (Hattingh and de Wet, 1996). The data have been high-pass filtered to remove the regional trend. See Figure 3-4 for additional details..... 92

Figure 3-9. Three-dimensional image showing the geometry of the dolerite sheets and sills (green, red, and light blue) in relation to the Whitehill Formation (ES, lower dark blue layer). See Figure 3-6 for location in the southeastern Karoo around the town of Somerset-East. These horizons are mapped using surface outcrop and north-south seismic lines BV05, BV06, BV12 and east-west line BV02. 93

Figure 3-10. (a) Geological map showing the Karoo sills in the southern Karoo. Dip intervals for dolerite sheets as measured from seismic sections are shown (red dots), with values increasing for sheets closer to the CFB (from 3˚ to 13˚). (b) The sheets are continuous across the Teekloof and Middleton lithological boundaries in the Beaufort, which are equivalent layers in the east and west (Table 3-1, Johnson *et al.* (2006)). Further west

these lithologies are removed by erosion and the deeper Abrahamskraal Formation is exposed, with considerably fewer outcropping sheets towards the south. (c) Gridded dip data mapped from sediments in the southern Karoo and CFB. Values change from ~50˚ within the CFB to ~2˚ in the north. The red line marks the southern extent of outcropping dolerites (dolerite line), and the green line marks the location of first tilting of the Whitehill Formation due to the CFB as seen on the seismic sections. The dolerite line does not seem to have any correlation with the dip of the sediments. 96

Figure 3-11. (a) Location plot for seismic profile SWK06 in the southwestern Karoo close to the town of Graaff-Reinet. The seismic profile (thick black line) on the geological map in (b) intersects a dolerite sill and several dykes (red arrows) and lies close to well KA1/66. A north-south magnetic profile in (c) shows how these outcropping dolerites correlate with magnetic anomalies (TMI, red arrows). These magnetic data are high-pass filtered to remove the region trend. The shallowest strong reflector in (d) correlates with a dolerite sill (D) intersected by well KA1/66. Below that the Whitehill Formation (ES) reflector is visible due to fewer dolerites at shallower levels, whereas the basement reflector (GG) is not. Strong reflections between ES and the lowest dolerite are interpreted as multiples. The southern mapped dyke in (b and c) correlates with a break in the picked continuous sill layer on the seismic data (southern red arrow). The red box marks a region with a complex magnetic signal, but no mapped dolerites. The reflections in this region are also weak. This highlights the

importance of using magnetic data when interpreting seismic data, and investigating for magnetic bodies that do not outcrop. See Figure 3-4 for additional details. 98

Figure 3-12. (a) Location map for a high resolution magnetic survey flown in the northwestern Karoo, southwest of the town of Fraserburg. (b) Geological map of the region with seismic line NWK06 indicated (thick black line). The total magnetic field of the area is shown using the c) regional (sun-shading at 45˚) and d) high resolution data (sun-shading at 135˚). Mapped NW-trending dykes are visible on the regional and high resolution data, while an ENE swarm is only visible on the high resolution data. This swarm corresponds with several mapped melilitite basalt dykes. The full extent of the swarm is mapped using the magnetic data and overlain on the geological map in (b). 104

Figure 4-1. Topographic map of South Africa (Amante and Eakins, 2009) with the major tectonic provinces outlined (thin black lines). These include the Archean Kaapvaal Craton (KVC), surrounded by the Namaqua-Natal mobile belt (NNMB), and the deformed Cape Fold Belt (CFB) in the south. The outline of the Southern Cape Conductive Belt (red lines), and the maximum axis of the Beattie Magnetic Anomaly are shown (thick black line). The location of deep SOEKOR boreholes that intersect basement is labelled (black circles, KA1/66, KC1/70, QU1/65 and WE1/66, Eglington and Armstrong (2003)). 110

Figure 4-2. Schematic diagram illustrating the evolution of the Natal Belt between 1170 to 1140 Ma and 1090 to 1070 Ma (modified from McCourt *et al.*,

2006). During the earlier period the Tugela terrane accreted onto the Kaapvaal Craton, and granites (oldest intrusives) intruded the supracrustals and associated rocks of the Mzumbe-Margate arc. Between 1090 and 1070 Ma the Mzumbe and Margate terranes accreted onto the Tugela terrane-KVC margin, and S-type granitoids intruded the Mzumbe-Margate terranes..... 114

Figure 4-3. (a) Aeromagnetic total intensity; (b) free-air gravity; (c) Bouguer gravity and (d) isostatic anomaly maps for South Africa. Major tectonic provinces are outlined (see Figure 4-1 for details). Coincident geophysical profiles collected over the south-western and south-central portion of the BMA are indicated in (a) (black lines), including a refraction seismic line (Stankiewicz *et al.*, 2007), magnetotelluric profiles (Weckmann *et al.*, 2007a, Weckmann *et al.*, 2007b), reflection seismic profile (Lindeque *et al.*, 2011), and offshore seismic lines (Parsiegla *et al.*, 2007, Parsiegla *et al.*, 2008). A vibroseis line (Loots, 2013) was collected between the two profiles. 119

Figure 4-4. Magnetic susceptibility measurements (x 10^{-3} SI) for several geological units within the Mzumbe Terrane, including the (a) supracrustal rocks of the Mapumulo Group, (b) orthogneisses (S-type), and (c) mafic intrusions and granitoids (S-type). Different suites or formations within these units are marked with different colours. Rock types are labelled, with the common ones abbreviated: AMPH – amphibolite, CH – charnockite, GN – gneiss, GR – granite, SERP - serpentinite. High magnetic susceptibility values which plot off the chart are included in brackets. For the supracrustal rocks in (a), the highest magnetic susceptibilities are for gneisses (> 20 x 10^{-3} SI). For the orthogneisses in (b) magnetic susceptibility values overall are

significantly lower (< 10 x 10^{-3} SI). For the Mzumbe mafics and granitoids (S-type) in (c), the highest magnetic susceptibility is 55 x 10^{-3} SI for a granite and for monzonite and syenite samples (< 25 x 10^{-3} SI), while the remaining samples have smaller values (< 10 x 10^{-3} SI). 123

Figure 4-5. Magnetic susceptibility measurements (x 10^{-3} SI) for several geological units within the Margate Terrane, including the (a) supracrustal rocks of the Mzimkulu Group and (b) orthogneisses (S-type), and (c) Oribi Gorge plutons (A-type) from both the Mzumbe and Margate terranes. See Figure 4-4 for details. For the supracrustal rocks in (a), the highest magnetic susceptibilities are for a basalt (12 x 10^{-3} SI), while the remaining recorded values are < 2 x 10^{-3} SI. For the orthogneisses in (b) the highest magnetic susceptibilities are for a diorite (54 x 10^{-3} SI) and serpentine (159 x 10^{-3} SI), while the remaining samples have magnetic susceptibilities of < 10 x 10^{-3} SI. For the Margate Plutons (A-type) in (c) magnetic susceptibilities of < 16 x 10^{-3} SI are recorded, while one granite has a measured magnetic susceptibility of 83 x 10^{-3} SI. 125

Figure 4-6. (a) Total magnetic intensity (TMI) and (b) high-pass (HP) filtered TMI for South Africa (using a 50 km wavelength cut-off). Alternating subparallel magnetic highs and lows are visible north and south of the BMA and are traced (black lines) and labelled according to Thomas et al. (1992b). The Lilani-Mabigulu shear zone (LSZ) north of these anomalies is labelled. From these traces the continuity of the Williston anomaly to the west is evident. These anomalies as well as borehole analysis by Eglington and Armstrong (2003) were used to define the border between the Natal and

Namaqua terranes (green line). The boreholes used (black circles) are labelled in (a) (KA1/66, KC1/70, QU1/65 and WE1/66). Tectonic provinces are outlined (see Figure 4-1 for details). 128

Figure 4-7. (a) Geological map showing the Mzumbe terrane associated with the Williston anomaly. Shear and thrust zones are marked (black lines, summarised by Voordouw (2010)). Geological time-scales during deposition include the Neoproterozoic (N), Ordovician (O), Carboniferous (C) through to Triassic (T), Jurassic (J) and Quaternary (Q). (b) Total magnetic intensity (TMI) map of the entire Mzumbe terrane with mapped Mzumbe supracrustal gneisses (and associated migmatites) marked. Shear and thrust zones are marked and labelled in (c). The terrane extends from the Lilani-Mabigulu shear zone (LSZ) in the north to the Melville thrust in the south (MT). South of this a small portion of the Margate terrane is exposed. The magnetic linear anomalies (Williston, BMA and Mbashe) are labelled. The Kaapvaal craton boundary is marked with a black line to the north of the LSZ (between these two boundaries is the Tugela terrane). The approximately northeast to southwest extent of younger sedimentary cover is marked (thick black line, Karoo and Natal sediments), east of which basement rocks outcrop. The magnetic highs of the LSZ, Williston and the high in-between are most closely associated with outcropping supracrustal rocks (Mapumulo group) and shear zones. More circular anomalies to the south are associated with the younger Oribi Gorge plutons. Towns include Amanzimtoti (AM), Pennington (PT), and Port Edward (PE) (black circles). 131

Figure 4-8. (a) High-pass (HP) filtered and (b) low-pass (LP) filtered magnetic data (50 km cut-off), as well as (c) tilt derivative (TDR) and (d) pseudogravity (PG) data and isostatic anomaly contours for the Natal mobile belt on the east coast of South Africa. Magnetic linear anomalies defined by Thomas *et al.* (1992b), as well as major shear zones (black lines) are indicated. See Figure 4-7 for details. There is a similar trend to the HP and LP anomalies and mapped shear zones. The TDR map can be used to better map these zones, while no correlation is seen between the PG and the isostatic anomaly contours (15 mGal interval). 132

Figure 4-9. TMI image with refined shear zones (black lines) constrained using geology data, previously mapped shear zones and magnetic tilt derivative data. 133

Figure 4-10. (a) Total magnetic intensity map over the BMA on the east coast of South Africa; (b) North-south profile over the BMA at its shallowest on the east coast (location marked with a black line in (a)). The data reveals the complex nature of the source. Towns indicated include Port Edward (PE) and Port St. Johns (PJ), as well as the Mkambati Nature Reserve (MB) (black circles). 134

Figure 4-11. (a) High-pass filtered TMI image for the region surrounding the western profile in Figure 4-3a. Traces of magnetic linear anomalies identified in Figure 4-6b are marked with black lines (M-Mbashe, BMA-Beattie Magnetic Anomaly, W-Williston). (b) 2D magnetic model along the profile shown in (a). The upper panel shows the observed magnetic anomaly (thick black line) and calculated anomaly (thin black line). The lower panel shows

the created 2D magnetic model, with the different bodies labelled. Seismic refraction velocities for these bodies are included in brackets, and the colour of the body represents the magnetic susceptibility (SI) of the body. Mid-crustal bodies with higher magnetic susceptibilities are used to fit the BMA, Williston and Mbashe anomalies. These bodies correlate with anomalous zones identified on seismic and MT data, and are modelled with increasing depth and magnetic susceptibilities towards the south. The location of SOEKOR deep boreholes used to constrain the depth of the Karoo basin is shown (KW1/67, SA1/67, QU1/65). (c) 2D density model corresponding with the magnetic profile in (b). The upper panel shows the observed free-air anomaly (thick black line) and calculated gravity (thin black line). The lower panel shows the 2D density model (density values in kg/m). (d) Correlated seismic reflection image (Lindeque *et al.*, 2007), (e) seismic refraction image (Stankiewicz *et al.*, 2008), and f) MT resistivity image (Weckmann *et al.*, 2007b) used to constrain the model. 139

Figure 4-12. (a) High-pass filtered TMI image for the region surrounding the central profile shown in Figure 4-3a. (b) 2D magnetic model along the profile shown in (a). The mid-crustal high susceptibility bodies used to fit the anomalies correlate with the magnetic traces in (a) as well as anomalous zones of high seismic velocity (Stankiewicz *et al.*, 2007), and are modelled with increasing depth towards the south. (c) 2D gravity model corresponding with the magnetic profile in (b). (d) Seismic refraction data from Stankiewicz et al. (2007) used to constrain the model. Boreholes used to constrain the

model are shown (SC3/67, CR1/68, VREDE1/66). See Figure 4-11 for details. 142

Figure 4-13. (a) Terrane map of western (WDML) and central Dronning Maud Land (CDML) with the different terranes labelled and delineated with black lines (Amante and Eakins, 2009). (b) Total magnetic intensity map of WDML and CDML (Golynsky *et al.*, 2006). Inset map shows the location of Africa, Eastern Antarctica and the Falkland Islands before Gondwana breakup (modified from Johnston, 2000), with the different tectonic terranes shaded (~1.1 Ga Namaqua, Natal and Droning Maud Land terranes; ~1.8-2.0 Ga and Archean terranes). Broad elongated magnetic highs and lows in (b) that characterise the western region have been linked with ~1.1 Ga orogenic basement, as well as similar basement and anomalies on the east coast of South Africa. Black lines mark terranes labelled in (a). The Heimefrontfjella region in the southwest, which includes the Vardeklettane terrane (V) and Mannefallknausane (M, Jacobs *et al.*, 1996), has been linked to the Margate terrane. 148

Figure 5-1. Topographic map of South Africa with the main tectonic terranes marked: KVC – Kaapvaal Craton; NNB – Namaqua-Natal Proterozoic Belt and CFB – Cape Fold Belt. The 1200 m topographic contour is marked (black contour). The divide between the Namaqua (west) and Natal (east) terranes as determined from borehole (Eglington, 2006) and magnetic data (Scheiber-Enslin *et al.*, 2014a) is shown (green line). The Karoo basin stretches over the inland plateau and lower-lying coastal regions (red line).

The location of the cities of Johannesburg (JHB) and Cape Town (CT) are shown, and the country of Lesotho (L). 156

Figure 5-2. (a) Cratonic blocks defined by De Wit *et al.* (1992) according to geology, geochronology and magnetic data. Several cratonic blocks accreted to the cratonic core (Southern and Northern Barberton and Ancient Gneiss terranes) between 3.7 and 2.5 Ga (De Wit *et al.*, 1992). These include the Witwatersrand block to the west (Wits, Boshoff and Southern terranes), Kimberley terrane further west (Colesburg, Amalia and Kraaipan terranes) and Pietersburg block to the north (Pieterburg/Giyani and unnamed terranes). The Colesburg Lineament (CL) separates the Wits and Kimberley blocks, while the Thabazimbi-Murchison Lineament (TML) separates the Wits and Pietersburg blocks. (b) Geological units overlying the craton are outlined (see geological key: Kheis – Kheis Belt; BVC – Bushveld Complex; Tvl & GW – Transvaal and Griqualand West Supergroup (SG); Wits – Wits SG; VD – Ventersdorp SG; GG – granite-greenstone belts). Extensions of units below the younger Karoo basin (red outline) are shown. See Figure 5-1 for details of the tectonic provinces (outlined in black). The divide between the Namaqua and Natal terranes is marked (brown line, Eglington, 2006, Scheiber-Enslin *et al.*, 2014a)..... 158

Figure 5-3. (a) GOCE satellite Bouguer gravity (Gz) and (b) gravity gradient (Gzz) data at 255 km height across South Africa. The effect of topography has been removed using tesseroids (Uieda, 2013). (c) Ground Bouguer anomaly (BA) and (d) isostatic anomaly map of South Africa (Venter *et al.*, 1999). The 1200 m topographic contour is marked in (c, black contour) and

roughly coincides with a low of -120 mGal. The isostatic map was calculated using a density contrast between the crust and mantle of 400 kg/m^3, an elastic thickness (Te) of 5 km and a reference depth of 35 km. Tectonic terranes are outlined (see Figure 5-1 and Figure 5-2. for details). The Karoo basin is outlined in white. The dashed line marks a profile from the southwest to northeast that is compared across several figures. 172

Figure 5-4. (a) Isostatic Moho calculated assuming an elastic thickness (Te) of 5 km and density contrast of 400 kg/m^3 between the crust and the mantle, and a reference depth of 35 km. These depths do not correlate well with teleseismic crustal thickness estimates from (b) Nguuri *et al.* (2001) and (c) Youssof *et al.* (2013). The dashed line marks a profile from the southwest to northeast that is compared across several figures. Tectonic terranes are outlined (see Figure 5-1 and Figure 5-2. for details). 173

Figure 5-5. (a) Moho depths from southwest to northeast across South Africa, from the Cape Fold Belt (CFB) and Namaqua-Natal Belt (NNB) to the Kaapvaal craton. These depths are determined from teleseismic data (Nguuri *et al.*, 2001), from which several depth models have been generated (Yang *et al.*, 2008, Nair *et al.*, 2006, Youssof *et al.*, 2013). The gravitational responses of these models are calculated (b) at ground-level (BA) and (c) at 255 km (SatGz) using a density contrast of 400 kg/m^3 at the Moho. The gravity gradient response (d) is also calculated at satellite height (SatGzz). The responses show variations of up to 75 mGal, 90 mGal and 1.0 Eötvös respectively, though none fit the broad signal of the observed gravity field (grey). See Figure 5-3 and Figure 5-4 for profile location. 175

Figure 5-6. Lithospheric mantle densities (kg/m^3) for satellite Gz inversion (Model 1, SatInv_Gz); Gzz inversion (Model 2, SatInv_Gzz); Gz and Gzz inversion (Model 3, SatInv_Gz_Gzz); ground gravity inversion (Model 4, GrdInv); forward modelling of satellite Gzz inversion density values to fit the long-wavelengths of the ground data (Model 5, SatInv_Gz_FM). Terranes include: Pietersburg (P, cratonic); Kimberley (K, cratonic); Kimberley2 (K2, cratonic); south-central (SC, cratonic); southeastern (SE, cratonic); Wits (W, cratonic); Kheis (Kh); Natal (NT); Namaqua (NM); CFB (C) and Ocean (Oc). 180

Figure 5-7. (a) Calculated Bouguer maps for the region covered by the Karoo basin for Model 5 (Table 5-4). The residual gravity map is shown in (b). The overall residual and P-correlation factor for the IGMAS+ model are listed in Table 5-4..... 181

Figure 5-8. Northwest to southeast on-craton density profiles from the main Karoo Basin three-dimensional (3D) model (top and bottom). The inset maps (centre) show: the 3D Moho and Karoo Supergroup interfaces and Bouguer anomaly (centre-left); and a two-dimensional map of the model upper mantle densities (centre-right). The northwest to southeast sections are marked on this map (dashed black lines), and the different mantle blocks are outlined (solid black lines) and labelled (see Figure 5-6 for details). The locations of the two profiles are also indicated on the map (black arrows and thick black lines). The northern profile (top, Section 13) passes over the Namaqua (NM), Kheis (KH), Kimberley (K), Wits (W), south-central (SC), Natal (NT) and ocean (OC) mantle blocks (the back view of the section). The southern

profile (bottom, Section 10) passes over the NM, KH, K, southeast (SE), NT and OC mantle blocks. For the profiles, the calculated (dashed) and observed (solid red) curves are fit to each other. The model is divided into the upper (UC, including Karoo Supergroup sediments), middle (MC), lower (LC) and lowest crust (LLC), mantle transition zone (MTZ) and mantle. Densities are in kg/m^3 (listed in Table 5-4) and coordinates are in UTM34S. 183

Figure 5-9. Northwest to southeast off-craton density profile from the main Karoo Basin 3D model. The inset map (top) shows a 2D map of upper mantle densities. The profile (bottom, Section 6) marks the divide between the Natal (NT, back of the section) and Cape blocks (C, front of the section), and Ocean (OC) blocks to the northwest and southeast. See Figure 5-8 for details 185

Figure 5-10. Crustal thickness map determined from the main Karoo Basin 3D gravity model (Model 5). Mantle vertices from the 3D model are marked (black dots). See Figure 5-1 and Figure 5-2. for details..... 186

Figure 5-11. Loading (kN/m) at the base of the model (300km depth) calculated for Model 5. The 1200 m topographic contour representing the edge of the escarpment is marked (blue line). Some of the greatest uncompensated loading occurs below the escarpment and Lesotho. See Figure 5-1 for details. 188

Figure 5-12. (a) Loading at the base of the model (kN/m), (b) gravity and (c) gravity residual (mGal) map for the buoyancy model. A 40 kg/m^3 density contrast exists between the region of asthenospheric buoyancy below the edge of the escarpment (dotted line) and the surrounding asthenosphere.

While the gravity effect is similar to Model 5, this model is closer to isostatic equilibrium compared to Figure 5-11. The outline of the extended craton is shown (dashed line). See Figure 5-1 for details..... 190

Figure 5-13. Crustal thickness map for the buoyancy model. See Figure 5-10 for details. 192

Figure 5-14. The long-wavelength gravity effect of the region of asthenospheric buoyancy outlined in Figure 5-12, with a 40 kg/m^3 density contrast. The thick black lines mark the -120 and -100 mGal isolines. 192

Figure 5-15. Density depth slices at (a) 100 km and (b) 200 km depth showing density contrasts relative to 3200 kg/m^3. In (a) an approximately 50 kg/m^3 change in lithospheric mantle densities from on to off-craton is evident. In (b) the extent of the region of asthenospheric buoyancy below the escarpment is evident, with a 40 kg/m^3 density contrast. 193

Figure 5-16. Lithosphere-Asthenosphere boundary (LAB) depths (Fishwick, 2010) above the region of asthenospheric buoyancy (thick black line). The Namaqua and Natal boundary and cratonic blocks defined by Youssof *et al.* (2013) are outlined (red lines), with the region of buoyancy correlating with the southeast and south-central blocks and Namaqua-Natal boundary. See Figure 5-1 for details. 195

Figure 6-1. Topographic map of South Africa with the main tectonic terranes marked: KVC – Kaapvaal Craton; NNB – Namaqua-Natal Proterozoic Belt and CFB – Cape Fold Belt. The divide between the Namaqua (west) and Natal (east) terranes as determined from borehole (Eglington, 2006) and magnetic data (Scheiber-Enslin *et al.*, 2014a) is shown (green line). The

Karoo basin stretches over the inland plateau and lower-lying coastal regions (red line). The country of Lesotho (L) is indicated as well as the cities of Johannesburg (JHB), Cape Town (CT), Hertzogville (HV) and Coffee Bay (CB) that mark the northeastern extent of the Whitehill Formation. 200

Figure 6-2. (a) The Karoo basin forming as a retroarc foreland basin. Accommodation space was created for the basin due to loading of the crust in the south by the Cape Fold Belt. This load was the result of subduction of oceanic crust below the belt further to the south. This thick-skinned folding and thrusting resulted in deformation of basement rocks. (b) The Karoo forming due to thin-skinned thrusting linked to subduction to the south and continent-continent collision. 202

Figure 6-3. Depth map of the Whitehill Formation relative to WGS84 with three flexure profiles marked (red north-south lines) (modified from Scheiber-Enslin *et al.*, 2015b). Data used to constrain the map are marked (seismic – black lines; boreholes – black circles and white triangles). The western flexure profile (P1) includes Lindeque *et al.* (2011) seismic profile and borehole data further north (white triangles, SA1/66, QU1/65, DV - Dubbelde Vlei). The profile in the east (P2) is constrained using Soekor seismic line BV06 in the south and boreholes in the north (white triangles: CR1/68. WE1/66, TU1/50, GLEN1/67, D731/1 and BBF1). The profile in the far-east (P3) is constrained only by borehole data (white triangles: SP1/69, WE1/66 and GLEN1/67). Dolerites intruded the basin following formation around ~180 Ma. The dolerite-line, south of which no dolerite intrusions occur is marked (red line). The northern extent of Cape

Supergroup is shown (yellow line; solid - definite and dashed – approximate location). The cities of Johannesburg (JHB), Cape Town (CT), Hertzogville (HV) and Coffee Bay (CB) are marked. Outcropping Whitehill Formation is shown in purple. See Figure 6-1 for details. 204

Figure 6-4. Map of Whitehill Formation thickness values (in metres), with the boreholes used shown (black triangles). In general, the layer thickens from around 40 m in the south to 5 m in the northeast on craton. Regions in the north-central, northwest and south showing local thickening, most likely due to structural features. See Figure 6-1 for details. 205

Figure 6-5. Simplified sketch of the (a) deposition and several stages of deformation, (b) burial and compaction, and (c) uplift and erosion of the Whitehill Formation. Flexure modelling provides an estimate of the difference in height (x) between the Whitehill Formation at deposition and deformation (in a), and its current location after uplift and erosion (in c). . 209

Figure 6-6. Best-fit flexure models of the lithosphere constrained by top of the Whitehill Formation depth profiles (thick black line) along the western (P1) and eastern profile (P2) for a load width of 100 km (see Figure 6-3 for locations). The load height for the flexure models is varied: 4 km (green line), 6 km (red line) and 8 km (blue line). The basin deepens towards the southeast resulting in a change in the best-fit model parameters across the two profiles. The load heights (h) and model elastic thickness (Te) values are listed (see Table 6-1 for model parameters). The topography (Topo) along each profile is shown (grey line for the western profile, black line for the eastern profile). 211

Figure 6-7. Best-fit flexure models (orange line) of the lithosphere constrained by top of the Whitehill Formation depth profiles (thick black line) along (a) the western (P1; load: 100 km wide and 4 km; Te 50 km) and (b) eastern profile (P2; load: 100 km wide and 8 km high; Te 85 km). Borehole data used to constrain the depth profile are shown (red dots with labels, see Figure 6-3 for locations). Divisions between terranes are marked (thin vertical black line): KVC - Kaapvaal craton, Namaqua and Natal terranes and CFB - Cape Fold Belt. The load representing the CFB is shown with dashed orange lines. See Figure 6-6 for details. 212

Figure 6-8. Best-fit flexure models of the lithosphere constrained by depths to the top of the Whitehill Formation as determined from borehole data (grey circles) along a profile extending north of borehole SP1/69 (P3; see Figure 6-3 for location). The Whitehill Formation only stretches along the southern portion of the profile. Borehole intercepts for the base of the Karoo Basin on-craton are therefore also plotted (red circles) (Scheiber-Enslin *et al.*, 2015b). An accurate flexure profile of the Whitehill Formation cannot easily be modelled. However, a high Te value is needed to fit the broad deepening of the Karoo Basin in this region (load height (h), model elastic thickness (Te) values and shift (s) are listed). The best-fit model for Profile 2 from Figure 6-7b is plotted for reference (h8_Te85_s1200). See Figure 6-6 and Figure 6-7 for details. 213

Figure 6-9. (a) Inverted Moho calculated using the topographic load and Moho depths from Nguuri *et al.* (2001) in Lithoflex. SASE sites are indicated (black dots). A reference depth of 30 km and density contrast of 400 kg/m^3

were used; (b) Residual when comparing (a) and Moho depths from Nguuri *et al.* (2001); (c) Te values needed to accommodate the topographic load with the Moho depths in (a). A reference depth of 35 km and density contrast of 400 kg/m^3 is used in (d), with the residual shown in (e) and calculated Te values in (f). The two north-south 2D flexure profiles are marked. See Figure 6-1 for details. 216

Figure 6-10. Topographic map of South Africa. The edge of the extensive inland plateau in the south (>1200 m) correlates closely with the northern extent of Cape Supergroup (yellow line; solid - definite and dashed – approximate location), as well as the divide between the Namaqua and Natal mobile belts (green line). The extent of the asthenospheric buoyancy anomaly along the edge of the escarpment is shown (dotted line). See Figure 6-1 and for details. 218

List of Tables

Table 2-1. Stratigraphy of the southern main Karoo Basin and Cape Basin, including groups and relevant formations, as well as depositional environments (McCarthy and Rubidge, 2005, Johnson *et al.*, 2006, Thamm and Johnson, 2006). 11

Table 2-2. Borehole database used to constrain the depths of Karoo strata (top of the Whitehill Formation and base of the Dwyka Group). Coordinates are converted relative to the WGS84 ellipsoid. Ground level (GL) is based on borehole logs. Measured depths (MD) and subsea depths are listed in metres. These data are taken from D. Cole's database, Rowsell and De Swardt (1976), as well as unpublished logs (UL)..... 20

Table 2-3. Average density values for Karoo and Cape Supergroup sediments from the Council for Geoscience Physical Properties Atlas (Maré, 2012). .. 28

Table 2-4. Crustal thickness estimates (including errors) for several studies in southern South Africa. Unknown errors are marked with '-'..... 29

Table 3-1. Stratigraphic table for the southern main Karoo Basin, listing groups, subgroups, formations and depositional environments (McCarthy and Rubidge, 2005, Johnson *et al.*, 2006)..... 57

Table 3-2. Dolerite groups within the Karoo basin defined by van van Zijl (2006a)..... 63

Table 3-3. Dolerite distribution from several deep wells within the main Karoo Basin, divided according to geographic region. The total thickness of the dolerites is listed (see text for more details) as well as the number of

intrusions in each well (some thinner intrusions might be excluded due to the resolution of well logs). The lithologies within which these dolerites have intruded are shaded grey (GG – granite-gneiss Namaqua-Natal basement, CGS – Cape Supergroup, DW – Dwyka Group, EC – Ecca Group, BF – Beaufort Group). The depth extent of the wells is indicated with thick black boxes. The general trend observed is intrusions at all stratigraphic levels in the northwestern and eastern/southeastern Karoo, while between these regions dolerites are restricted to shallower lithologies (Beaufort Group)..... 69

Table 3-4. Sill and inclined sheet geometries determined from geological and seismic data, including the horizontal and vertical extent of the bodies and dips of the inclined sheets. Sill geometries were determined from those around Queenstown in the southeastern Karoo, while sheet geometries were determined from those further south, around Somerset-East. Lithologies in which they intrude are listed (Fm – Formation, Grp – Group)..... 101

Table 4-1. Density and magnetic susceptibility values used for potential field modelling..... 136

Table 5-1. Summary of the geological history of South Africa (De Wit *et al.*, 1992, Thomas *et al.*, 1993) and corresponding geophysical studies (including references). 159

Table 5-2. Crustal density (kg/m^3) and velocity (km/s) values from: the Council for Geoscience Physical Properties Atlas (1 - Maré, 2012), refraction seismic studies (2 - Green and Durrheim, 1990, Durrheim and Green, 1992, Durrheim, 1998) (3 - Stankiewicz *et al.*, 2007), xenolith studies (4 - Schmitz

and Bowring, 2004) and teleseismic studies (5 - James *et al.*, 2003). Upper crustal rocks units (SG - Supergroups) are divided into on- and off-craton units. Rock types are listed in brackets (sst – sandstone, qtzite – quartzite). Refraction velocities are converted to densities using the velocity-depth curve from Zoback and Mooney (2003) and Ludwig *et al.* (1970). 166

Table 5-3. Starting model densities (kg/m^3) and depths (km). The geological units are divided into on- and off-craton units. SG – Supergroup. 176

Table 5-4. Lithospheric mantle density results (kg/m^3) for: Model 1 – satellite Gz inversion (SatInv_Gz), 2 – Gzz inversion (SatInv_Gzz), 3 – Gz and Gzz inversion (SatInv_Gz_Gzz), 4 – ground gravity inversion (GrdInv), 5 – Forward modelling of density values from Model 2 to fit the long-wavelengths of the ground data (SatInv_Gzz_GrdFM). The different on- and off-craton tectonic terranes are listed including the various cratonic blocks from Youssof *et al.* (2013) (shaded grey). Residuals (Res) and P-correlation factors (Pf) measuring the fit of calculated data to observed satellite (Sat) and ground data (Grd) are given..... 179

Table 5-5. Lithospheric mantle density results (kg/m^3) for Model 5 and the buoyancy model (40 kg/m^3 density contrast). See Table 5-4 for details..... 191

Table 6-1. Basic 2D best-fit flexure models of the lithosphere, constrained using two north-south top of the Whitehill Formation depth profiles (see Figure 6-3 for locations). The width and height of the Cape Fold Belt load, as well as the elastic thickness (Te) and shift of the modelled plate are listed. The minimum model residual (Resid) for each combination is recorded (10^3). 210

List of symbols and nomenclature

ρ	Density
x	Distance
Te	Effective elastic thickness
D	Flexural rigidity
g	Gravitational acceleration
h	Height/depth
m/ka	meters per thousand years
MD	Measured depth within borehole
P-factor	P-correlation factor
V	Poisson's ratio (0.25)
Res	Residual
TWT	two-way travel-time
Gz	Vertical component of gravity
Gzz	Vertical component of gravity gradient
E	Young's modulus (10^{11} N/m^2)
BMA	Beattie Magnetic Anomaly
CFB	Cape Fold Belt
CIA	Cape Isostatic Anomaly
KVC	Kaapvaal Craton
NNB	Namaqua-Natal Belt
SASE	Southern African Seismic Experiment

Chapter 1

Introduction

1.1 Thesis Objective

The objective of this thesis was to investigate the formation of the main Karoo Basin, which covers a large part of South Africa. Several Karoo aged basins exist across south-central Africa (Catuneanu *et al.*, 2005), but the focus of this study was the largest of these basins in South Africa. This was to be done through the creation of a three-dimensional (3D) model of the basin, constrained by existing geological and geophysical data. This model would then be used to carry out isostasy and flexure studies of the lithosphere.

1.2 Organization of the Thesis

Comprehensive depth maps of the basin are presented in Chapter 2. These maps were created using vintage seismic data combined with new computational capacity and an extensive borehole database. In this chapter, I also investigate the gravitational response of these sediments, and whether they can account for the source of the Cape Isostatic Anomaly

These seismic and borehole data allow, in Chapter 3, for the distribution and geometry of dolerite intrusions within the basin to be constrained. The shape of the basin and its internal stratification significantly impacted emplacement of these dolerites, as they intruded preferably between layers with varying mechanical properties. These bodies can cause heating of the shale reservoir in their vicinity and rapid conversion of organic material to gas (CH_4 and CO_2). This in turn can result in over maturation and loss of gas, or alternatively an increase in the maturity of the shale reservoir to a favourable level. The delineation of these bodies is therefore of importance for future shale gas exploration.

In order to use potential field, seismic and borehole data to construct a 3D model of the Karoo basin, an understanding is needed of the underlying basement rocks. The Beattie Magnetic Anomaly (BMA) that stretches across the entire southern part of the basin forms part of the basement Namaqua-Natal Belt. In Chapter 4 filtered magnetic data is used to show that the BMA is part of a group of linear magnetic anomalies making up the Natal Belt. The anomaly itself will therefore not have an individual effect on basin formation, and the effect of the Natal Belt can be modelled as a whole.

In Chapter 5, I present a 3D lithospheric model of the basin area. The relatively well-constrained crustal structure of the model allows for inversion modelling of lithospheric mantle densities using GOCE (Gravity Field and Steady-State Ocean Circulation Explorer) satellite gravity data. These satellite data provide a better constraint of the long-wavelength mantle signal compared to ground gravity data. In this chapter, isostasy studies using this 3D model shed light on loading at the base of the model. As South Africa is not experiencing rapid uplift or subsidence, it is expected to be in isostatic compensation. This provides a method to determine the accuracy of the model. It also provides an explanation for how the high topography of the main Karoo Basin in South Africa is compensated.

In Chapter 6, depth estimates for the shale layer (Whitehill Formation) within the main Karoo Basin are compared with 2D flexure profiles. This is done to determine the effective elastic thickness (Te) during basin formation, and hence better understand the formation. Moho depth estimates and topography are used to determine the current day Te of the lithosphere. These two Te estimates are compared to understand how Te changes through time. Closing remarks are included in Chapter 7.

1.3 Contribution of Thesis

This study has led to the creation of the best-constrained sediment thickness map of the main Karoo Basin to date using borehole and seismic data. Through this thesis work the borehole database used to create this map has been published. These borehole and seismic data have also allowed for a more accurate delineation of the northern extent of the Cape Supergroup.

The vintage seismic data in this thesis have been used to confirm the distribution of dolerites emplaced within the basin, and constrain their subsurface geometry. Understanding of their vertical distribution was previously limited to a handful of historic low-resolution seismic images and intersections of sills by boreholes, while understanding their vertical geometry was limited to surface

outcrops. This new study also quantifies for the first time the impact of sediment deformation due to the Cape Fold Belt in the south on the emplacement of these intrusions.

These seismic data along with geological and structural data have allowed for a more geologically reasonable explanation of the source of the Cape Isostatic Anomaly in the southern Cape. The existing explanation for the anomaly, namely deepening Moho geometry in this region Hales and Gough (1960), was shown to be invalid after the SASE experiment of 1997 to 1999 and has not been re-examined in the literature since.

This thesis has contributed towards a greater understanding of the Natal basement rocks that underlies a large part of the Karoo basin. This study confirmed the results of previous borehole and low resolution magnetic studies that suggest the Namaqua and Natal Belts are two separate belts. Filtering of magnetic data, for the first time, allowed for a more accurate delineation of the boundary of the Natal belt. This study also confirmed that the BMA is part of a series of anomalies that together make up the Natal Belt. Filtered magnetic data allowed for the western extent of the other anomalies to be accurately delineated for the first time. The source of these strong magnetic anomalies, which has been debated since 1909, was determined during this study using previously unused geological evidence on the east coast of South Africa.

The 3D model of the Karoo basin from this thesis, for the first time, has constrained the change in lithospheric mantle density from on- to off-craton through the use of satellite gravity and gravity gradient data. These high elevation datasets (255 km) provide information on the long-wavelength component of the field linked to deeper sources. Previous gravity estimates are limited to ground gravity data whose signal contains a large crustal component.

Through this research, I have analytically determined how the large inland plateau covering a significant portion of the Karoo basin is isostatically compensated. Previous tomographic studies have suggested plume activity, but here it is shown for the first time that the gravity and isostasy data over South

Africa cannot be modelled without including an asthenospheric buoyancy anomaly.

Furthermore, I present the first flexure models for the southern Karoo basin using the new basin sediment thickness maps. These models allow for the Te of the lithosphere during the deposition of the Karoo basin to be determined. The results from these models have shown that it is west to east changes in Te that have impacted the shape of the Karoo basin, rather than previously suggested lateral changes in lithospheric rheology linked to the different terranes (approximately north to south). These flexure studies have confirmed mathematically that the Karoo basin could have been formed due to flexural loading in the south, which was previously only assumed or argued against due to the size of the basin.

Chapter 2

Karoo Basin

This chapter includes a manuscript that is published in the South African Journal of Geology (2015, volume 118, pages 261-284). I conceived this study in discussion with my supervisors. Work for this manuscript and write-up was completed by me, with the remaining authors helping to improve the manuscript. The extensive borehole table in this manuscript was provided by Dr Doug Cole, previously at the Council for Geoscience.

NEW DEPTH MAPS OF THE MAIN KAROO BASIN, USED TO EXPLORE THE CAPE ISOSTATIC ANOMALY

STEPHANIE E. SCHEIBER-ENSLIN
Geophysics Unit, Council for Geoscience, Pretoria, 0184, South Africa
School of Geosciences, University of the Witwatersrand,
Private Bag 3, WITS 2050, South Africa
email: steph.scheiber@gmail.com

JÖRG EBBING
Department of Geosciences, Christian-Albrechts University,
Kiel, 24118, Germany
email: jebbing@geophysik.uni-kiel.de

SUSAN J. WEBB
School of Geosciences, University of the Witwatersrand,
Private Bag 3, WITS 2050, South Africa
email: susan.webb@wits.ac.za

2.1 Abstract

Here we present a comprehensive depth and thickness map of the main Karoo and Cape Basins using borehole and reflection seismic data. The depth to the Whitehill Formation, which is the focus of current shale gas interest within the Karoo, is also mapped. The deepest part of the basin is in the south, along the northern boundary of the Cape Fold Belt (~4000 m in the southwest Karoo and ~5000 m in the southeast; ~5500 to 6000 m sediment thickness). The Whitehill Formation along this boundary reaches a depth of ~ 3000 m in the southwest and ~4000 m in the southeast. Limited borehole data in the southeastern Karoo show a broad deepening of the basin here compared to the southwestern Karoo. In the southeast near East London faulting has resulted in deepening of the basin close to

the coast, with the Whitehill Formation deepening to over ~5000 km. Seismic and borehole data show that the Cape Supergroup pinches out below the Karoo Basin around Beaufort West and Graaff-Reinet in the southern Karoo (32.6˚S for the Bokkeveld and 32.4˚S for the Table Mountain Group). The Cape Supergroup reaches thicknesses of around 4 km in the south. The gravity effect of these sediments does not account for the Cape Isostatic Anomaly (CIA) in the southern part of the Karoo Basin near Willowmore and Steytlerville, i.e., an ~45 mGal Bouguer gravity low. A refraction seismic profile over the anomaly shows this region is associated with a large volume of low velocity/density shallow sediments (4.5 m/s^2, 2500 kg/m^3), as well as a low velocity/density anomaly associated with a normal fault and the Klein Winterhoek thrust fault (5.5 m/s^2, 2650 kg/m^3). These low density shallow sediments are explained by uplift of Karoo and Cape Supergroup sediments of ~2 km or greater that is evident in this south-central region of the basin based on Soekor seismic data. This deformation has brought lower density shales (1800 – 2650 kg/m^3) of the Ecca Group closer to the surface. These shallower features along with a deeper lower crust (6.5 m/s^2, 2900 kg/m^3) in this region are interpreted to account for the CIA.

2.2 Introduction

The main Karoo Basin covers ~700,000 km^2 of Southern Africa (Figure 2-1, Johnson *et al.*, 2006) and is the current focus of shale gas exploration (Decker and Marot, 2012, Cole *et al.*, 2011). An understanding of how the depth of the basin changes from region to region is therefore important. Previous studies have relied on extensive borehole data in the basin (Rowsell and De Swardt, 1976). Recently digitized historical seismic data in the southern part of the basin (Fatti, 1987, Fatti, 1970, Fatti and Du Toit, 1970), along with reflection seismic data (Loots, 2013, Lindeque *et al.*, 2011) from the Inkaba yeAfrica project now allow for infilling of this map. These seismic data also allow for a better understanding of the upper crustal contributors to the Cape Isostatic Anomaly (CIA) in the central part of the Cape Fold Belt (CFB), at the southern edge of the basin. This

anomaly was previously attributed to a remnant crustal root below the fold belt (Hales and Gough, 1960).

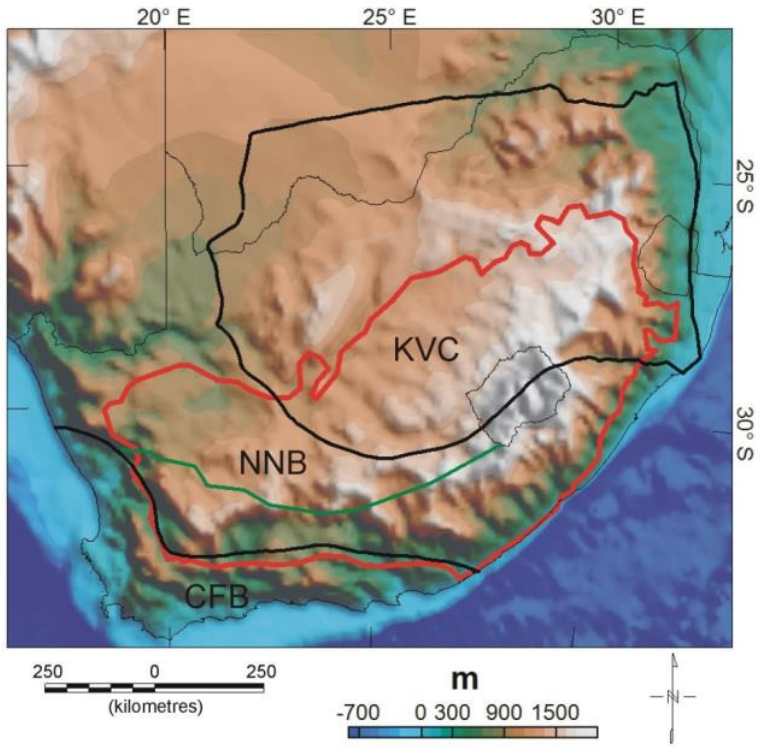

Figure 2-1. Topographic map of South Africa showing the tectonic provinces: KVC – Kaapvaal craton, NNB – Namaqua-Natal Belt and CFB – Cape Fold Belt. The divide between the Namaqua (west) and Natal (east) terranes as determined from borehole (Eglington, 2006) and magnetic data (Scheiber-Enslin *et al.*, 2014a) [Chapter 4] is shown (green line). The main Karoo Basin (red outline) covers a large portion of the high inland plateau (Johnson *et al.*, 2006).

2.3 The Karoo and Cape Basins

Karoo Supergroup sediments were deposited from the Late Carboniferous (300 Ma) to Middle Jurassic (180 Ma) (Johnson *et al.*, 2006), forming after a 30 Ma hiatus following the deposition of Cape Supergroup (Thamm and Johnson, 2006). The sediments were deposited on the stable Archean Kaapvaal Craton

(KVC) in the northeast and on the surrounding Proterozoic Namaqua-Natal Belt (NNB) in the southwest (Figure 2-1). Magnetic data (Scheiber-Enslin *et al.*, 2014a - Chapter 4) and borehole data (Eglington, 2006, Eglington and Armstrong, 2003) have been used to determine the boundary between the older Namaqua (2.0-1.7 Ga from U-Pb and Sm-Nd dating; Raith *et al.*, 2003, Robb *et al.*, 1999, Cornell *et al.*, 1986, Geringer *et al.*, 1994) and entirely juvenile Natal crust (~1.5 Ga from Rb-Sr, Sm-Nd and U-Pb dating; Eglington *et al.*, 1989, Thomas and Eglington, 1990) (Figure 2-1).

Depositional environments within the basin changed glacial to aeolian as Gondwana migrated from the poles to hotter regions (Johnson *et al.*, 2006). The marine shales of the Whitehill Formation in the southern part of the basin are currently being explored for shale gas (Cole *et al.*, 2011, Decker and Marot, 2012). The stratigraphic sequences in the southern part of the basin along with depositional environments are summarized in Table 2-1, and the distribution of the sediments is shown in Figure 2-2. A significant portion of the basin was eroded in the mid- to late-Cretaceous during two periods of uplift (i.e., 2 – 7 km of mostly basalt that caps the basin, De Wit, 2007).

Table 2-1. Stratigraphy of the southern main Karoo Basin and Cape Basin, including groups and relevant formations, as well as depositional environments (McCarthy and Rubidge, 2005, Johnson *et al.*, 2006, Thamm and Johnson, 2006).

Super-group	**Group**	**Formation**	**Depositional Environments**
Karoo (~300 – 180 Ma)	Drakensberg		Lavas
	Stormberg	Clarens	Aeolian and playa
		Elliot	Meandering rivers and playa
		Molteno	Braided rivers
	Beaufort		Fluvial
	Upper Ecca		Deltaic and basin plain turbidites
	Lower Ecca	Collingham	Marine shales
		Whitehill	
		Prince	
		Albert	
	Dwyka		Glacial diamictites and muds
Cape (~500 – 330 Ma)	Witteberg		Shallow marine, marginal marine and deltaic.
	Bokkeveld		Wave-dominated deltas
	Table Mountain		Shallow marine to fluvial, separated by a glacial interlude

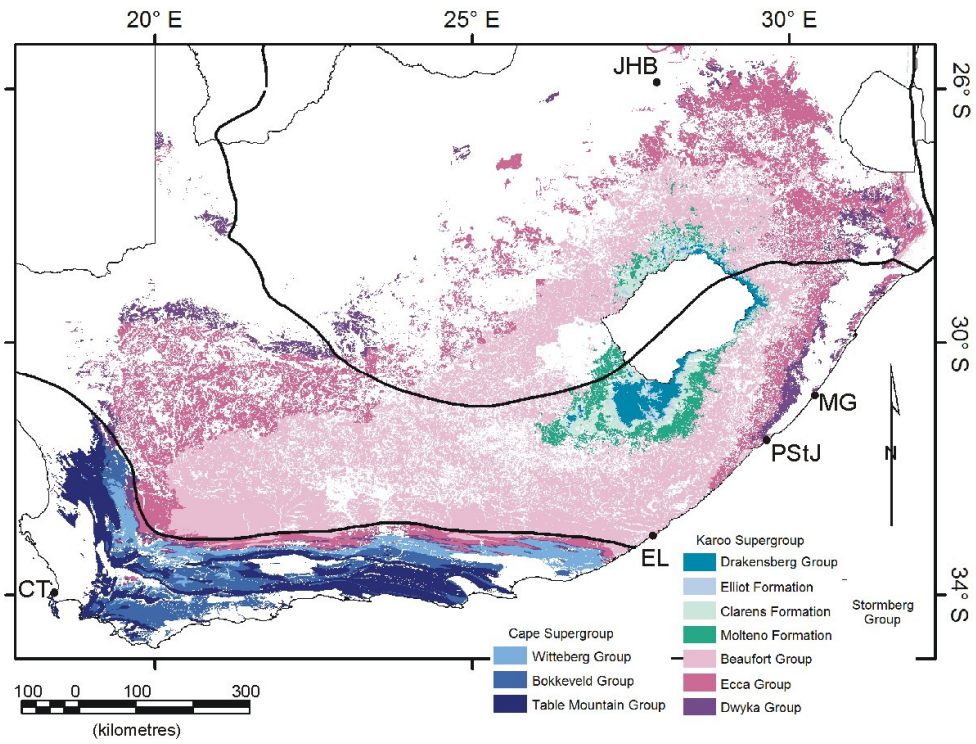

Figure 2-2. Distribution map of the geological units of the main Karoo Basin across South Africa, and the Cape Basin in the southern part of the country (Stratigraphy), 1980). Major tectonic provinces are outlined (see Figure 2-1 for details). Several cities and towns are indicated include Cape Town (CT); Johannesburg (JHB); East London (EL); Margate (MG) and Port St Johns (PStJ).

Several models have been proposed for the formation of the basin. Four to five different compressional events are associated with the Cape orogeny between 300 Ma and 215 Ma ($^{40}Ar/^{39}Ar$ dating), and linked to the Late Palaeozoic amalgamation of Gondwana (Gresse *et al.*, 1992, Hälbich *et al.*, 1983). While problems can be associated with $^{40}Ar/^{39}Ar$ dating (Turner and Thomson, 2005), these dates have been confirmed by stratigraphy and biostratigraphic ages (Bordy *et al.*, 2005), giving eight events in total (Catuneanu *et al.*, 1998), and have been reproduced by other studies (e.g., Gresse *et al.*, 1992, Thomas *et al.*, 1992b). These events have been linked to the subduction of the palaeo-Pacific plate below the Gondwana plate towards the north, and to the formation of the Karoo as a

retroarc foreland basin (Catuneanu *et al.*, 1998, De Wit and Ransome, 1992, Johnson, 1991, Cole, 1992). Turner (1999) argues that evidence in the Upper Karoo (Upper Triassic-Jurassic) sequence supports an extensional depositional environment and uplift. Extension is said to have resulted from a thermal anomaly off the current southeast coast of South Africa, which is argued against by Bordy *et al.* (2005).

Pysklywec and Mitrovica (1999) suggest that due to the large size of the basin, additional mechanisms are needed to explain subsidence along with flexure due to thrusting. Their numerical models estimate that 20 to 30% of sediment accumulation space in the Karoo could have been created by mantle flow (with the subducting slab dipping at 25˚ to 40˚, and a distance to the trench of between 600 and 1300 km). An extensive geological and geophysical study by Tankard et al. (2009) attributes both Cape and Karoo Basin formation to fault-controlled subsidence of crustal blocks, followed by long periods of regional subsidence due to subduction-driven mantle flow (Pysklywec and Mitrovica, 1999). These thick-skinned tectonic models involve basement deformation and movement along crustal-scale structures (Coward, 1983).

Recent studies in the southwestern Karoo using reflection seismic data, however, suggest the Karoo Basin does not fulfil the criteria of a foreland basin (Lindeque et al., 2011). The lack of basement deformation on seismic data instead suggests that the Karoo and the Cape Basin developed from a wide, thin-skinned fold belt that formed in response to far-field southward subduction (Lindeque et al., 2011). Lindeque *et al.* (2011) interpret a series of low-angle listric thrusts and folds in the Cape Supergroup sediments (down to ~ 10km depth in the south of the profile) that are not connected to the underlying basement or overlying Karoo. In addition, deformation within the Karoo occurs along low-angle listric faults linked to local décollement surfaces within the Whitehill and Prince Albert Formations in the Ecca Group (Lindeque *et al.*, 2011). This interpretation is supported by a recent interpretation of historic Soekor seismic data (Mowzer, 2013). Soekor (Pty) Ltd was established by the South African government in the 1960s to investigate for onshore hydrocarbon deposits in the country.

Paton *et al.* (2006) argue, using constructed onshore geological cross-sections from surface geology and offshore seismic data, that instead of describing the CFB as thin- or thick-skinned end-members, it should rather be described as being controlled by a south dipping mega-décollement that exhibits aspects of both models, e.g. shallow dipping controlling structures in the north that are associated with low relief and the southern limit of Karoo rocks (Booth and Shone, 2002) and progressively steeper dipping structures in the south associated with the Cape Supergroup sediments and higher relief that may coalesce at depth onto a common south-dipping décollement (Hälbich, 1993, Söhnge and Hälbich, 1983, De Wit and Ransome, 1992) below the Cape Supergroup and within the pre-Cape Group (Paton *et al.*, 2006). This décollement is supported by seismic receiver function analysis by Harvey *et al.* (2001). Receiver function analysis shows a discontinuity at ~8 (and ~18 km) depth at four stations in the Cape region, with the upper discontinuity increasing to 11 km further west.

The Karoo rocks unconformably overly those of the Cape Supergroup (Thamm and Johnson, 2006). The Cape Supergroup was deposited from the Early Ordovician (~500 Ma) to the Early Carboniferous (~330 Ma). Table 2-1 summarizes the Cape geological units (Witteberg, Bokkeveld and Table Mountain Groups) and depositional environments, and Figure 2-2 shows the distribution of sediments. Previous interpretations from borehole and outcrop data suggest the youngest Cape Supergroup sediments, the Witteberg Group, do not continue north below the Karoo Basin and are restricted to the CFB (Winter and Venter, 1970). Recent seismic reflection data in the southwestern Karoo, however, suggest that these Witteberg Group sediments extend for approximately 60 km to the north below the Karoo, and pinch out before any borehole intersections (just south of 32.77˚ S; Lindeque *et al.*, 2011). These seismic data show that the entire succession of Cape Supergroup sediments reach a maximum thickness of ~10 km south of the Karoo Basin, and pinch out north of the profile in this region, i.e. north of Slingersfontein (31.07˚ S).

The majority of Cape Supergroup sediments outcrop along the southern coast of South Africa, though a portion (~ 1000 m) outcrops between Margate and Port St Johns on the east coast (Karpeta and Johnson, 1979; Figure 2-2, Kingsley,

1975, Hobday and Mathew, 1974). This Msikaba Formation was previously mapped as the Natal Group, but has been reassigned to the Cape Supergroup and most likely correlates with the Witteberg Group (Thomas *et al.*, 1992b, Thamm and Johnson, 2006, Stratigraphy), 1980), or is possibly younger than the Witteberg Group (Shone and Booth, 2005)

It is unclear what basement rocks underlie the Cape Supergroup. Exposed pre-Cape metasediments within the CFB include the Gamtoos, Kango and Kaaimans Group (Söhnge and Hälbich, 1983). Metasediments from the Kango Group have been dated (U/Pb dating of detrital zircon) at 1100 Ma (NNB source) and 518 Ma (NNB and Cape Granite Suite source), the younger subgroup has been described as a precursory rift sequence to the Cape Basin (Barnett *et al.*, 1997). Recent seismic studies have supported the idea that the NNB continues below the Cape Supergroup (Lindeque *et al.*, 2011).

Several studies agree that the Cape Supergroup represents an Atlantic-type passive margin basin, i.e., sedimentation occurs above an ancient rift that forms a transitional zone between continental and oceanic crust (Tankard *et al.*, 1982, Johnson, 1991, Winter, 1984, Winter, 1989, Thamm and Johnson, 2006). Shone and Booth (2005) expands on this model suggesting passive rifting linked to the formation of the Cape Supergroup due to the absence of volcanics, but active rifting in the northern Natal where volcanism has been recorded. Their study recognizes several shortfalls in their model and any other model due to limited data.

In the south, lower Karoo Supergroup sediments (Dwyka, Ecca and Beaufort Group) and Cape Supergroup sediments were deformed during the formation of the north-south and east-west arms of the CFB (Hälbich, 1992, Söhnge and Hälbich, 1983). This belt extends for approximately 1300 km across the southern part of South Africa (Figure 2-2). Two main models have been proposed for the formation of this belt, namely an Andean model with subduction ~1500 km further south, resulting in folding and thrusting (Johnson, 1991, De Wit and Ransome, 1992), and a right-lateral transpressional model with the CFB joining regions of strike-slip deformation in South America and Antarctica during

Gondwana times (Johnston, 2000, Tankard *et al.*, 2009). Booth (2011) details problems associated with each model by pointing out that structural styles in the western and eastern sectors of the fold belt show opposite senses of movement.

In the eastern branch rocks are deformed up to 250 km from the coast, with folds/faults being northward verging (De Wit and Ransome, 1992, Hälbich, 1992). This region is characterized by thrust faults, as well as along-strike normal faults and strike-slip faults. These normal and strike-slip faults are linked to the Mesozoic breakup of Gondwana (Bate and Malan, 1992, Booth and Shone, 1999). Thrusting and erosion makes it difficult to determine the original thickness of the Cape Supergroup, as well as the location of the basin depocentre (Shone and Booth, 2005).

Recent mapping of several thrust faults in the eastern arm of the belt have allowed for a better understanding of the CFB (e.g., Witteberg units around the town of Steytlerville; Booth *et al.*, 2004, Booth and Shone, 2002, Booth and Shone, 1999, Brunsdon and Booth, 2009). This region is characterized by several thrust sheets occurring as parallel belts up to 5 km wide, with the sheets themselves being hundreds of metres thick (Booth, 1996, Booth *et al.*, 2004, Booth and Shone, 2002, Booth and Shone, 1999, Brunsdon and Booth, 2009) (Figure 2-3).

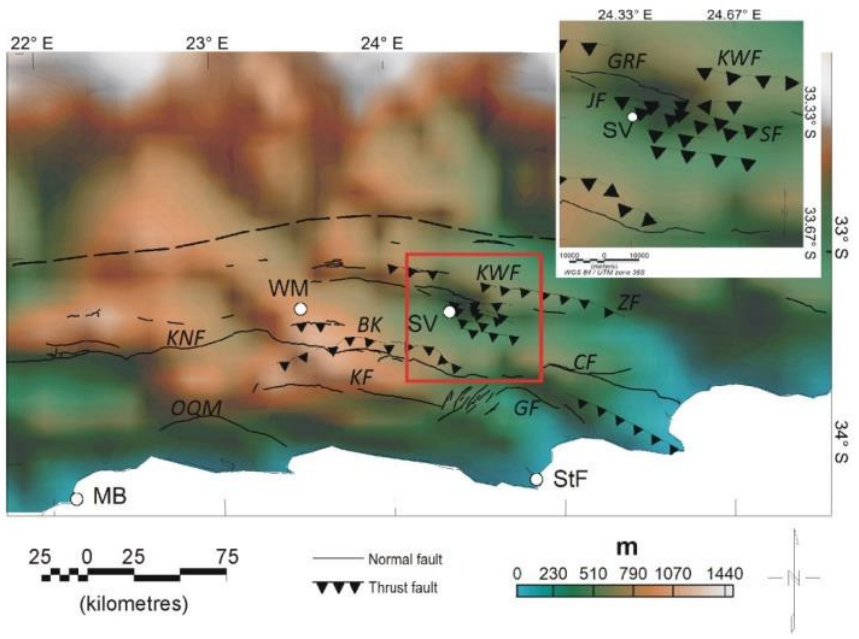

Figure 2-3. Topographic map of the central portion of the eastern arm of the Cape Fold Belt (Amante and Eakins, 2009). Willowmore (WM), Steytlerville (SV), Mossel Bay (MB) and Cape St Francis (StF) are shown as white circles. The dashed line marks the approximately northern extent of the fold belt. Mapped and inferred faults in the region are indicated (normal – black lines; thrust – black line with black triangles), and labelled (normal faults: CF – Coega, GF – Gamtoos, GRF – Grootrivier, KNF – Kango, KF – Kouga, OQM – Outenique Mountains; thrust faults: BK – Baviaanskloof, JF – Jackalsbos, KWF – Klein Winterhoek, SF-Soutkloof, ZF – Zuurberg) (Booth *et al.*, 2004, Booth and Shone, 1999, Roby *et al.*, 1995, Toerien, 1991, Toerien and Roby, 1979). The area outlined (red box) is shown on the zoomed in inset map.

In the central part of the eastern arm, around Steytlerville, the Grootrivier fault is one of the largest and most continuous of the normal faults with a displacement of ~ 800 m (Toerien, 1986, Booth *et al.*, 2004) (Figure 2-3). Several east-west striking thrust faults have been mapped (Booth *et al.*, 2004, Booth and Shone, 2002), and include the Soutkloof (Booth *et al.*, 2004) and Jackalsbos faults (Toerien, 1991) that cut through Witteberg sediments (Figure 2-3). Movement

along the Klein Winterhoek thrust fault to the north has been recorded but not studied in detail (Booth *et al.*, 2004; Figure 2-3). These faults in general dip to the south, with dips increasing from north to south, e.g. Jackalsbos fault dips at 37˚ while the Soutkloof fault 4 km further south dips at ~65˚. Thrusts within the Bokkeveld sediments ~ 6 km further south (Figure 2-3) are characterized by shallow south-dipping low-angle thrust fault plane which are displaced by steep south-dipping thrust planes and subordinate north-dipping backthrusts (Booth *et al.*, 2004, Brunsdon and Booth, 2009). It appears therefore that rock types influence fault frequency (Booth *et al.*, 2004). The dip of these thrust faults also appears to shallow with depth (Booth, 1996). Displacement also varies from north to south, with larger displacement along the prominent Jackalsbos thrust (estimated 500 m of displacement), and less along the steeper thrusts to the south (Booth *et al.*, 2004). In this region it appears that thrusting has taken place before, during and after folding (Booth and Shone, 2002).

2.4 Cape Isostatic Anomaly

This region of faulting around Steytlerville (Figure 2-3) roughly coincides with the Cape Isostatic Anomaly (CIA). This anomaly was recognized in the 1960s during surveying of the Cape region (Hales and Gough, 1960, Hales and Gough, 1961). The anomaly is visible on the free-air, Bouguer and isostatic gravity anomaly maps as a gravity low around the towns of Willowmore and Steytlerville, near the boundary between Karoo and Cape Supergroup sediments, (Figure 2-4a-c). In the case of the free-air and isostatic maps the anomaly extends to the coast northeast of Port Elizabeth (Figure 2-4).

The anomaly was attributed to a remanent crustal root below a section of the CFB, thought to have compensated topography that has since been removed by erosion. No crustal thickness data existed at the time to confirm this hypothesis. Hales and Gough (1960) model the low-density root using a 80 km wide by 6.2 km thick slab at 35 km depth, and assume a density difference of 600 kg/m^3 between the mantle and overlying crust. Erosion of this region and the resulting isostatic uplift is the suggested cause of historic and small-scale current

seismic activity along several faults in the region, including the Kango-Baviaanskloof-Coega and Kouge-Gamtoos fault sections, and possibly the Zuurberg fault to the north (Goedhart *et al.*, 2011; Figure 2-3). A recent GPS station set up east-southeast of Willowmore (Figure 2-3; on the Willowmore "high", i.e., outcropping Table Mountain Group within Bokkeveld sediments) will be used to quantify the amount of uplift taking place (Goedhart *et al.*, 2011).

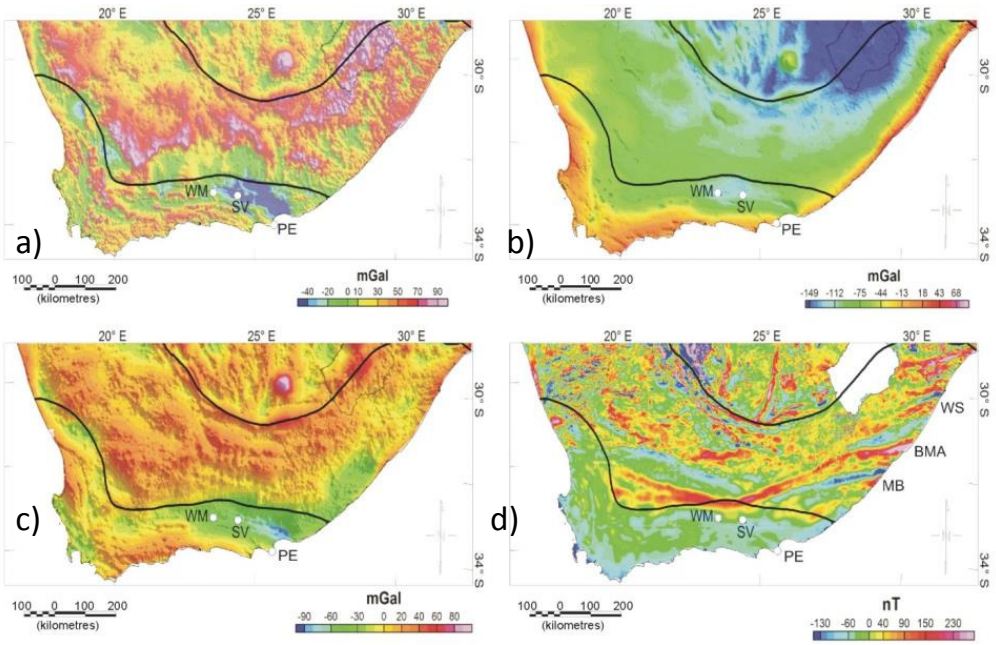

Figure 2-4. (a) Free-air, (b) Bouguer, (c) isostatic gravity anomaly and (d) total magnetic intensity maps for South Africa. Major tectonic provinces are outlined (see Figure 2-1 for details). The Cape Isostatic Anomaly extends from Willowmore (WM) through to Steytlerville (ST) and Port Elizabeth (PE) on the east coast (white circles). The Williston (WS), Beattie (BMA) and Mbashe (MB) anomalies are indicated in (d) (Thomas *et al.*, 1992b).

2.5 Data

The datasets used to create the depth map for the top of the Whitehill Formation and the base of the Karoo Basin (i.e., the base of the Dwyka Group, or top of the underlying Cape Supergroup and basement) are shown in Figure 2-5.

These include the extensive borehole database compiled by Doug Cole at the Council for Geoscience (CGS), which is made up of industry (Anglo American), deep Soekor (Rowsell and De Swardt, 1976) and CGS boreholes (Table 2-2). Depths are listed as measured depths (MD) within the boreholes and as subsea depths, i.e., depths relative to the WGS84 ellipsoid. Original coordinates are assumed to be relative to the Clarke 1880 ellipsoid and Cape Datum (except for borehole G39974). Recorded elevations and depths are assumed to be in British feet, not Cape feet. Published industry boreholes were used in the northeastern basin (Rutherford, 2009).

Table 2-2. Borehole database used to constrain the depths of Karoo strata (top of the Whitehill Formation and base of the Dwyka Group). Coordinates are converted relative to the WGS84 ellipsoid. Ground level (GL) is based on borehole logs. Measured depths (MD) and subsea depths are listed in metres. These data are taken from D. Cole's database, Rowsell and De Swardt (1976), as well as unpublished logs (UL).

Borehole	Long	Lat	GL (m)	Top Whitehill		Base Dwyka		Source
				MD (m)	Subsea (m)	MD (m)	Subsea (m)	
AB1/65	22.6164	-31.8020	1415	1881	-466			Rowsell
AM1/70	20.8933	-31.3741	1067			1536	-469	Cole
AXT1	22.6087	-30.6131	1218	259	959			Cole
B390/1	19.7154	-32.6420	451	73	378			Cole
BBF1	25.3747	-28.4525	1255	104	1151	179	1076	Cole
BE1/67	29.3863	-28.6779	1151			1056	95	Cole
BH 47	25.3068	-30.2790	1395			1390	5	Cole
BH1 Sambokskraal	21.3333	-32.6751	738	2754	-2016			Cole
BH6 Rietfontein	23.7934	-32.9712	867	68	799			Cole
BKP1	22.8034	-30.6783	1208	356	852			Cole
CFK1	25.8072	-30.3559	1471			1764	-293	Cole
CR1/68	25.0078	-32.4859	793	3671	-2878	4290	-3497	Rowsell
D731/1	25.3741	-28.5703	1242	114	1129	184	1058	Cole
DD1/63	25.4592	-28.5414	1257	132	1125	198	1059	Cole
DP1/78	24.4354	-29.4004	1250	77	1173			Cole
Dubbelde Vlei	21.5194	-30.5403	1036	140	896	640	396	Cole
E1288/1	25.2188	-28.6530	1254	131	1123	178	1076	Cole
EP1/78	23.7996	-29.8695	1189					Cole

FI1/72	27.8470	-28.8945	1572			1873	-301	Cole
G39974	19.8973	-31.4905	1044	344	700			Cole
GLEN1/67	26.3330	-28.9533	1292	732	560	774	518	Rowsell & Cole
GP1/78	25.5769	-28.0564	1271	15	1256	85	1186	Cole
HDA2	26.0622	-28.2181	1326			292	1034	Cole
HDA3	25.8675	-28.2203	1323			195	1128	Cole
HG1/84	20.2902	-30.7964	976	230	746			Cole
HGK1	23.7254	-30.2706	1112	73	1039			Cole
HLP1	23.1865	-30.4667	1105	64	1041			Cole
HM1/78	25.3225	-28.3639	1241	32	1209	106	1135	Cole
KA1/66	23.4195	-32.0202	1036	2083	-1047	2531	-1495	Rowsell
KC1/70	20.5821	-31.3588	1181			1745	-564	Cole
KD1/71	21.8156	-31.0547	1315			1451	-136	Cole
KFN1	25.3077	-30.5592	1224			1330	-106	Cole
KL1/65	20.4523	-32.6172	729	1359	-630	2035	-1306	Rowsell
KL1/78	24.4502	-29.3796	1250	67	1183			Cole
KW1/67	22.3350	-32.9847	969	4360	-3391			Rowsell
LA1/68	27.4797	-29.0864	1614			1710	-96	Cole
OL1/69	19.8592	-32.0006	542	246	296	753	-211	Cole
QU1/65	21.4371	-31.8270	1261	1636	-375	2409	-1148	Rowsell

RM1/78	24.3296	-29.6065	1151	30	1121			Cole
S1460/1	19.7987	-32.9420	536	92	444			Cole
SA1/66	21.3274	-32.6700	741	2754	-2013	3572	-2831	Rowsell
SC3/67	24.2985	-32.7741	792	3972	-3180	5343	-4551	Rowsell
SP1/69	27.7696	-33.0047	237	3668	-3431	4283	-4046	Rowsell
SW1/67	29.2663	-30.1545	1682			2792	-1110	Cole
TG1	25.6744	-29.9167	1355			1129	226	Cole
TG2	25.6300	-29.9480	1399			1142	257	Cole
TG3	25.6131	-29.9376	1388			1125	263	Cole
TG4	25.5949	-29.9241	1380			1115	265	Cole
TG5	25.5897	-29.8899	1384			1142	242	Cole
TG6	25.6001	-29.8975	1370			1068	302	Cole
TGX	25.7538	-30.0115	1400			1560	-160	Cole
TU1/50	25.4996	-29.9003	1380	1045	336			Rowsell
VB122	25.5291	-28.0223	1301	92	1209	160	1141	Cole
VB123	25.7278	-27.9792	1311	124	1187	201	1110	Cole
VB124	25.9464	-28.0075	1280			188	1092	Cole
VP1/78	25.2111	-28.4980	1220	48	1172	104	1116	Cole
VREDE1/66	24.2118	-32.2248	875	2679	-1804	3307	-2432	Rowsell
WE1/66	26.8391	-30.8986	1532	3491	-1959	3732	-2200	Rowsell

WI1/72	27.6882	-28.7091	1695			1512	183	Cole & UL
ZWT1	23.0906	-30.6861	1138	381	757			Cole

Depths to the base of Karoo strata from two 100 km reflection seismic lines were included in this study. One extends south of Fraserburg (Lindeque *et al.*, 2011) and the other is a vibroseis line just west of Beaufort West (Loots, 2013), in the southwestern Karoo. Seismic data in the southern Karoo originally collected by Soekor in the late 1960s and early 1970s, and recently digitized by Falcon Oil and Gas, were also included. Several of these seismic lines have previously been interpreted (Fatti, 1987, Fatti, 1970, Fatti and Du Toit, 1970, Mowzer, 2013). These seismic data include the King William's Town (KW) survey in the eastern Cape; however, these data were not digitized by Falcon Oil and Gas. A depth map (in feet) was instead digitized from Fatti (1970). Velocities for this survey were determined using expanded spread velocity profiles in this region. Additional Soekor lines were shot around Lesotho, but were not included in this study due to interpretation difficulties.

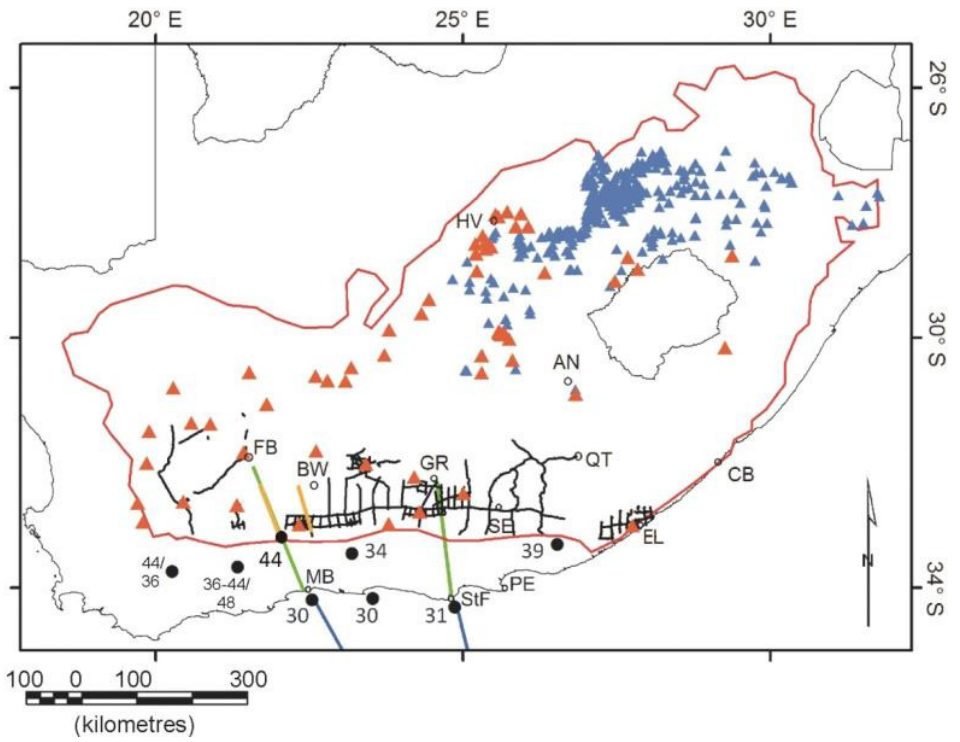

Figure 2-5. Available data used to constrain main Karoo Basin (red line) depth maps. These include deep SOEKOR boreholes (Rowsell and De Swardt, 1976), Council for Geoscience and industry boreholes (D. Cole, pers. comm.) in the southwestern part of the basin (orange triangles), and industry boreholes giving basement depths in the northeastern part of the basin (blue triangles, Rutherford, 2009). Seismic data include reflection seismic (yellow, Lindeque *et al.* (2011) and Loots (2013)), refraction seismic profiles (green, Stankiewicz *et al.* (2007)), offshore seismic lines (blue, Parsiegla *et al.* (2007) and Parsiegla *et al.* (2008)) and Soekor seismic data (black lines). These Soekor data include survey KW in the southeastern Karoo around East London (EL, Fatti, 1970). Moho depth estimates are indicated (black circles, values in kilometres) (Parsiegla *et al.*, 2008, Parsiegla *et al.*, 2007, Muller, 1991, Durrheim, 1987, Graham and Hales, 1965, Nguuri *et al.*, 2001, Lindeque *et al.*, 2011, Harvey *et al.*, 2001). For some sites, due to duplicate studies, multiple estimates are listed. In some cases Cities indicated include Aliwal North (AN), Beaufort West (BW), Coffee Bay (CB), Fraserburg (FB), Graaff-Reinet (GR), Hertzogville (HV), Mossel Bay (MB), Port

Elizabeth (PE), Queenstown (QT), Somerset-East (SE) and Cape St Francis (StF) (white circles).

The Bouguer anomaly (Figure 2-4b), which is calculated from the regional free air anomaly data (Figure 2-4a, Venter *et al.* (1999)), was used to study the CIA. The gravity data were collected with a station spacing of approximately 14 km. The terrain corrected gravity data released by the CGS does, however, have an error of 2 – 5 mGal as several of the elevation measurements were made using barometers (Leaman, 1984). The ETOPO1 topographic model with a resolution of 1 arc-min (Amante and Eakins, 2009) was used during the study with a vertical uncertainty of 10 m. The isostatic anomaly map (Figure 2-4c) is calculated assuming an elastic thickness (Te) of 5 km, reference depth of 35 km and density contrast of 400 kg/m^3 between the crust and the mantle.

Density values used for the study are based on hand sample data from the CGS Physical Properties Atlas (Maré, 2012) (Table 2-3), as well as p-wave seismic velocity to density conversion curves (Zoback and Mooney (2003), adaped from Christensen and Mooney, 1995). Hand samples for stratigraphic groups are averaged over the entire basin, though average density values for formations in the southern part of the basin are also listed. Shale rocks making up the Prince Albert and Whitehill Formations have relatively low average densities (1800 – 2650 kg/m^3). Out of the eight shale samples included in the CGS petrophysical database (Maré, 2012), two samples record densities below 2000 kg/m^3, five have densities between 2000 kg/m^3 and 2300 kg/m^3, and one a density of 2650 kg/m^3. Other rock types making up the formation include gypsum (1800 kg/m^3), mudstone/siltstone (1900 – 2200 kg/m^3) (Maré, 2012).

Table 2-3. Average density values for Karoo and Cape Supergroup sediments from the Council for Geoscience Physical Properties Atlas (Maré, 2012).

Stratigraphic Group	**Density (kg/m^3)**	**Number of samples**	**Stratigraphic Formation**	**Density (kg/m^3)**	**Number of samples**
Beaufort	2478	223			
Ecca			Waterford	2513	6
			Fort Brown	2561	5
			Ripon	2621	6
			Collingham	2634	4
			Whitehill	2111	10
			Prince Albert	2274	2
Dwyka	2642	23			
Witteberg	2576	29			
Bokkeveld	2536	47			
Table Mountain	2535	60			

Several individual seismic surveys (Graham and Hales, 1965, Durrheim, 1987, Muller, 1991, Parsiegla *et al.*, 2008, Lindeque *et al.*, 2011) have been carried out in the eastern arm of the CFB (Figure 2-5), along with a local receiver function study (Harvey *et al.*, 2001). This receiver function study formed part of the larger Southern African Seismic Experiment to study crustal thicknesses (Nguuri *et al.*, 2001). It must be noted, however, that data quality in this region (SA02 and SA03) is poor (Harvey *et al.*, 2001). In addition, small scale variations in crustal thickness are recorded at each station (~4 km), and are most likely due to crustal structure and tectonic history (e.g., at SA03 thinning is attributed to throw along the Kango Fault to the East; Harvey *et al.*, 2001). Individual estimates of Mohorovičić (Moho) depths exist from these different studies and are summarized in Table 2-4. Crustal thinning towards the southern coastline is

attributed to Jurassic-Cretaceous extensions, and the absence of a thick crustal root below the CFB (Harvey *et al.*, 2001).

These seismic survey data as well as two refraction seismic profiles in the southwestern Karoo (Stankiewicz *et al.*, 2008, Stankiewicz *et al.*, 2007) were used to investigate the deeper crustal structures associated with the CIA. The western refraction profile extends from just south of the town of Fraserburg to Mossel Bay on the south coast, while the eastern profile extends from Beaufort West to Cape St Francis.

Table 2-4. Crustal thickness estimates (including errors) for several studies in southern South Africa. Unknown errors are marked with '-'.

Long	**Lat**	**Depth**	**Error**	**Measurement Type and Reference**
23.20	-33.45	34	5	Refraction seismics (Graham and Hales, 1965)
23.54	-34.17	30	5	Reflection and refraction seismics (Durrheim, 1987)
26.53	-33.30	39	5	P-wave analysis (Muller, 1991)
20.27	-33.74	44	1	Teleseismic data (SA02) (Harvey *et al.*, 2001)
20.27	-33.74	36	2	Teleseismic data (SA02) (Nguuri *et al.*, 2001)
21.34	-33.66	36-44	1	Teleseismic data (SA03) (Harvey *et al.*, 2001)
21.34	-33.66	48	-	Teleseismic data (SA03) (Nguuri *et al.*, 2001)
24.87	-34.31	31	-	Offshore seismics (Parsiegla *et al.*, 2008)
22.55	-34.19	30	-	Offshore seismics (Parsiegla *et al.*, 2007)
22.06	-33.19	44	-	Reflection seismics (Lindeque *et al.*, 2011)

Regional aeromagnetic data are used to study the Beattie Magnetic Anomaly (BMA), which stretches from west to east across a large portion of

South Africa (Figure 2-4d). These data were collected by the Council for Geoscience from the 1980s to late 1990s, flown at a line spacing of 1 km and sample spacing of around 60 m (Stettler *et al.*, 1999). The flight height for the survey was between 100-150 m. The final aeromagnetic anomaly was calculated with respect to the normal Earth magnetic field (Intensity: 28 500 nT, Declination: -23˚, Inclination: -66˚).

2.6 Methodology

Seismic data used to better understand the subsurface geometry of the Karoo Basin were interpreted in IHS Kingdom Suite. Picking of horizons is based on historic descriptions of reflectors (Fatti 1970; Fatti and Du Toit 1970) and previously interpreted seismic sections (Lindeque *et al.*, 2011, Loots, 2013). Two strong reflectors have previously been identified on the Soekor seismic data, namely "Old Faithful", which is interpreted here as the top of the Whitehill Formation, and the second being the top of the NNB basement. This interpretation is based on the interpretation of Soekor seismic data by Fatti (1970). Two weaker reflectors are often visible between these strong reflectors and represent the Bokkeveld-Witteberg transition and the Table Mountain Group horizon (Fatti, 1970). Since the Witteberg-Bokkeveld contact is gradational, the first weak reflector is most likely a sandstone layer in the Bokkeveld (Fatti and du Toit, 1970). Horizons were correlated from line to line, which was especially important due to the limited number of deep boreholes (Rowsell and De Swardt, 1976). See Scheiber-Enslin *et al.* (2014b) [Chapter 3] for interpreted seismic sections.

Survey limitations are detailed in Scheiber-Enslin *et al.* (2014b) [Chapter 3]. These include difficulties in identifying horizons due to extensive dolerites intruded at shallower depths (e.g., on lines BV12, BV13 and BV14 in the east and all NW3 lines in the western part of the survey area, though borehole QU1/65 is available in this region), as well as poor data quality (e.g., approximately north-south lines NWK05 and WK06 that run along the western extent of the survey area).

Two-way-travel-times (TWT) were converted to depth using a second-order polynomial (Equation 2-1) fit to TWT-depth pairs (i.e., using strong reflectors of the Ecca Shales and their corresponding borehole intersections (MacKay, 2013)), along with a sonic velocity log (Fatti, 1987) and velocity estimates in the western Karoo (Fatti and Du Toit, 1970). This method averages values across the basin, even though it is likely that velocities vary laterally. See Scheiber-Enslin *et al.* (2014b) [Chapter 3] for more details.

$$\text{Measured depth} = 231.5\ \text{TWT}^2 + 2022.6\ \text{TWT} \qquad (2\text{-}1)$$

All depth estimates were converted to subsea values for the depth maps. A reference datum of 700 m above sea-level was used for the Soekor survey, and therefore basin sediment thicknesses were converted to subsea depths by removing this datum. Similarly a datum of 750 m was used by Loots (2013). Measured depths within the boreholes were converted to subsea depths. The digitized depths from the seismic reflection profile (Lindeque *et al.*, 2011) and KW survey (Fatti, 1970) were originally plotted relative to sea-level. There will be a discrepancy between the KW survey data and Soekor data as the depth conversions are different. Outcrops of the Dwyka Group and Whitehill Formation were also used to constrain the maps.

All depth estimates from seismic and borehole data were combined into a database and gridded using Geosoft's minimum curvature algorithm at a resolution of 30 km. Thicknesses of stratigraphic units shown on the maps were derived from depth estimates for the top and base of the Supergroups, i.e. topography and base of the Dwyka Group for the Karoo Supergroup thickness, and base of the Dwyka Group and top of the basement for the Cape Supergroup thickness.

Lithoflex software (Braitenberg *et al.*, 2007) and the ETOPO1 topographic model were applied to calculate the gravity effect of sediments. For the forward calculation a linear density increase with depth ($\rho(z)$, Equation 3-2) is used.

$$\rho(z) = \rho_{top} + \left(\frac{h_{seds}(\rho_{low} - \rho_{top})}{(h_{low} - h_{top})} \right) \qquad (2\text{-}2)$$

For this calculation we assume a density at the surface (h_{top}) of 2550 kg/m^3 (ρ_{top}) and a density at 6 km depth (h_{low}) of 2650 kg/m^3 (ρ_{low}). We assume that the density at the base of the model (i.e., below the linear variation, h_{bottom}) is 2800 kg/m^3 (ρ_{bottom}). These estimates are based on velocity-density conversions from seismic refraction data in the southwestern Karoo (Stankiewicz *et al.*, 2007). This equation only holds if the sediment thickness (h_{seds}) is less than the absolute value of the depth (h_{low}), otherwise $\rho(z) = \rho_{bottom}$. A reference model is used with top (surface) and bottom (10 km depth) densities of 2700 and 2800 kg/m^3 respectively. The data is initially low-pass filtered with a cut-off wavelength of 20 km.

2.7 Results

2.7.1 Depth and Thickness Maps

Depth maps were created for the base of the main Karoo Basin (Figure 2-6a) and the Whitehill Formation (Figure 2-6b), as well as thickness maps for the Karoo (Figure 2-7a) and Cape Supergroups (Figure 2-7b). The deepest section of the basin is adjacent the northern boundary of the CFB. The depths are not equal along this boundary, with greater depths in the southwestern Karoo and southeastern Karoo (~4000 and ~5000 m respectively relative to the WGS84 ellipsoid; ~5500 to 6000 m sediment thickness). The Whitehill Formation mimics trends displayed by the base of the basin, reaching a depth of ~3000 m in the southwest and ~4000 m in the southeast. This formation does not, however, extend into the northeastern part of the basin (Cole *et al.*, 2011). For both the base of the Karoo Basin and the Whitehill Formation, limited boreholes in the southeastern Karoo show broad deepening of the basin in this region. Just south of borehole SP1/69 near East London, major faults have lead to deepening of the Whitehill Formation to over 5000 m (Figure 2-6b; Fatti, 1970). Similar thickening

is seen in the underlying Cape Supergroup, but are not shown here on the base of the Karoo depth map due to a lack of depth estimates (Fatti, 1970).

Care must be taken when interpreting the gridded maps as the large low south of Queenstown is a gridding artifact, with only the western part of the low being associated with seismic data. Additional data is needed in this region to help reduce uncertainties. These basin sediment thicknesses are also calculated assuming the Witteberg Group does not extend below the Karoo Basin and that the Bokkeveld Group represents the top of the Cape Supergroup in this region. Lindeque *et al.* (2011), however, show that the Witteberg Group in the southwestern part of the Basin extends for around 60 km below the Karoo Basin. Our assumption, therefore, will lead to a slight over-estimation of the Karoo thickness in the south of the basin, and under-estimation of the thickness of the Cape Supergroup (of 2 to 3 km or less, Lindeque *et al.* (2011)).

The northern pinch-outs of the Bokkeveld (red) and Table Mountain Groups (yellow) are shown in Figure 2-6a (around 32.6˚S and 32.4˚S in the south-central part of the basin respectively) and include outcrops of the Msikaba Formation along the east coast. The western and eastern extents are approximated due to poor seismic data and limited borehole data in the east. These extents are in line with the fact that Lindeque *et al.* (2011) did not observe any pinch out on their seismic reflection profile in the southwestern Karoo.

The Cape Supergroup reaches thicknesses of around 4 km below the Karoo Basin in the south (Figure 2-7b), which are in line with previous estimates in this area (5-6 km, Lindeque *et al.*, 2011, ~3 km, Loots, 2013). Thickening of the supergroup in the west should be interpreted with caution as seismic data in this area is poor.

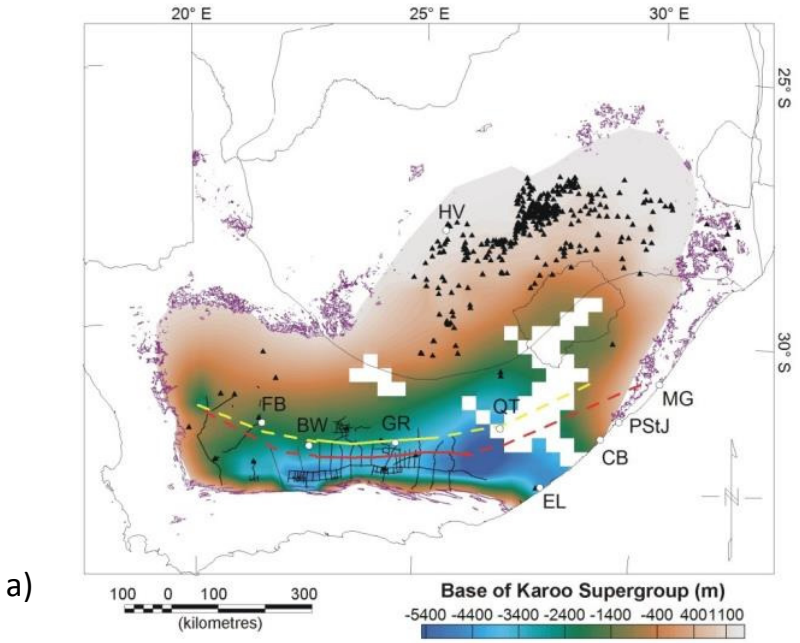

a)

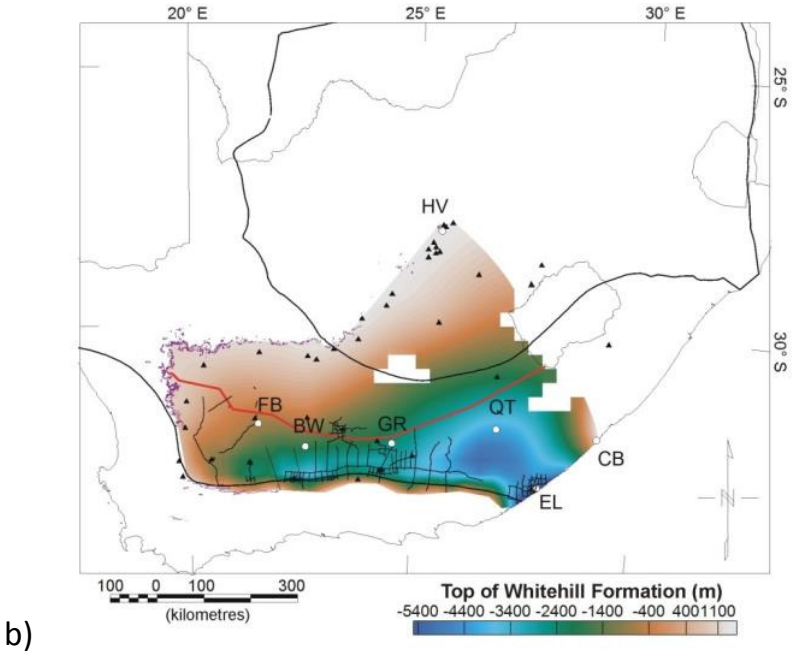

b)

Figure 2-6. Depth maps for a) the base of the main Karoo Basin (base of the Dwyka Group) and b) the top of the Whitehill Formation (relative to the WGS84 ellipsoid). In (a) the northern extent of the Table Mountain Group (yellow line; solid - definite and dashed – approximate location) and Bokkeveld Group (red line; solid - definite and dashed – approximate location) are shown. The outlines of major tectonic provinces are shown (see Figure 2-1 for details). Data used to create the maps are shown (seismic – black lines; boreholes – black triangles).

Outcropping strata of the Dwyka Group and Whitehill Formation are shown in (a) and (b) respectively (purple). The Msikaba Formation of the Cape Supergroup outcrops between the towns of Margate (MG) and Port St Johns (PStJ) on the east coast. Several towns are indicated (white circles, see Figure 2-5 for details).

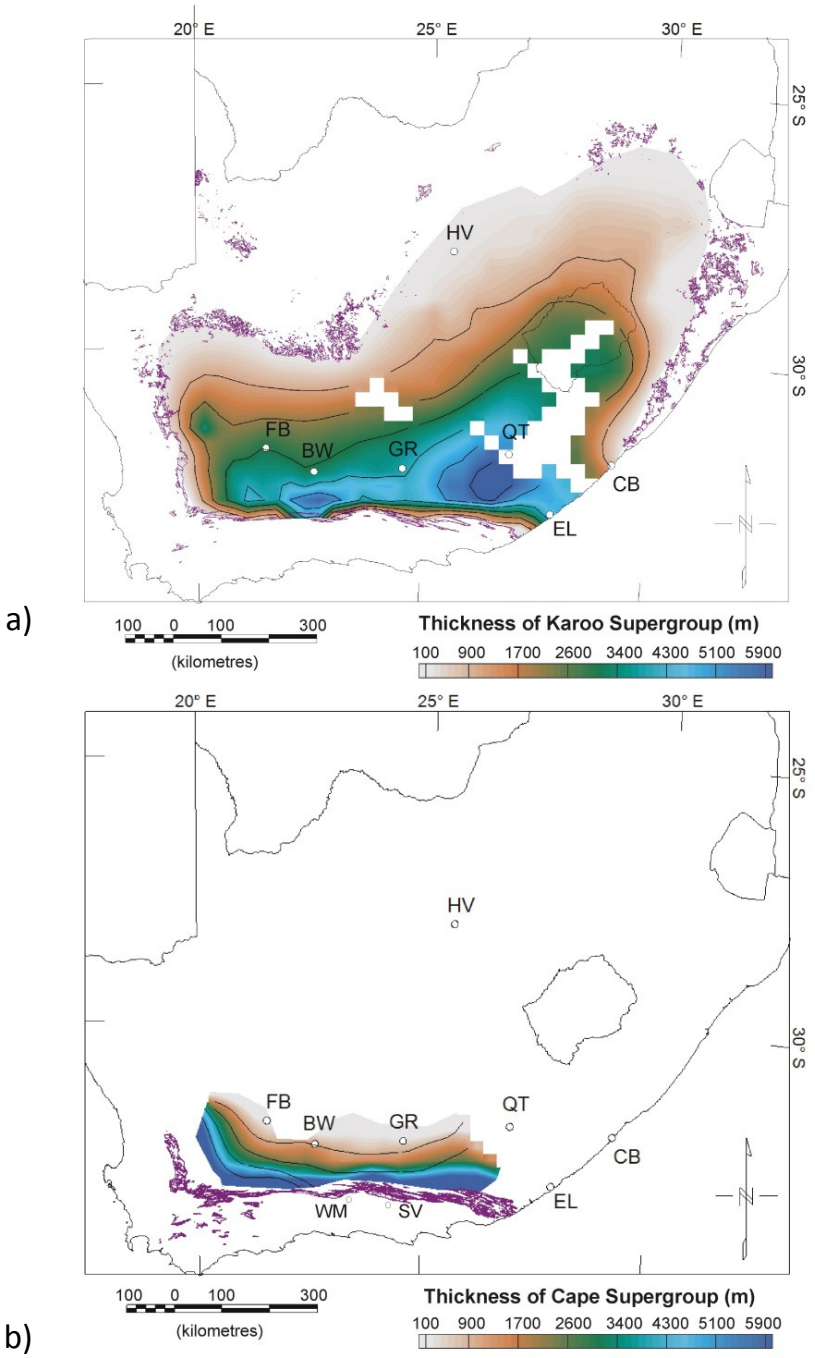

Figure 2-7. Thickness maps for a) the main Karoo Basin and b) Cape Supergroup (1000 metre contour intervals shown). Outcropping Dwyka and Witteberg Group rocks are shown in (a) and (b) respectively (purple). Several towns are indicated (white circles, see Figure 2-5 for details). The towns of Willowmore (WM) and Steytlerville (SV) are marked (white circles).

The gravity effect of the sediment thicknesses (Karoo, Cape and combined thicknesses from Figure 2-7) are shown in Figure 2-8. While there are no sediment thickness data around Willowmore and Steytlerville, i.e., the central part of the CIA, the anomaly does extend to the northern boundary of the CFB. At this boundary there is recorded sediment thinning on both maps in Figure 2-7. Conclusions from this region are therefore applied to the entire CIA. This thinning is associated in Figure 2-8c with a gravity increase to around -20 mGal (from -30 mGal further to the west and east). However, a Bouguer gravity low of -100 mGal is associated with the CIA (Figure 2-4b), therefore sediment thickness alone cannot explain the CIA low.

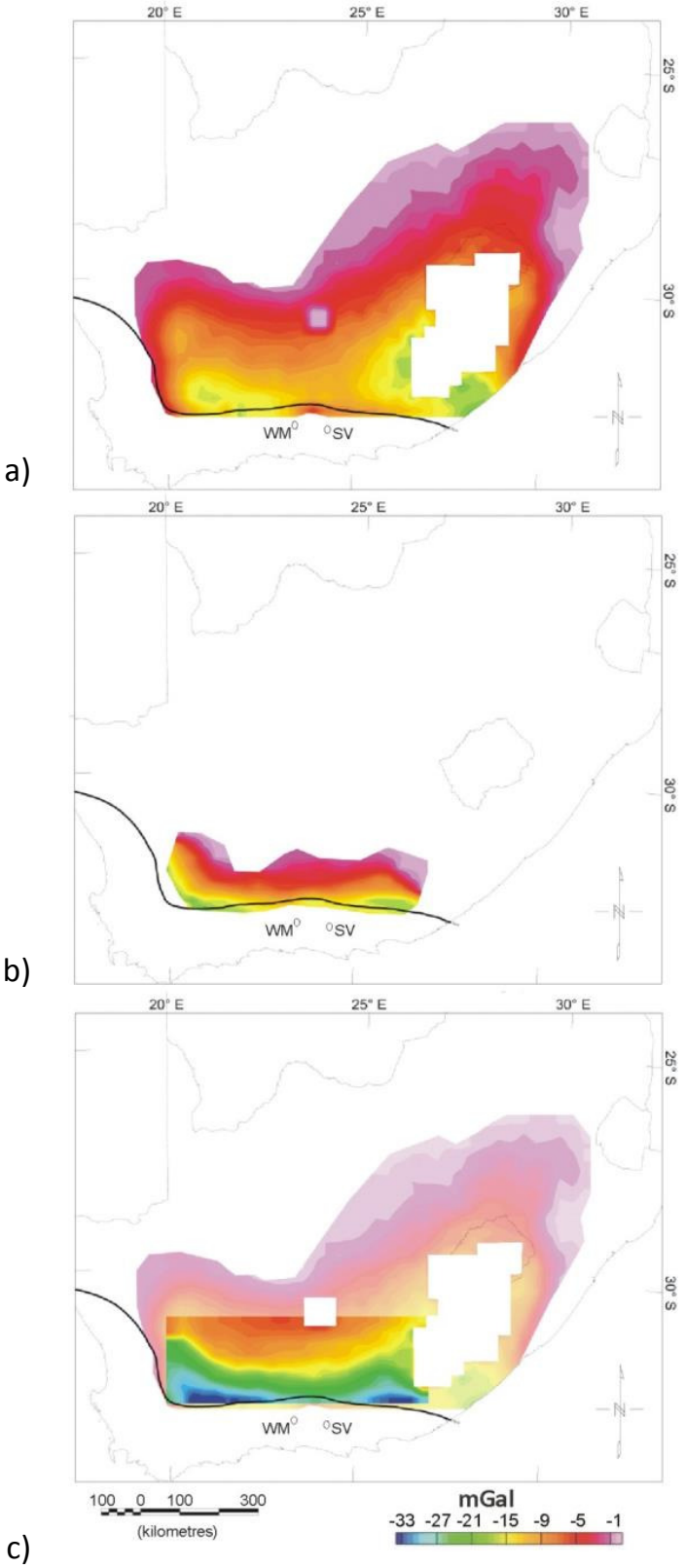
a)
20° E
25° E
30° E
25° S
30° S
WM
SV
b)
20° E
25° E
30° E
25° S
30° S
WM
SV
c)
20° E
25° E
30° E
25° S
30° S
WM
SV
100 0 100 300
(kilometres)
mGal
-33 -27 -21 -15 -9 -5 -1

Figure 2-8. Gravity effect of (a) Karoo and (b) Cape Supergroup sediments shown in Figure 2-7a and b respectively. The gravity effects are combined in (c). See Figure 2-7 for details.

2.7.2 Cape Isostatic Anomaly

Deformation, uplift and subsequent erosion of Karoo and Cape Supergroups between Willowmore and Steytlerville (Figure 2-9a) has resulted in Dwyka and Ecca sediments outcropping further north in this region (Figure 2-9b). This shallowing of the Whitehill Formation and top of the Bokkeveld Group is evident on north-south seismic profiles BV01, BV03 and P01, and more clearly on the east-west profile KL04C (Figure 2-9 and Figure 2-10, at a distance of around 80 km). These sections therefore outline the extent of uplift. This deformation makes it difficult to identify the Whitehill Formation (i.e., Ecca shale horizon, ES) on the seismic profile, though it is clear that lower density shales in the lower Ecca (1800 – 2650 kg/m^3) are closer to the surface in this region. The Bokkeveld (BV) horizon below is easier to pick and shows ~1.5 to 2.5 km of upward displacement. This deformation has, therefore, resulted in lower density Ecca shales (Table 2-3) being positioned closer to the surface. The underlying basement is not deformed in the same manner as the sediments, though uplift of ~1 km is evident.

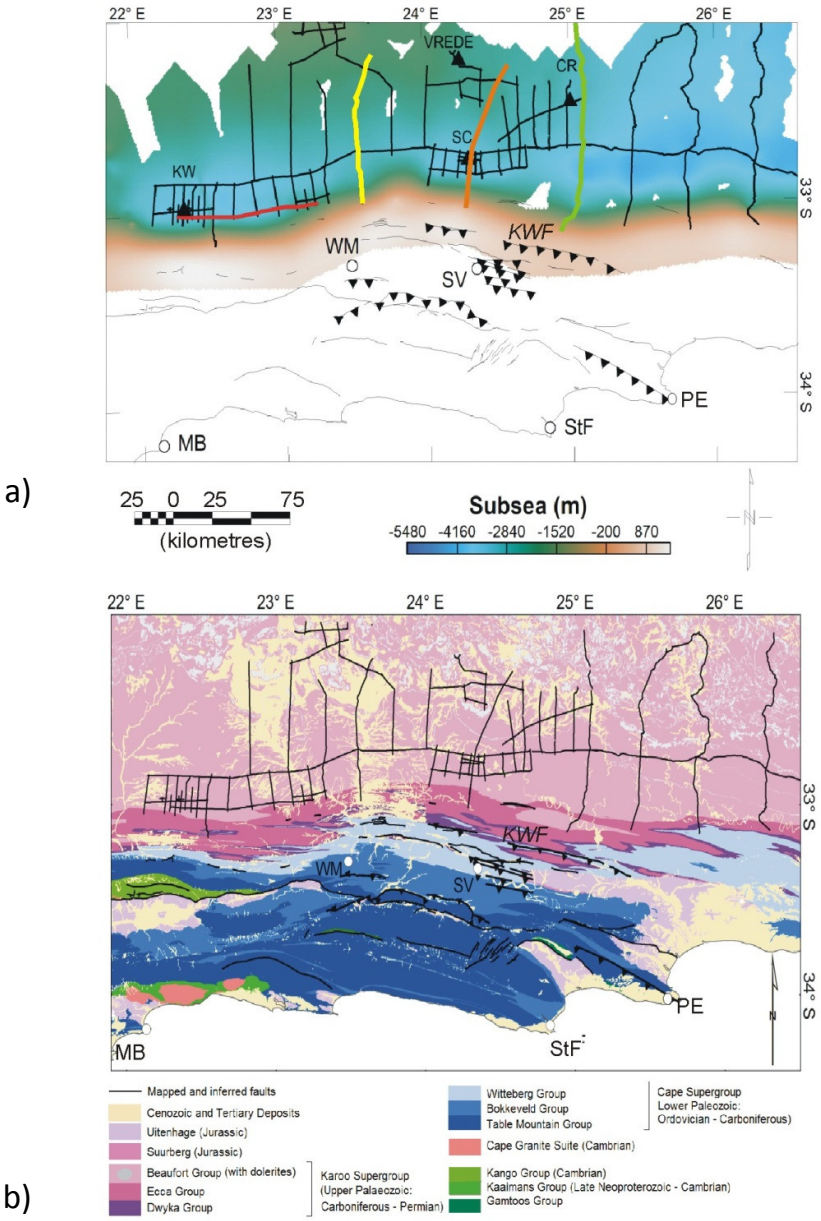

Figure 2-9. (a) Depth map of the Whitehill Formation (from Figure 2-6b) and (b) corresponding geological map of the region surrounding the town of Willowmore (WM) and Steytlerville (SV) (Stratigraphy), 1980). Faults in the Cape Fold Belt are indicated (normal – black line, thrust – black line with triangles; KWF – Klein Winterhoek thrust fault, see Figure 2-3 for more details) (Booth *et al.*, 2004, Booth and Shone, 1999, Roby *et al.*, 1995, Toerien, 1991, Toerien and Roby, 1979). Soekor seismic profiles (black lines) and boreholes (black triangles) are indicated. The coastal towns of Mossel Bay (MB), Port Elizabeth (PE) and Cape

St Francis (StF) are marked (white circles). The location of east-west seismic profile KL04C is indicated in (a) (red line), as well as the north-south profiles BV01 (green line), BV03 (yellow line) and P01 (orange line). Deformation of Karoo and Cape Supergroup sediments is recorded further north on these sections compared to other sections in the surrounding southern Karoo.

a)

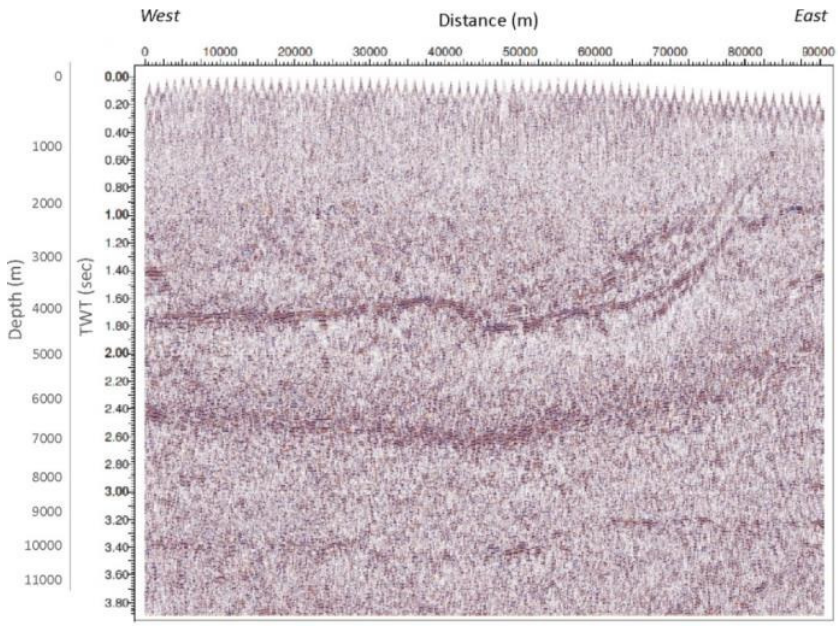

b)

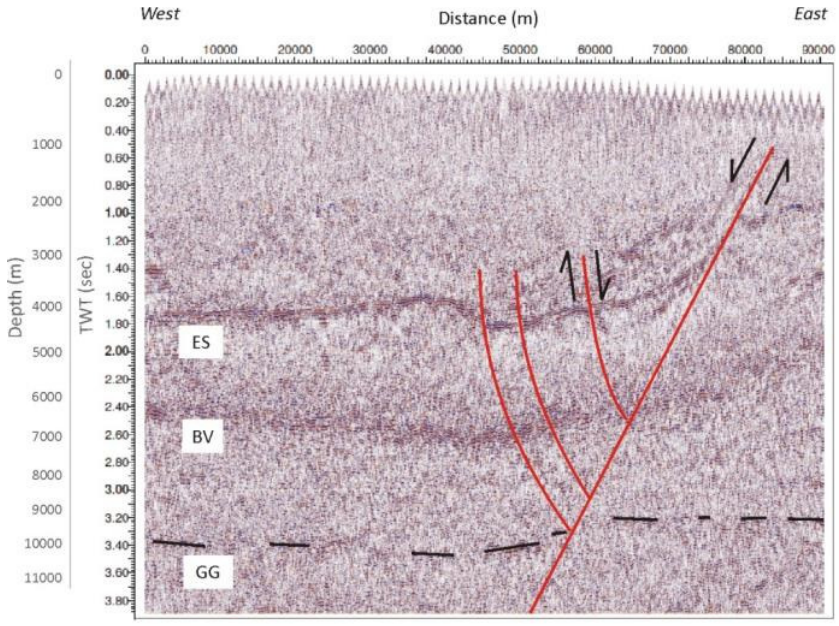

Figure 2-10. (a) East-west seismic section KL04C (location indicated in Figure 2-9a). (b) Interpreted section with horizons marked: Whitehill Formation (ES, Ecca Shales), top of the Bokkeveld (BV) Group and top of the basement (GG, black dashed line). Interpreted faults and direction of movement are indicated (red lines and black arrows). Displacement along the smaller listric faults is evident in the ES horizon. These faults have been continued down through the BV horizon

though displacement is not easily resolved. Depths are given as two-way travel-times and as a non-linear depth scale. Peaks are filled red and troughs blue.

We investigated further to see if the CIA is associated with any other shallow geological features. The CIA does not correlate with any significant topographical features (Figure 2-3), though there is a correlation with several faults. The Bouguer gravity low appears to correlate with normal and thrust faults around the town of Steytlerville, though thrust faults do not correlate with the low around Willowmore (Figure 2-11a). Additional faults could exist northeast of Willowmore but have not been mapped. From the Isostatic and Bouguer gravity maps it appears that several of these faults can be mapped using the gridded gravity data (Figure 2-11).

On the isostatic anomaly map the anomaly instead extends to the southeast to the coast (north of Port Elizabeth, Figure 2-11b). This region at the coast is covered by Cenozoic and Tertiary sediments, as well as the Jurassic sediments of the Uitenhage Group that were deposited in graben-related structures (Figure 2-9b and 2-11b; Shone, 2006), that could contribute to the anomaly. The isostatic map is, however, dependent on the density contrast used at the Moho as well as lithospheric thickness and strength values used during calculation.

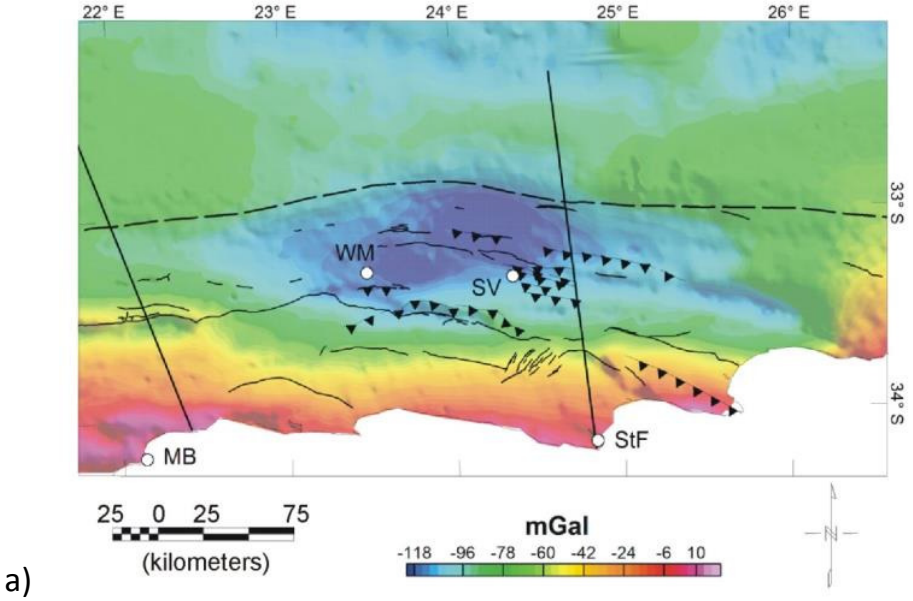

a)

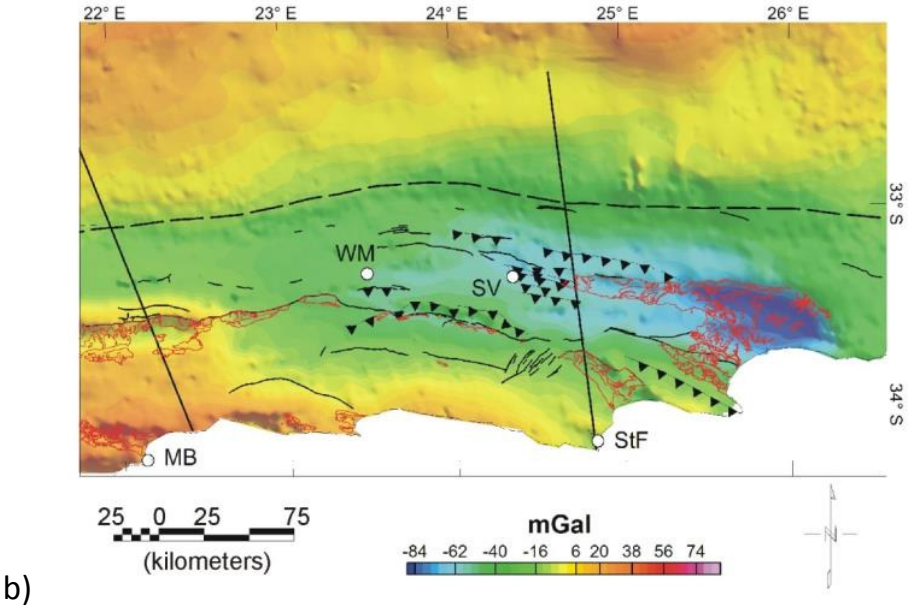

b)

Figure 2-11. (a) Bouguer gravity and (b) isostatic gravity anomaly map of the region surrounding Willowmore (WM) and Steytlerville (SV), showing the low of the Cape Isostatic Anomaly. Faults in the Cape Fold Belt are indicated (normal – black line, thrust – black line with triangles, see Figure 2-3 for more details) (Booth *et al.*, 2004, Booth and Shone, 1999, Roby *et al.*, 1995, Toerien, 1991, Toerien and Roby, 1979). Jurassic sediments of the Uitenhage Group are outlined in red. Two refraction seismic profiles are indicated (solid black line) (Stankiewicz *et al.*, 2007). The approximate northern limit of the Cape Fold Belt

is shown (dashed black line), as well as the towns of Mossel Bay (MB), Port Elizabeth and Cape St. Francis (StF) (white circles).

The geology and Bouguer anomaly along two refraction seismic profiles (see Figure 2-11 for locations; Stankiewicz *et al.*, 2007) were assessed to further investigate which other crustal structures could be associated with the CIA (Figure 2-12). These profiles are dominated by the gravity decrease across the oceanic-continental transition due to crustal thickening, with gravity minima existing just north of the coastline (-90 mGal and -110 mGal respectively). This stronger gravity low along the eastern profile is associated with the CIA.

Along the western profile, the deepest part of the Karoo Basin (Figure 2-12a) is associated with a gravity low (-90 mGal, Figure 2-12b) and a shallow low velocity anomaly (5.5 m/s^2, Figure 2-12c). The major fault intersected along this western profile just south of the Karoo Basin is the Kango Fault, which is a normal fault and is not associated with a velocity anomaly (Stankiewicz *et al.*, 2007). Stankiewicz *et al.* (2007) indicates a thrust fault north of the Kango Fault along this profile, while investigation of available structural data for this study show only normal faults in this region (Figure 2-12a).

Along the eastern profile, Jurassic Uitenhage Group, Dwyka and Ecca Groups sediments (Figure 2-12a) are associated with the CIA gravity low (Figure 2-12b) and a large, shallow, low velocity anomaly (4.5 m/s^2, Figure 2-12c). Along this profile Dwyka and Ecca Groups sediments outcrop further north than the surrounding regions, and lower density Ecca shales are closer to the surface, due to the deformation seen on seismic section KL04C in Figure 2-10. The east-west extent of this deformation is shown in Figure 2-9. The gravity low also correlates with a stronger low velocity anomaly extending to a depth of 11 to 12 km (5.5 m/s^2, Figure 2-12c). Stankiewicz *et al.* (2007) correlates this low velocity anomaly with the Kango Normal Fault and a thrust fault further north (Figure 2-12c). On investigation of available structural data during this study, it appears that the Kango Fault does not extend east to this profile (Figure 2-12a). However, a

normal fault would be expected in this area, north of the Uitenhage Group sediments that were deposited in graben-related structures. On the seismic section this fault dips at around 40˚ near surface and shallows to ~20˚ dip around 5 km depth. The thrust fault is associated with the Klein Winterhoek Mountains. Along this thrust fault, Dwyka Group, lower density Ecca Group shales (e.g., Prince Albert and Whitehill Formations) as well as other Ecca Group sediments (e.g., Collingham, Ripon and Fort Brown Formations) in the north are displaced below sediments of the Witteberg Group in the south.

At deeper levels in the crust, the gravity lows on both profiles correlate with a lower crust (6.5 – 7.0 m/s^2) that is deeper (19-20 km depth) than surrounding areas (16-17 km) (Figure 2-12c, Stankiewicz *et al.*, 2007). In addition, crustal thickness studies show possible thinning in the region of the CIA as the thickness changes from 45 km in the west to 34 km around the CIA and 39 km further east. A shallower Moho in this region would result in a gravity increase. These velocity anomalies were combined into density models along both profiles (Scheiber-Enslin *et al.*, 2014a) [Chapter 4].

.

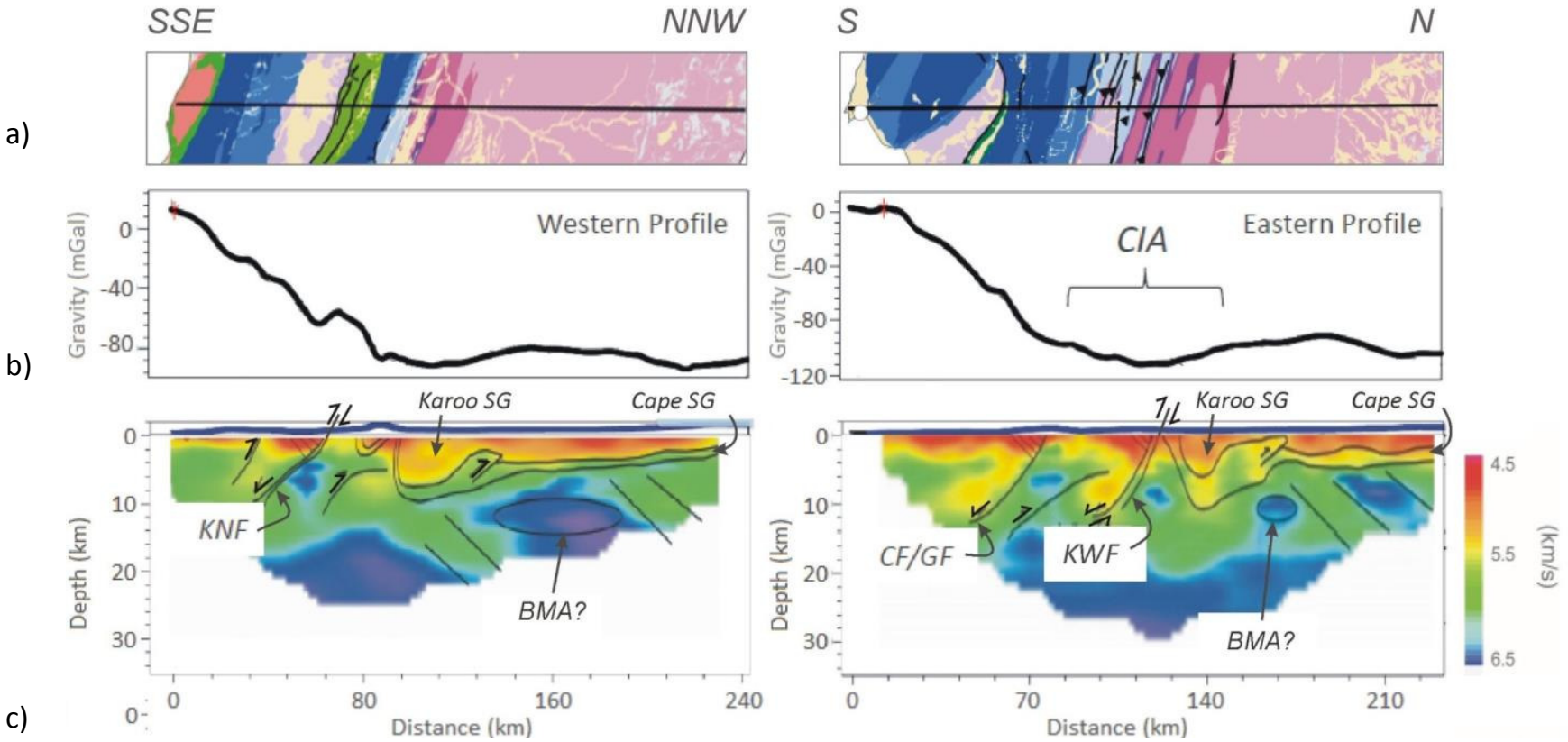
a)
SSE
NNW
S
N
b)
Western Profile
Eastern Profile
CIA
Gravity (mGal)
0
-40
-80
-120
c)
Karoo SG
Cape SG
KNF
BMA?
CF/GF
KWF
Depth (km)
0
10
20
30
0
80
160
240
70
140
210
Distance (km)
4.5
5.5
6.5
(km/s)

Figure 2-12. (a) Geological map and (b) 2D Bouguer gravity profile along the western (left) and eastern (right) seismic refraction profiles shown in (c) (locations shown in Figure 2-11, modified from Stankiewicz *et al.*, 2007). Seismic velocities are in km/s (Stankiewicz *et al.*, 2007). The extent of the Cape Isostatic Anomaly (CIA) is marked on the eastern gravity profile. The Karoo and Cape Supergroups (SG) are labelled. Faults south of the Karoo Basin are labelled (normal faults: Kango (KNF), Coega (CF) and Gamtoos (GF); thrust fault: Klein Winterhoek (KWF)) and direction of movement determined by Stankiewicz *et al.* (2007) are indicated (black arrows). South of the Karoo Basin, along both profiles, Stankiewicz *et al.* (2007) indicates a closely associated normal and thrust fault (c), while on the geological map in (a) only a normal fault (KNF) is evident along the western profile. The possible source of the Beattie Magnetic Anomaly (BMA) is marked.

2.8 Discussion

The depth configuration and shape of the Karoo Basin determined from seismic and borehole data show that the main Karoo Basin shallows over the stable Archean KVC and deepens over the Proterozoic NNB. The basin also appears so be shallower over the Namaqua section of the mobile belt compared to the Natal section (Eglington, 2006, Eglington and Armstrong, 2003, Scheiber-Enslin *et al.*, 2014a - Chapter 4). However, in the area between Queenstown and East London additional data are needed to better define basin sediment thickness. The deepest section of the basin around East London continues into the Falklands, which was linked to South Africa during Gondwana times (Johnston, 2000, Adie, 1952). These basin thickness maps are not sufficient, however, to explain the CIA in the southern Cape.

These depth estimates are in line with isopach maps of the Whitehill Formation from Cole *et al.* (2011) based on borehole data. Thicknesses are in general > 30 m in the southern part of the basin, while depocentres near Calvinia, Laingsburg and Graaff-Reinet contain up to 50 – 70 m of sediments. A depth map of the Whitehill Formation shows a similar trend of increasing depth to the south

and southeast (depth to top of >3000 m, and ~ 4000 m in some parts in the southern part of the basin; Cole *et al.*, 2011).

The CIA has previously been attributed to greater crustal thickness below a section of the CFB due to delayed isostatic rebound linked to erosion (Hales and Gough, 1960, Hales and Gough, 1961). However, crustal thickness studies show that the Moho does not deepen across this region of the CFB (Figure 2-5; Muller, 1991, Durrheim, 1987, Nguuri *et al.*, 2001, Lindeque *et al.*, 2011, Harvey *et al.*, 2001). Density models over the CIA (Scheiber-Enslin *et al.*, 2014a) [Chapter 4] constrained by seismic refraction data (Stankiewicz *et al.*, 2007) instead show that the low of the CIA can be explained by a shallow large volume of low velocity sediments, a low velocity fault zone and deepening of the lower crust in this region. The low velocity/density shallow sediments are linked to the uplift of lower density shales of the Ecca Group as seen on the Soekor seismic data (Figure 2-10). The extent of this uplift is outlined by seismic sections BV01, BV03, P01 and KL04C (Figure 2-9a) and coincide well with the extent of the CIA (Figure 2-11a). Outcrops of Ecca Group shales and Jurassic Uitenhage Group sediments in this region also contribute to the anomaly, particularly towards the southeast coast. The low velocity fault zone appears to be linked to a Mesozoic normal fault that has created a graben-related structure into which lower density Uitenhage Group sediments were deposited. The velocity low could also be linked to lower density sediments (particularly the Ecca Group shales) being underthrust below Witteberg Group sediments along the Klein Winterhoek fault further to the north. Density modelling shows that these low density anomalies are sufficient to offset the density high due to the shallower Moho depths in this region (Scheiber-Enslin *et al.*, 2014a).

A comparison of magnetic and gravity data shows a correlation between the CIA and the change in direction of the BMA, from east-southeast to northeast (Figure 2-13). This change in direction is also evident in the Williston anomaly north of the BMA (Thomas *et al.*, 1992b). The BMA is thought to be associated with the NNB basement (Thomas *et al.*, 1992b, Scheiber-Enslin *et al.*, 2014a, Weckmann *et al.*, 2007b, Stankiewicz *et al.*, 2007, Lindeque *et al.*, 2007, de Beer *et al.*, 1982, de Beer and Meyer, 1983, Hälbich, 1993, de Beer *et al.*, 1974, Gough

et al., 1973, Corner, 1989). This structural change in the basement could be a zone of weakness that influenced the overlying sediments during the Cape orogeny, resulting in deformation of Karoo and Cape Supergroup sediments further north in this region. Deformation of basement in this region (~1 km of uplift on KL04C) was, however, not seen on a seismic reflection section further west (Lindeque *et al.*, 2011), though small-scale deep deformation may be difficult to image. Lindeque *et al.* (2011) explains this lack of deformation as a result of thin-skinned instead of thick-skinned folding, related to subduction of the Gondwana plate to the south. Basement deformation in the region of the CIA may therefore be localized, however, additional high resolution seismic profiles are needed to clarify this.

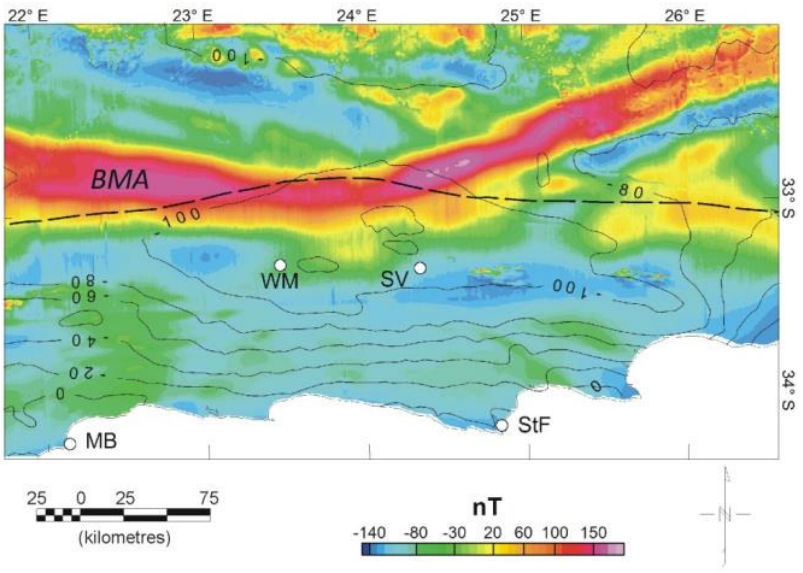

Figure 2-13. Total magnetic intensity map over the Cape Isostatic Anomaly (contours at 20 mGal intervals). The gravity low correlates with a change in direction of the high intensity Beattie Magnetic Anomaly (BMA).

Additional high resolution refraction seismic profiles and additional boreholes are needed in the Karoo to better constrain the depth maps in this study. Additional seismic data is also needed in the southern Karoo to assess whether

these anomalous shallow, low velocity zones are continuous across the CIA and not just a feature of this one seismic profile. These data would also better constrain Moho depths below the fold belt. Increased density sampling of Karoo rocks would provide better average values, and additional structural mapping of the CFB would help constrain the relationship between faults, low density shales of the Ecca Group and the CIA.

2.9 Conclusions

Here we present a comprehensive depth map of the entire main Karoo Basin using borehole data throughout the basin, including reflection seismic data in the southern part of the basin. As expected the deepest part of the main Karoo Basin is in the south (~4000 m in the southwest and ~5000 m in the southeast relative to the WGS84 ellipsoid; ~5500 to 6000 m sediment thickness). Limited borehole data in the southeastern Karoo show a broad deepening of the basin here compared to the southwestern Karoo. This trend is reflected in the overlying Whitehill Formation, with depths of between ~3000 to 4000 m in the southwest and southeast respectively, deepening to over 5000 m in the southeast due to faulting (Fatti, 1970).

The Bokkeveld Group pinches out around 32.6˚S, while the Table Mountain Group pinches out around 32.4˚S in the south-central part of the basin. The pinch-out extends further north in the eastern and western parts of the basin (corresponding with the outcropping of the Msikaba Formation between Margate and Port St Johns, and the western branch of the CFB respectively). Estimates for the thickness of sediments of the Cape Supergroup below the southern part of the Karoo Basin are in line with previous estimates and are around 4 km.

Seismic refraction profiles (Stankiewicz *et al.*, 2007) and existing density models (Scheiber-Enslin *et al.*, 2014a) in the region show the CIA can be explained by a large volume of low velocity/density shallow sediments (4.5 m/s^2, 2500 kg/m^3) and a low velocity/density body (5.5 m/s^2, 2650 kg/m^3) associated with a normal and a thrust fault extending to 11-12 km depth.

In the southern part of the basin at the CFB boundary, north of Willowmore (WM) and Steytlerville, there has been uplift of a section of Karoo and Cape strata (and to a lesser extent basement) further north than the surrounding sediments. This deformation has resulted in lower density shales (1800 – 2650 kg/m^3) of the Ecca Group being closer to the surface (by ~2 km or greater). These sediments can therefore explain the shallow low velocity anomaly seen on the seismic section across this region, and contributes to the gravity low of the Cape Isostatic anomaly (CIA). Jurassic Uitenhage Group sediments that extend from this region to the southeast coast also contribute to the gravity low in this region.

The low velocity fault zone associated with the CIA can be explained by displacement of lower density Uitenhage Group sediments along a Mesozoic normal fault, and/or lower density Karoo Supergroup sediments being underthrust along the Klein Winterhoek fault. In addition, a slightly deeper lower crust (6.5 m/s^2, 2900 kg/m^3) is interpreted to be present in this region (19-20 km compared to 16-17 km).

2.10 Acknowledgements

This project was funded by the National Research Foundation (NRF), Council for Geoscience (CGS), University of the Witwatersrand and the Society of Exploration Geophysicists (SEG), with software support from IHS Kingdom and Geosoft. We thank Falcon Oil and Gas and the Council for Geoscience for data access and the Petroleum Agency of South Africa and John Decker for assistance with the data. The authors are grateful to Marc Goedhart for sharing their knowledge on the topic; Doug Cole for sharing his knowledge and extensive borehole database; and Lindsay Linzer, Jean-Claire Trickett and Musa Manzi for software support. The authors are grateful to Wayne Barnett, Professor Peter W.K. Booth and an anonymous reviewer for improving this manuscript through the review process.

Chapter 3

Karoo Dolerites

This chapter includes a manuscript published in the South African Journal of Geology (2014, volume 117, pages 275-300). I conceived this study in discussion with my supervisors. Work for this manuscript and write-up was completed by me, with the remaining authors helping to improve the manuscript. John Decker at the Petroleum Agency of South Africa (PASA) helped greatly to improve the discussion of this publication through the review process.

GEOPHYSICALLY PLUMBING THE MAIN KAROO BASIN, SOUTH AFRICA

STEPHANIE E. SCHEIBER-ENSLIN
Geophysics Unit, Council for Geoscience, Pretoria, 0184, South Africa
School of Geosciences, University of the Witwatersrand,
Private Bag 3, WITS 2050, South Africa
email: steph.scheiber@gmail.com

SUSAN J. WEBB
School of Geosciences, University of the Witwatersrand,
Private Bag 3, WITS 2050, South Africa
email: susan.webb@wits.ac.za

JÖRG EBBING
Department of Geosciences, Christian-Albrechts University,
Kiel, 24118, Germany
email: jebbing@geophysik.uni-kiel.de

3.1 Abstract

Recent interest in the main Karoo Basin of South Africa has been sparked by the possibility of extensive shale gas resources. Historical reflection seismic, petroleum exploration wells and regional magnetic data are used to better understand the distribution and geometry of dolerite intrusions within the basin that could have impacted the shale reservoir. The lowest concentration of dolerites is found in a region stretching from the southwestern to the southeastern part of the basin around the town of Graaff-Reinet. These intrusions are confined to the Beaufort Group, ~1000 m shallower than the shale reservoir. In the southeastern Karoo around Queenstown, 5 to 30 km wide saucer-shaped sills extend down to ~ 800 m, with dips of between 2˚ and 8˚. Further south, dolerite sheets around Somerset-East extend for over 150 km at dips of between 3˚ and

13˚, and are imaged down to ~ 5 km. These dips appear to increase closer to the Cape Fold Belt in the south, although there is no correlation between the southern edge of these dolerites (i.e., the dolerite line) and the dip of sediments due to folding. Magnetic data are useful in shale gas exploration to detect shallower (<200 m) dykes that can extend to reservoir depth and are not visible on seismic data. Karoo dykes are usually between 1 and 10 m thick and are shown to often be beyond the resolution of the regional aeromagnetic data. Integrated studies using seismic and higher resolution magnetic data are therefore necessary to better understand the complex dolerite network of the Karoo.

3.2 Introduction

The main Karoo Basin remnant covers ~700 000 km^2, although at the time of formation the entire basin covered a much larger portion of southern Africa and the surrounding Gondwana continents (Johnson *et al.*, 2006). It is capped by a thick basaltic lava succession (the Drakensburg Group) and is riddled at depth with dolerite sills and dykes (Duncan and Marsh, 2006) that form part of the Karoo Large Igneous Province (LIP). The significant exposure of the main Karoo Basin due to uplift and erosion, with 2 to 7 km of rock being eroded during two episodes of uplift in the Early and Mid-Cretaceous (De Wit, 2007), make it ideal for studying this intricate network. However, questions still remain regarding the 3D geometries and distribution of these dolerites that cannot be gleaned from outcrop and wells. The need to investigate these questions has arisen due to recent attention focused on possible shale gas resources in the main basin (Cole, 2011, Decker and Marot, 2012, De Wit, 2011).

This study focuses on exploration wells, Soekor seismic and regional magnetic data in the southern portion of the basin (20-28˚E, 31-33˚S), as well as on wells surrounding Lesotho. This is part of the region across which the shale gas reservoir extends (i.e., the Whitehill Formation, and possibly the Prince Albert Formation). We investigate the lateral variations in dolerite thicknesses, as previous studies have focused on the high percentages of dolerite in the eastern part of the basin (Winter and Venter, 1970). We also investigate changes in the

vertical distribution of dolerites that are said to be concentrated within the Beaufort Group (van Zijl, 2006a). Both lateral and vertical variations can shed light on the source location for these magmas.

While initial studies using these seismic data shed light on several dolerite geometries (Fatti, 1987, Fatti, 1970, Fatti and Du Toit, 1970), recent digitization of the data has allowed for a more extensive study of the sills and inclined sheets within the basin. Digitization has also allowed for easy correlation with regional magnetic data and the mapping of sills and dykes not exposed at surface, and dykes not visible on seismic data. These historic seismic data also allow for a greater understanding of how tilting of Karoo Supergroup sediments during the Cape tectonic event has affected the later emplacement of these dolerites, and what link can be drawn (if any) to the so-called dolerite line.

While regional magnetic data can be correlated with the seismic data, a small higher-resolution aeromagnetic survey flown in the northwestern Karoo highlights the limitations of this regional survey. High resolution surveys will therefore be important during any shale gas exploration phases. This approach indicates the importance of combining geological and geophysical studies.

3.3 The Main Karoo Basin

The main Karoo Basin sediments into which these dolerites intruded, were deposited from the Late Carboniferous (300 Ma) to Mid-Jurassic (180 Ma) (Johnson *et al.*, 2006). These sediments are subdivided into the Dwyka, Ecca and Beaufort Groups (Johnson *et al.*, 2006). The overlying Stormberg Group, made up of the Molteno, Elliot and Clarens Formations, formed as the basin shrank towards the northeast (Johnson *et al.*, 2006). The geological units making up the basin, as well as the depositional environments are listed in

Table 3-1. The sediments of the underlying Cape Basin (500 to 330 Ma) are separated from the Karoo by a ~30 m.y. hiatus (Johnson *et al.*, 2006), with the

formation of the two basins often being linked. The Cape Supergroup is made up predominantly of the sandstone formations of the Witteberg, Bokkeveld and Table Mountain Group (Thamm and Johnson, 2006).

Table 3-1. Stratigraphic table for the southern main Karoo Basin, listing groups, subgroups, formations and depositional environments (McCarthy and Rubidge, 2005, Johnson *et al.*, 2006).

Group	**Formation**		**Depositional Environments**
Drakensberg			Lavas
Stormberg	Clarens		Aeolian and playa
	Elliot		Meandering rivers and playa
	Molteno		Braided rivers
Upper Beaufort	Tarkastad Subgroup:		
	Burgersdorp		Alluvial fan and braided rivers
	Katberg		Meandering rivers
Lower Beaufort	Adelaide Subgroup:		
	Southwestern Karoo	*Southeastern Karoo*	Meandering rivers
		Balfour	
	Teekloof	Middleton	
	Abrahamskraal	Koonap	
Upper Ecca	Waterford		Delta front sands
	Fort Brown		Prodelta slope muds
	Southwestern Karoo	*Southeastern Karoo*	
	Laingsburg	Ripon	Basin plain turbidites
	Vischkuil		
Lower Ecca	Collingham		
	Whitehill		Marine shales
	Prince Albert		
Dwyka			Glacial diamictites and muds

Several hypotheses exist regarding the formation of the main Karoo Basin. Its proposed formation as a retroarc foreland basin (Johnson, 1991, Cole, 1992, De

Wit and Ransome, 1992, Catuneanu *et al.*, 1998) is linked to compressional events in the Cape region recorded between 300 Ma and 215 Ma (Hälbich *et al.*, 1983, Gresse *et al.*, 1992), with a combined total of eight events (Catuneanu *et al.*, 1998). This thick-skinned deformation (i.e., involving basement and movement along crustal structures, Coward (1983)) is thought to result from subduction of the palaeo-Pacific plate below the Gondwana plate over 1500 km further south (Cole, 1992). An extensive geological and geophysical study by Tankard *et al.* (2009) attributes both Cape and Karoo basin formation to periods of crustal uplift, followed by subsidence along crustal faults, and then finally long periods of regional subsidence resulting from subduction-driven mantle flow (Pysklywec and Mitrovica, 1999). Turner (1999) proposes a polyphase successor basin to explain the Karoo and the earlier Cape Basins. In this model deposition of the upper Table Mountain Group of the Cape sequence occurred during extension, while the lower Karoo is characteristic of a foreland basin, followed by extension during the deposition of the upper Karoo (Stormberg Group). Extension is said to have resulted from a thermal anomaly off the current southeast coast of South Africa, which is argued against by Bordy *et al.* (2005).

More recent explanations for basin formation are based on recently acquired seismic data. A reflection seismic profile in the southwestern Karoo emphasizes that lithostratigraphic attributes typical of a foreland basin are missing (e.g., absense of a notable fore-deep basin in the southern Karoo, Lindeque *et al.* (2011)). The lack of basement deformation on seismic data instead suggests that the Cape Fold Belt (CFB) and Karoo basin developed as a result of wide, thin-skinned folding. This folding is said to have resulted from far-field southward subduction leading to continent-continent collision, arc collision, or suturing south of the CFB (Lindeque *et al.*, 2011). Lindeque *et al.* (2011) interprets a series of low-angle listric thrusts and folds in the Cape Supergroup that are not connected to the underlying basement or overlying Karoo, as well as low-angle listric faults in the Karoo Supergroup linked to local décollement surfaces in the lower Ecca Group. This interpretation is supported by a more recent interpretation of historic Soekor seismic data (Mowzer, 2013). Paton *et al.* (2006) argues using constructed onshore geological cross-sections from surface geology and offshore

seismic data, that instead of describing the CFB as thin- or thick-skinned end-members it should be described as being controlled by a south dipping mega-décollement that exhibits aspects of both models.

Soekor studies in the late 1960s and early 1970s revealed that lower Ecca shales (Prince Albert and Whitehill Formations) south of 29˚S had dry gas potential (Rowsell and De Swardt, 1976). This dry gas (methane) is formed during the final stage of hydrocarbon thermal maturation (i.e., between 5 and 6 km burial depth, Hunt (1996)). In the case of the Karoo basin, the general trend is increasing maturity southwards across the basin due to increased burial (Rowsell and De Swardt, 1976).

The Whitehill Formation covers the deeper section of the basin in the south, pinching out north of Hertzogville in the Free State and Coffee Bay in the Eastern Cape (Figure 3-1, Cole and McLachlan (1994)). Total organic carbon (TOC) values of between 3 and 7 wt % have been measured for the Whitehill Formation in regions within the basin (Rowsell and De Swardt, 1976), which are within the range of values suggesting the layer could be productive (Cole *et al.*, 2011). Several other parameters are used to measure shales productivity, such as vitrinite reflectance. Reflectance values for the shales of the lower Ecca and Dwyka Groups vary between 1.75 and 4.39 % Ro in some areas (Rowsell and De Swardt, 1976), within ideal values (Cole *et al.*, 2011). The thickness of a shale layer is also important, with borehole studies showing the Whitehill shales are thickest (> 30 m) in the south-central part of the basin, with some depocentres (near Calvinia, Laingsburg and Graaff-Reinet) containing up to 72 m of strata (Rowsell and De Swardt, 1976, Cole and McLachlan, 1994). A depth of ~4 to 5 km is estimated in the south based on seismic and well data (Rowsell and De Swardt, 1976, Lindeque *et al.*, 2011). The productivity of these shales could also have been affected by the large volume of dolerites that have intruded the main Karoo Basin.

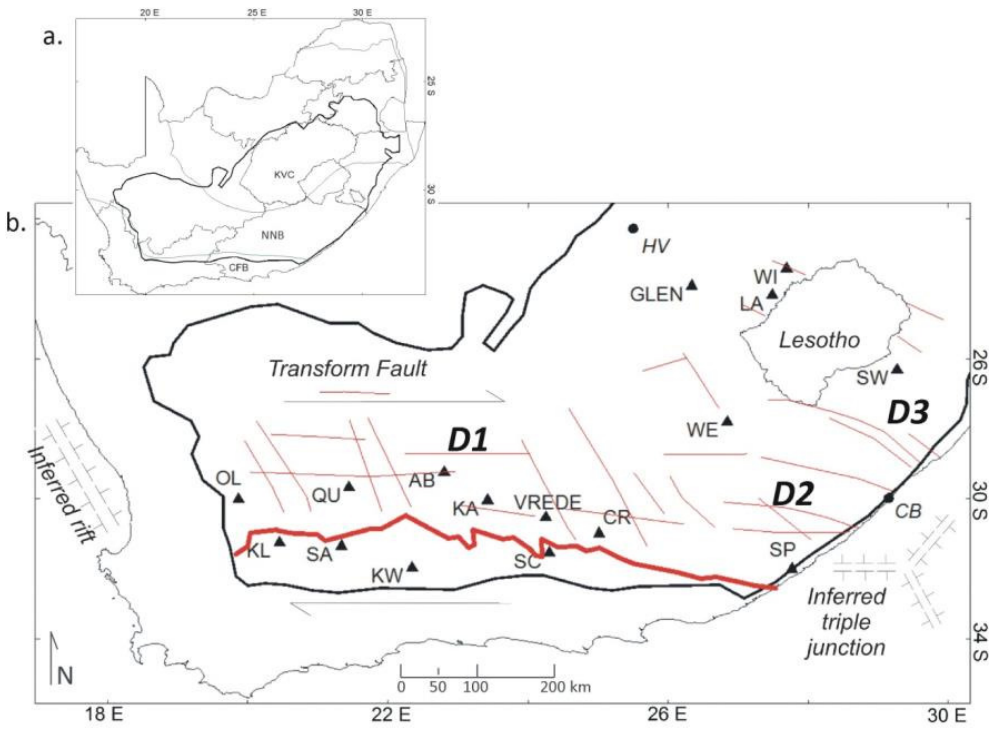

Figure 3-1. (a) Map of South Africa with the major tectonic provinces indicated. The Archean Kaapvaal Craton (KVC) is surrounded by the Proterozoic Namaqua-Natal Belt (NNB), and the younger Cape Fold Belt in the south. All of these provinces are overlain by the Late Carboniferous to Early Jurassic main Karoo Basin (thick black line) (Johnson *et al.*, 2006). (b) Simplified structural map of the southern Karoo. The main dyke trends determined from the 1:1,000,000 map are east-west and north-northwest. These trends are associated with an inferred transform fault in the central Karoo linking inferred rifts off the west and east coast (Chevallier *et al.*, 2001). Chevallier *et al.* (2001) divided the dykes into three domains (*D1, D2* and *D3*). The dolerite line defines the southern limit of the outcropping dolerites (thick red line). Deep wells in the Karoo are indicated (black triangles). The northeastern limit of the Whitehill Formation (the source of possible shale gas) is indicated by the towns Hertzogville (HV) and Coffee Bay (CB) (Cole *et al.*, 2011).

3.4 The Karoo Igneous Province

The Karoo magmatic activity has been closely linked to the breakup of Gondwanaland (Johnson *et al.*, 2006). Today the thickest succession of lavas (maximum 1.65 km) covers a portion of the main Karoo Basin within Lesotho and South Africa, with smaller packages throughout southern Africa (Duncan and Marsh, 2006). In the case of the extensive network of sills and dykes emplaced at the same time, it is estimated that sills in carbon-rich sediments cover ~390 000 km^2 of the main Karoo Basin (Svensen *et al.*, 2007). These dolerites intruded over a relatively short period, with 40Ar/39Ar dating from throughout Gondwanaland estimating emplacement between ~190 and ~178 Ma (Riley and Knight, 2001, Riley *et al.*, 2005, Jourdan *et al.*, 2008), with more recent U-Pb dating suggesting a rapid emplacement between 183 and 182 Ma over <1 m.y. (Encarnación *et al.*, 1996, Svensen *et al.*, 2012, Svensen *et al.*, 2007).

Studies have inferred the source location for these magmas using percentage dolerite maps that show the highest percentage in the east (Rowsell and De Swardt, 1976, Winter and Venter, 1970). This analysis is, however, skewed by the depth of wells and thickness of the basin. Other source locations are based on dyke swarms. A significant number of swarms are concentrated in the northeast Karoo and this has led to the proposal that the source is a triple junction in southern Zimbabwe (Burke and Dewey, 1973). Hastie *et al.* (2014) provide a comprehensive summary of field evidence, structure and geochronology of dyke swarms in the Karoo in relation to magma source locations, and highlight the limited work in the southern portion of the basin (Neumann *et al.*, 2011) that is the focus of this study.

Extensive mapping of dykes and fractures in the southern main Karoo Basin has shown that there are regions with different dominant dyke trends (Chevallier and Woodford, 1999). Chevallier and Woodford (1999), and later Chevallier *et al.* (2001) and Woodford and Chevallier (2002) sub-divided these dykes into three domains (Figure 3-1): the western domain (D1); an eastern domain branching off from the east coast (*D2*); and the northern domain (*D3*). This variation is most likely due to changes in stress conditions in the crust at the

time of emplacement (Stettler *et al.*, 1989). These northern Karoo dykes are those associated with triple junction studies (Burke and Dewey, 1973).

From these groups it is clear that the dominant trend of the dykes in the main basin is east-west and north-northwest. These trends are attributed to a dominant NW compressive stress field at the beginning of Gondwana breakup; while the east-west dykes are attributed to a similarly oriented shear/dislocation zone linking inferred rifts off the west and east coasts (Figure 3-1, Chevallier *et al.* (2001) and Woodford and Chevallier (2002)). Chevallier *et al.* (2001) propose that the rift off the east coast is a triple junction and represents the source of the main Karoo magmas. These observations of dyke trends show that the event cannot be oversimplified to one magma source. Although significant work has been done in this field to better understand the magma source, more studies will have to be focused on the southern part of the basin to gain a full understanding of the Karoo magmatic event.

3.5 The Karoo Dolerite Network

Our understanding of this Karoo dolerite network has been enhanced by several geophysical studies. These include electrical sounding measurements that allowed van Zijl (2006a) to divide the dolerites into three zones (Table 3-2). The lower zone consists of flat extensive sills (~30 km) in the lowest stratigraphic units of the basin. These units include the glacial deposits of the Dwyka Group and submarine laminated shales of the lower Ecca (

Table 3-1). Inclined sheets that formed at the tips of these sills outcrop in the lower Beaufort in the southeastern basin. Well data record instances where these sills have intruded close to the shales of the Whitehill Formation within the lower Ecca Group (Cole *et al.*, 2011).

Table 3-2. Dolerite groups within the Karoo basin defined by van van Zijl (2006a).

Zones	**Dominant dolerite geometry**	**Occurrence**	**Stratigraphy**
Lower	Flat extensive sills (~30 km)	Dolerite-poor	Dwyka Group Lower Ecca Group
Middle	Saucer- or basin-shaped, usually coalescing to form ring complexes	Dolerite-rich	Upper Ecca Group Beaufort Group
Upper	Dykes (and smaller basin structures)	Dolerite-poor	Molteno, Elliott and Clarens Formations

The second dolerite zone is thought to consist of the most significant number of intrusions. These intrusions occur within the Upper Ecca and Beaufort Groups and in some instances into the higher formations (

Table 3-1). The reason for this abundance is thought to correspond to the first thick sandstone unit, emphasizing the importance of horizontal, as well as vertical transport of magma in the system. This second group of intrusions is mostly saucer- or basin-shaped, with these structures usually coalescing to form ring complexes (Du Toit, 1920).

The third zone that has intruded the Stormberg Group (

Table 3-1) is the most dolerite-poor and consists predominantly of dykes that are thought to feed the overlying lavas (i.e., northern domain, D3, from Chevallier *et al.* (2001)). van Zijl (2006a) and van Zijl (2006b) suggest that due to the low overburden pressure in this zone the intrusion style is independent of lithology. These zones are expanded upon with additional well data in this study.

Preferred emplacement horizons determined from wells are the Dwyka-Ecca Group contact, the Prince Albert-Whitehill Formation contact in the lower Ecca and the upper Ecca-lower Beaufort Group contact, as well as lithological boundaries within the Beaufort (Du Toit, 1920, Cole and McLachlan, 1994). Burchardt (2008) highlights that sills are more likely to intrude between layers of varying mechanical properties due to a change in the stress field, for example between rhyolitic intrusion and basaltic lava flows.

In some instances sills have penetrated below the basin into basement, as well as Cape Supergroup rocks that underlie the basin in the south. Basement rocks include the Proterozoic Namaqua-Natal mobile belt in the central part of the basin, while in the northeast it is underlain by the Archean Kaapvaal craton.

The areal extent of the dolerites is limited in the southern part of the basin, with the southern boundary defined as the dolerite line. This "line" crosses from northwest to southeast across the Beaufort Group. This limitation is thought to be due to previous northward tilting of southern Karoo Supergroup sediments due to tectonic activity in the Cape region (Planke and Svensen, 2012). A quantitative investigation of the correlation between the dolerite line and dip of Karoo Supergroup sediments is carried out in this study.

3.6 Dolerite Geometries

From observations in the Karoo, dykes are usually between 2 and ~10 m wide and 5 to 30 km long, although some extend for up to 80 km (Duncan and Marsh, 2006). Dykes are in general compositionally homogeneous across their extents (Marsh and Mindaweni, 1998), and some show *en-échelon* segmentation.

Recent studies have expanded our knowledge of the subsurface geometries and mechanisms of formation of these sills, inclined sheets and dykes. It has been suggested from field observations that dykes develop into inclined sheets, which in turn develop into an inner and outer sill (Chevallier and Woodford, 1999). More recent experimental work by Malthe-Sørenssen *et al.* (2004) using discrete element modelling has shown that a symmetrical sill

can develop from a central injection point. These studies showed how a sill develops into a complex network, with the sill emplacement causing doming of the overlying sediment surface. As the edges of the dome reach a critical angle, stress at the tips causes the sills to develop into an inclined sheet, cross-cutting layers. These inclined sheets continue until the magma pressure decreases and the intrusion again follows the bedding and forms an outer sill higher up in the stratigraphy. Numerical modelling results, as well as geological examples suggest that the size of the inner sill is proportional to the overburden thickness, which Polteau *et al.* (2008) proposed is a four or five to one relationship using numerical and field data including Karoo sills. Scatter in these sill size-overburden thickness data, however, suggests a ratio of anywhere between two and six to one.

Recent experimental work has expanded on the relationship between overburden depth and intrusion shape (Galerne *et al.*, 2011). Experiments show that sub-circular saucer-shaped sills form above pipe feeders. Galerne *et al.* (2011) suggests that a pipe feeder is similar to a feeder dyke whose extent is small relative to its depth of emplacement. Alternatively, a feeder that is long with respect to its emplacement depth, such as for a shallow dyke, results in the formation of an elliptical saucer-shaped sill. A feeder length-to-depth of emplacement ration of L/D = 4 or larger is needed in such a case. For the elliptical Golden Valley Sill near Queenstown in the southeastern Karoo, a ratio of between 10 and 20 is calculated, since emplacement depth is estimated as 1 to 2 km and the sill has a long axis of approximately 20 km.

These analytical and experimental studies, therefore, show that sills can be fed by dykes and other sills. These types of feeder systems are also supported by field evidence. Recent geochemical work in the Golden Valley Sill (GVS) Complex suggests that the Golden Valley Sill is fed by a dyke, and has the same geochemistry as two shallower sills within the complex that it is in contact with (i.e., Mountain Valley Sill and Glen Sill). The sill, however, has a different geochemical signature compared to a deeper sill in the complex (Morning Sun Sill) (Galerne *et al.*, 2011).. It is evident in this region that dykes

can cross-cut sills and not represent the system feeder as they could have been linked to different magma pulses over short periods of time (Galerne *et al.*, 2011). Further afield in the Faroe-Shetland basin seismic data point towards a sill-feeding- sills system (Hansen *et al.*, 2004). These seismic data also shed light on the subsurface geometry of the sills, with dips of inclined sheets of approximately 10°. In this study, seismic data help to constrain the dip and subsurface structure of the dolerites that have previously not been investigated in the Karoo. These low-resolution data, however, have limited resolution of the horizontal extent of the sills and do not show vertical structures such as dykes. Regional aeromagnetic data are therefore used to resolve dykes, although the data is strongly aliased and insufficient for detailed analysis. Through this study we will highlight how higher resolution aeromagnetic data are needed to further understand this complex feeder system.

3.7 Data

We divide our investigation in the southern portion of the basin into four regions, with the towns and wells used to define them shown in Figure 3-2a. These include a region in the northwestern main Karoo Basin focused around the town of Fraserburg in the Northern Cape and well QU1/65. A second region includes the southwestern main Karoo Basin centred on the town of Graaff-Reinet. This region spans the border between the Western and Eastern Cape, as well as wells KA1/66 and VREDE1/66. The final two regions in the southeastern main Karoo Basin focus on the town of Somerset-East and well CR1/68, and Queenstown in the Eastern Cape.

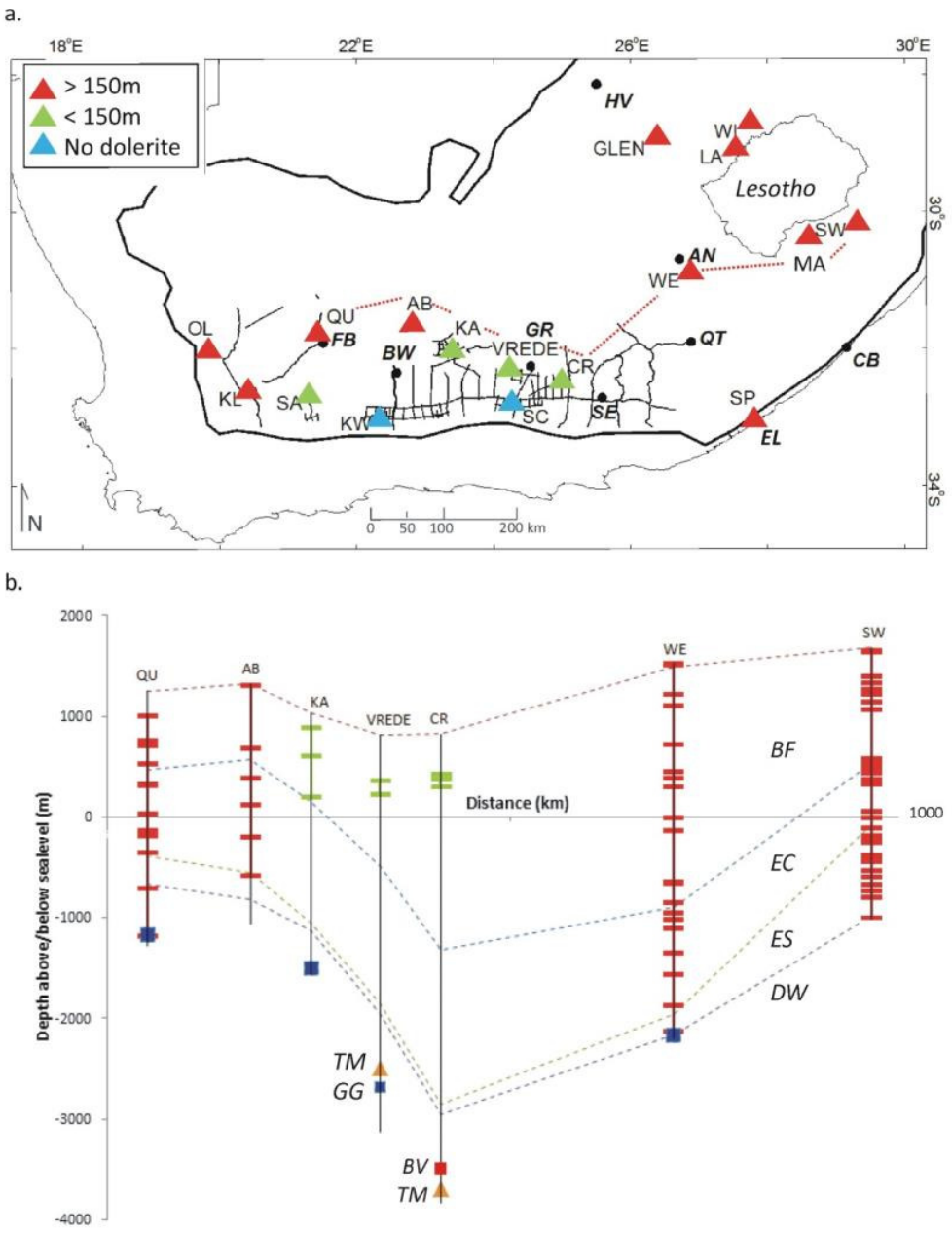

Figure 3-2. (a) Plot of the dolerite thickness distribution as determined from existing reports (Rowsell and De Swardt, 1976) and unpublished log data. Dolerite thickness are indicated: greater than 150 m (red triangles), less than 150 m (green triangles), and zero dolerite further south of the dolerite line (blue triangles). Soekor seismic lines in the southern part of the basin are marked (black lines). The surveys (and corresponding wells) are divided into regions, namely the northwestern region around Fraserburg (FB) in the Northern Cape; southwestern

region around the town of Graaff-Reinet (GR); and two regions in the southeastern main Karoo Basin close to Somerset-East (SE), and Queenstown (QT) further north. Additional wells exist around Lesotho and the towns of Aliwal North (AN) and East London (EL). Previously interpreted seismic line SWK01 stretches south from Beaufort West (BW) (Fatti and Du Toit, 1970). See Figure 3-1 for details. The dotted line indicates the profile shown in (b). (b) Approximately southwest- northeast profile through the main Karoo Basin, showing the dolerite distribution (horizontal lines) in deep wells QU1/66, AB1/65, KA1/66, VREDE1/66, CR1/68, WE1/66 and SW1/67. Stratigraphic boundaries between wells are marked (dotted lines): BF – Beaufort Group, EC – upper Ecca Group, ES – Ecca shales (lower Ecca shales topped by the Whitehill Formation), DW – Dwyka Group, BV – Bokkeveld Group (red square), TM – Table Mountain Group (orange triangle), GG – Granite-gneiss basement (blue square). The total well depths are indicated with solid black lines. Over 400 m of dolerite occurs in each well in the east/southeast and northwest at all stratigraphic levels, while <150 m of dolerite is found in the southwest wells within the Beaufort Group.

3.7.1 Soekor Deep Wells

Additional datasets include deep Soekor core well data (Rowsell and De Swardt, 1976) and unpublished logs (recorded in British feet, Fatti, personal communication, 13 May 2014), with some reaching depths in excess of 5 km. Dolerite thickness values shown in Figure 3-2a and Table 3-3 are not only highest (>400 m) for wells in the east/southeast (wells WE1/66 and SP1/66) closer to the proposed source of the LIP, but also in the northwest (wells QU1/65 and AB1/65) (Cole *et al.*, 2011, Cawthorn, 2012). In addition, dolerites have intruded at all stratigraphic levels within these wells (Figure 3-2b and Table 3-3). It should be noted that Rowsell and De Swardt (1976) show borehole SW1/67 ends in Ecca sediments, while unpublished logs show it intersects basement.

Table 3-3. Dolerite distribution from several deep wells within the main Karoo Basin, divided according to geographic region. The total thickness of the dolerites is listed (see text for more details) as well as the number of intrusions in each well (some thinner intrusions might be excluded due to the resolution of well logs). The lithologies within which these dolerites have intruded are shaded grey (GG – granite-gneiss Namaqua-Natal basement, CGS – Cape Supergroup, DW – Dwyka Group, EC – Ecca Group, BF – Beaufort Group). The depth extent of the wells is indicated with thick black boxes. The general trend observed is intrusions at all stratigraphic levels in the northwestern and eastern/southeastern Karoo, while between these regions dolerites are restricted to shallower lithologies (Beaufort Group).

Wells	Total dolerite thickness	Number of intrusions	Lithologies					
			GG	CSG	DW	EC	BF	Molteno
Southern Karoo								
KL1/65 *(Klipdrift)*	170	1						
SA1/66 *(Sambokskraal)*	15	1						
KW1/67 *(Klein Waterval)*	0							
SC3/67 *(Schietfontein)*	0							
Northwestern Karoo								
QU1/65 *(Quaggafontein)*	434	12						
AB1/65 *(Abrahamskraal)*	622	6						
OL1/69 *(Olyvenbosch)*	273	4						
Southwestern Karoo								
KA1/66 *(Karee Bosch)*	121	3						
VREDE1/66 *(Uitkomst)*	55	2						
Southeastern Karoo								
CR1/68 *(Cranemere)*	27	4						
SP1/66 *(Springfontein)*	200	1						
WE1/66 *(Weltevreden)*	966	18						
Eastern Karoo								
MA1/69 *(Matatiele)*	391	21						
SW1/67 *(Swartberg)*	710	24						
Northeastern Karoo								
WI1/72 *(Wittekrans)*								
LA1/68 *(Olney)*	331	14						
GLEN1/67 *(Klipfontein)*	208	8						

An isopach map of dolerite within and/or adjacent to the Whitehill Formation from Cole *et al.* (2011) show thicknesses > 100 metres in the Aliwal North area, with >75% dolerites within the formation. In the regions of Calvinia (>100 km northwest of Fraserburg), Britstown (>100 km north of Beaufort West and Graaff-Reinet) and northeast of Kimberley (around the region of Hertzogville) >50 m of dolerite occurs within and/or adjacent to the Whitehill Formation (Figure 3-2a). In terms of percentages, there are >50% dolerite within the formation around Calvinia and northeast of Kimberley and >75% in the Britstown region. Considering the basin sediment thicknesses in these regions, Cole *et al.* (2011) suggests the Aliwal North region can be excluded from exploration. The investigations of Svensen *et al.* (2007) in Loeriesfontein and Calvinia confirm this high concentration of dolerites.

In contrast, the wells in the band between these two regions (wells KA1/66, VREDE1/66 and CR1/68) show reduced thicknesses of dolerite (<150 m) and intrusions only in the Beaufort Group. It is very important to note, however, that a lack of intersected dolerites in these limited wells does not necessarily mean a complete absence of dolerites in the surrounding sediments. This is evident in well CR1/68 as bleaching of the shales and tillites at the top of the Dwyka most likely represents a contact aureole due to an adjacent dolerite that is not intersected (Leith, 1970).

When investigating the preferred horizons into which these dolerites intrude, initial studies on well KA1/66 show that 4 of the 6 dolerite sills intrude between sandstone layers above and siltstone below. In the case of the fifth dolerite the lithologies are reversed, and for the final dolerite it intrudes into shale. The thickness of dolerites south of the dolerite line is obviously minimal, with some thin intrusions in KL1/65 and SA1/66 that lie close to the line. In four of the wells, GLEN1/67 and LA1/68 in the northeast and OL1/66 and KL1/65 in the west, dolerites intrude into basement and Cape Supergroup rock below the Karoo respectively.

3.7.2 Soekor Seismic Data

Approximately 13,000 line-kilometres of 2D seismic data were shot in the southern Karoo by Soekor from 1966 to 1971 (Figure 3-2). The original exploration target for the project was the pinch-out of the Bokkeveld below the Karoo where porous deltaic sands were thought to be a possible oil target if it occurred with a structural trap (Fatti, 1987). The second target was the Dwyka tillites and Ecca shales (lower Ecca), where domes and anticlines were thought to provide reservoirs by fracture porosity. However, no economically recoverable oil and gas was found, although well CR1/68 did yield gas at a rate of 1.83 million scf/day over a 23 hour period (Leith, 1970; Rowsell and De Swardt, 1976).

A dynamite source with an average charge of 50 lbs (20 kg) was used in 15-18 m deep holes for the survey (Fatti and du Toit, 1970). Some lines in the eastern Free State were shot with vibroseis and some using weight-drop methods; however, they have not been digitized for this study (Fatti, 1970). The majority of the lines are single fold with an average of 24 traces per shot point, although a few three and six fold stacks were shot in the east.

Data were corrected for a low-velocity layer (2130 m/s) at the surface. All data were corrected to the elevation datum using a velocity of 4,570 m/s. These analog data were processed using static corrections, NMO correction, CDP stacking (where available) and band-pass filtering (see Fatti and du Toit (1970) for further details). These paper seismic sections were recently scanned and digitized by Falcon Oil and Gas. The dominant frequency for the survey is 40 Hz; therefore, assuming a velocity of 5.55 km/sec for the dolerites, the data have a dominant half wavelength/resolution of 70 m. This limited resolution means that imaging of smaller features is not possible.

Four strong reflectors were detected due to differences in acoustic impedance in the subsurface. The two strongest reflectors are “Old Faithful” as described by Fatti (1970) that is almost continuous across the study area, as well as the top of the basement (GG). “Old Faithful” is thought to represent either the top of the Dwyka Group or the Whitehill Formation within the lower Ecca (ES)

(Fatti, 1970; Lindeque et al., 2011). Exact stratigraphic correlation is difficult due to limited velocity data that would allow for accurate time-depth conversion. Lindeque et al. (2011) show that an accurate correlation is only possible with knowledge of the local geology. In this study we assume that "Old Faithful" represents the top of the Whitehill Formation. This highly carbonaceous layer is distinctive due to the strong contrast between the lower velocity of the carbon layer (~4000 m/s) and the surrounding rock (~5000 m/s) (Fatti and du Toit, 1970). The weaker reflectors are the Witteberg-Bokkeveld contact (BV) and the top of the Table Mountain Group (TBM) of the Cape Supergroup. Since the Witteberg-Bokkeveld contact is gradational, the first weak reflector is most likely a sandstone layer in the Bokkeveld (Fatti and du Toit, 1970). The brightest reflectors at shallower levels, however, are the dolerite sills and inclined sheets of the Karoo LIP. No dolerite reflectors are resolvable below the shales in the lower Ecca from these seismic data.

Interpreted Soekor seismic profiles from the southern Karoo (Fatti, 1970; Fatti and du Toit, 1970; Fatti, 1987), as well as Inkaba yeAfrica reflection seismic profiles from the southwestern Karoo (Loots, 2013, Lindeque *et al.*, 2011) were used to identify reflectors on the remaining Soekor seismic data, and these horizons were continued across sections. No direct velocity measurements were made during the survey in the southwest Karoo, so an expanding spread velocity profile was used from line SWK01 (Figure 3-2) to calculate interval velocities (Fatti and du Toit, 1970). For this, 5 successive shots were fired with different offsets. The interval velocities were determined with a maximum error of 5% (i.e., 5,060 m/s for the ES-BV interval; 5,350 m/s for the ES-TBM interval; 5,560 m/s for the ES-Basement interval). These velocities are similar to those determined during more recent seismic tomography studies in the southwestern Karoo (Stankiewicz *et al.*, 2008, 4,500 – 5,300 m/s; Stankiewicz *et al.*, 2007). These interval velocities were used to calculate velocities for individual horizons using depth and velocity ratios. In the eastern Karoo, sonic logs were recorded down wells WE1/66 and SP1/69 (Fatti, 1987). For SP1/69 the sandstone rocks within the well have less than 1% primary porosity and therefore relatively high velocities that only increase slightly with depth (Fatti,

1987). Several dolerites are intersected by both wells and have high velocities around 6,200 m/s and hence produce strong reflections. Fatti (1970) recorded lateral reflection changes from the dolerite sheets from high to lower frequency pulses due to variations in, for example, sill thickness.

These depth-time data from the sonic logs and expanding spread velocity profile are compared in Figure 3-3 with time and depth data from the seismic sections-wells pairs. These pairs are determined using the two-way-travel-times (TWT) of the first continuous strong reflector representing the Whitehill Formation (labelled on the seismic sections as Ecca shales, ES), and the corresponding measured-depths (MD) from Soekor wells (MacKay, 2013). The best-fit second order polynomial to the data gives an estimate of the change in velocity with depth, and was used to convert TWT to depth for the survey. This method has the obvious disadvantage that prior knowledge is need of which strong reflection represents which lithological horizon. As the horizons focused on in this study are relatively strong and easily identified, this was not a problem, although wells were excluded from the plot if the corresponding reflectors were not clear on the seismic profile (e.g., well QU1/65, where several dolerite sills have intruded above the Whitehill Formation). Another shortcoming of this method is the assumed constant lateral velocity in the study area, although the method does average over a large number of the wells. Varying dolerite distribution within the basin will also have an effect on velocities, as the intrusions have higher seismic velocities. Velocities will also be affected by undocumented duplications of lithologies due to tectonic events, for example, folding and faulting in the CFB.

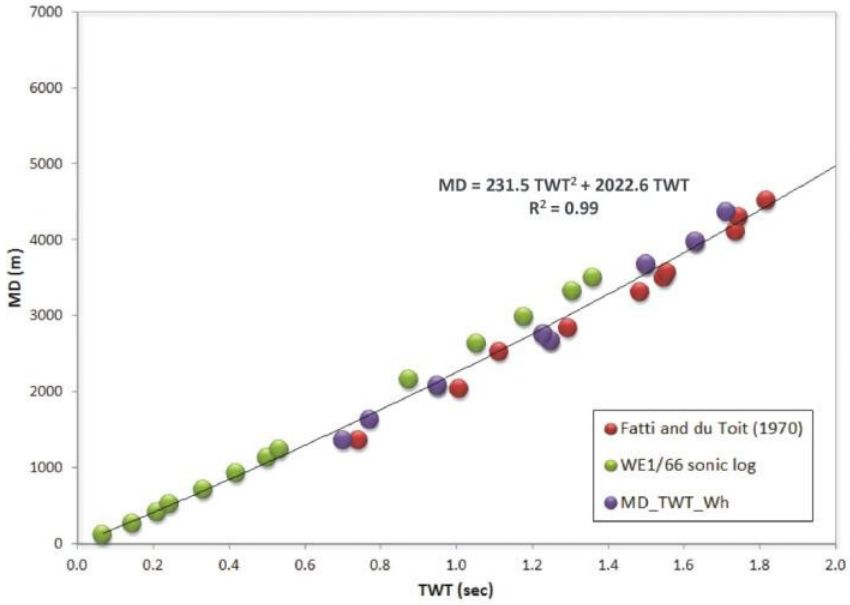

Figure 3-3. Time-depth plots for Soekor seismic data. The measured depths (MD) of the Whitehill Formation from wells (Rowsell and De Swardt 1976) and the two-way travel times (TWT) of the first continuous strong reflector (i.e., Whitehill Formation) are plotted (MD_TWT_Wh). Interval velocities determined by Fatti and du Toit (1970) are also plotted, as well as the sonic velocity log from well WE1/66 (Fatti, 1987). A second-order binomial curve is fit to the data with a y-intercept of zero ($R^2 = 0.99$).

Seismic imaging below intrusions or lava flows, called sub-basalt imaging, is a common problem in the oil and gas industry. These high impedance bodies cause energy to be attenuated, resulting in a loss of amplitude. In such cases imaging may not be clear. In the case of shallow dolerites, energy is reflected back leading to a poor signal-to-noise ratio for the deeper reflectors. Often "ringing" or multiples are seen below sills that cannot be differentiated from actual intrusions without well controls. Sill termination can also be difficult to resolve due to interference and the large dominant half-wavelength for the survey of 70m. This large wavelength also means that the tops and bottoms of sills cannot be resolved, and as a result a series of thin sills might not be distinguishable from a single thick sill. Attempts were made to improve

the resolution during data collection using 6-fold CDP stacking (although most are single fold), large geophone patterns and shot-hole patterns, with limited success (Fatti, 1987). In the case of the Karoo data, quality is obviously better south of the dolerite line.

Limitations specifically related to this survey include few deep wells (Table 3-3) to constrain horizons as well as dolerite intrusions. The utmost care was taken, therefore, to ensure realistic continuity of horizons in regions with no wells. In addition, deviation data for these wells were not used in this study. For some seismic sections the data quality is also poor, as the old paper sections were damaged, and/or during scanning and digitization these sections were not well aligned. The error in the navigation file also needs to be considered, as shot point maps were digitized with an error of usually a few hundred metres or less (Bada, personal communication, 13 December 2011). In terms of data processing it is recorded that variable velocities in the weathered and sub-weathered layers made it difficult to compute the static corrections accurately (Fatti, 1987). Limited Soekor seismic data also exist around Lesotho but were excluded due to interpretation difficulties. Despite these limitations, this dataset provides us with a wealth of subsurface information in an area with limited exploration. This study aims to expand on previous work (Fatti, 1970; Fatti and du Toit, 1970; Fatti, 1987).

3.7.3 CGS Aeromagnetic Data

Several geophysical datasets were used during this study, including regional aeromagnetic data. These data were collected by the Council for Geoscience (CGS) from the 1980s to late 1990s. The magnetic data were flown at a line spacing of 1 km and sample spacing of around 60 m. The flight height for the survey was between 100-150 m (Stettler *et al.*, 2000). We use the topographic model ETOPO1 with a resolution of 1 arc-minute (Amante and Eakins, 2009). The final aeromagnetic anomaly was calculated with respect to

the normal Earth magnetic field (Intensity: 28 700 nT, Declination: -22.6˚, Inclination: -66.1˚).

These regional data are compared with a smaller high resolution aeromagnetic survey (2.4 by 3 km) (Chevallier, personal communication, 3 December 2013) to compare what geological features each can resolve. The high resolution survey was flown in the northwestern Karoo, southwest of the town of Fraserburg (Figure 3-2) in 2003. The smaller survey was collected at a flight height of approximately 80 m (varied due to terrain) and a line spacing of 200 m. The sample spacing for the survey is around 13 m (200 km/h flight speed). The final aeromagnetic anomaly was calculated with respect to the normal Earth magnetic field (Intensity: 26 600 nT, Declination: -22.4˚, Inclination: -66.0˚).

In some instances these aeromagnetic data were modelled using petrophysical properties from the CGS Atlas (Maré, 2012) compiled from hand samples, with an average magnetic susceptibility for the sills and dykes of 0.15 SI. Knowledge of the magnetic field at the time of dolerite emplacement is necessary for magnetic modelling. Several palaeomagnetic studies have been carried out in the Karoo basin and are summarized by (Hargraves and Rehacek, 1997). A single magnetic reversal has been measured in the lower 300 m of the Drakensberg Group volcanic sequence which caps the Karoo, and is followed by 200 m of transitional poles and then 900 m of normal polarized rocks (Hargraves and Rehacek, 1997, van Zijl *et al.*, 1962). Palaeomagnetic investigations of the large Insizwa complex in the Eastern Cape revealed a magnetization direction with a declination of 334° and inclination of -62°, which is very similar to the current field (Hattingh and de Wet, 1996). Some samples show a reversed magnetization with a mean natural remanent magnetization (NRM) direction, with a declination of 116° and inclination of 39°.

3.8 Methodology

In order to better understand the source location of the magmas, we investigate the distribution of the sills within wells and confirm the broader distribution trend using seismic data. Seismic data interpreted in IHS Kingdom Suite are used to better understand the subsurface geometry of sills and inclined sheets within the Beaufort Group of the main Karoo Basin. Picking of horizons is based on historic descriptions of reflectors (Fatti, 1970; Fatti and du Toit, 1970), as well as on well intersections and the time-to-depth conversion method described above. An elevation datum of 700 m was used in the project.

In many instances outcrop and/or magnetic data are used to confirm sills and sheets on the seismic sections where they meet the Earth's surface. Aeromagnetic data are dealt with using the built-in functions of Geosoft Oasis Montaj. A 2D magnetic profile is modelled using Geosoft's GM-SYS. Magnetic model responses were calculated using the methods of Talwani *et al.* (1959) and Talwani and Heirtzler (1964), and using the algorithms described by Won and Bevis (1987).

In order to better understand the limits on the Karoo LIP feeder system, we investigate whether the Karoo dolerite distribution has been influenced by the Cape Fold Belt. This is done by comparing the dolerite line and dip of the southernmost inclined sheets with the dip of the folded Beaufort sediments mapped at the surface, as well as deformation of the Whitehill Formation from seismic data. Dip intervals are reported, as the dip of a sheet may vary along its length. In addition, the TWT to depth conversion is non-linear. Hence, if a constant dip is measured in the time-domain, it will vary in the depth domain. This effect is mainly seen for sheets that extend below one second TWT, i.e. sheets in the southeastern Karoo, as the TWT to depth conversion becomes increasingly non-linear. Dip intervals were calculated using depths recorded at the beginning, middle and end of the sheet (i.e., TWTs were converted to metres). The distance along the profile was recorded at those locations (in metres), and then the apparent dips were calculated. True dips were calculated using the azimuth of the seismic line and the strike of the intersected dolerites. The dip

could be calculated at smaller intervals to get a more accurate picture as to how it changes.

Finally, to highlight the need for higher-resolution magnetic data in the basin to fill the gaps left by geological, seismic and regional aeromagnetic surveys, we investigate a high resolution magnetic survey in the northwestern Karoo. These magnetic data are used to investigate the size of dyke intrusions identifiable on higher resolution data compared to regional data, and what source depth is resolvable.

3.9 Results

The distribution of sills as seen in well data (Figure 3-2a) is mimicked in the seismic data where coincident coverage exists. The seismic data can be divided into a northwestern region close to the town of Fraserburg and southeastern region close to Queenstown, where extensive intrusions at multiple depths make imaging of stratigraphic layers difficult. Further south in the southeastern Karoo close to the town of Somerset-East, extensive sheets are imaged, stretching from just above the Whitehill Formation to the surface. In the southwestern Karoo around the town of Graaff-Reinet fewer dolerites allow for clear imaging of deeper Karoo layers.

3.9.1 Northwestern Main Karoo Basin (Fraserburg)

In the northwestern Karoo, seismic profile NW3-9 coincides with well QU1/65 (Figure 3-4a and b). The profile passes over a dolerite sill that coincides with peaks on the magnetic data (Figure 3-4c). This profile displays the complex effect on seismic imaging of multiple sills (Figure 3-4d): Twelve sills are intersected by QU1/65 between the surface and 2.5 km depth, ranging in thickness from <1 m to 130 m, and with a total thickness of 434 m. Several of these thicker sills coincide with strong reflectors in the seismic data above the Ecca shale layer, while other strong reflections are interpreted as

artefacts/multiples. The high velocities of these dolerites will, however, affect the time-depth curve for this region, making accurate picking difficult. For example, between 0 and 1 seconds 10 sills are identified within QU1/65, but a maximum of 5 are resolvable on the seismic data.

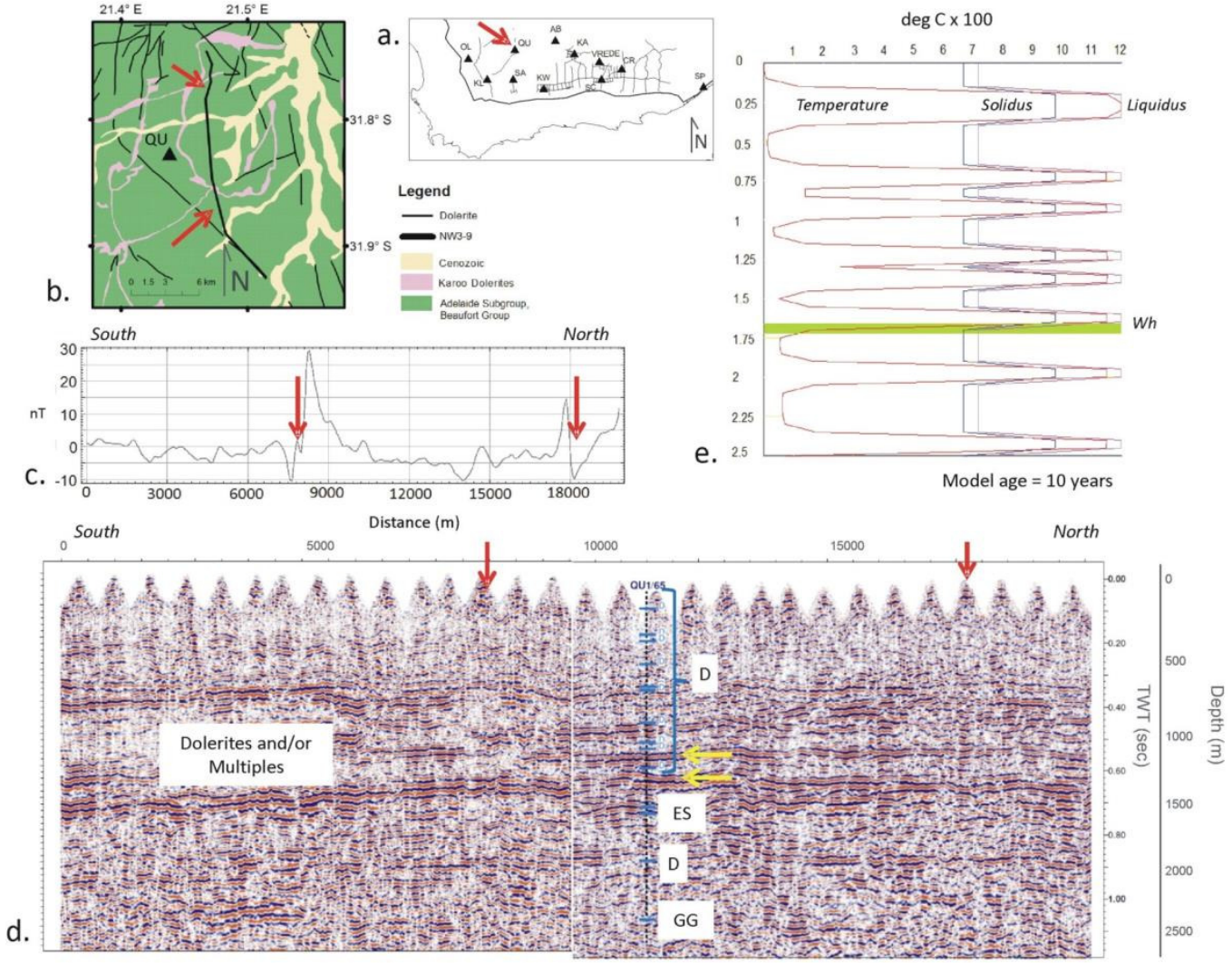
a.
b.
c.
d.
e.
21.4° E
21.5° E
31.8° S
31.9° S
QU
N
Legend
Dolerite
NW3-9
Cenozoic
Karoo Dolerites
Adelaide Subgroup, Beaufort Group
South
North
nT
Distance (m)
Dolerites and/or Multiples
D
ES
GG
TWT (sec)
Depth (m)
deg C x 100
Temperature
Solidus
Liquidus
Wh
Model age = 10 years

Figure 3-4. (a) Location map of seismic profile NW3-9 (black line) and well QU1/65 (black triangle, marked with red arrow) in the northwest Karoo (thick black outline). (b) Geological map of the region north of Fraserburg with the seismic profiles (thick black line) and well QU1/65 marked. The line was shot over Beaufort Group sediments (green), a Karoo dolerite sill (pink, marked with red arrows) and dykes (thin black lines). (c) The profile is correlated with a north-south magnetic profile. The magnetic data have been high-pass filtered to remove the regional field. The edges of the sill are clearly visible on the filtered magnetic data (red arrows). (d) The seismic profile NW3-9 is shown (red = peaks and blue = troughs) with the vertical axis displayed as two-way travel time in seconds and depth in metres (non-linear). Formation tops recorded down well QU1/65 are marked (blue dashes). Expected strong reflectors at depth should correlate with the Whitehill Formation (ES, Ecca shales) and granite-gneiss basement (GG) as constrained by wells data, but none are visible. This is due to strong shallower reflectors interpreted as dolerite sills (D) from well intersections. Other strong shallow reflectors that do not correlate with dolerites in the well are interpreted as multiples (yellow arrows, although the lack of correlation could be due to an inaccurate velocity curve because of the large number of dolerites). The shallow sill visible in outcrop (red arrows in b) is not resolvable on the seismic data, and neither are vertical structures such as dykes. (e) Temperature (˚C x 100) versus depth (km) curve calculated for the dolerite sills in well QU1/65 ten years after emplacement (Cawthorn and Walraven, 1998). The location of the Whitehill Formation is marked (green line, Wh). The temperature curve (red line), solidus curve (blue line) and liquidus curve (pink line) are indicated relative to the original emplacement temperature (1200˚C). The temperature after 10 years of cooling is still approximately 700-800˚C within the Whitehill Formation due to dolerite emplacement.

One of these sills has intruded above the Whitehill Formation at a depth of ~ 1,600 m and we investigate its heating effect on the shales. Figure 3-4e shows the temperature curve for well QU1/65 calculated using the program

THERMS32 (Cawthorn and Walraven, 1998) using a thermal conductivity of 0.006 cal/˚/cm^2 and intrusion temperature for the sills of 1,200˚C and solidus temperature of 980˚C. Temperatures within the Whitehill Formation due to heating from the sill are between 700 and 800˚C after 10 years of emplacement. More extensive work on the heating effect of these sills is currently being carried out (Maré *et al.*, 2014, Maré *et al.*, 2013).

The low horizontal resolution of these seismic data make the individual sills appear as an extensive continuous dolerite layer (L. Hermann 2013, personal communication, 26 September 2013). High resolution seismic data from the Faroe-Shetland basin, however, show how smaller sills can form a continuous intrusive layer, with the touching sill edges resolvable (Hansen *et al.*, 2004). The four/five to one ratio from Polteau *et al.* (2008) of sill diameter to overburden thickness would also suggest that these horizontally continuous reflectors are made up of individual sills.

3.9.2 Southeastern Main Karoo Basin (Queenstown)

Extensive sills are also found in the eastern Karoo as seen in well WE1/66, although in this region they have intruded higher up in the Karoo stratigraphy and are more saucer-shaped. Further south the overlapping nature of these saucer-shaped sills is highlighted within the well-studied Golden Valley Sill complex (Figure 3-5a). This region has no well constraints, though from outcrop data and seismic profiles BV12E and BV14 (Figure 3-5b and c) we can see that the horizontal extent of these sills (~5 to 10 km) is more limited than those in the northwestern Karoo, and the dip of the inclined sheets connected to these sills is between 3 and 7°. The depths of these shallow sills are < 800 m (<0.4 seconds).

Strong reflections are visible below these saucer-shaped sills, although without well constraints we cannot conclude whether they are sills or multiples. A magnetic profile over the Golden Valley Sill complex (Figure 3-5d and e) shows that the larger shallower sills are clearly visible on the aeromagnetic

data, while the deeper sills are at the resolution of the data. The magnetic signal over the Golden Valley sill itself is a lot more complex than expected for a simple sill, suggesting there are additional body/ies at depth below the northern part of the sill.

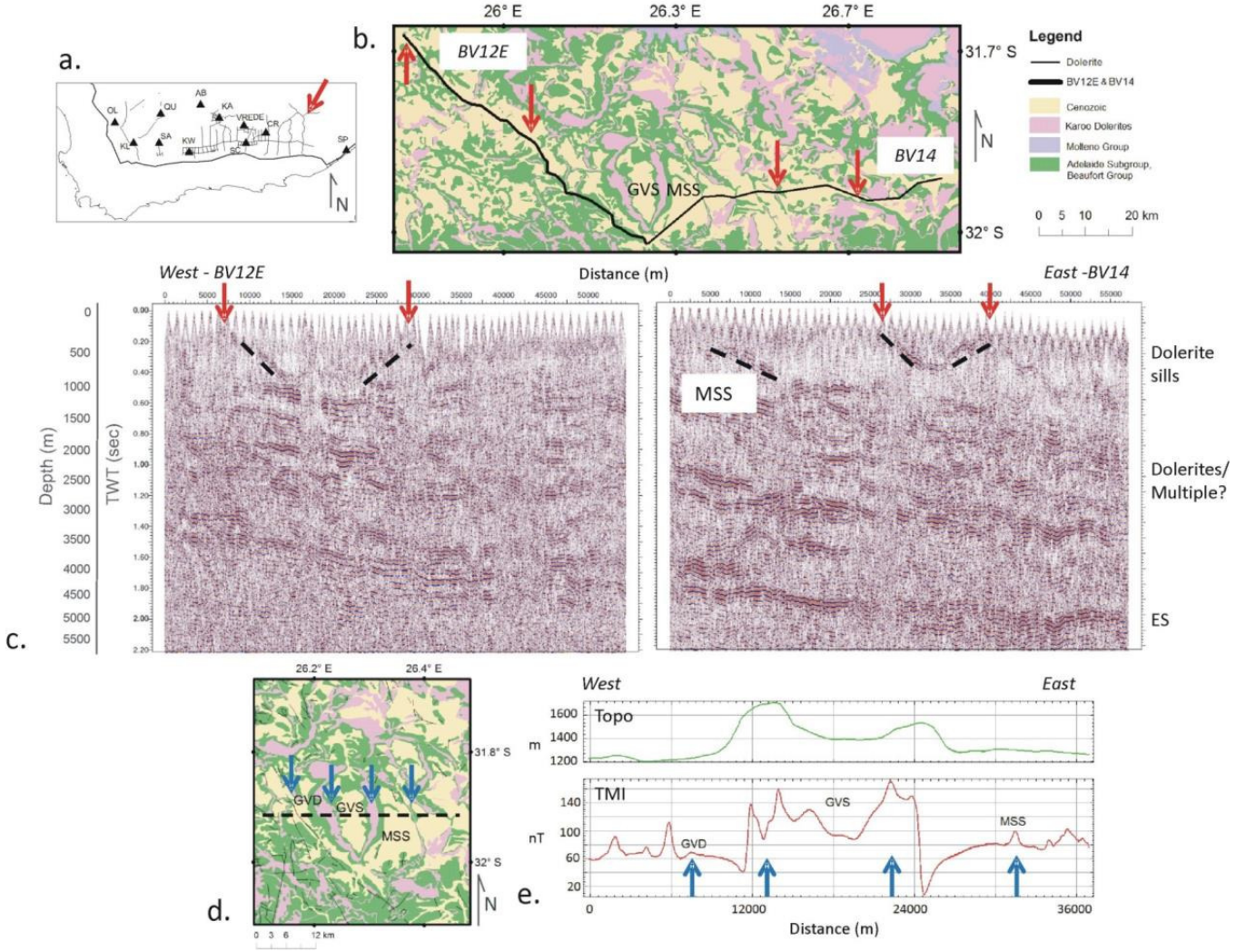
a.
OL
OU
AB
KA
VREDE
CR
SP
KL
SA
KW
SC
N
b.
26° E
26.3° E
26.7° E
BV12E
BV14
GVS MSS
31.7° S
32° S
N
Legend
Dolerite
BV12E & BV14
Cenozoic
Karoo Dolerites
Molteno Group
Adelaide Subgroup, Beaufort Group
0 5 10 20 km
c.
West - BV12E
Distance (m)
East -BV14
Depth (m)
TWT (sec)
MSS
Dolerite sills
Dolerites/ Multiple?
ES
d.
26.2° E
26.4° E
31.8° S
32° S
GVD
GVS
MSS
N
0 3 6 12 km
e.
West
East
Topo
m
1600
1400
1200
TMI
nT
140
100
60
20
GVD
GVS
MSS
0
12000
24000
36000
Distance (m)

Figure 3-5. (a) Location map for seismic profile BV12W (west) and BV14 (east) in the eastern Karoo (in the region of Queenstown). The proximity of these lines to the well-studied Golden Valley Sill (GVS) complex is shown on the geological map in (b). Outcropping sills clearly seen on the seismic profiles (c) are marked on the geological map with red arrows. The depth extent of these shallow sills is around 800 m, while the inclined sheets dip at between 2 to 8˚ (dashed black lines below sheets). The base of the Morning Sun Sill (MSS), which forms part of the complex, is visible of the seismic data (dashed black line below sill) although the inclined sheets that outcrop are not. The reflector representing the Whitehill Formation (ES) is marked (constrained from nearby seismic lines), with shallower reflectors representing other sills or multiples. (d) Focusing in on the GVS complex, a magnetic (TMI) profile (e) over the centre of the GVS complex shows that the shallower GVS has a strong signal, while the deeper MSS and thin Golden Valley Dyke (GVD) have signals close to the resolution of the data (blue arrows). The signal over the GVS is more complex than expected for a simple sill, implying additional dolerite structures at depth. A topographic profile (Topo) shows the high relief of the GVS. See Figure 3-4 for additional details.

3.9.3 Southeastern Karoo (Somerset-East)

In the lower Beaufort Group in the southeastern Karoo (

Table 3-1), extensive sheets outcrop from east to west over more than 150 km. These sheets represent the edge of outcropping dolerite (the dolerite line). These sheets are visible on the seismic data (seismic lines BV02, BV05, BV06, BV07 and BV12 shown in Figure 3-6) as subparallel reflectors cross-cutting the Beaufort and Ecca layers and connect to deeper sills, though they are not constrained by any well data. In this region a dolerite sheet (green arrow, Figure 3-6) is mapped in outcrop for approximately 140 km across seismic profiles BV02, BV05, BV06 and BV12. Further west this sheet cross-cuts a second sheet

intersected by line BV07. Two other sheets are mapped in outcrop (red and blue arrows, Figure 3-6) and are visible on BV02, BV06 and BV12, and BV05, BV06 and BV12 respectively.

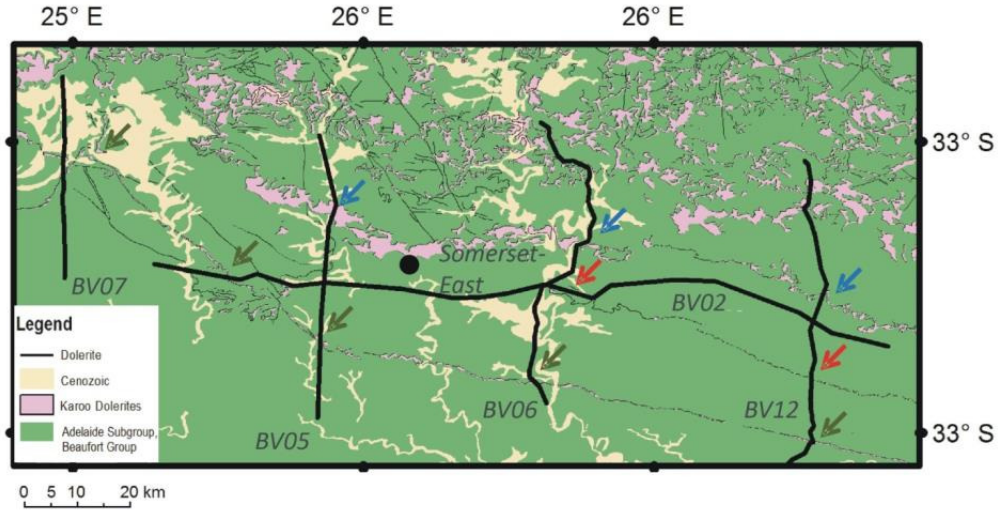

Figure 3-6. Geological map of the region in the southeastern Karoo close to the town of Somerset-East. This region is covered by five seismic profiles: part of BV02, BV05, BV06, BV07 and part of BV12. Extensive dolerite sheets can be mapped in outcrop from profile to profile (green, red and blue arrows).

On seismic line BV07 (Figure 3-7a-b), the above-mentioned sill is evident as a strong horizontal reflector at depth (at 0.8 sec, ~2 000 m, Figure 3-7c and d). This sill is connected by an inclined sheet to saucer-shaped sills at shallower levels (at 0.4 sec, < 1000 m, Figure 3-7c and d) that outcrops. This sheet extends from a depth of ~1 km over a distance of ~ 30 km, dipping at approximately 5° at depth to 3° near the surface. Well CR1/68 is ~2.3 km away from line BV07 and intersects four intrusions that are confined to the Beaufort Group. These sills range in thickness from 5 to 8 m at measured depths of between 390 m and 525 m, the lowest of which is detected on the seismic data. Well CR1/68 continues down into the Cape Supergroup, and therefore it appears that in this area the Whitehill Formation has not been directly affected by the dolerites. However, as mentioned above, bleaching of the shales and tillites

at the top of the Dwyka is evident in CR1/68 and is most likely due to a dolerite that is not intersected (Leith, 1970).

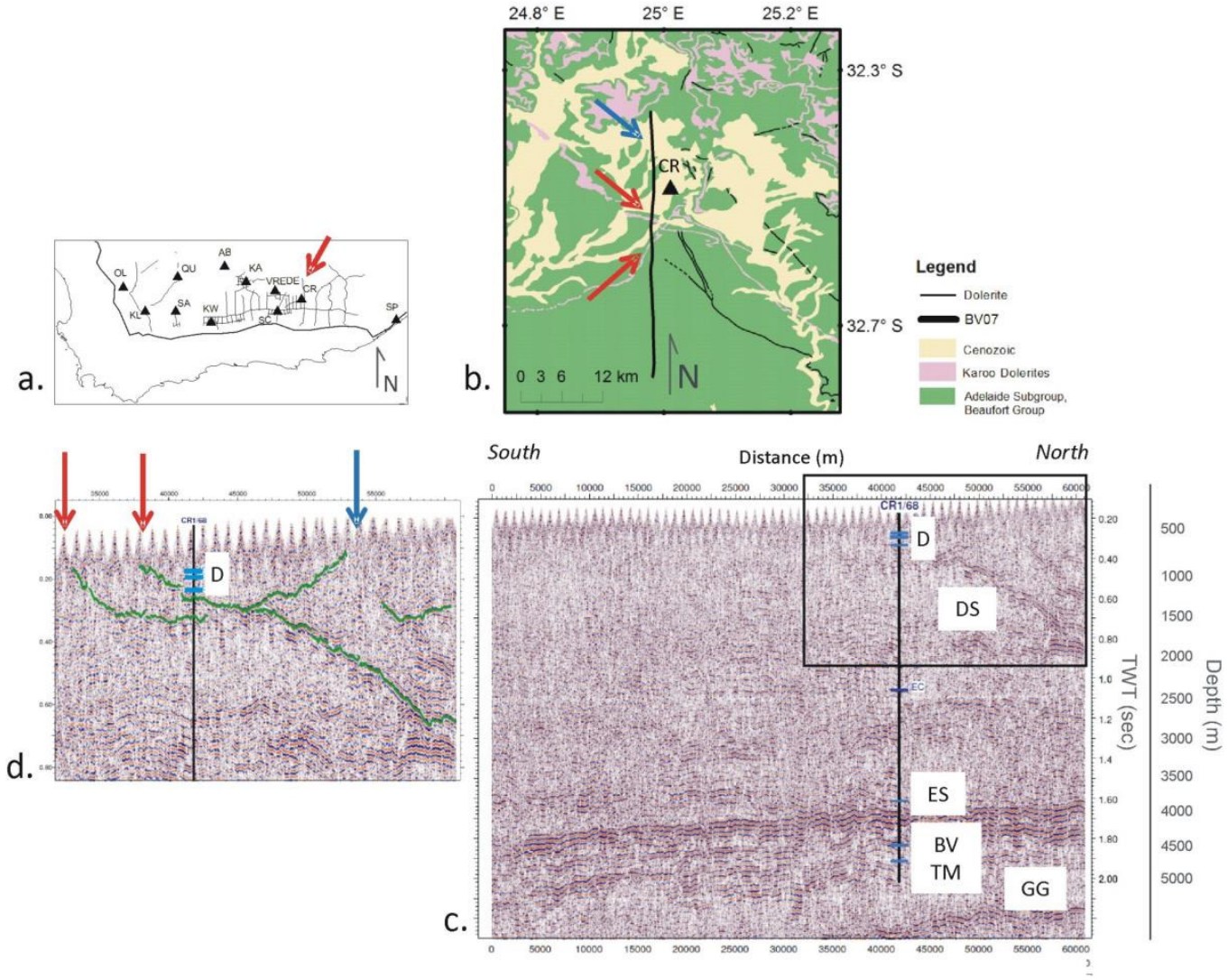
a.
OL
OU
AB
KA
VREDE
CR
KL
SA
KW
SC
SP
N
b.
24.8° E
25° E
25.2° E
32.3° S
32.7° S
CR1
0 3 6 12 km
N
Legend
Dolerite
BV07
Cenozoic
Karoo Dolerites
Adelaide Subgroup, Beaufort Group
d.
CR1/68
D
c.
South
Distance (m)
North
CR1/68
D
DS
EC
ES
BV
TM
GG
TWT (sec)
Depth (m)

Figure 3-7. (a) Location plot of seismic profile BV07 in the southeastern Karoo, west of the town of Somerset-East. On the geological map (b) it can be seen that BV07 intersects two dolerites sheets close together (red arrow) and lies close to well CR1/68. (c) Seismic profile BV07 with the deep reflectors of the Whitehill Formation (ES), Bokkeveld (BV), Table Mountain (TM) Groups and basement (GG) marked, as constrained by well data (CR1/68) and nearby seismic lines. An interpreted inclined sheet (DS) is marked. A black box marks the region focused on and interpreted in (d, green horizons). It appears that a deeper sill is connected by this inclined sheet to a shallower sill that outcrops (red arrows). The interpreted northern limb of the shallow sill (blue arrow) does not outcrop. See Figure 3-4 for additional details.

Seismic section BV06 (Figure 3-8a) intersects three sheets that are visible in outcrop (Figure 3-8b). The middle sheet is mapped to the east of the line, although its limited extent to the west is only definable from magnetic data (Figure 3-8c). This highlights the importance of geophysical datasets to gain a clear geological understanding of an area. These three sheets are clearly visible on seismic data (Figure 3-8d), with the southernmost sill having been identified by Fatti and Du Toit (1970) during their initial interpretation of the data. The deepest of these sills has intruded close to the Whitehill Formation (>4 000 m depth). However, due to poor vertical resolution and what are interpreted as multiples, it is difficult to determine if these sheets connect to the same sill at depth or whether they are stacked vertically. Deeper horizons on this profile are not picked in the south, because of folding and faulting of sediments due to the Cape tectonic event that makes accurate picking difficult. A magnetic model of the profile is shown in Figure 3-8e, with sills and sheets modelled with susceptibilities of 0.15 SI (Maré, 2012) and remanence similar to the present day field (declination of 334° and inclination of -62°). This model is non-unique and cannot constrain whether or not the sills are connected at depth.

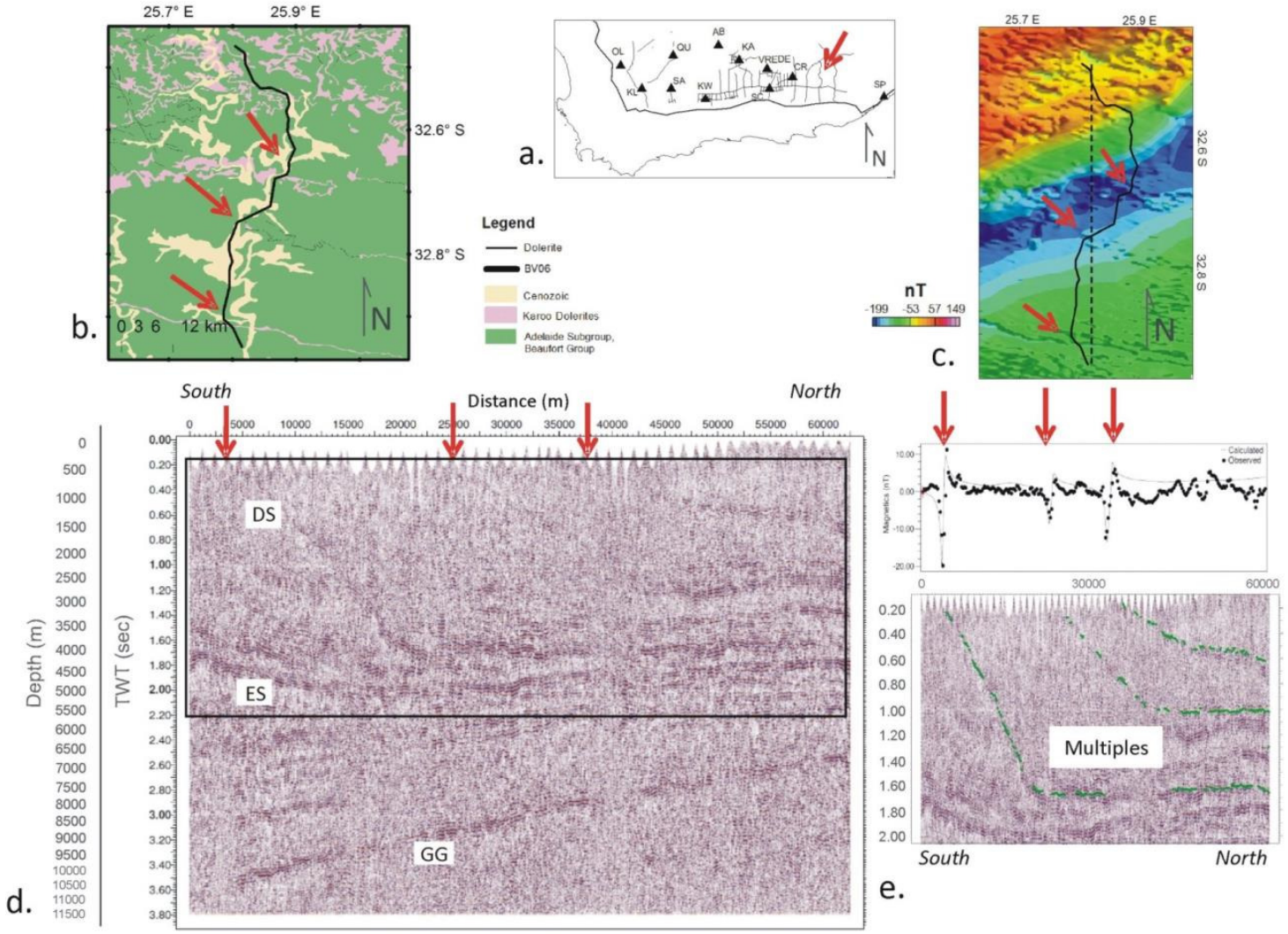
25.7° E
25.9° E
32.6° S
32.8° S
b.
0 3 6 12 km
N
a.
OL
OU
AB
KA
VREDE
CR
SP
KL
SA
KW
SC
N
Legend
Dolerite
BV06
Cenozoic
Karoo Dolerites
Adelaide Subgroup, Beaufort Group
nT
-199 -53 57 149
c.
25.7 E
25.9 E
32.6 S
32.8 S
N
South
Distance (m)
North
DS
ES
GG
Depth (m)
TWT (sec)
Calculated
Observed
Multiples
South
North
d.
e.

Figure 3-8. (a) Location map for seismic profile BV06 in the southeastern Karoo, east of the town of Somerset-East. The profile (thick black line) passes over three dolerites sheets (red arrows) that show up clearly on the (b) geological map and (c) gridded magnetic data. (d) Seismic profile BV06 with the deep reflectors of the Whitehill Formation (ES) and basement (GG) constrained by surrounding seismic lines (reflectors are labelled from below). Shallower reflectors represent dolerite sheets (DS) that connect to sills at depth and cut through the Beaufort sediments to the surface. One such sheet appears to have intruded close to the Whitehill Formation (ES). Multiples have been interpreted between these sills. (e) A south-north magnetic model coincident with the profile (dotted line in (c) and black box in (d)). This model shows how these interpreted sheets/sills on the seismic profile (green horizons) can be easily modelled using a susceptibility value of 0.15 SI (Maré, 2012) and remanent magnetism close to the present-day field (Hattingh and de Wet, 1996). The data have been high-pass filtered to remove the regional trend. See Figure 3-4 for additional details.

Fatti (1970) mapped one of these sheets across multiple seismic lines. In Figure 3-9 we show how three of the main sheets and sills (green, red and blue arrows, Figure 3-6) interconnect in 3-dimensions over an area of approximately 60 km by 100 km. This is done using north-south lines BV05, BV06, a section of BV12 and a section of east-west profile BV02. The continuation of the middle sill (red arrow, Figure 3-6) to BV05 is assumed, as there is no outcrop evidence. The continuation of the green sill/sheet west of BV05 to BV02 and BV07 is also complicated by several crisscrossing intrusions.

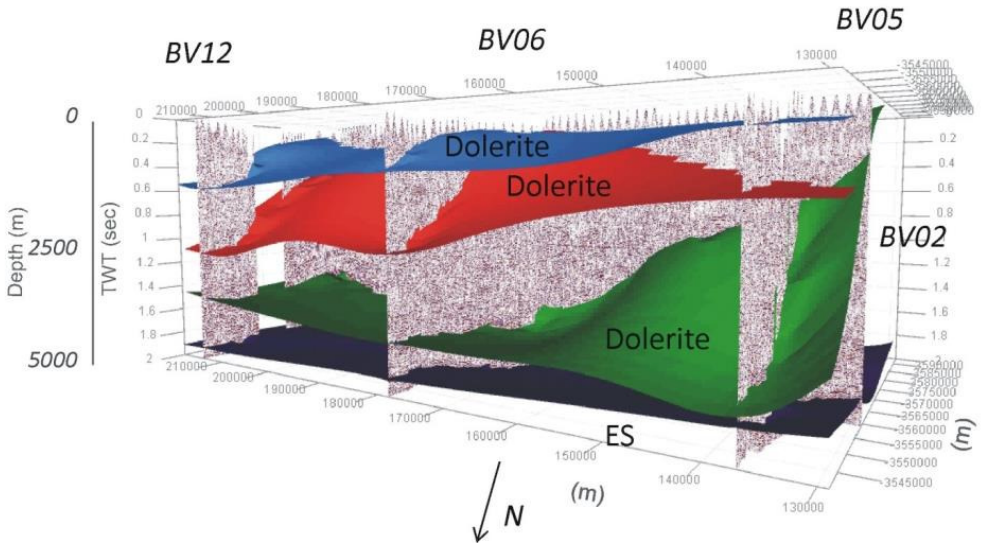

Figure 3-9. Three-dimensional image showing the geometry of the dolerite sheets and sills (green, red, and light blue) in relation to the Whitehill Formation (ES, lower dark blue layer). See Figure 3-6 for location in the southeastern Karoo around the town of Somerset-East. These horizons are mapped using surface outcrop and north-south seismic lines BV05, BV06, BV12 and east-west line BV02.

In Figure 3-8d, it is evident that the dip of the sheets on line BV06 increases from north to south towards the CFB, i.e. sheets closer to the fold belt exhibit a steeper dip. The measured dip for the shallowest sheet is approximately 3°, while the middle sheet dips at 5˚ to 6˚, and the sheet furthest to the south dips at 8˚ to 13°, with a total profile distance of ~60 km. Several of these sheets in the southeastern Karoo have been investigated using seismic data and show a similar trend with increasing dip closer to the CFB (Figure 3-10a). This general trend shows that the tilting of the Karoo Supergroup sediments due to earlier deformation in the south had an effect on the emplacement of dolerites, but the extent to which it has impacted the location of the dolerite line is unclear.

In the southwest, the dolerite line lies ~ 60 km north of the CFB boundary while in the east the two meet (Figure 3-10a). The dip of sheets closest

to the dolerite line therefore vary from 2-4˚ in the west to 8-12˚ in the east. We investigate whether variations in the type of sediments and/or dip of these sediments due to the CFB could be impacting the location of the line. These sheets have intruded various Beaufort Group sediments (

Table 3-1 and Figure 3-10b), with those sheets in the southeast extending for several km within the Balfour and Middleton Formations of the Beaufort Group (Figure 3-10d). In the western part of the basin these sheets continue in the Teekloof Formation, the equivalent of the Middleton Formation (Johnson *et al.*, 2006). In the west these sheets continue to a lesser extent further north, within the underlying Abrahamskraal Formation.

Lateral variations in dip also exist within different stratigraphic units. In the centre of the region plotted in Figure 3-10c, between approximately 22.3˚ and 24.8˚ east, Beaufort sediments dipping at approximately 15˚ are found further north. This lateral variation in maximum dip location does not seem to continue into the Ecca. The point at which Ecca shales first begin to dip to the north is mapped using seismic sections (Figure 3-10b, green line), and remains approximately parallel to the plotted CFB boundary. Several sheets in the southeast extend past this point of first northward dipping of the Ecca shales, although the sills do not. In general, sheets appear to not intrude into sediments that have a dip of greater than 15 - 20° (Figure 3-10c). This argument cannot be used to explain the more northerly extent of the dolerite line in the southwestern Karoo compared to the southeast, as Beaufort sediments dip to the same extent in the east as in the west.

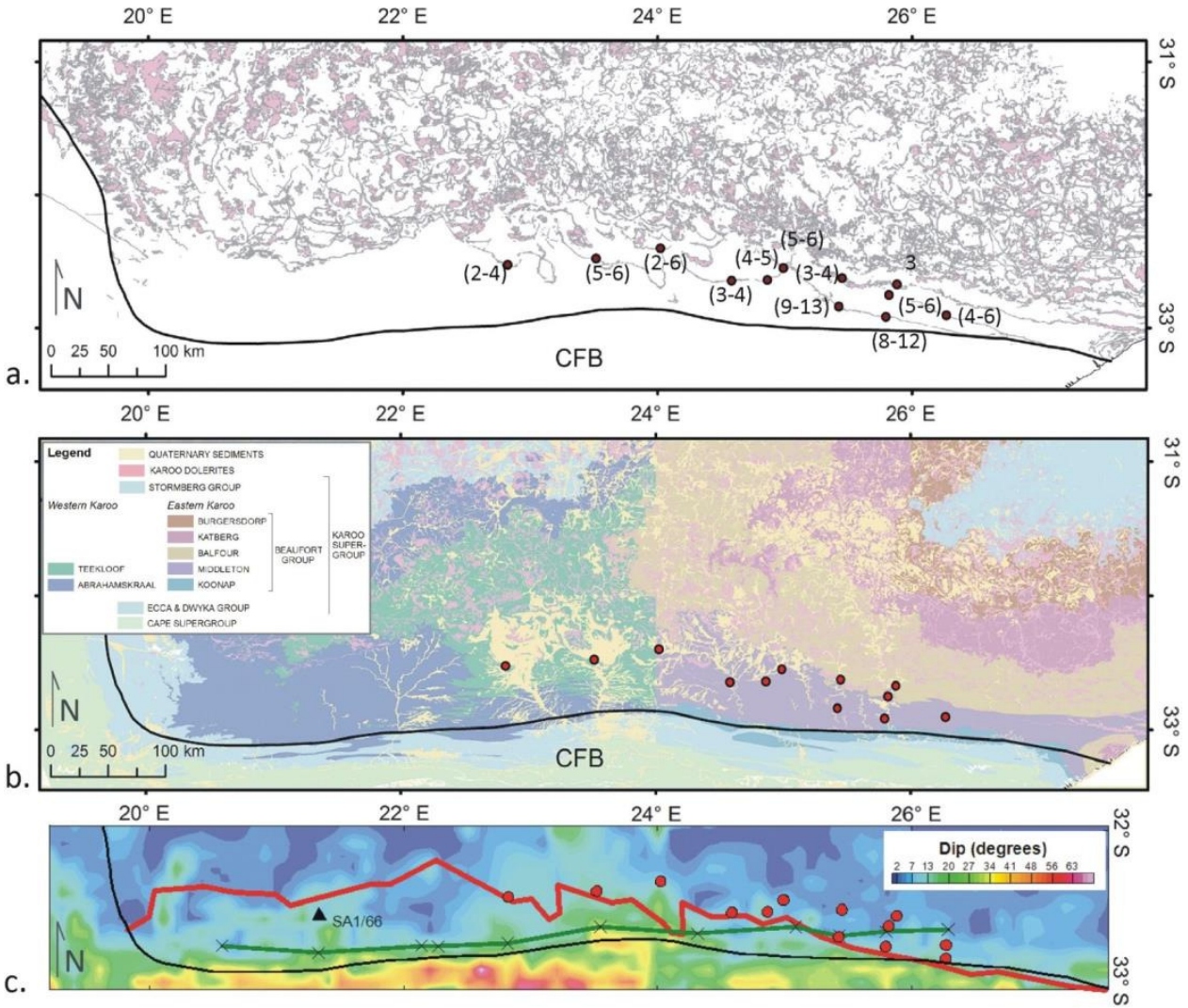
20° E
22° E
24° E
26° E
31° S
33° S
a.
(2-4)
(5-6)
(2-6)
(4-5)
(5-6)
(3-4)
(3-4)
3
(9-13)
(5-6)
(4-6)
(8-12)
N
0 25 50 100 km
CFB
b.
Legend
QUATERNARY SEDIMENTS
KAROO DOLERITES
STORMBERG GROUP
Western Karoo
Eastern Karoo
BURGERSDORP
KATBERG
BALFOUR
MIDDLETON
KOONAP
TEEKLOOF
ABRAHAMSKRAAL
BEAUFORT GROUP
KAROO SUPER-GROUP
ECCA & DWYKA GROUP
CAPE SUPERGROUP
c.
32° S
SA1/66
Dip (degrees)
2 7 13 20 27 34 41 48 56 63

Figure 3-10. (a) Geological map showing the Karoo sills in the southern Karoo. Dip intervals for dolerite sheets as measured from seismic sections are shown (red dots), with values increasing for sheets closer to the CFB (from 3˚ to 13˚). (b) The sheets are continuous across the Teekloof and Middleton lithological boundaries in the Beaufort, which are equivalent layers in the east and west (

Table 3-1, Johnson *et al.* (2006)). Further west these lithologies are removed by erosion and the deeper Abrahamskraal Formation is exposed, with considerably fewer outcropping sheets towards the south. (c) Gridded dip data mapped from sediments in the southern Karoo and CFB. Values change from ~50˚ within the CFB to ~2˚ in the north. The red line marks the southern extent of outcropping dolerites (dolerite line), and the green line marks the location of first tilting of the Whitehill Formation due to the CFB as seen on the seismic sections. The dolerite line does not seem to have any correlation with the dip of the sediments.

It must be kept in mind, however, that this dolerite line is based on surface exposure of dolerites. Wells SA1/66 and KL1/65 both lie just south of the dolerite line (25-35 km), but SA1/66 intersects an approximately 6 m thick sill at ~3,350 m depth within the Dwyka Group (although the sill could be thicker due to no coring after this point for a section of the well) and well KL1/65 intersects an approximately 170 m thick dolerite at ~ 2,250 m depth within the Bokkeveld. Therefore dolerites could exist south of the line in the southwest that do not outcrop, although a decreasing trend of dolerites is still evident towards the south. It must be noted that for this study the CFB is interpreted as a zone of deformation with a northern boundary that coincides with the southern extent of Beaufort sediments (Figure 3-10b) where Cape and Karoo lithologies dip at around 30˚ (Figure 3-10c). The Beaufort sediments north of this line dip more gently (<15° in the south and <5° in the north).

3.9.4 Southwestern Main Karoo Basin (Graaff-Reinet)

In the southwestern part of the basin, seismic profile SWK06 runs close to well KA1/66 (Figure 3-11a and b). Outcropping dolerite sills and dykes (Figure 3-11b) correlate with small anomalies on the magnetic data (Figure 3-11c, red arrows). A region with a complex magnetic signal is viewed in the north of the profile that coincides with limited dolerite outcrop and most likely buried sources (red box). Three dolerites within the Beaufort Group are intersected by the well at 0.24, 0.35 and 0.5 seconds (measured depths of 140 m, 431 m, and 838 m), with thicknesses of 78 m, 6 m and 34 m, respectively. The deepest sill correlates with a strong reflector on the seismic data (Figure 3-11d). In the south, a "break" in the "continuous" sill layer is correlated with mapped dykes at the surface (southernmost red arrow), although vertical features are not resolvable on seismic data. From seismic and well data it appears that in this section of the basin, sills are emplaced approximately 1,000 m above the Whitehill Formation. It must be noted again, however, that due to limited data, sills could exist closer to the Whitehill but have not been imaged or intersected. Sills intruded along the Whitehill south of KA1/66 could also be the reason for the strong Whitehill reflector in this region, instead of good imaging due to a lack of sills at shallower levels which is the interpretation for this study.

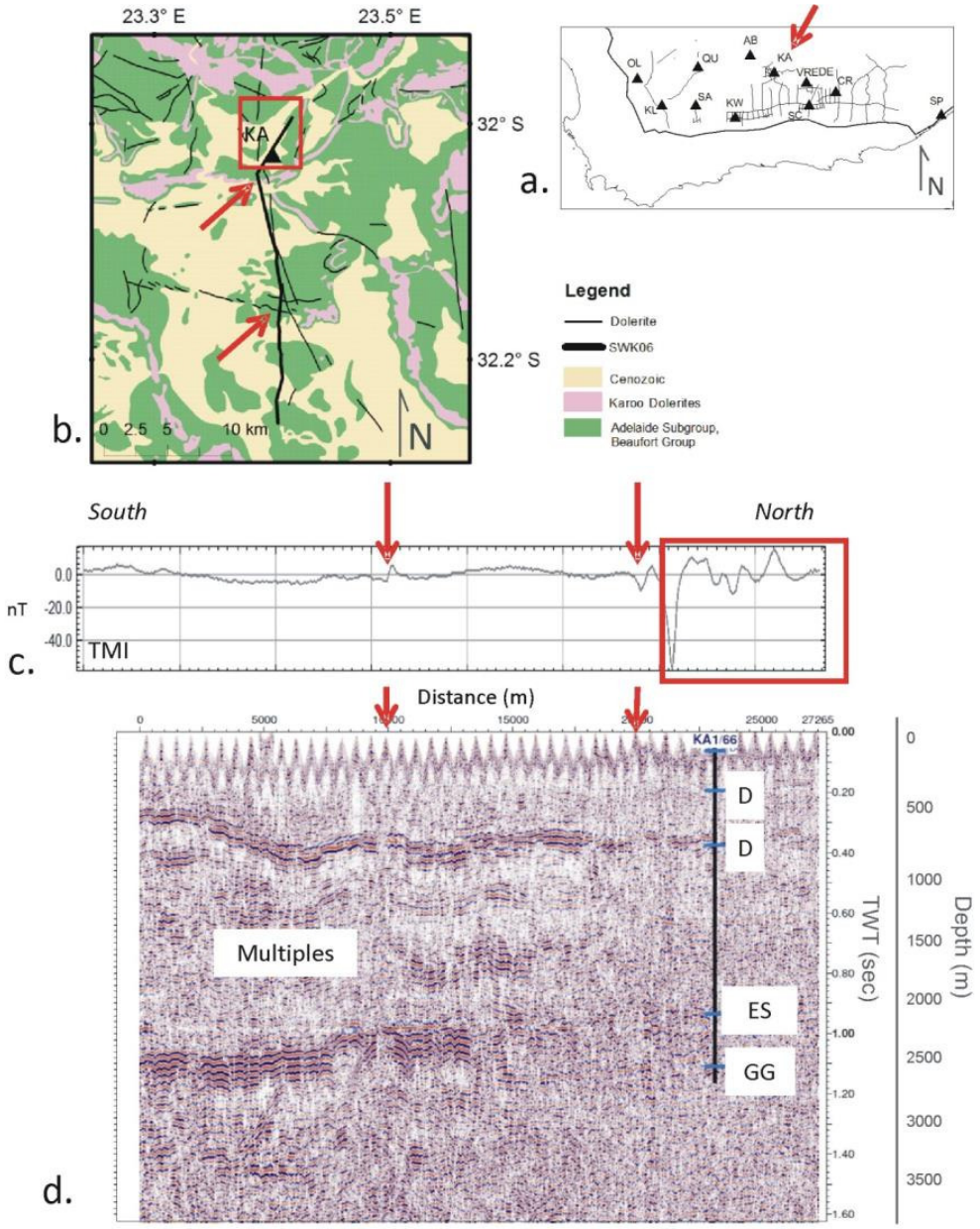

Figure 3-11. (a) Location plot for seismic profile SWK06 in the southwestern Karoo close to the town of Graaff-Reinet. The seismic profile (thick black line) on the geological map in (b) intersects a dolerite sill and several dykes (red arrows) and lies close to well KA1/66. A north-south magnetic profile in (c) shows how these outcropping dolerites correlate with magnetic anomalies (TMI, red arrows). These magnetic data are high-pass filtered to remove the region trend. The shallowest strong reflector in (d) correlates with a dolerite sill (D) intersected by well KA1/66. Below that the Whitehill Formation (ES) reflector

is visible due to fewer dolerites at shallower levels, whereas the basement reflector (GG) is not. Strong reflections between ES and the lowest dolerite are interpreted as multiples. The southern mapped dyke in (b and c) correlates with a break in the picked continuous sill layer on the seismic data (southern red arrow). The red box marks a region with a complex magnetic signal, but no mapped dolerites. The reflections in this region are also weak. This highlights the importance of using magnetic data when interpreting seismic data, and investigating for magnetic bodies that do not outcrop. See Figure 3-4 for additional details.

3.10 Discussion

This study expands on the vertical dolerite distribution defined by van Zijl (2006a). From well and seismic studies we see that in the northwestern portion of the basin around Fraserburg (wells QU1/65, AB1/65, OL1/66 and KL1/65) and eastern/southeastern basin extending from East London (SP/66) up to Aliwal North (WE1/66) and around Lesotho (GLEN1/67, LA1/68 and WI1/72) towards the eastern Karoo (MA1/69 and SW1/67), a large number of intrusions are recorded at all stratigraphic levels (Figure 3-2). In the region stretching from the southwestern to southeastern Karoo, centred around the town of Graaff-Reinet, fewer dolerites have only intruded in the Beaufort Groups (VREDE1/66, KA1/66 and CR1/68) (Figure 3-2). However, it must be noted that borehole CR1/68 shows signs of bleaching at the top of the Dwyka due to a possible dolerite in the vicinity (Leith, 1970). Initial studies highlight how the dolerites appear to intrude along lithological boundaries with different mechanical properties, such as siltstone and sandstone (, and this studyBurchardt, 2008).

This horizontal distribution is in line with observations by Cole *et al.* (2011) of dolerite thicknesses within the Whitehill Formation, and sheds light on the source location of these Karoo magmas. It is evident in Figure 3-1 that these wells with lower dolerite concentrations (<150 m) lie close to the border between the *D1* and *D2* regions defined by Chevallier *et al.* (2001). The largest dolerite concentrations (>150 m, with some total dolerite thicknesses > 400 m) are

in line with the suggestion by Chevallier *et al.* (2001) that sources existed off the west and east coast of South Africa. These sources are closer to the study area compared to the triple junction suggested as the feeder for dyke swarms in the northeast of the basin. This could be tested further with more geochronology and geochemical studies (Neumann *et al.*, 2011, Hastie *et al.*, 2014), although it is an extensive region to cover.

The apparent lack of dolerites in the southwestern part of the basin around the town of Graaff-Reinet at measured depths greater than 1,000 m highlights the importance of horizontal magma transport in the basin. Limited intrusions in this region could be due to loss of energy during magma transport away from the western and eastern sources. It has also led other researchers to suggest that this part of the basin would be the best place to carry out shale gas exploration, as the Whitehill Formation has been least affected by dolerites (Decker, 2013). A gas release from well CR1/68 within this region has historically been recorded (Leith, 1970, Rowsell and De Swardt, 1976). Cole *et al.* (2011) propose the region 50 km north of the dolerite line to 30 km north of the southernmost CFB exposures as the best location for shale gas exploration, along with a few small (~ 10 km²) dolerite-free regions between intrusions within the southern basin (Cole and McLachlan, 1994).

These seismic data have also allowed us to better constrain the subsurface geometries (vertical extent and dip) of shallower sills in the southeastern Karoo around Queenstown and extensive sheets around Somerset-East, and are summarized in Table 3-4. The effect of the CFB on the sill and sheet geometries is most evident from the dip of these sheets, which become steeper close to the CFB. Sheets appear to not intrude sediments dipping more than 15 to 20°. However, the CFB does not appear to affect the location of the dolerite line, as we find no correlation between the line and the dip of the Beaufort sediments. These sheets also appear continuous across lithological boundaries.

Table 3-4. Sill and inclined sheet geometries determined from geological and seismic data, including the horizontal and vertical extent of the bodies and dips of the inclined sheets. Sill geometries were determined from those around Queenstown in the southeastern Karoo, while sheet geometries were determined from those further south, around Somerset-East. Lithologies in which they intrude are listed (Fm – Formation, Grp – Group).

	Sills	**Sheets**
Lateral Extent:	5 – 30 km	Over 150 km in the subsurface
Depth extent:	800 m to surface	From ~ 5 km up to surface
Dip:	2 – 8˚	3-13˚
Stratigraphy:	Burgersdorp Fm, Beaufort Grp	Teekloof/Middleton and Abrahamskraal Fm, Beaufort Grp

Additional physical experiments and numerical modelling expanding on the current knowledge (Galland *et al.*, 2007, Galland *et al.*, 2006, Galland *et al.*, 2003, Malthe-Sørenssen *et al.*, 2004) looking at the impact of already tilted sediments during sill emplacement, could help shed light on the impact of the tilted Karoo Supergroup sediments. Pore pressures might also have played a role and should be further investigated (Gressier *et al.*, 2010). Higher resolution seismic data across the dolerite line would allow for imaging of possible sills south of the line that do not outcrop. Comprehensive mapping of the basement below this region would also help determine if the dolerite line is a result of a deep crustal structure.

Despite this greater understanding of the sill geometries, we have been unable to draw further conclusions regarding their feeder system. Evidence for a sill-feeding-sill relationship is seen on line BV07 (Figure 3-7c and d), where an inclined sheet branches and then flattens out at shallower depths (< 1000 m) to form a second sill. Additional geochemical work, such as that carried out in the Golden Valley Sill (Galerne *et al.*, 2011), would be needed to confirm this relationship and conclusively show dyke-feeding-sill relationships.

With a better understanding of dolerite distribution and geometry, the next step for companies exploring in the Karoo is to drill several deep wells to better understand variations in shale rock properties (e.g., depth, shale thickness, organic carbon content, porosity and mineralogy) and the effect that the dolerites have had on the maturity of these shales (Cole *et al.*, 2011, Decker and Marot, 2012, Geel *et al.*, 2013, Smithard *et al.*, 2013).

Studies have shown that heating of shale reservoirs by adjacent dolerites (up to 1000˚C) can result in the rapid conversion of organic material to gas, namely CH_4 and CO_2 (Aarnes *et al.*, 2011b, Svensen *et al.*, 2007). A rapid build-up of reservoir pressure in the Karoo during dolerite emplacement was accompanied in regions by violent degassing to the surface in the form of breccia pipes (Svensen *et al.*, 2007). An example of the impact of these sills is seen in the TOC values for shales in borehole QU1/65 in the northwestern Karoo, where extensive intrusions have resulted in high values of 14.8 wt % (Cole and McLachlan, 1994). Recent studies, have estimated the impact zone of these dolerites on adjacent shales as being half the width of the sill, but is dependent on the host rock and heat flow (Aarnes *et al.*, 2011a, Aarnes *et al.*, 2011b, Maré *et al.*, 2013).

These intrusions can also have positive effects on surrounding shales. Shallower shale layers can produce dry gas if exposed to dolerite intrusions that locally increase their thermal maturity (Aarnes *et al.*, 2011a, Aarnes *et al.*, 2011b). Larger volumes of gas (> 60%) have also been concentrated in shales close to these dolerites, possibly in fractures created by dolerite heating (Rowsell and De Swardt, 1976). Additional exploration wells in regions where sills have been emplaced close to the Whitehill Formation will shed light on the reservoirs gas retention ability and permeability, and on current maturity levels. Despite the significant impact that these dolerites have had on the shale reservoir, recent estimates of the shale resources taking into account these dolerites still suggest the basin is economical (Cole *et al.*, 2011, Decker, 2014)

The maturity levels of these Karoo rocks are also not only affected by these dolerites, as lower Ecca shales in the southeastern Karoo near Port Elizabeth

have been shown to be over-mature due to the Cape tectonic event (Geel *et al.*, 2013). Shales further west within the basin (well SA1/66) have also been shown to be over-mature (Branch *et al.*, 2007).

Once regions for further exploration are identified, high resolution aeromagnetic and seismic data should be collected. Although aeromagnetic data cannot image dolerites at the depth of the shale reservoir (1.5 km), shallower dykes (<200 m) would be resolvable and can commonly extend down to reservoir depths. High resolution seismic data would allow for better mapping of the geometry of sills and sheets closer to the shale reservoir. New techniques and higher resolution seismic data might also allow for imaging of these vertical dykes (Wall *et al.*, 2009).

An example of the usefulness of higher resolution aeromagnetic data exists in the northwestern Karoo and correlates with seismic profile NWK06 (Figure 3-12a and b). A NW dyke swarm is evident on geological and regional data (Figure 3-12c); while a virtually unmapped east-northeast melilitite basalt swarm (kimberlitic magma) is evident on the higher resolution data (Figure 3-12d) and is marked on the geological map (Figure 3-12b). This swarm is identifiable, as the dykes have similar signals, i.e., they are reversely magnetized due to remanent magnetization. One NNE kimberlite dyke is mapped but is not easily visible on the magnetic data. The thinnest dyke, perpendicular to the flight direction, that can be identified using these high resolution data, is approximately 10 m thick at a shallow depth (~3 m, ~5 nT signal), or thinner if intruded at shallow depths. The regional data will not be able to resolve said dykes, as the signal will be very close to the resolution of the data (~15 – 20 nT).

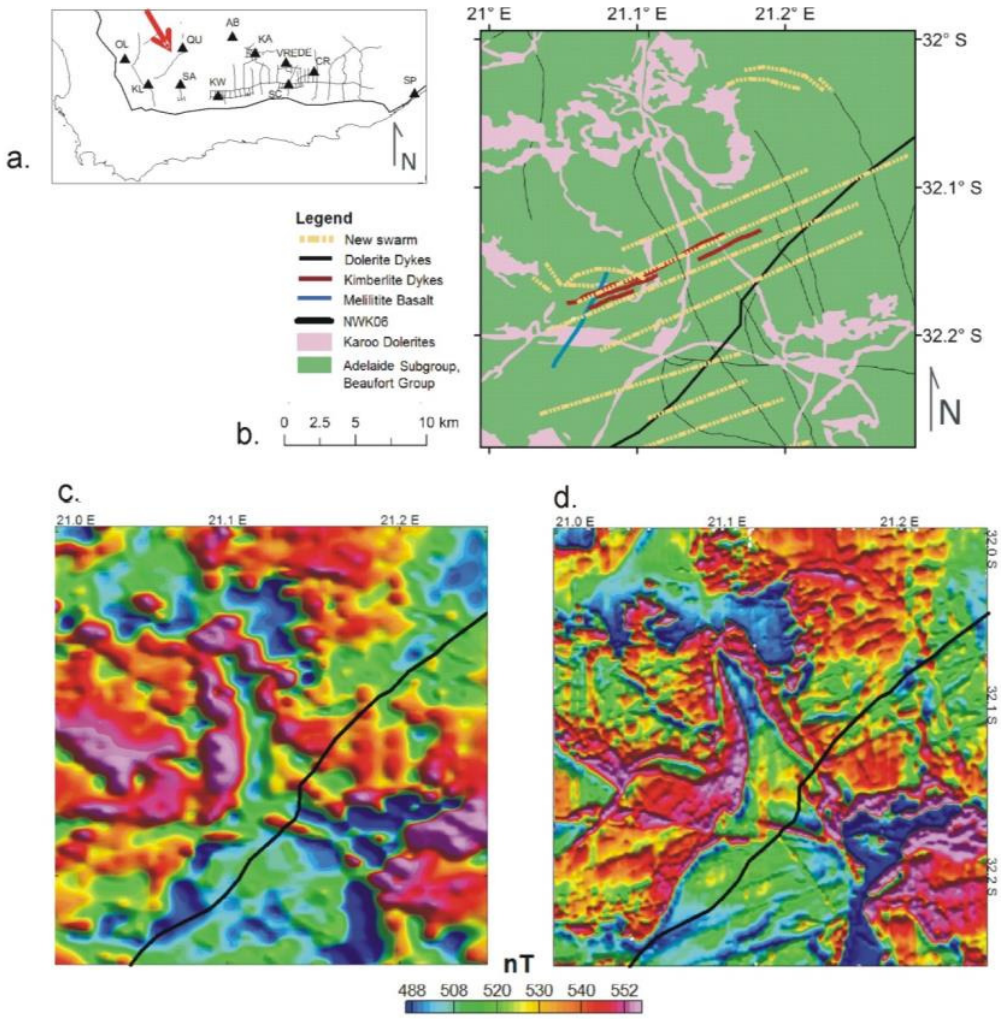

Figure 3-12. (a) Location map for a high resolution magnetic survey flown in the northwestern Karoo, southwest of the town of Fraserburg. (b) Geological map of the region with seismic line NWK06 indicated (thick black line). The total magnetic field of the area is shown using the c) regional (sun-shading at 45˚) and d) high resolution data (sun-shading at 135˚). Mapped NW-trending dykes are visible on the regional and high resolution data, while an ENE swarm is only visible on the high resolution data. This swarm corresponds with several mapped melilitite basalt dykes. The full extent of the swarm is mapped using the magnetic data and overlain on the geological map in (b).

Other electromagnetic (EM) geophysical techniques, such as resistivity and IP (induced polarization), will prove useful when investigating the fracture networks associated with these dolerites (Chevallier *et al.*, 2004, Chevallier *et al.*, 2001). This study therefore shows the usefulness of integrated studies, and how existing geophysical data (aeromagnetic and seismic) over the main Karoo Basin allow for a more continuous picture of the distribution of dolerites within the Karoo.

3.11 Conclusions

Seismic and exploration well data within the main Karoo Basin point towards a change in the distribution of dolerites within the basin that has not been highlighted by historical studies (Rowsell and De Swardt, 1976, Winter and Venter, 1970). These borehole data, and confirmed by seismic data, indicate a maximum dolerite concentration in the northwestern part of the basin around Fraserburg, as well as in the east/southeastern Karoo around Queenstown, further northeast around Lesotho and south around East London in the Eastern Cape. In these regions sills were emplaced at all stratigraphic level.

In a region stretching from the southwestern to the southeast of the basin, around the town of Graaff-Reinet, sills are concentrated in the upper lithologies (Beaufort Group) away from the Whitehill Formation. This region includes wells KA1/66, VREDE1/66 and CR1/68, with well CR1/68 historically having released gas (Leith, 1970, Rowsell and De Swardt, 1976).

This high dolerite concentration in the east and the west, with decreased concentration in the centre points towards two magma sources during emplacement off of the east and west coasts of South Africa.

In the southeastern Karoo around Queenstown, 5 to 30 km wide saucer-shaped sills are imaged extend down to ~ 800 m with dips of between 2˚ and 8˚. Dolerite sheets around Somerset-East that extend for over 150 km are imaged down to ~ 5 km, with dips of between 3 and 13˚. From well data it appears that these sills are emplaced at layer boundaries of contrasting mechanical strengths (e.g., siltstone and sandstone).

From seismic data and mapping we determine that previous tilting of Karoo Supergroup sediments does affect the dip of the dolerite sheets. Sheets intruded closer to the CFB have a steeper dip, and appear not to intrude sediments dipping at more than 15-20˚. However, this does not explain the cause of the dolerite line, as similar dips are recorded in the west and east, but dolerites do not extend as far south in west.

This study highlights the importance of including geophysical data in any investigation of the Karoo LIP feeder system. Seismic data helps to image the subsurface geometry of the sill feeder systems, while magnetic data helps image shallow (<200 m) dykes that are not visible on the seismic data. These magnetic data can also be used to identify shallow sills and dykes that do not outcrop. A higher resolution survey flown in the northwestern Karoo (flight height 80 m, line spacing 200 m, sample spacing ~13 m) is able to detect 10 m wide dykes (common in the Karoo) at shallow depths (~3 m) that are approximately perpendicular to the flight direction, which is beyond the resolution of the regional magnetic dataset. Modern surveys can be flown at even higher resolution levels than these.

3.12 Acknowledgements

This project was funded by the National Research Foundation (NRF), Council for Geoscience (CGS), University of the Witwatersrand and the Society of Exploration Geophysicists (SEG), with software support from IHS Kingdom and Geosoft. We thank Falcon Oil and Gas and the Council for Geoscience for data access and the Petroleum Agency of South Africa for assistance with the data. The authors are grateful to Leonie Mare and Luc Chevallier for sharing their knowledge on the topic; Doug Cole for sharing his knowledge and extensive borehole database; and Lyndsay Lindser, Jeanne Tricker and Musa Manzi for software support. The authors are grateful to Johan de Beer and John Decker for improving this manuscript greatly through the review process.

Chapter 4

Basement

This chapter includes a manuscript published in the journal of Tectonophysics (2014, volume 636, pages 228-243). I conceived this study in discussion with my supervisors. Work for this manuscript and write-up was completed by me, with the remaining authors helping to improve the manuscript and assisting with field work.

AN INTEGRATED GEOPHYSICAL STUDY OF THE BEATTIE MAGNETIC ANOMALY, SOUTH AFRICA

Stephanie Scheiber-Enslin[ab,*], Jörg Ebbing[c], Susan J. Webb[b]

[a] *Geophysics Unit, Council for Geoscience, Pretoria, 0184, South Africa*

[b] *School of Geoscience, University of the Witwatersrand, Johannesburg, 2000, South Africa*

[c] *Department of Geoscience, Christian-Albrechts University, Kiel, 24118, Germany*

* Corresponding author. Tel.: +27 11 717 6606; Fax: +27 86 672 8967;

Email addresses: 0211594d@students.wits.ac.za (S. Scheiber-Enslin), jebbing@geophysik.uni-kiel.de (J. Ebbing), susan.webb@wits.ac.za (S.J. Webb)

4.1 Abstract

The source of the Beattie magnetic anomaly (BMA) still remains unclear, with several competing hypotheses. Here we add a piece to the puzzle by investigating available potential field data over the anomaly. Filtered magnetic data show the BMA as part of a group of linear magnetic anomalies. As the linear anomaly north of the BMA is associated with exposed supracrustals, migmatites and shear zones within the Natal thrust terranes we assume a similar source for the BMA. This source geometry, constrained by seismic and MT data, fits potential field data over the BMA and other magnetic linear anomalies in the south-central and south-western Karoo. In these models the bodies deepen from ~5 km towards the south, with horizontal extents of ~20-60 km and vertical extents of ~10-15 km. Densities range from 2800- 2940 kg/m^3 and magnetic susceptibilities from 10 to 100 x 10^{-3}

SI. These magnetic susceptibilities are higher than field values from supracrustal rocks (10-60 x 10^{-3} SI) but could be due to the fact that no remanent magnetisation was included in the model. The lithologies associated with the different linear anomalies vary as is evident from varying anomaly amplitudes. The strong signal of the BMA is linked to high magnetic susceptibility granulite facies supracrustals (~10-50 x 10^{-3} SI) as seen in the Antarctic, where the mobile belt continued during Gondwana times.

Keywords: Beattie anomaly; mobile belt; magnetic field; forward modelling

4.2 Introduction

The Beattie magnetic anomaly (BMA) that runs along almost the entire southern portion of South Africa (Figure 4-1) was first recognised in the early 1900s (Beattie, 1909) but even today its source is the matter of an ongoing debate. On the east coast, where the BMA source is at its shallowest, it is truncated by the Agulhas fracture zone, implying that the body causing the anomaly formed prior to Gondwana breakup (Pitts *et al.*, 1992).

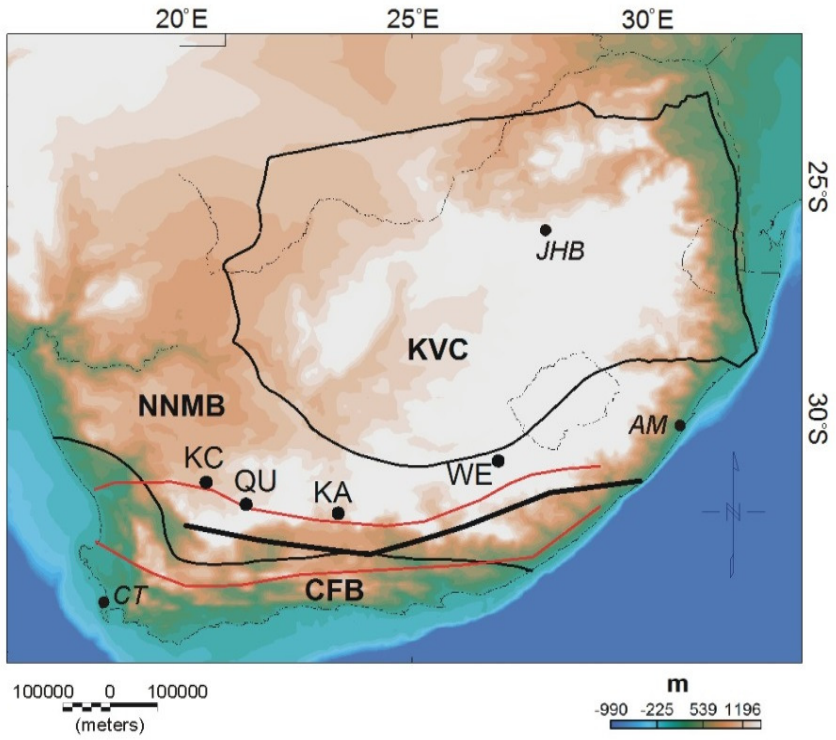

Figure 4-1. Topographic map of South Africa (Amante and Eakins, 2009) with the major tectonic provinces outlined (thin black lines). These include the Archean Kaapvaal Craton (KVC), surrounded by the Namaqua-Natal mobile belt (NNMB), and the deformed Cape Fold Belt (CFB) in the south. The outline of the Southern Cape Conductive Belt (red lines), and the maximum axis of the Beattie Magnetic Anomaly are shown (thick black line). The location of deep SOEKOR boreholes that intersect basement is labelled (black circles, KA1/66, KC1/70, QU1/65 and WE1/66, Eglington and Armstrong (2003)). The cities of Johannesburg (JHB), Cape Town (CT) and Amanzimtoti (AM) are shown.

Several geophysical studies have been conducted to better understand the source of the magnetic anomaly. One of these includes a large-scale magnetic survey carried out in southern South Africa in the early 1970s (and later extended), which led to the identification of the Southern Cape Conductive Belt (SCCB, Figure 4-1) (Gough *et al.*, 1973, de Beer *et al.*, 1982, de Beer and Gough, 1980). This 140 km broad and 1000 km long conductive zone that runs east-to-

west across southern South Africa was suggested to be linked to a lower crustal or upper mantle source. The rough coincidence of the SCCB and BMA led to the proposal of a common source, namely a dipping slab of serpentinized oceanic crust representing a Pan African suture zone (~500 Ma) (de Beer *et al.*, 1982, de Beer and Meyer, 1983, Hälbich, 1993, de Beer *et al.*, 1974). A receiver function study recognised discontinuities at ~8-11 km and ~18 km depth at four seismic stations in this region that were attributed to this slab (Harvey *et al.*, 2001). The BMA and SCCB show no special correlation with younger (≤180 Ma) large-scale geological features such as the edge of the inland plateau (Figure 4-1).

Studies by Corner (1989) correlating geological and magnetic data, led to the hypothesis that the BMA forms part of the NNMB basement rocks. Corner (1989) proposed water movement and mineralization along low-angle thrust zones within the basement as the source, as well as the extension of the BMA into Antarctica. Thomas et al. (1992b) in turn suggested that the BMA is one of several magnetic linear anomalies visible along the east coast of South Africa, which are associated with shear zones within the Natal basement. The magnetic linear anomaly north of the BMA close to Amanzimtoti was labelled the Williston anomaly (Figure 4-1), and the Mbashe anomaly was identified to the south of the BMA (Thomas *et al.*, 1992b).

Several geophysical studies have been conducted in recent years in the south-western Karoo linked to the Inkaba yeAfrica project, which have explored deeper basement structures including the BMA. These include magnetotelluric (MT) studies (Weckmann *et al.*, 2007a, Weckmann *et al.*, 2007b), as well as a near-vertical reflection study (Lindeque *et al.*, 2007, Lindeque *et al.*, 2011) and wide-angle refraction studies (Stankiewicz *et al.*, 2007, Stankiewicz *et al.*, 2008). These studies placed the source of the anomaly in the south-western Karoo at a depth of between 5 and 15 km within the mid-crust.

A comprehensive magnetic modelling study by Quesnel et al. (2009) showed that two wide, highly-magnetised sheet-like prisms (~80 km, > 5 $A.m^{-1}$) provide the best-fit for the BMA. Tankard et al. (2009) used geological and

geophysical data to attribute the BMA to volcanic rift fill, while the SCCB is linked to upthrust mantle using teleseismic Moho depths.

Despite these comprehensive studies of the BMA, a more detailed investigation of existing magnetic and gravity data over the anomaly is needed. In this study we present an integrated analysis using these and other geophysical data to identify the source of the anomaly. We also investigate similar linear magnetic anomalies within the Natal Belt, one of which partly outcrops north of the Beattie on the east coast of South Africa. Newly investigated links between geology and magnetic anomalies in this region are extended to the source of the Beattie.

4.3 Geology of the Namaqua-Natal Metamorphic Belt and Cape Fold Belt

The source of the BMA is covered across its entire extent by younger sediments. To the north of the anomaly Namaqua-Natal mobile belt (NNMB) basement rocks are exposed, while to the south deformed Cape Supergroup rocks are exposed in the Cape Fold Belt (CFB). As several previous geophysical studies have linked the anomaly to this mobile belt (Corner, 1989, Thomas *et al.*, 1992b, Weckmann *et al.*, 2007b), we investigate the exposed Natal portion of the belt on the east coast of South Africa.

The NNMB abuts the KVC and dates to the formation of Rodinia around 1 Ga (Jacobs *et al.*, 1993). This belt can be traced through the Falkland Plateau to Western Dronning Maud Land in east Antarctica as these regions were joined during Gondwana times (Jacobs *et al.*, 1997, Grantham *et al.*, 2001, Frimmel, 2004).

While commonly thought of as one continuous belt, several studies have highlighted differences between the Natal and Namaqua belts. The Natal crust in the east has been identified as entirely juvenile with isotope model ages younger than ~1.5 Ga (using Rb-Sr, Sm-Nd and U-Pb dating; Eglington *et al.*, 1989, Thomas and Eglington, 1990); while the Namaqua crust in the northwest contains older fragments of crust (2.0-1.7 Ga, using U-Pb and Sm-Nd dating; Raith *et al.*,

2003, Robb *et al.*, 1999) as well as juvenile fragments identified using isotope dating (Geringer *et al.*, 1994, Cornell *et al.*, 1986). Isotopic analysis of basement rocks from deep SOEKOR boreholes (KA1/66, KC1/70, QU1/65 and WE1/66 in Figure 4-1) was used to define a boundary between the Namaqua and Natal Belts in the south-western Karoo (Eglington and Armstrong, 2003, Eglington, 2006). Most importantly, borehole QU1/65 contains basement rocks from both terranes and is therefore on the boundary between the two belts. These data confirm the boundary previously suggested using geophysical data (de Beer and Meyer, 1984, Thomas *et al.*, 1992b).

The Natal Belt developed as a result of oceanic-arc tectonics, with arc complexes forming in a basin to the south and accreting onto the KVC to the north during basin closure (Cornell *et al.*, 2006) (Figure 4-2). The oceanic/island-arc of the Tugela terrane was emplaced onto the craton boundary between 1155 and 1140 Ma, followed by the accretion of the Mzumbe-Margate terranes between ~1091 and ~1070 Ma (age estimates vary slightly from study to study) (McCourt *et al.*, 2006). Subsequent crustal thickening resulted in regional deformation fabrics and metamorphism. During the intrusion of the Oribi Gorge Suite (pulses at 1070 and 1030 Ma), the regime of deformation changed from northward-vergent fold and thrust tectonics, to ENE-trending sinistral shear (Eglington and Armstrong, 2003, Jacobs *et al.*, 1993), resulting in the formation of large shear zones. This change in the tectonic regime was most likely due to continued northeast-southwest convergence along the approximately east-west craton margin (Jacobs and Thomas, 1994).

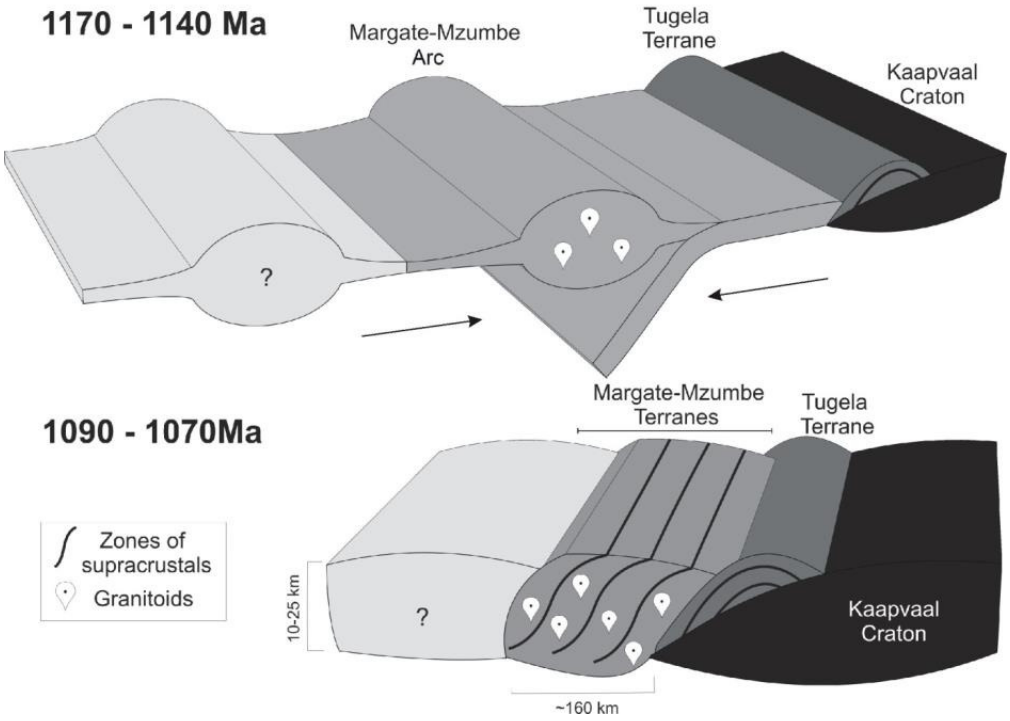

Figure 4-2. Schematic diagram illustrating the evolution of the Natal Belt between 1170 to 1140 Ma and 1090 to 1070 Ma (modified from McCourt *et al.*, 2006). During the earlier period the Tugela terrane accreted onto the Kaapvaal Craton, and granites (oldest intrusives) intruded the supracrustals and associated rocks of the Mzumbe-Margate arc. Between 1090 and 1070 Ma the Mzumbe and Margate terranes accreted onto the Tugela terrane-KVC margin, and S-type granitoids intruded the Mzumbe-Margate terranes.

These large-scale shear zones commonly define terrane boundaries. The Tugela terrane at amphibolite and greenschist facies is separated by the ENE-trending Lilani-Mabigulu shear zone from the upper amphibolite (and locally granulite) facies Mzumbe terrane. The Melville thrust and associated shear zone (Lovat shear zone) in turn forms the boundary to the Margate terrane in the south, which has been metamorphosed to granulite facies (Jacobs *et al.*, 1993, Thomas, 1989). An additional shear zone, the Vungu shear zone, has most recently been mapped by Voordouw (2010) further south of the Melville thrust.

Lithostratigraphic units making up the Mzumbe and Margate terranes include the supracrustal gneisses of the Mapumulo and Mzimkulu Groups respectively, as well as S-type orthogneisses that are the oldest intrusives (Stratigraphy), 1980). Younger rocks within the Mzumbe terrane include S-type granitoids and mafic intrusions (Equeefa Suite), and the more recent A-type plutons of the Oribi Gorge Suite (McCourt *et al.*, 2006).

The Mapumulo metamorphic rocks of the Mzumbe terrane are subdivided into the Quha and Ndonyane Formations in the south, while rocks in the northern part of the terrane are yet unclassified. There formations comprise heterogeneous layered gneisses (supracrustals) and migmatites with a wide range of compositions (Thomas, 1992). These deformed units originate mainly from sedimentary and volcanic/volcaniclastic rocks, and to a less extent extruded and/or eroded products from juvenile volcanic arcs (Thomas *et al.*, 1992a, Thomas and Eglington, 1990). Several rocks within this terrane would be expected to be highly magnetic, such as prominent layers (~1 m) of fine-grained banded magnetite quartzite, grunerite and garnet in the north of the Mzumbe terrane (Scogings *et al.*, 1984). Serpentinite and amphibolite are found closely associated with these supracrustals.

A study by Maré and Thomas (1998) of one of these Oribi plutons led to the proposal that the strong magnetic signal associated with these plutons is due to the plutons themselves, as well as remnants of the supracrustal Mapumulo suite gneisses beneath the plutons. More specifically those from the Ndonyane Formation displayed the largest measured magnetic susceptibilities (0.2 to 22.8 x 10^{-3} SI) and a Königsberger ratio of ~4, i.e. significant remanent magnetisation. A range of palaeomagnetic results were collected for these supracrustal rocks though a single virtual palaeomagnetic pole position could not be defined. Microscope studies by Máre and Thomas (1998) show that magnetite is the dominant opaque phase in the Ndonyane gneisses of the Mapumulo group, while within the Oribi Gorge suite ilmenite dominates. Opaque mineral grains in the study range from 10 to 200 μm.

Exposed older rocks exist within the Cape Supergroup south of the BMA (including the Gamtoos, Kango and Kaaimans Groups; Söhnge and Hälbich, 1983). These rocks have been used to support the ideal that the BMA forms part of a Pan African suture zone between the NNMB and these Saldanian rocks below the CFB (de Beer *et al.*, 1982, Pitts *et al.*, 1992, Harvey *et al.*, 2001, Hälbich, 1993). More recent work, however, has suggested that these metasediments form part of the precursor rift sequences of the Cape Supergroup (Barnett *et al.*, 1997). The question still, therefore, exists whether the NNMB continues below the Cape Supergroup.

4.4 Previous Geophysical Studies

Recent geophysical studies in the western Cape have attempted to shed light on the broader tectonic setting of the BMA, as well as the horizontal and vertical extents of the source body. During Inkaba yeAfrica geophysical surveying in the western Cape, Weckmann et al. (2007a, 2007b) identified anomalous MT zones associated with the BMA that are attributed to a crustal-scale shear zone in the NNMB, with graphite mineralization, similar to those suggested by Thomas et al. (1992b). Weckmann et al. (2007a) also attributed the SCCB to higher than expected conductivity levels within the NNMB. Initial suggestions of serpentinized oceanic crust as the source of the SCCB (de Beer *et al.*, 1982, de Beer and Meyer, 1983, Hälbich, 1993, de Beer *et al.*, 1974) can also be argued against as serpentinite has been shown to be a poor electrical conductor (Airo and Loukola-Ruskeeniemi, 2004, Reynard *et al.*, 2011, Kawano *et al.*, 2012). Studies have shown that it is high salinity fluids moving through the serpentinite that increases its conductivity (e.g. serpentinite in the mantle wedge above a subduction zone has a conductivity of 0.001 S/m, while with circulating saline fluids this value increases to 0.1–1 S/m (Reynard *et al.*, 2011)). In addition, the SCCB stretches from the east to the west coast of South Africa whereas the BMA does not.

From reflection seismic data, Lindeque et al. (2007) suggested that the BMA is a strata bound massive sulphide-magnetite deposit flanked by smaller

deposits with overlapping metasomatic aureoles, with some of these deposits being conductive and magnetic while others are one or the other. Several of these regions correlate with high velocity zones on the refraction seismic data (Stankiewicz *et al.*, 2007). Lindeque et al. (2007) compared this deposit to the Bushmanland ore district within the Namaqua basement, though the Bushmanland deposits are significantly smaller (<10 km extent) (Bailie *et al.*, 2007). Lindeque *et al.* (2011) also suggested that since no suture zone is visible on the seismic data, the NNMB continues below the Cape Supergroup. However, near-vertical features are not easily visible on seismic data. Anomalous geophysical regions are correlated across datasets in the modelling section of this study. Similar parabolic reflectors are seen on some of the historic SOEKOR seismic profiles collected in the 1970s (Fatti, 1970).

Basic potential field modelling of the anomaly by Pitts et al. (1992) showed the BMA as a 30 km wide south dipping slab. This model could not, however, clearly resolve whether serpentinized crust or another rock type is the cause of the anomaly. Similarly, basic magnetic modelling by Weckmann et al. (2007a) defined the BMA source as 100 to 150 km wide (with a minimum width of 50 km if remanence is included). This body correlates with mid-crustal zones of high resistivity on the MT data and regions of high seismic velocity (Stankiewicz *et al.*, 2007), while the high conductivity anomaly is modelled as a fault or shear zone within this magnetic body.

The two wide highly-magnetised sheet-like prisms identified as the source geometry by Quesnel et al. (2009) were modelled at depths of 9-12 km and 13-18 km, one of which coincides with a high velocity region. Quesnel et al. (2009) proposed that these prisms represent granulite-facies mid-crustal rocks within the NNMB. These models are a good starting point; however, predefined geometrical shapes used during modelling seldom reflect geology and therefore will be expanded on in this study.

Tankard et al.'s (2009) suggestion that the SCCB can be attributed to upthrust mantle can be argued against as the teleseismic data are interpolated to

draw this conclusion, and no evidence for upthrusting is seen on the refraction seismic images from Stankiewicz et al. (2008).

In this study we use these geological observations, as well as magnetic filtering and potential field modelling constrained by these seismic and MT data, to better understand which of these anomaly sources are more feasible.

4.5 Data

4.5.1 Regional

Datasets used to investigate the BMA in this study include the regional free air anomaly data (Venter *et al.*, 1999) as well as regional aeromagnetic data (Stettler *et al.*, 1999) (Figure 4-3). The magnetic data (Figure 4-3a) were collected by the Council for Geoscience from the 1980s to late 1990s, flown at a line spacing of 1 km and sample spacing of around 60 m. The flight height for the survey was between 100-150 m. Poor magnetic data in the south over the Cape Fold Belt due to variable flight heights over the mountains make interpretation of these data difficult. The final aeromagnetic anomaly has been calculated with respect to the normal Earth magnetic field (Intensity: 28,500 nT, Declination: -23˚, Inclination: -66˚).

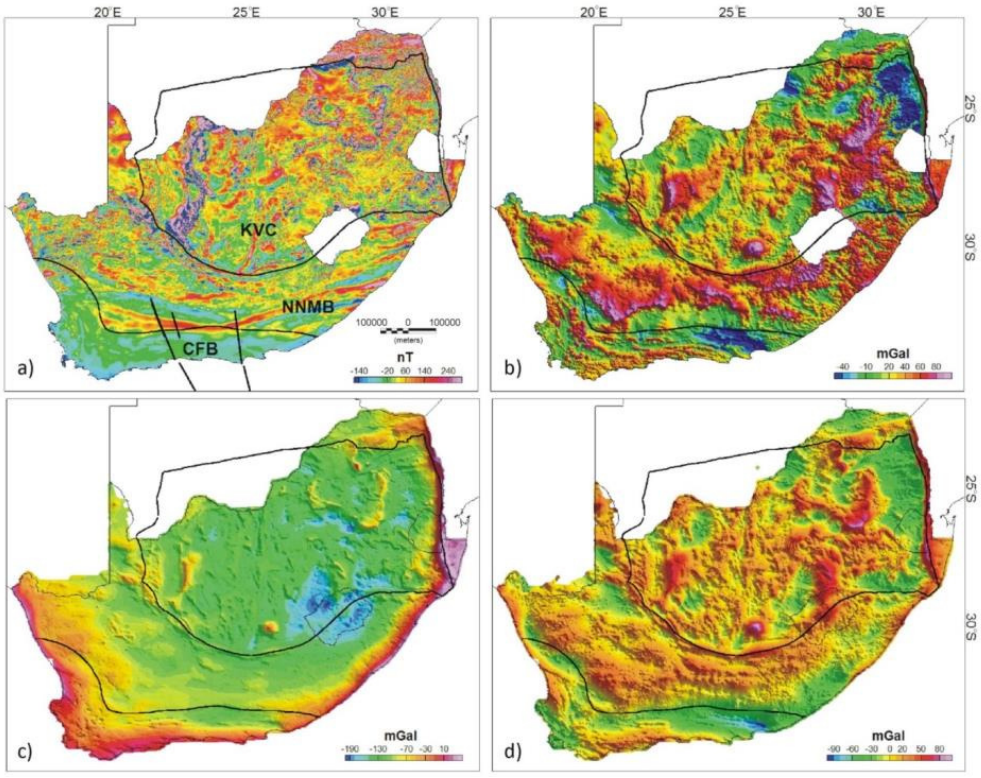

Figure 4-3. (a) Aeromagnetic total intensity; (b) free-air gravity; (c) Bouguer gravity and (d) isostatic anomaly maps for South Africa. Major tectonic provinces are outlined (see Figure 4-1 for details). Coincident geophysical profiles collected over the south-western and south-central portion of the BMA are indicated in (a) (black lines), including a refraction seismic line (Stankiewicz *et al.*, 2007), magnetotelluric profiles (Weckmann *et al.*, 2007a, Weckmann *et al.*, 2007b), reflection seismic profile (Lindeque *et al.*, 2011), and offshore seismic lines (Parsiegla *et al.*, 2007, Parsiegla *et al.*, 2008). A vibroseis line (Loots, 2013) was collected between the two profiles.

The gravity data were collected with a station spacing of approximately 14 km. The free-air gravity anomaly map is shown in Figure 4-3b. The ETOPO1 topographic model with a resolution of 1 arc-min (Amante and Eakins, 2009) was used for the calculation of the Bouguer anomaly (BA, Figure 4-3c). The density used for the Bouguer correction is 2670 kg/m^3. The terrain corrected gravity data released by the CGS was not used, as several of the elevation measurements were

made using barometers which can introduce an error of 2–5 mGal (Leaman, 1984). In addition, the vertical uncertainty of the ETOPO1 data is 10 m therefore making it insufficient to recalculate the terrain correction. The isostatic anomaly map is calculated assuming an elastic thickness (Te) of 5 km, reference depth of 35 km and density contrast of 400 kg/m between the crust and the mantle (Figure 4-3d).

4.5.2 Petrophysical studies

Petrophysical data are necessary for constructing realistic potential field models over the BMA, and are drawn from the Natal mobile belt. Field observations reveal the rapid change in rock types and magnetic susceptibilities over small distances within this highly sheared Natal terrane. For example, magnetic susceptibility measurements made close to the boundary between the Mapumulo metamorphic rocks and Margate Granite Suite showed a change from granite (3 x 10^{-3} SI), to gneiss (6 x 10^{-3} SI), to migmatite (12 x 10^{-3} SI), and back to the gneiss and granite (9 and 2 x 10^{-3} SI respectively) over a distance of ~0.5 m. Less than 100 m further west a magnetic susceptibility measurement of less than 1 x 10^{-3} SI was obtained for a similar gneiss. Thin section analysis confirmed that the dominant opaque mineral is magnetite, with samples containing between 1 and 3% opaque minerals.

Magnetic susceptibility data from the CGS Petrophysical Properties Atlas (Maré, 2012) help identify which rock types are associated with magnetic anomalies in this region. Data for the Mzumbe terrane and associated rock types are shown in Figure 4-4 and for the Margate terrane in Figure 4-5. For the supracrustal rocks in the Mzumbe terrane, a large number of samples have magnetic susceptibilities > 10 x 10^{-3} SI, with the highest value recorded for a gneiss (62 x 10^{-3} SI). Several serpentinite and amphibolite samples are closely associated with the Mzumbe supracrustal rocks, with two samples displaying high susceptibilities (41 and 45 x 10^{-3} SI respectively). For the Mzumbe orthogneiss suites the highest magnetic susceptibilities are for gneisses, which are an order of

magnitude smaller than several of the supracrustal samples (< 10 x 10^{-3} SI). For the Mzumbe mafics and younger granitoids (S-type) the magnitudes are similar to those for the orthogneisses, except for a granite sample that is an order of magnitude larger (55 x 10^{-3} SI) and several monzonite and syenite samples (10 - 25 x 10^{-3} SI). These high susceptibility samples form part of the Sezela Suite that is concentrated just inland from the town of Pennington on the east coast.

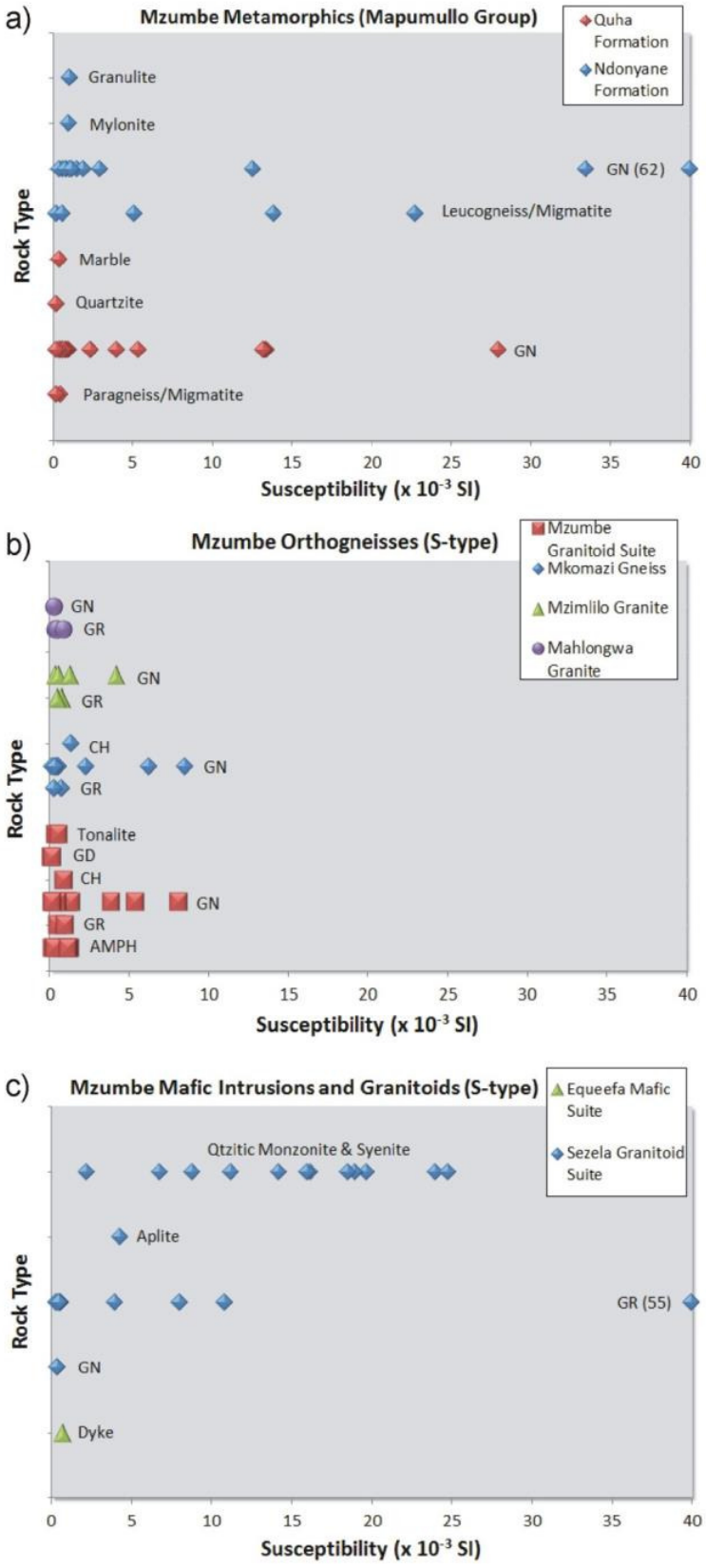
a)
Mzumbe Metamorphics (Mapumullo Group)
Quha Formation
Ndonyane Formation
Granulite
Mylonite
GN (62)
Leucogneiss/Migmatite
Marble
Quartzite
GN
Paragneiss/Migmatite
Rock Type
0 5 10 15 20 25 30 35 40
Susceptibility (x 10-3 SI)
b)
Mzumbe Orthogneisses (S-type)
Mzumbe Granitoid Suite
Mkomazi Gneiss
Mzimlilo Granite
Mahlongwa Granite
GN
GR
GN
GR
CH
GN
GR
Tonalite
GD
CH
GN
GR
AMPH
Rock Type
0 5 10 15 20 25 30 35 40
Susceptibility (x 10-3 SI)
c)
Mzumbe Mafic Intrusions and Granitoids (S-type)
Equeefa Mafic Suite
Sezela Granitoid Suite
Qtzitic Monzonite & Syenite
Aplite
GR (55)
GN
Dyke
Rock Type
0 5 10 15 20 25 30 35 40
Susceptibility (x 10-3 SI)

Figure 4-4. Magnetic susceptibility measurements (x 10^{-3} SI) for several geological units within the Mzumbe Terrane, including the (a) supracrustal rocks of the Mapumulo Group, (b) orthogneisses (S-type), and (c) mafic intrusions and granitoids (S-type). Different suites or formations within these units are marked with different colours. Rock types are labelled, with the common ones abbreviated: AMPH – amphibolite, CH – charnockite, GN – gneiss, GR – granite, SERP - serpentinite. High magnetic susceptibility values which plot off the chart are included in brackets. For the supracrustal rocks in (a), the highest magnetic susceptibilities are for gneisses (> 20 x 10^{-3} SI). For the orthogneisses in (b) magnetic susceptibility values overall are significantly lower (< 10 x 10^{-3} SI). For the Mzumbe mafics and granitoids (S-type) in (c), the highest magnetic susceptibility is 55 x 10^{-3} SI for a granite and for monzonite and syenite samples (< 25 x 10^{-3} SI), while the remaining samples have smaller values (< 10 x 10^{-3} SI).

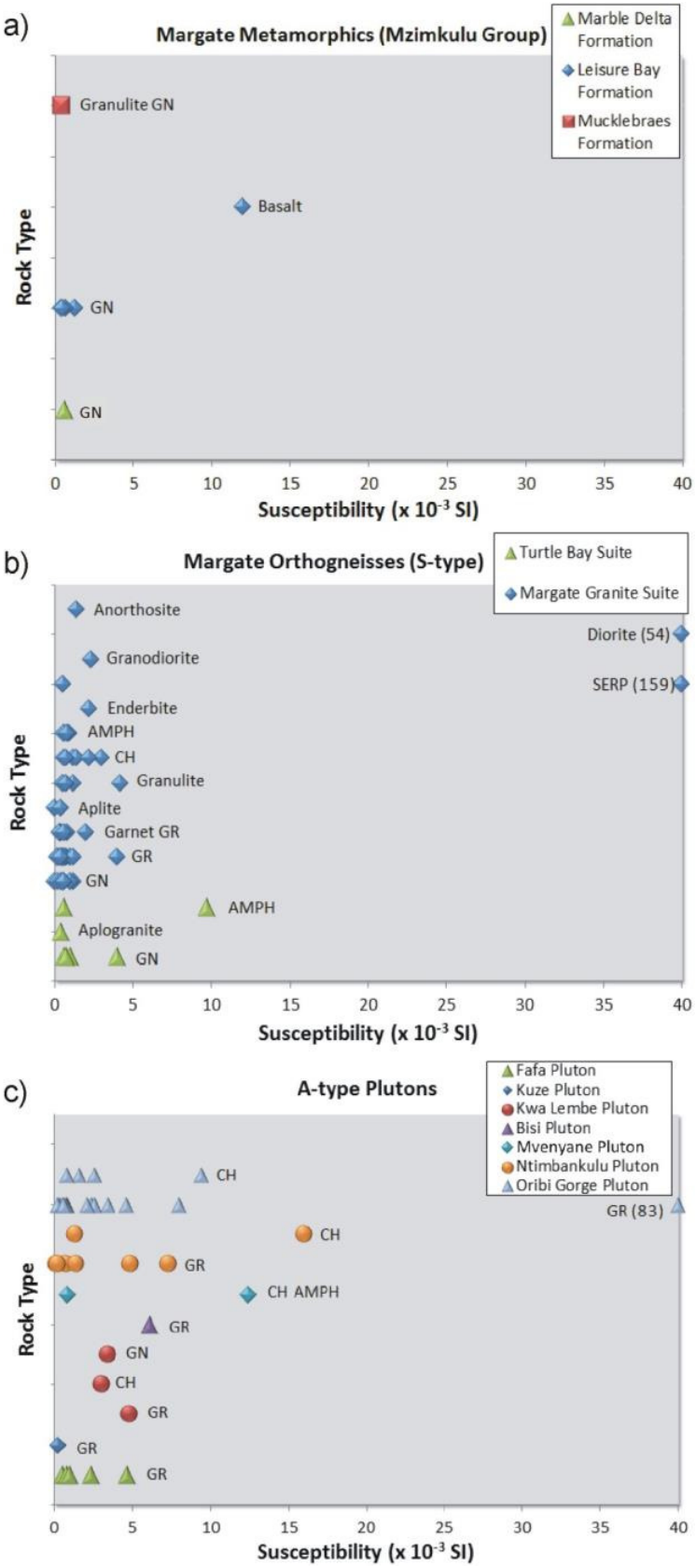
a)
Margate Metamorphics (Mzimkulu Group)
Marble Delta Formation
Leisure Bay Formation
Mucklebraes Formation
Granulite GN
Basalt
GN
GN
Rock Type
0 5 10 15 20 25 30 35 40
Susceptibility (x 10-3 SI)
b)
Margate Orthogneisses (S-type)
Turtle Bay Suite
Margate Granite Suite
Anorthosite
Diorite (54)
Granodiorite
SERP (159)
Enderbite
AMPH
CH
Granulite
Aplite
Garnet GR
GR
GN
AMPH
Aplogranite
GN
Rock Type
0 5 10 15 20 25 30 35 40
Susceptibility (x 10-3 SI)
c)
A-type Plutons
Fafa Pluton
Kuze Pluton
Kwa Lembe Pluton
Bisi Pluton
Mvenyane Pluton
Ntimbankulu Pluton
Oribi Gorge Pluton
CH
GR (83)
CH
GR
CH AMPH
GR
GN
CH
GR
GR
GR
Rock Type
0 5 10 15 20 25 30 35 40
Susceptibility (x 10-3 SI)

Figure 4-5. Magnetic susceptibility measurements (x 10^{-3} SI) for several geological units within the Margate Terrane, including the (a) supracrustal rocks of the Mzimkulu Group and (b) orthogneisses (S-type), and (c) Oribi Gorge plutons (A-type) from both the Mzumbe and Margate terranes. See Figure 4-4 for details. For the supracrustal rocks in (a), the highest magnetic susceptibilities are for a basalt (12 x 10^{-3} SI), while the remaining recorded values are < 2 x 10^{-3} SI. For the orthogneisses in (b) the highest magnetic susceptibilities are for a diorite (54 x 10^{-3} SI) and serpentine (159 x 10^{-3} SI), while the remaining samples have magnetic susceptibilities of < 10 x 10^{-3} SI. For the Margate Plutons (A-type) in (c) magnetic susceptibilities of < 16 x 10^{-3} SI are recorded, while one granite has a measured magnetic susceptibility of 83 x 10^{-3} SI.

Within the Margate terrane, magnetic susceptibility values for supracrustal rocks are lower than for the Mzumbe terrane, though there are fewer samples most likely due to a lack of exposure. The highest magnetic susceptibility for the supracrustal rocks is for a basalt sample (12 x 10^{-3} SI), while the remainder of samples (gneiss and granulite) display magnetic susceptibility values of < 2 x 10^{-3} SI. For the Margate orthogneiss suite, amphibolite, gneiss, granite and granulite samples have magnetic susceptibilities < 10 x 10^{-3} SI, while two diorite and serpentine samples have magnetic susceptibility values > 50 x 10^{-3} SI. The younger Oribi Gorger Pluton (A-type) samples show magnetic susceptibilities of < 15 x 10^{-3} SI, with one granite with a high magnetic susceptibility (83 x 10^{-3} SI).

Magnetic susceptibility measurements in Figure 4-4 and Figure 4-5 show a broad range of magnetic rocks within these terranes, though the supracrustal rocks of the Mzumbe terrane show consistently higher values distributed over a larger area. To confirm whether these supracrustals (and associated migmatites) are the source of the magnetic linear anomalies north of the BMA, it is necessary to investigate the distribution of the lithologies relative to the anomalies. This analysis focuses on the Mzumbe terrane as the Margate terrane has limited exposure.

4.6 Magnetic Field Analysis and Forward Modelling

To gain a broader tectonic understanding of these magnetic linear anomalies identified by Thomas et al. (1992b), we investigate the high-pass (HP) filtered map for South Africa. We test a range of cut-off wavelengths for this filter (25, 50, 70, 100 and 125 km) to isolate short, long and intermediate wavelength patterns. Additional filters are applied to the magnetic data on the east coast of South Africa. While there is not an exact correlation between anomaly wavelength and source depth, automatic depth methods commonly use wavelength as a proxy for depth to source, i.e., longer wavelengths are associated with deeper sources. Hence here we have used these filters to approximate the depth of the sources associated with these anomalies. High-pass filtered data is used to highlight shallower magnetic features, while low-pass (LP) filtered data highlights regional structures at mid-crustal levels. The tilt derivative (TDR) map highlights the orientation of the linear tectonic fabric of the basement as the TDR is positive over a source and negative elsewhere (Miller and Singh, 1994, Verduzco *et al.*, 2004). The pseudogravity, which is calculated from the magnetic data, allows for comparison with the Bouguer anomaly map. Similarities between the two would imply common deeper sources for the anomalies (Baranov, 1957). The magnetic signal over the BMA at its shallowest on the east coast was also investigated to shed light on the nature of the source.

In addition, we carried out 2D modelling of potential field data using GM-SYS (Geosoft Oasis Montaj). Gravity and magnetic model responses were calculated using the methods of Talwani *et al.* (1959) and Talwani and Heirtzler (1964), and using the algorithms described by Won and Bevis (1987). Models were created along the two approximately north-south Inkaba yeAfrica profiles in the south-western Cape shown in Figure 4-3a. During modelling free-air anomalies were modelled using an accurate terrain model.

4.7 Results

4.7.1 Magnetic Linear Anomalies within Mobile Belts

The extent of the Natal Belt has previously been defined using the change in the magnetic signal in the west from broad highs and lows to a more complex signal over the Namaqua terrain (Figure 4-6a). This pattern of magnetic linear anomalies is more easily seen on a HP filtered image of the region (50 km wavelength cut-off, Figure 4-6b). Magnetic linear anomalies north and south of the BMA that are subparallel to the craton are easily delineated. The extent of the Williston anomaly to the north of the BMA was debated by Thomas et al. (1992b) who previously studied the total magnetic intensity (TMI) map. From this HP-filtered image we confirm that the Williston anomaly extends further to the west where the signal is dwarfed by the BMA. These anomalies, as well as isotopic analysis by Eglington and Armstrong (2003) help define a rough boundary between the Natal and Namaqua mobile belts as shown in Figure 4-6. This is a refinement of the boundary suggested by previous studies (de Beer and Meyer, 1984, Thomas *et al.*, 1992b).

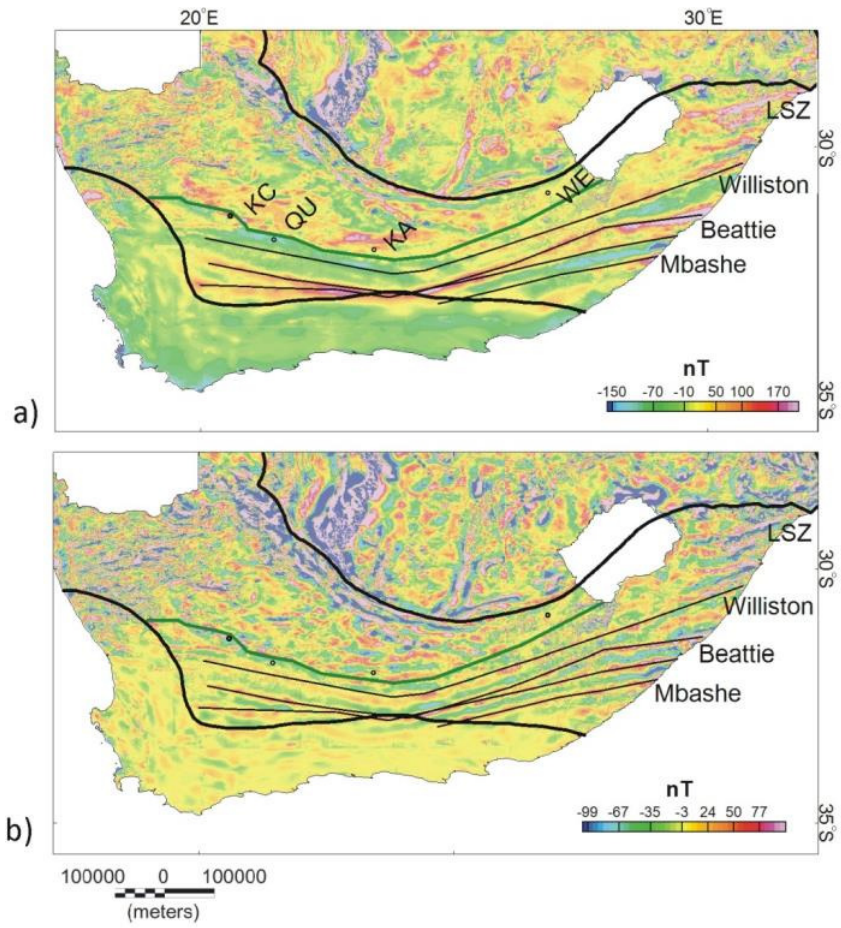

Figure 4-6. (a) Total magnetic intensity (TMI) and (b) high-pass (HP) filtered TMI for South Africa (using a 50 km wavelength cut-off). Alternating subparallel magnetic highs and lows are visible north and south of the BMA and are traced (black lines) and labelled according to Thomas et al. (1992b). The Lilani-Mabigulu shear zone (LSZ) north of these anomalies is labelled. From these traces the continuity of the Williston anomaly to the west is evident. These anomalies as well as borehole analysis by Eglington and Armstrong (2003) were used to define the border between the Natal and Namaqua terranes (green line). The boreholes used (black circles) are labelled in (a) (KA1/66, KC1/70, QU1/65 and WE1/66). Tectonic provinces are outlined (see Figure 4-1 for details).

Figure 4-7 focuses on these magnetic anomalies on the east coast of South Africa within the Natal Belt. A detailed comparison of different lithologies

(Figure 4-7a) with magnetic anomalies (Figure 4-7b) shows the highest correlation with the Mapumulo supracrustal rocks, and more specifically the Ndonyane formation and unmapped formations in the north. The difficulty of mapping rock types in such a complex region where rocks are heavily weathered can add errors to this correlation. There is also a similar trend to these anomalies and the mapped shear zones (Figure 4-7c): the LSZ in the north has a strong magnetic signature, while the Williston anomaly is associated with the Jolivet and Amanzimtoti shear zones; and the high in-between these two anomalies is associated with the Mvoti and Mgeni shear zones. The newly identified Vungu shear zone south of the Melville thrust is not associated with a strong anomaly. It is evident that strong anomalies are also associated with the Oribi Gorge plutons, though these anomalies are more circular in nature.

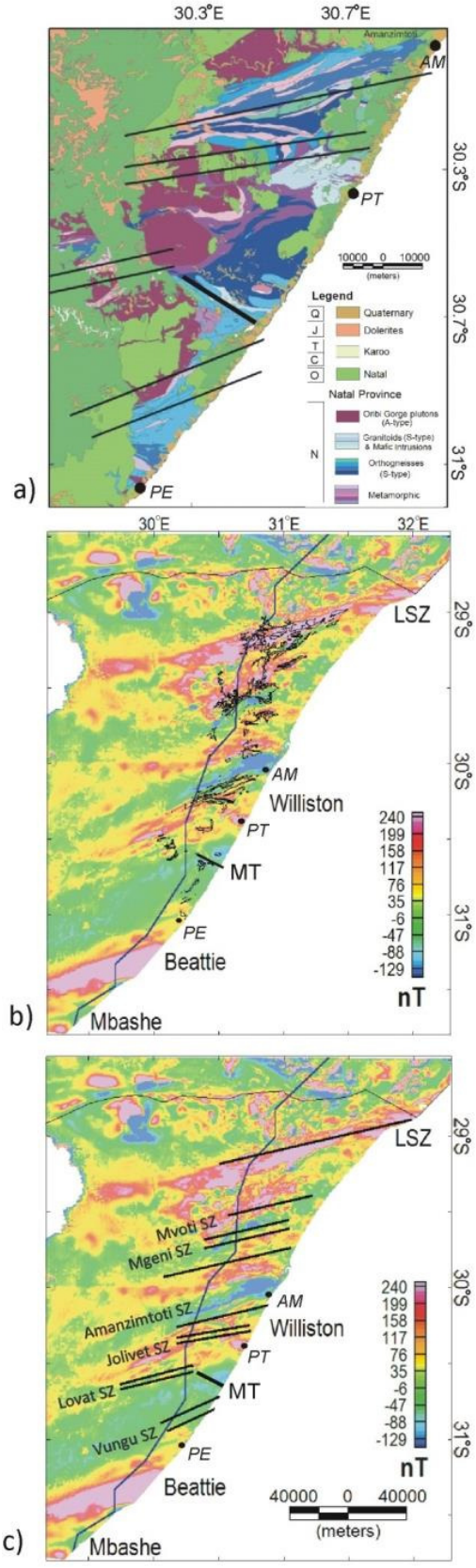
30.3°E
30.7°E
AM
PT
PE
30.3°S
30.7°S
31°S
10000 0 10000
(meters)
Legend
Quaternary
Dolerites
Karoo
Natal
Natal Province
Oribi Gorge plutons (A-type)
Granitoids (S-type) & Mafic intrusions
Orthogneisses (S-type)
Metamorphic
a)
30°E
31°E
32°E
LSZ
29°S
30°S
31°S
AM
Williston
PT
MT
PE
Beattie
Mbashe
240
199
158
117
76
35
-6
-47
-88
-129
nT
b)
Mvoti SZ
Mgeni SZ
Amanzimtoti SZ
Jolivet SZ
Lovat SZ
Vungu SZ
40000 0 40000
(meters)
c)

Figure 4-7. (a) Geological map showing the Mzumbe terrane associated with the Williston anomaly. Shear and thrust zones are marked (black lines, summarised by Voordouw (2010)). Geological time-scales during deposition include the Neoproterozoic (N), Ordovician (O), Carboniferous (C) through to Triassic (T), Jurassic (J) and Quaternary (Q). (b) Total magnetic intensity (TMI) map of the entire Mzumbe terrane with mapped Mzumbe supracrustal gneisses (and associated migmatites) marked. Shear and thrust zones are marked and labelled in (c). The terrane extends from the Lilani-Mabigulu shear zone (LSZ) in the north to the Melville thrust in the south (MT). South of this a small portion of the Margate terrane is exposed. The magnetic linear anomalies (Williston, BMA and Mbashe) are labelled. The Kaapvaal craton boundary is marked with a black line to the north of the LSZ (between these two boundaries is the Tugela terrane). The approximately northeast to southwest extent of younger sedimentary cover is marked (thick black line, Karoo and Natal sediments), east of which basement rocks outcrop. The magnetic highs of the LSZ, Williston and the high in-between are most closely associated with outcropping supracrustal rocks (Mapumulo group) and shear zones. More circular anomalies to the south are associated with the younger Oribi Gorge plutons. Towns include Amanzimtoti (AM), Pennington (PT), and Port Edward (PE) (black circles).

Filtering of the magnetic data allows for an estimation of the source depth for these magnetic linear anomalies. The HP filtered image (Figure 4-8a) shows a similar trend to the magnetic rocks within these mapped shear zones and the high-pass anomalies (Voordouw, 2010). This correlation is also seen on the LP filtered image (Figure 4-8b), except in the case of the most recently mapped Vungu shear zone north of the BMA. This suggests that these shear zones are regional structures extending from upper to mid crustal levels within the basement rocks. The BMA in the south and Lilani-Mabigulu shear zone in the north displays the strongest low-pass anomalies, while the Williston anomaly and magnetic linear anomaly to the north show up as smaller anomalies (which are not continuous to the west on the low-pass map). The tilt derivative image (Figure 4-8c) is used for

mapping these magnetic zones below younger sediments. There is no correlation between the pseudogravity and the isostatic anomaly contours (Figure 4-8d), confirming the Beattie is not associated with a strong gravity anomaly. From these gravity data it can be seen that the BMA is an intra-crustal feature that is not associated with a significant gravity anomaly, and is isostatically compensated.

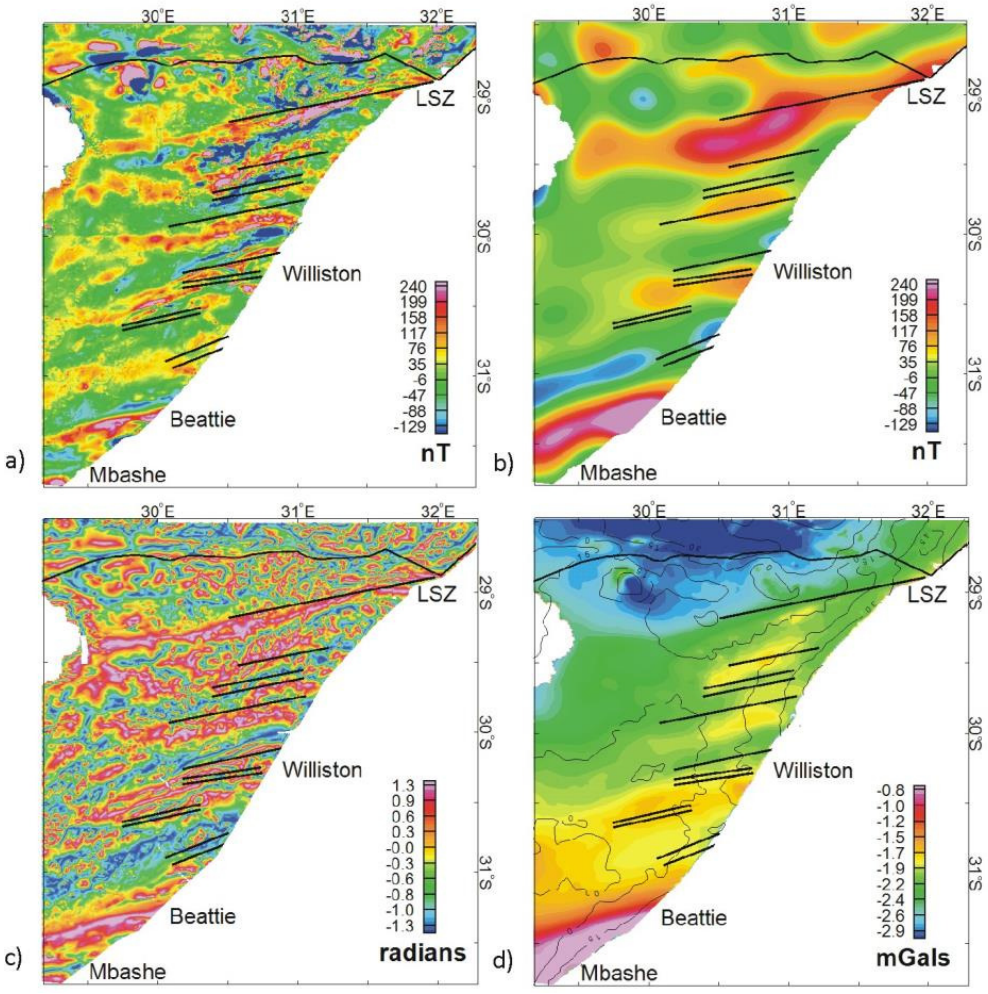

Figure 4-8. (a) High-pass (HP) filtered and (b) low-pass (LP) filtered magnetic data (50 km cut-off), as well as (c) tilt derivative (TDR) and (d) pseudogravity (PG) data and isostatic anomaly contours for the Natal mobile belt on the east coast of South Africa. Magnetic linear anomalies defined by Thomas *et al.* (1992b), as well as major shear zones (black lines) are indicated. See Figure 4-7

for details. There is a similar trend to the HP and LP anomalies and mapped shear zones. The TDR map can be used to better map these zones, while no correlation is seen between the PG and the isostatic anomaly contours (15 mGal interval).

The tilt data, as well as the geological data and existing mapped shear zones, are used to refine the orientation of previously mapped zones of supracrustal gneisses (and associated migmatites) and shear (Figure 4-9). These tilt data also confirm previous extensions by Schmitz and Bowring (2004) of the Tugela and Mzumbe terrane boundaries to the west below younger sediments (Karoo and Natal) using kimberlite studies of lower crustal granulites. The general orientation of shear zones is southwest to northeast, though the trend is east-west closer to the coast. These zones are around 25-40 km wide, though more detailed field mapping is needed wherever possible to confirm or adjust these boundaries.

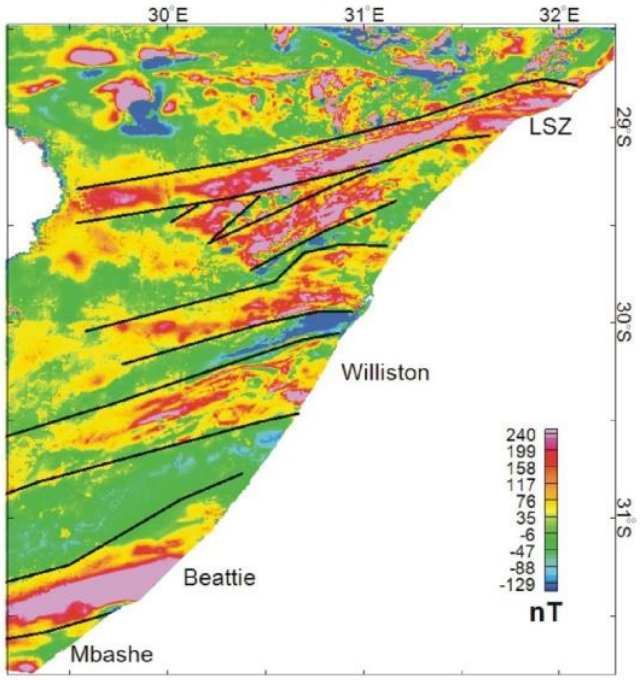

Figure 4-9. TMI image with refined shear zones (black lines) constrained using geology data, previously mapped shear zones and magnetic tilt derivative data.

These magnetic linear anomalies allow us to conclude that the BMA has a similar source as the Williston anomaly, namely Natal supracrustal rocks which form part of thrust sheets later cut by shear zones. This complex nature of the BMA is supported by aeromagnetic data on the east coast where the source is at its shallowest (Figure 4-10). Instead of a smooth broad signal as seen in the south-western Karoo, in the east the broad high of the BMA is more complex. Shorter wavelength anomalies in this region represent younger Karoo dolerite dykes (< 2000 m).

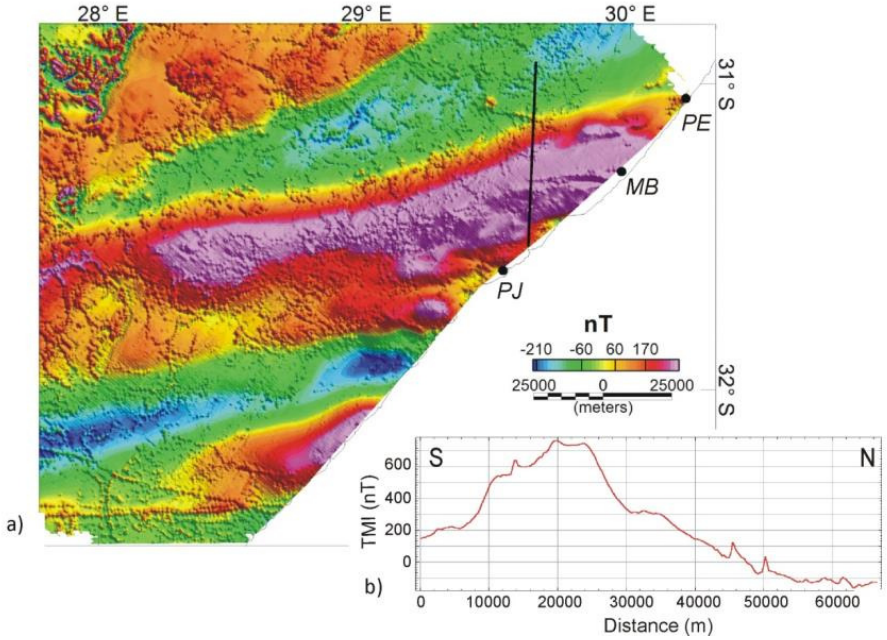

Figure 4-10. (a) Total magnetic intensity map over the BMA on the east coast of South Africa; (b) North-south profile over the BMA at its shallowest on the east coast (location marked with a black line in (a)). The data reveals the complex nature of the source. Towns indicated include Port Edward (PE) and Port St. Johns (PJ), as well as the Mkambati Nature Reserve (MB) (black circles).

4.7.2 Forward Modelling

2D potential field models were created over the BMA in the south-western and south-central Karoo to investigate whether the Natal mobile belt magnetic source geometry can be reconciled with the geophysical data, and to better constrain the petrophysical properties of the source. The western profile was constrained using offshore seismic data from Parsiegla et al. (2007) and onshore refraction data from Stankiewicz et al. (2007, 2008). These seismic data were reprocessed into a single velocity model by Stankiewicz et al. (2008) focusing on deeper structures. Reflection seismic data from Lindeque *et al.* (2011) and magnetotelluric data from Weckmann et al. (2007b) were also used. The existence of a high velocity zone in the lower crust was determined from seismic data (Stankiewicz *et al.*, 2008, Lindeque *et al.*, 2007), and was therefore inferred for the central profile. The shallower lithologies were constrained using borehole data (Rowsell and De Swardt, 1976).

The central profile is less constrained with offshore seismic data from Parsiegla et al. (2008) and onshore refraction data from Stankiewicz et al. (2007), and magnetotelluric data from Weckmann et al. (2007b). We do not model a profile over the eastern extent of the BMA due to limited deep boreholes and a complete lack of seismic data. Previous potential field models over these two profiles were exclusively constrained using seismic data without including the connection to the Natal Belt (Scheiber-Enslin *et al.*, 2012). Teleseismic data collected during the Southern Africa Broadband Seismic Experiment were used to constrain the Moho depths in both models (Nguuri *et al.*, 2001, Harvey *et al.*, 2001).

The density and magnetic susceptibility values used during modelling are shown in Table 4-1. Density values are based on borehole (Rowsell and De Swardt, 1976) and hand sample data from the CGS Physical Properties Atlas (Maré, 2012), as well as P-wave seismic velocity to density conversion curves (Christensen and Mooney, 1995). Magnetic susceptibility values are based on recent field investigations of the Williston anomaly, as well as the physical properties atlas. Maré and Thomas (1998) showed that more comprehensive

studies are needed to better understand the complex remanent magnetisation of the Natal supracrustal rocks, therefore here we include only simplistic models with induced magnetisation.

Table 4-1. Density and magnetic susceptibility values used for potential field modelling.

	Velocity (km/s)	**Density (kg/m3)**	**Susceptibility (x10-3 SI)**
Karoo	5	2550	1
Cape	5.5	2650-2700	1
Upper crust	5.75	2700	1
Middle crust	6.0	2800	8
Magnetic Bodies (MB)	6.25-6.5	2840-2900	100-10
Lower crust	6.5	2900	3
Lowest crust	7.0	3000	-
High velocity zone	7.5	3100-3200	-
Mantle	8.0	3300	-

Figure 4-11 shows the modelled western profile where the BMA appears to split. Due to geological observation from the Natal terrane we model these high amplitude magnetic linear anomalies as thrust sheets, i.e. near vertical slabs of highly magnetic supracrustal rock separated by slabs with lower magnetic susceptibilities that represent either weakly-magnetic supracrustal rocks or later weakly-magnetic intrusives. The dip of these sheets to the south is assumed from the direction of movement during formation of the Natal Belt, i.e. overlap onto the craton in the north, and the dip of high conductivity anomalies from MT data (Weckmann *et al.*, 2007b). This direction is opposite to that determined from reflection seismic data (Lindeque *et al.*, 2011). The density and magnetic

susceptibility values for these anomalous bodies are slightly higher than the surrounding middle crust, with bodies deepening towards the south.

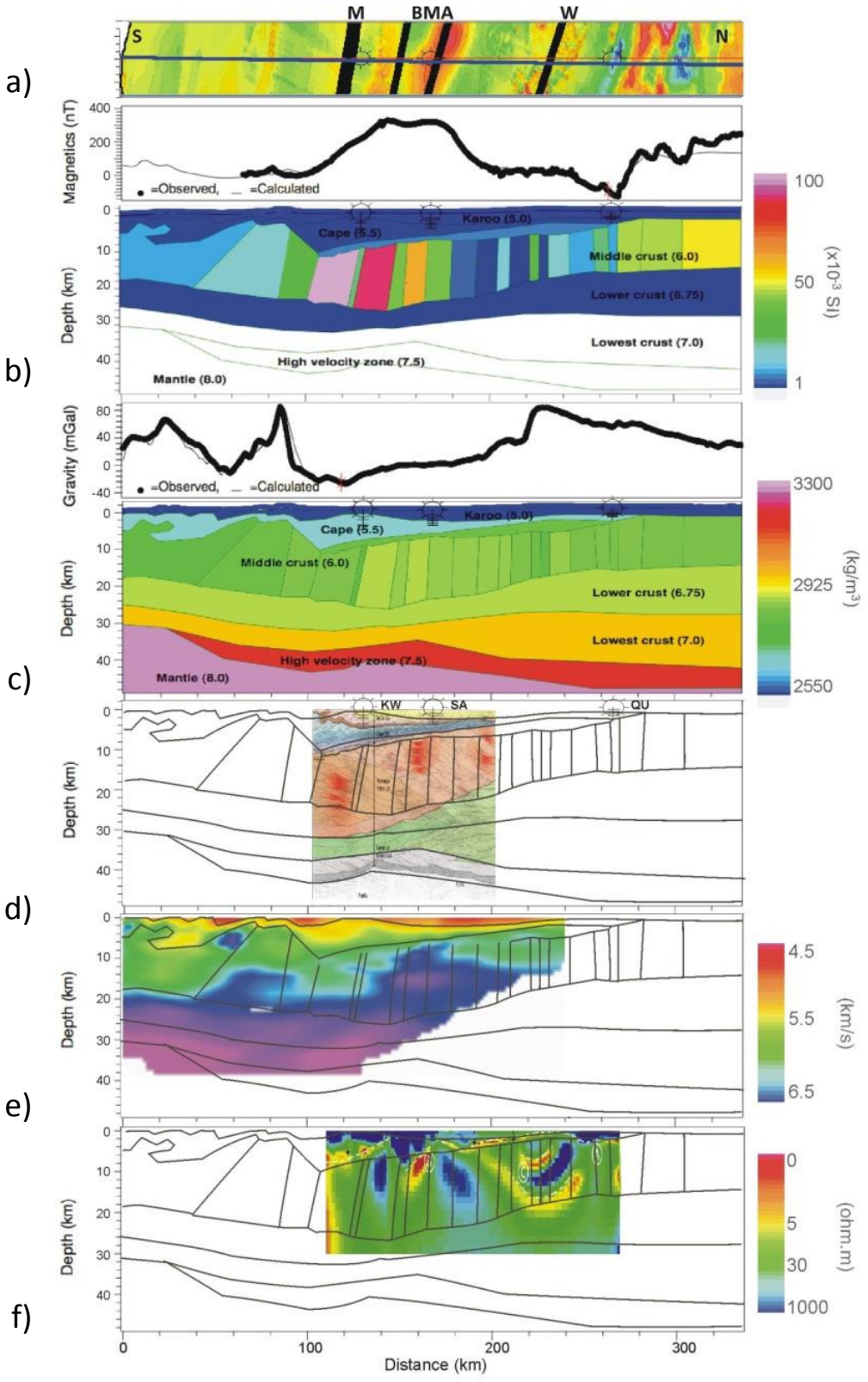
a)
b)
c)
d)
e)
f)
M
BMA
W
S
N
Magnetics (nT)
=Observed, =Calculated
Depth (km)
Cape (5.5)
Karoo (5.0)
Middle crust (6.0)
Lower crust (6.75)
Lowest crust (7.0)
High velocity zone (7.5)
Mantle (6.0)
Mantle (8.0)
Gravity (mGal)
(x10-3 SI)
(kg/m3)
KW
SA
QU
(km/s)
(ohm.m)
Distance (km)

Figure 4-11. (a) High-pass filtered TMI image for the region surrounding the western profile in Figure 4-3a. Traces of magnetic linear anomalies identified in Figure 4-6b are marked with black lines (M-Mbashe, BMA-Beattie Magnetic Anomaly, W-Williston). (b) 2D magnetic model along the profile shown in (a). The upper panel shows the observed magnetic anomaly (thick black line) and calculated anomaly (thin black line). The lower panel shows the created 2D magnetic model, with the different bodies labelled. Seismic refraction velocities for these bodies are included in brackets, and the colour of the body represents the magnetic susceptibility (SI) of the body. Mid-crustal bodies with higher magnetic susceptibilities are used to fit the BMA, Williston and Mbashe anomalies. These bodies correlate with anomalous zones identified on seismic and MT data, and are modelled with increasing depth and magnetic susceptibilities towards the south. The location of SOEKOR deep boreholes used to constrain the depth of the Karoo basin is shown (KW1/67, SA1/67, QU1/65). (c) 2D density model corresponding with the magnetic profile in (b). The upper panel shows the observed free-air anomaly (thick black line) and calculated gravity (thin black line). The lower panel shows the 2D density model (density values in kg/m). (d) Correlated seismic reflection image (Lindeque *et al.*, 2007), (e) seismic refraction image (Stankiewicz *et al.*, 2008), and f) MT resistivity image (Weckmann *et al.*, 2007b) used to constrain the model.

A HP-filtered TMI image is shown in (a) with magnetic linear anomalies from Figure 4-6 marked. Magnetic and gravity models for this profile are shown in (b) and (c) respectively. These magnetic data are correlated with seismic and MT data over the profile. It can be see that the magnetic linear anomalies correlate with zones of complex reflectivity identified on reflection seismic data in (d), and anomalous zones on the seismic refraction and MT data (e-f). This supports the idea of a similar source for the individual bodies. In (e) the linear anomalies correlate with high velocity zones (as would be expected from velocity to density conversion curves), except for the shallowest body associated with the Williston

anomaly. In (f) the Williston anomaly correlates with alternating high-low conductivity synform structures, and the BMA correlates with a steeply dipping high conductivity zone flanked by resistive zones. Quesnel et al. (2009) and Weckmann et al. (2007a) assume during magnetic modelling that the high resistivity regions identified on MT data are the source of the BMA, separated by a shear zone or fault. In our model the bodies are closely associated with the highly resistive regions, though the region of high conductivity does overlap with a high magnetic susceptibility body.

The depths of these bodies range from 5 to 15 km for the Williston anomaly, 7.5 to 16 km for the BMA and 15 – 25 km for the Mbashe anomaly. Accurate magnetic modelling of the Williston anomaly is not possible unless the magnetic terrane further to the north is taken into account, which is attempted here. More detailed studies of this northern terrane (Namaqua) are, however, needed.

The free-air gravity anomaly follows the terrain (Figure 4-11c). A low-amplitude gravity high is measured over the BMA, though densities used during modelling do not differ significantly from the surrounding mid-crust. The modelled density values for the BMA and other bodies are affected by the modelling of the shallower, less dense layers. These shallower layers are defined using refraction seismic data (Stankiewicz *et al.*, 2008, Stankiewicz *et al.*, 2007) and therefore are not exact, which in turn will affect the accuracy of the density model.

These models largely follow the velocity layers of the seismic refraction data, giving the appearance of a layered model without much depth variation in the middle crust (~5-10 km). This is a simplified model compared to the reflection seismic data, which shows a more complicated middle and lower crustal structure with different overlapping terranes.

Potential field models along the central Inkaba profile are shown in Figure 4-12. HP-filtered magnetic linear anomalies are shown in (a), while magnetic and gravity models for this profile are shown in (b) and (c) respectively. The

correlation of these magnetic linear anomalies with high-velocity zones is evident on the refraction seismic profile in (d), except in the case of the Mbashe anomaly in the south. The magnetic signal, however, cannot be properly modelled without including a body at depth below the Mbashe anomaly. This refraction seismic profile images shallower depths compared to the western profile, limiting deeper modelling. The BMA also correlates with a high conductivity zone that stretches down to ~ 25 km on MT data along a shorter central profile that is not shown here (Weckmann *et al.*, 2007a). Separate thrust sheets associated with supracrustal rocks, similar to the western profile, are modelled in the mid-crust and constrained by the magnetic linear anomalies and anomalous seismic zones. The source of the BMA along this profile is more limited in width compared to the western profile.

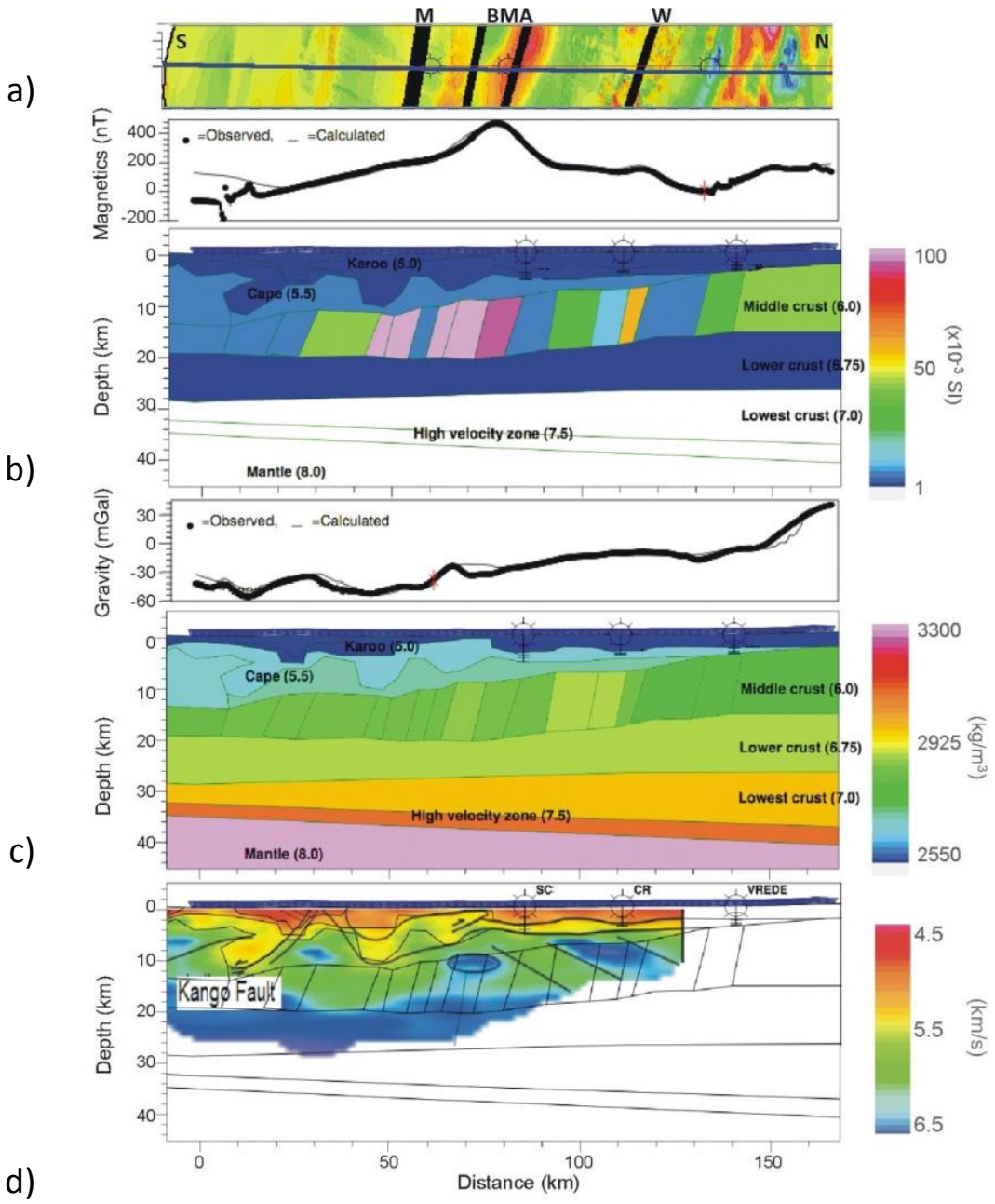

Figure 4-12. (a) High-pass filtered TMI image for the region surrounding the central profile shown in Figure 4-3a. (b) 2D magnetic model along the profile shown in (a). The mid-crustal high susceptibility bodies used to fit the anomalies correlate with the magnetic traces in (a) as well as anomalous zones of high seismic velocity (Stankiewicz *et al.*, 2007), and are modelled with increasing depth towards the south. (c) 2D gravity model corresponding with the magnetic profile in (b). (d) Seismic refraction data from Stankiewicz et al. (2007) used to

constrain the model. Boreholes used to constrain the model are shown (SC3/67, CR1/68, VREDE1/66). See Figure 4-11 for details.

Similar to the western profile, the main gravity feature along this central profile *(c)* is due to terrain. Again only a slight gravity high is measured over the BMA. An anomalous low density body is needed in the upper crust below the CFB to model the gravity data south of the Cape Isostatic anomaly (Hales and Gough, 1960). This model, however, is non-unique and bodies in the lower crust or upper mantle below this region could also produce the observed gravity anomaly.

In the 2D magnetic models shown in Figure 4-11 and Figure 4-12 we model the zones of complex seismic reflectivity that correlate with the magnetic linear anomalies as 20 - 60 km wide bodies. Previous magnetic models over the BMA have included 30 to 150 km wide bodies, with vertical extents of ~5 km down to 30 km (controlled by Curie temperature, de Beer *et al.*, 1982, Pitts *et al.*, 1992, Weckmann *et al.*, 2007a). The depth extent of the bodies in this study is approximately 10 - 15 km as determined from seismic data, starting at a depth of ~5 km in the north and deepening to the south. MT data along the central profile, however, suggest that the conductive body linked to the BMA could continue down to around 25 km (Weckmann *et al.*, 2007a). The deepening of the bodies to the south is similar to what is seen on the east coast, with the Mzumbe terrane outcropping, while the southern part of the Margate terrane is not exposed. In addition, further south of the Margate terrane (close to East London) borehole SP1/69 does not intersect basement even though it extends to a depth of ~4.5 km (Rowsell and De Swardt, 1976).

The 20 - 60 km wide bodies modelled here are sometimes made up of several sheets with variable physical property values that are higher than the surrounding crust. Modelled density and magnetic susceptibility values (2840 – 2900 kg/m^3, 10-100 x 10^{-3} SI) are similar to those used in previous models (2870 - 2900 kg/cm3, 50-90 x 10-3 SI; de Beer *et al.*, 1982, Pitts *et al.*, 1992, Weckmann

et al., 2007a), though magnetic susceptibility values are higher than those measured in the field for supracrustal rocks of the Mzumbe terrane (10-60 x 10^{-3} SI).

4.8 Discussion

In this study we show that although the magnitude of the BMA is significant (~400 nT), the anomaly itself is not unique as was previously thought. It forms part of a group of magnetic linear anomalies which define the extent of the Natal basement. This link is further confirmed by similar anomalous zones on other geophysical datasets (seismic and MT). Our study therefore does not support the proposal by de Beer and Meyer (1983), de Beer et al. (1982) and Hälbich (1993) that the BMA is a suture zone, as the Mbashe anomaly is visible south of the BMA.

Due to this link, conclusions can be drawn regarding the source of the BMA from geological observations linked to the Williston anomaly. These anomalies' elongate magnetic signature is therefore linked to the original thrust terranes and supracrustal rocks making up the belt that extend down to mid-crustal depths, as well as the associated shear zones. The difference in magnitude of the anomalies does, however, suggest that rocks within each linear anomaly have different magnetic properties.

It appears that shear zones have preferentially formed in these supracrustal regions, resulting in the elongate nature of the rocks and magnetic signals. This is an extension of the source models proposed by Corner (1989) and Thomas et al. (1992b), and previously supported by Weckmann et al. (2007a, 2007b). It appears that the shear zones marking the edge of terranes (e.g., Lilani-Mabigulu shear zone) have higher amplitude and more laterally extensive low-pass filter anomalies, while those occurring within terranes have weaker low-pass anomalies. As the Lilani-Mabigulu shear zone represents a terrane boundary we assume the horizontal and vertical size of the zone explains the larger anomaly. Using these

observations the BMA would be expected to represent a terrane boundary. Due to poor magnetic data over the Mbashe anomaly no conclusions can be drawn.

In the east and west it appears as if the BMA splits, which we would attribute to truncation of two thrust terranes with the middle section of the terranes merged or one removed. From the two seismic reflection profiles (Stankiewicz *et al.*, 2007) it is evident that the source of the BMA does not shallow significantly over the western ~800 km portion, but shallows rapidly towards the east (~100 to 150 km from the coast). It is unclear why this is the case and could be linked to the breakup of Gondwanaland.

In a global sense, these magnetic signatures allow us to better understand how Proterozoic mobile belts amalgamated, in some cases as continuous terranes over ~1000 km. This characteristic magnetic signal could also allow for identification of mobile belts that are not yet exposed. This principle could not, however, be applied to the more complicated Namaqua belt as it is made up of several smaller terranes of varying ages (Raith *et al.*, 2003, Robb *et al.*, 1999, Geringer *et al.*, 1994, Cornell *et al.*, 1986).

The 2D models produced in this study show that thrust sheet geometries for the BMA, Williston and Mbashe anomalies fit the potential field data. The complex nature of the magnetic signal over the BMA on the east coast supports this idea as the signal appears to be made up of several overlapping narrow magnetic anomalies. It must be noted, however, that without addition constrains this model is non-unique. Magnetic susceptibility values are on the higher-end of those measured in the field for (weathered) supracrustal rocks, and could be due to the lack of remanent magnetisation included in the model. High Königsberger ratios determined by Máre and Thomas (1998) suggest that remanent magnetisation cannot be excluded and needs to be studied in more detail for better constraints. The modelled density values are in line with those expected for supracrustal rocks, and correlate with higher seismic velocities calculated using velocity-to-density curves (Christensen and Mooney, 1995). High resistivities are expected for the igneous/metamorphic rocks making up the Natal basement not cut by shear zones.

There is, however, no clear correlation between zones of complex reflectivity identified on reflection seismic data and zones of high conductivity on MT data. This is explained by geological field observations within sheared regions in the Natal mobile belt. These regions are made up of a complex array of elongate geological units and zones of intense shear that can change over less than a kilometre and are not easily delimited. We therefore assume that the entire zone would be characterised by complex reflectivity patterns (Wall *et al.*, 2009, Welford and Clowes, 2006), and that only larger shear zones would be resolvable as high conductivity anomalies on the MT data. For the Williston anomaly it appears that the zones of complex reflectivity do correlate with conductive zones, which we assume to be shear zones within the amphibolite facies Mzumbe terrane. For the BMA the zones of complex reflectivity correlate broadly with resistive regions, which we assume to be the boundary between the Margate granulite terrane and a terrane further to the south, cut by a conductive shear zone. An even better correlation with MT and refraction seismic data may also be possible with the introduction of remanent magnetisation to the model.

Despite the fact that the strongest of these magnetic linear anomalies (BMA) is assumed to be closely associated with the granulite facies of the Margate terrane, there appears to be no direct correlation between metamorphic grade and the strength of the magnetic anomalies. This conclusion is drawn as the granulite facies rocks within the Margate terrane do not display particularly high magnetic susceptibilities (Figure 4-5a). However, this could be due to limited exposure of the Margate terrane. In addition, as can be seen in the Mzumbe terrane, only certain supracrustals (and associated migmatites) display high magnetic susceptibilities (Figure 4-4a).

A different picture is painted for granulite facies rocks in the Antarctic at the proposed continuation of the BMA (Jacobs *et al.*, 2004). Gondwana reconstructions link the NNMB in South Africa to an orogenic belt stretching from western (WDML) to central Dronning Maud Land (CDML) in the Antarctic (Jacobs *et al.*, 1998, Gose *et al.*, 1997), with the Falklands Island fragment fitted between the two regions. Terranes within WDML and CDML, namely

Mannefallknausane, Heimefrontfjella, Kirwanveggen and HU Sverdripfjella are associated with broad elongated magnetic highs and lows (Figure 4-13) that have been linked through limited outcrops to the ~1.1 Ga orogenic basement (Jacobs *et al.*, 1996). These terranes consist of supracrustal gneisses of volcanic and sedimentary origin that have been intruded mainly by granitoids (Jacobs *et al.*, 1996).

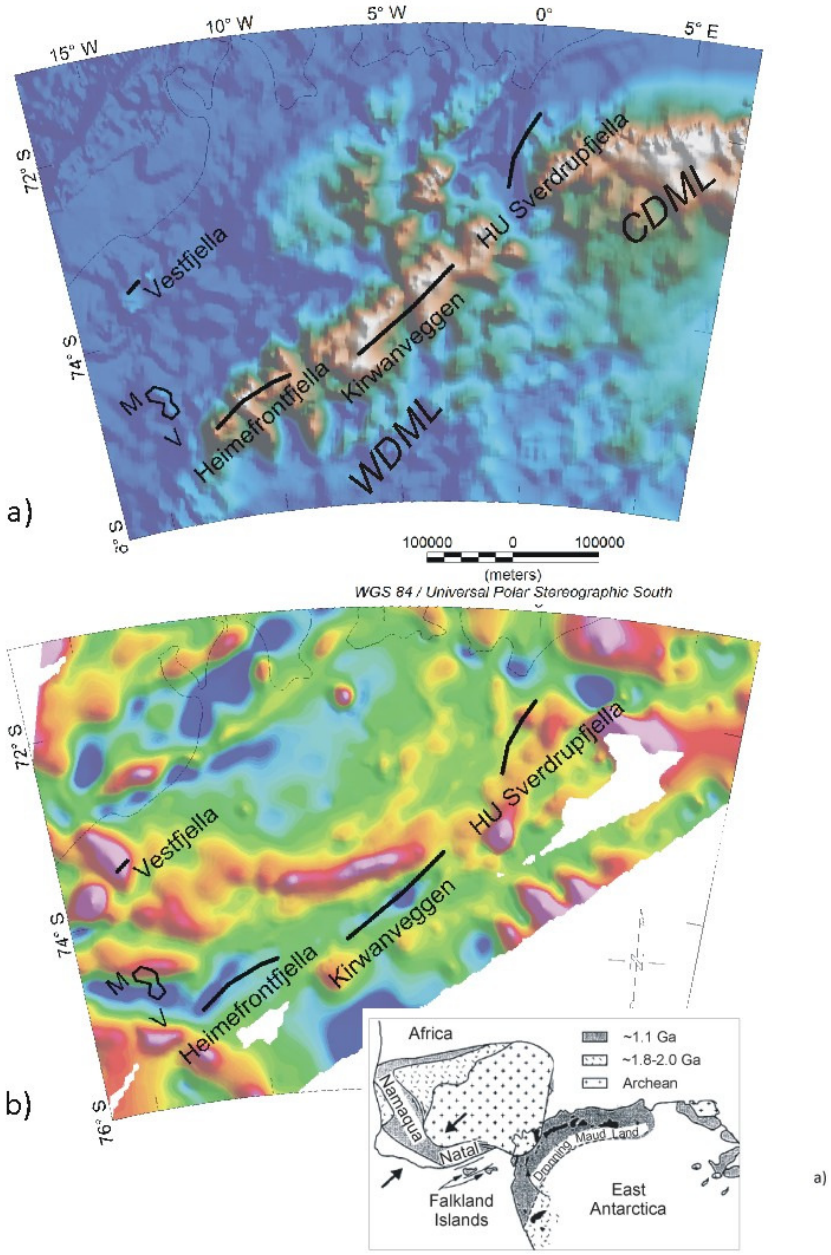

Figure 4-13. (a) Terrane map of western (WDML) and central Dronning Maud Land (CDML) with the different terranes labelled and delineated with black lines (Amante and Eakins, 2009). (b) Total magnetic intensity map of WDML and CDML (Golynsky *et al.*, 2006). Inset map shows the location of Africa, Eastern Antarctica and the Falkland Islands before Gondwana breakup (modified from

Johnston, 2000), with the different tectonic terranes shaded (~1.1 Ga Namaqua, Natal and Droning Maud Land terranes; ~1.8-2.0 Ga and Archean terranes). Broad elongated magnetic highs and lows in (b) that characterise the western region have been linked with ~1.1 Ga orogenic basement, as well as similar basement and anomalies on the east coast of South Africa. Black lines mark terranes labelled in (a). The Heimefrontfjella region in the southwest, which includes the Vardeklettane terrane (V) and Mannefallknausane (M, Jacobs *et al.*, 1996), has been linked to the Margate terrane.

Jacobs *et al.* (1996) link the Vardeklettane and Mannefallknausane rocks within the Heimefrontfjella terrane to the Margate terrane using geological, geochemical, age and magnetic similarities. Magnetic susceptibility measurements made on a handful of granulite rocks from this terrane range from ~10 to 50 x 10^{-3} SI, significantly higher than for granulites in the Margate terrane (Jacobs *et al.*, 2004). Thus the granulites in the Margate terrane could be the cause of the large amplitude of the BMA.

Another explanation for the large signal of the BMA was put forward by Quesnel *et al.* (2009), i.e., exsolved hematite-ilmenite within the granulite-facies mid-crustal rocks of the NNMB. These lamellae can result in high natural remanent magnetisation (up to 30 A/m, McEnroe *et al.*, 2001, McEnroe *et al.*, 2002, McEnroe *et al.*, 2009, Robinson *et al.*, 2002). Martelat *et al.* (2014) suggest a similar source for magnetic anomalies associated with a granulitic metamorphic belt with a complex Proterozoic shear zone network in southern Madagascar. In these belts, metamorphic reactions have resulted in the breakdown of biotite to orthopyroxene and iron-rich oxides. These oxides are shown to have exsolved iron-rich oxide intergrowths on cooling (e.g., magnetite and ilmenite) resulting in strong lamellar magnetism.

Thin section analysis of several supracrustal samples collected in the region of the Williston anomaly during this study shows similar lamellae, and therefore provides support for the proposal by Quesnel *et al.* (2009). Samples

contain 1-3% opaque minerals (approximately 70% magnetite and 30% ilmenite), with ilmenite lamellae in magnetite grains. Other reactions within the belt could also have contributed to the production of magnetite, and therefore a comprehensive sampling study in the region would be needed to confirm these observations.

World-wide other large magnetic anomalies similar to the Beattie, e.g., along the Cascadia convergent margin in North America, have been explained by Blakely *et al.* (2005) as being linked to a serpentinized mantle wedge. This lower crustal body is associated with a long wavelength magnetic anomaly and weak gravity anomaly (<20 mGal, Blakely *et al.*, 2005), and a low velocity anomaly compared to the surrounding mantle (Carlson and Miller, 2003). The fact that the BMA source is a mid-crustal feature makes it unlikely, however, to be a serpentinized mantle wedge. The wedge could have somehow been brought to shallower levels during terrain formation, though it is unlikely it would have remained intact as a large crustal block (~20 km in width according to reflection seismic estimates, Lindeque *et al.* (2011)) considering the deformation of other supracrustal rocks. However, serpentinization is a complicated processes and dependant on pressure and temperature conditions and water content (Hyndman and Peacock, 2003), and cannot be ruled out without sampling of the BMA source. MT data show highly resistive zones (500 – 1000 Ω.m, i.e. 0.001 – 0.05 S/m) that appear to correlate with the Beattie (Weckmann *et al.*, 2007a, Weckmann *et al.*, 2007b). These values are in line with those determined for a serpentinized mantle wedge above a subduction zone (0.001 S/m, Reynard *et al.*, 2011) though are at shallower depths (5 – 15 km).

The question regarding the source of the anomaly can only be solved by drilling the anomaly at its shallowest point on the east coast. Attempts have been made in the past to drill the BMA just south of Mkambati reserve (Figure 4-10), but due to the drill rig scheduling conflicts was not successful. Care would need to be taken during drilling as this study has shown that the anomaly is made up of zones of high magnetic susceptibility instead of one large body. A high resolution

ground magnetic profile and/or airborne survey should be completed over the anomaly before an ideal drilling location can be determined.

4.9 Conclusions

We have developed a new model for the BMA that combines geological, petrophysical and potential field data, along with seismic and MT data and existing models. The final model contributes to our understanding of the formation of mobile belts similar to the Natal Belt.

Filtering of aeromagnetic data allows us to investigate the regional tectonic fabric within the NNMB. These magnetic data suggest that the BMA forms part of a group of magnetic linear anomalies visible along the east coast of South Africa, including the Williston anomaly to the north and Mbashe anomaly to the south. These linear anomalies together form the Natal Belt, and allow the boundary of the belt to be easily delineated in the west.

Investigation of Natal basement rocks associated with the Williston anomaly reveals a complex ENE-oriented sheared zone of predominantly high magnetic susceptibility supracrustal rocks.

Potential field modelling confirms that a similar geological setting can account for the source of the BMA. Our model allows us to refine the basement architecture and constrain density and magnetic susceptibility distributions for these anomalous zones.

The significant amplitude of the BMA is attributed to high magnetic susceptibility granulite supracrustals of the Margate terrane, which are cut by conductive shear zones and mark the southern boundary of this Natal terrane.

A previous study in the region highlights the complex remanent magnetisation of these Natal basement rocks. A more detailed study is needed to better constrain this magnetism, therefore allowing for more accurate modelling.

Though no clear geological evidence exists for the BMA source, this study has shown that several other hypotheses can be ruled out as they only explain parts of the available geophysical data.

4.10 Acknowledgements

This project was funded by the National Research Foundation (NRF), Council for Geoscience (CGS), University of the Witwatersrand and the Society of Exploration Geophysicists (SEG), with software support from Geosoft. Field work was made possible by Greg Botha and the Pietermartizburg CGS office. We thank Ute Weckmann, Jacek Stankiewicz, Bob Thomas, Johan de Beer, Reinie Meyer, Branco Corner, Bruce Eglington and Lew Ashwal for sharing their knowledge on the topic. The authors are grateful to Eric Ferré and Edgar Stettler for improving this manuscript through the review process.

Chapter 5

3D Model

The contents of this chapter have been submitted to the Geophysical Journal International (1 August 2015). I conceived this study in discussion with my supervisors. Work for this manuscript and write-up was completed by me, with the remaining authors helping to improve the manuscript.

AN ISOSTATIC STUDY OF THE KAROO BASIN AND UNDERLYING LITHOSPHERE IN 3-D

STEPHANIE E. SCHEIBER-ENSLIN
Geophysics Unit, Council for Geoscience, Pretoria, 0184, South Africa
School of Geosciences, University of the Witwatersrand,
Private Bag 3, WITS 2050, South Africa
email: steph.scheiber@gmail.com

JÖRG EBBING
Department of Geosciences, Christian-Albrechts University,
Kiel, 24118, Germany
email: jebbing@geophysik.uni-kiel.de

SUSAN J. WEBB
School of Geosciences, University of the Witwatersrand,
Private Bag 3, WITS 2050, South Africa
email: susan.webb@wits.ac.za

5.1 Summary

A three-dimensional density model of the crust and upper mantle beneath the Karoo basin is presented here. The model is constrained using potential field, borehole and seismic data. Uplift of the basin by the end of the Cretaceous has resulted in an unusually high plateau (>1000 m) covering a large portion of South Africa. Isostatic studies show the topography is largely compensated by changes in Moho depths (~35 km on-craton and >45 km off-craton) and changes in lithospheric mantle densities between the Kaapvaal Craton and surrounding regions (~50 kg/m^3 increase from on- to off-craton). This density contrast is determined by inverted satellite gravity and gravity gradient data. The highest topography along the edge of the plateau (>1200 m) and a strong Bouguer gravity

low over Lesotho, however, can only be explained by a buoyant asthenosphere with a density decrease of around 40 kg/m^3.

Keywords: Satellite gravity; 3D model; lithospheric mantle; asthenosphere; isostasy

5.2 Introduction

The main Karoo Basin currently covers ~700 000 km^2 of South Africa (Johnson *et al.*, 2006) and stretches across several different crustal terranes. These include the Archean Kaapvaal Craton (KVC) in the northeast and the surrounding Proterozoic Namaqua-Natal Belt (NNB) (Figure 5-1). Depositional environments vary from glacial to submarine, fluvial and aeolian as the basin shallowed to the northeast (Johnson *et al.*, 2006). The cover is thinnest over the craton (Winter and Venter, 1970, Rowsell and De Swardt, 1976), deepens over the NNB in the south and is deepest in the southern Cape at the edge of the Cape Fold Belt (CFB) (Scheiber-Enslin *et al.*, 2015b, Rowsell and De Swardt, 1976).

The high topography of southern Africa (>1000 m), a large part of which constitutes Karoo Supergroup, represents a significant load on the crust whose origin is poorly understood (Figure 5-1). A better understanding of how this high topography is isostatically compensated requires better insights into the lithospheric and/or asthenospheric mantle structure below the Karoo basin. Different mechanisms have been proposed for compensation (e.g., buoyancy in the mantle or plate tectonic forces), but neither have been confirmed by an in-depth isostatic study.

In this study, a well constrained crustal 3D model of the basin and satellite gravity data are used to study the mantle density structure below the basin. This model, which includes a buoyancy anomaly in the asthenosphere, is shown to be in isostatic equilibrium, thus confirming previous hypotheses of how the topography is compensated.

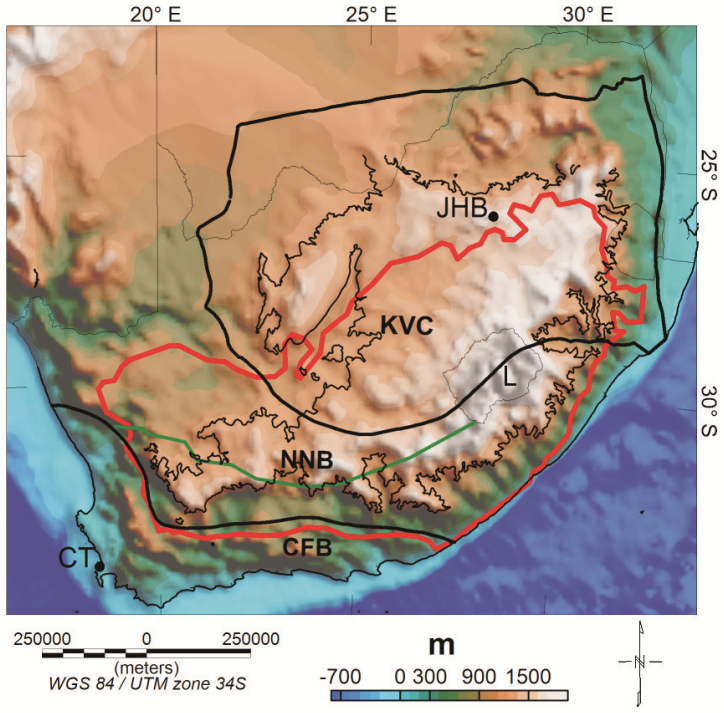

Figure 5-1. Topographic map of South Africa with the main tectonic terranes marked: KVC – Kaapvaal Craton; NNB – Namaqua-Natal Proterozoic Belt and CFB – Cape Fold Belt. The 1200 m topographic contour is marked (black contour). The divide between the Namaqua (west) and Natal (east) terranes as determined from borehole (Eglington, 2006) and magnetic data (Scheiber-Enslin *et al.*, 2014a) is shown (green line). The Karoo basin stretches over the inland plateau and lower-lying coastal regions (red line). The location of the cities of Johannesburg (JHB) and Cape Town (CT) are shown, and the country of Lesotho (L).

5.3 Overview of South African Geology

The geological history of South Africa relevant to this study's 3D model is summarised from De Wit *et al.* (1992) and Thomas *et al.* (1993) in Table 5-1 and Figure 5-2. . The KVC was formed by the amalgamation of several terranes defined by De Wit *et al.* (1992) based on geological mapping, geochronology and aeromagnetic characteristics. The core of the Archean craton (or Southeastern

Terrane) consists primarily of granite-greenstone belts, which include at least the Southern and Northern Barberton and Ancient Gneiss terranes, though these belts extend further north around Pietersburg and into the Natal terrane to the south and further west (Figure 5-2a; De Wit *et al.*, 1992). The narrow Witwatersrand (or Central) terrane in the centre of the KVC that accreted to cratonic core, consists of granitic gneisses and migmatites with granitoid domes and is devoid of greenstones (Wits, Boshoff and Southern terranes, Figure 5-2a; De Wit *et al.*, 1992, Webb, 2009). The Kimberley (or Western) terrane west of the Colesburg Lineament, consists of granitic gneisses and unfoliated granitoids with narrow greenstone belts (Colesburg, Amalia and Kraaipan terranes, Figure 5-2a; De Wit *et al.*, 1992). The Pietersburg terrane north of the Thabazimbi-Murchison Lineament consists of tonalitic–trondhjemitic gneisses and younger granites, with greenstone belts in-between (Pieterburg/Giyani and unnamed terrane, Figure 5-2a; De Wit *et al.*, 1992, Thomas *et al.*, 1993). The extent of these lineaments are based here on geophysical signatures (Webb, 2009). Later accretion during the Proterozoic of the Namaqua belt in the west and Natal Belt to the south is associated with arc-related, volcano-sedimentary rocks (~1.3-1.1 Ga), with some older basement rocks in the west (~2 Ga) and only juvenile rocks in the east (Thomas *et al.*, 1993).

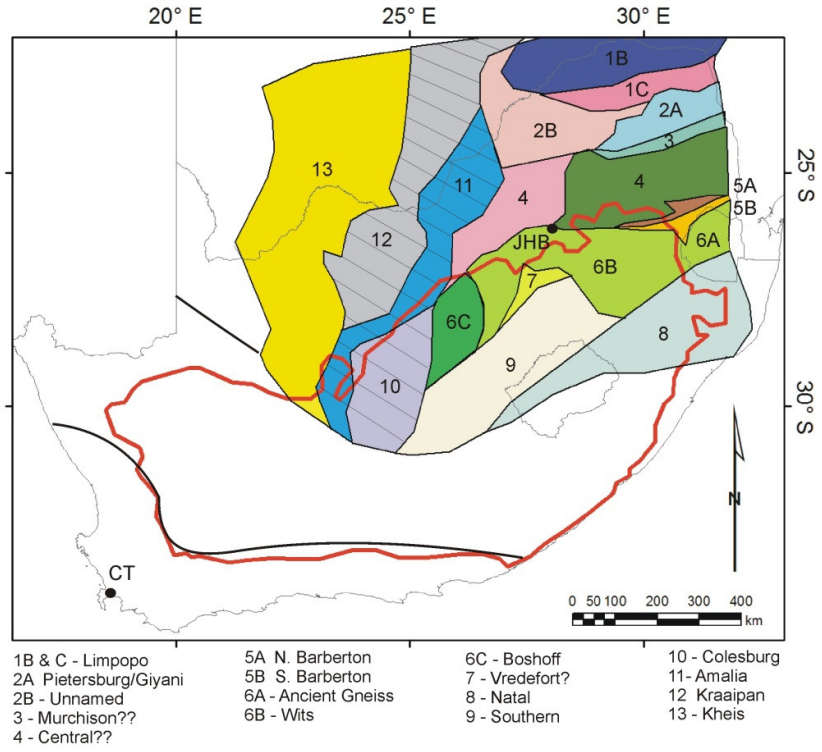

a)

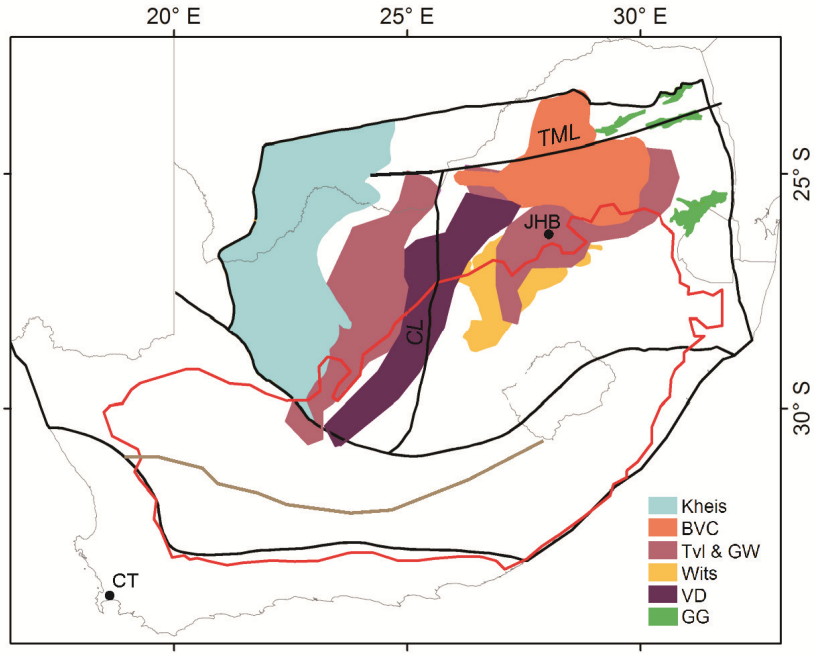

b)

Figure 5-2. (a) Cratonic blocks defined by De Wit *et al.* (1992) according to geology, geochronology and magnetic data. Several cratonic blocks accreted to the cratonic core (Southern and Northern Barberton and Ancient Gneiss terranes)

between 3.7 and 2.5 Ga (De Wit *et al.*, 1992). These include the Witwatersrand block to the west (Wits, Boshoff and Southern terranes), Kimberley terrane further west (Colesburg, Amalia and Kraaipan terranes) and Pietersburg block to the north (Pieterburg/Giyani and unnamed terranes). The Colesburg Lineament (CL) separates the Wits and Kimberley blocks, while the Thabazimbi-Murchison Lineament (TML) separates the Wits and Pietersburg blocks. (b) Geological units overlying the craton are outlined (see geological key: Kheis – Kheis Belt; BVC – Bushveld Complex; Tvl & GW – Transvaal and Griqualand West Supergroup (SG); Wits – Wits SG; VD – Ventersdorp SG; GG – granite-greenstone belts). Extensions of units below the younger Karoo basin (red outline) are shown. See Figure 5-1 for details of the tectonic provinces (outlined in black). The divide between the Namaqua and Natal terranes is marked (brown line, Eglington, 2006, Scheiber-Enslin *et al.*, 2014a).

Table 5-1. Summary of the geological history of South Africa (De Wit *et al.*, 1992, Thomas *et al.*, 1993) and corresponding geophysical studies (including references).

Age (Ga)	**Geological History**	**Geophysical studies**	**References**
3.7 - 3.2	Formation of cratonic core	Teleseismic study (Crustal thickness estimates)	(Yang *et al.*, 2008, Youssof *et al.*, 2013, Nair *et al.*, 2006, Nguuri *et al.*, 2001, Kgaswane *et al.*, 2009)
3.2	Witwatersrand (Wits) terrane accretes to cratonic core		
3.1 – 2.6	Dominion, Wits and Ventersdorp rift basins form		
3.0 – 2.5	Kimberley terrane accretes to Wits terrane in the West	Refraction seismics (Mine tremor studies down to lower crust and Moho)	(Durrheim, 1998, Durrheim and Green, 1992, Durrheim and Mooney, 1991)
3.0 – 2.7	Accretion of Pietersburg terrane in the north		

2.6 – 2.1	Formation of the Transvaal and Griqualand West extensional basins	Reflection seismics (16 sec TWT down to lower crust and Moho; 6 sec TWT down to mid-crust)	(De Wit and Tinker, 2004 outlines possible extensions to the Wits, Ventersdorp and Transvaal Supergroups, Tinker *et al.*, 2002)
2.05	Emplacement of the Bushveld Igneous Complex	Reflection seismics (crustal structure down to 4.5 TWT or ~ 13 km)	(Odgers *et al.*, 1993)
1.75	Amalgamation of Kheis province (sediments and volcanic rocks) to the western margin of the Kimberley block	Teleseismic study	See above references
		Reflection seismics	(Tinker *et al.*, 2004)
1.3 – 1.1	Accretion of mobile belts to the western (Namaqua belt) and southern border (Natal Belt) of the craton; Reactivation of the Kheis province resulting in the formation of the thin-skinned fold-and-thrust Kheis belt (high to low grade metamorphic and plutonic rocks)	Teleseismic study	See above and Harvey *et al.* (2001)
		Reflection and refraction seismics; P-wave analysis (Crustal structure and thickness)	(Graham and Hales, 1965, Durrheim, 1987, Muller, 1991, Green and Durrheim, 1990, Stankiewicz *et al.*, 2008, Stankiewicz *et al.*, 2007, Lindeque *et al.*, 2011)
		Boreholes	(Eglington, 2006, Eglington and Armstrong, 2003)
1.5 - 1.1	Kimberlite magmatism on craton (Smith, 1983)	Xenolith studies	(Schmitz and Bowring, 2004, Griffin *et al.*, 2009, Griffin *et al.*, 2003, James

			et al., 2004)
0.6 – 0.5	Possible orogeny along the southern margin of the Namaqua–Natal Mobile Belt and formation of several smaller basins; Intrusion of Cape granites (Thomas *et al.*, 1993).		
0.5 – 0.33 0.3	Assembly of Gondwana. Formation of the Cape Basin Deposition of the Karoo Basin	Reflection seismics (Crustal structure and Moho depths)	(Lindeque *et al.*, 2011, Loots, 2013, Scheiber-Enslin *et al.*, 2015b, Fatti and Du Toit, 1970)
		Refraction seismics (Crustal structure and Moho depths)	(Stankiewicz *et al.*, 2008, Stankiewicz *et al.*, 2007)
		Boreholes	(Rowsell and De Swardt, 1976, Rutherford, 2009)
0.18	Emplacement of Karoo basalts closely linked to the breakup of Gondwana (Duncan and Marsh, 2006)	Off-shore seismics in the west and south (Coastal crustal structure and Moho depths)	(Hirsch *et al.*, 2009, Parsiegla *et al.*, 2008, Parsiegla *et al.*, 2009)
0.9 – 0.6	Kimberlite magmatism on- and off-craton, with a peak around 90 Ma (Smith, 1983)		See above references

5.4 South Africa's High Topography

The inland plateau (>1000 m) that covers a larger part of South Africa is bordered by the Great Escarpment, at which elevations decrease towards the coast (Figure 5-1). Several time-frames have been proposed for the formation of this high topography. Partridge and Maud (1987) used geomorphological observations to suggest that this escarpment formed during the late Jurassic to early Cretaceous after the breakup of Gondwana. De Wit (2007) used thermo-chronology and stratigraphy studies to determine that major uplift had occurred by the end of the Cretaceous. De Wit (2007) shows that the time-scale of this uplift is strongly correlated with the break-up of Gondwana; significant basaltic magmatism (at

~132 Ma linked to the Etendeka LIP and at 90 Ma due to the Agulhas oceanic LIP, though not the Karoo LIP at 180 Ma); and spikes in kimberlite emplacement (90 Ma and 120 Ma; De Wit, 2007).

Buoyancy in the mantle best explains support of this high topography, though different sources have been proposed. The fact that the escarpment has not been smoothed by erosion was used to suggest recent plume activity (~30 Ma; Burke, 1996, Burke and Gunnell, 2008), however, this is not supported by recent tomography data (Nyblade and Sleep, 2003). A low-wave speed anomaly (LWA) at the core-mantle-boundary (CMB), detected from global seismic tomography studies was proposed as the source of mantle flow that in turn supports the anomalous southern African topography (Lithgow-Bertelloni and Silver, 1998). Mulibo and Nyblade (2013) show that this "African superplume" extends to shallow depths (100-200 km) beneath the active East African rift. While Steinberger and Torsvik (2012) suggest that instead of the entire region reaching shallow depths, smaller plume-like upwellings rise off of these regions. Steinberger and Torsvik (2012) identified a seismically slow and chemically anomalous region below Africa at the core-mantle boundary (CMB), called the African Large Low Shear Velocity Province (LLSVP). They suggest that the upwellings form as a subducting slab reaches the LLSVP, and material is pushed to the edges of the LLSVP where it is forced upward. Recent studies using seismic anisotropy confirm that mantle flow is limited to the asthenosphere (>160 km) beneath southern Africa (Vinnik *et al.*, 2012, Behn *et al.*, 2004).

Alternative suggestions for the source of this high topography include dynamic rebound due to slab detachment at the end of the Triassic, linked to previous subduction below the CFB (Pysklywec and Mitrovica, 1999). Another explanation for the high topography of the escarpment is upward forces at a rift flank associated with the breakup of Gondwana(Ten Brink and Stern, 1992, Gilchrist *et al.*, 1994). Any systematic valuation of these concepts requires geophysical modelling or analysis of geophysical data.

5.5 Crustal Thickness and Mantle Variations Below South Africa

Earlier studies trying to decipher the crustal structure, and to link topography to depth, include a global seismology study by Durrheim and Mooney (1994). They showed that old Archean cratons are underlain by thinner-than-expected crust while the crust below mobile belts is generally thicker, regardless of the overlying topography. This was confirmed by teleseismic data in southern Africa with depths of ~35 km below the KVC compared to ~45 km below the mobile belts (James *et al.*, 2001, Nguuri *et al.*, 2001). However, the KVC is associated with a strong Bouguer gravity low (Venter *et al.*, 1999) but not a large isostatic anomaly (Webb, 2009).

To understand Bouguer anomalies and topographic compensation one, therefore, needs to consider a more complex model. The large-scale gravity study by Webb (2009) in South Africa highlighted the need to include mantle density variations, as well as crustal thickness variations in 3-dimensional modelling of large areas across several geological terranes. Webb (2009) shows lower density mantle exists below the craton, with a best-fit for a density contrast across the Moho of 300 kg/m^3. In-depth modelling, however, shows a better fit if varying density contrasts across tectonic regions are taken into account. This model provides a baseline estimate of mantle density variations as only limited crustal structure is accounted for.

Variations in lithospheric mantle P-wave velocities of 0.5 to 1.5% are also seen below the KVC in delay-time tomography (James *et al.*, 2001, James *et al.*, 2003, Fouch *et al.*, 2004). Fast velocities are recorded under the central and western craton and extending under the Kheis belt. The thickest keel and most intense velocity perturbations are towards the centre of the craton (Fouch *et al.*, 2004, James *et al.*, 2001). For the NNB, the velocity perturbations are slightly lower than for the craton, ranging from 0.5 to -0.5%, but velocities are in general slower than on-craton, with increasingly negative perturbations within the CFB (-0.2 to -0.5%, with -0.9% at one site). Downward smearing on the delay time tomography makes resolving of the depth extent of the keel difficult (~200-250 km depth; Fouch *et al.*, 2004). These tomographic data are limited to the region covered by SASE stations and have a resolution of 50-100 km.

Xenolith studies show that these fast mantle velocities below the craton can be linked to a 1% density decrease from off- to on-craton (James *et al.*, 2004). Comparisons of garnet xenocrysts in older (>110 Ma) and younger kimberlites (≤95 Ma) on-craton by Griffin *et al.* (2003) further confirm that variations are linked to changes in bulk composition of the mantle, as they do not indicate large variations in the geotherm. They show that the high-Vp region below the craton correlates with depleted Archean lithospheric mantle, while low-Vp region below the craton corresponds with iron enrichment and progressive refertilisation/metasomatisation, most likely due to intraplate magmatism (e.g., Bushveld Complex). A similar correlation is seen for the low-Vp Kheis and NNB regions, where it is possible that Archean mantle has mixed with younger fertile material (Griffin *et al.*, 2009).

Griffin *et al.* (2009) further suggests that these kimberlites only sample the margins of these mantle regions as seen on tomographic data. To determine the primitive, more depleted composition of craton cores, i.e., a dunite/harzburgite composition that formed at high degrees of partial melting (≥ 5 GPa) that correlate with high-Vp data, Griffin *et al.* (2009) instead used the Norwegian massifs and most depleted xenoliths from around the world. Griffin *et al.* (2009) and Carlson *et al.* (2005) predict an approximately 50 kg/m^3 contrast between mantle below the craton and below the Proterozoic mobile belts. The keel below the craton is also, in general, characterized by lower than average heat flow (Jones, 1992, Jones, 1988).

The fast lithospheric mantle evident on delay time tomography images is therefore linked using three-dimensional (3D) gravity modelling (Webb, 2009) and xenolith data (Griffin *et al.*, 2003, Griffin *et al.*, 2009, James *et al.*, 2004) to a depleted, lower density keel. This depleted mantle has higher velocities due to a higher magnesium number (Mg# = Mg/Mg+Fe) but lower densities due to the removal of iron and aluminium during partial melting (Griffin *et al.*, 1998, Griffin *et al.*, 1999). Density variations on- and off-craton are therefore shown to be controlled by composition, while temperature controls velocity variations between these terranes (with lower temperatures resulting in higher velocities; James *et al.*, 2004). Previous studies have suggested that it is this cratonic buoyancy that would

have resulted in the Karoo forming only a shallow basin over the craton, compared to greater basin sediment thicknesses over the surrounding mobile belt (Catuneanu *et al.*, 1998) that is underlain by slow lithospheric mantle (Fouch *et al.*, 2004).

5.6 Data

In order to construct a 3D model, information is needed on the lithospheric geometry and petrophysical properties. We therefore considered several geophysical datasets.

5.6.1 Seismic Data

Several ground studies used to constrain the crustal structure of the model are summarised in Table 5-1, with velocities and converted densities from these studies in Table 5-2. P-wave velocities were converted to densities using the velocity-depth equation and coefficients from Zoback and Mooney (2003) (adapted from Christensen and Mooney (1995)) and Ludwig *et al.* (1970)'s Nafe-Drake curve. The Zoback and Mooney (2003) curve is optimal for crystalline rocks with velocities ranging from 5.5 km/s to 7.5 km/s, while the Ludwig *et al.* (1970) curve covers sedimentary to crystalline rocks from 1.5 to 8.5 km/s. Depth maps of the basin are taken from Scheiber-Enslin *et al.* (2015b). These maps were created using borehole (Cole, unpublished; Rowsell and De Swardt, 1976) and published seismic data (Lindeque *et al.*, 2011, Loots, 2013), including Soekor seismic data (Fatti, 1987).

These studies, in general, agree on greater depths (>45 km) in tectonically reworked regions such as the NNB, and shallower on-craton depths (35-40 km) (Durrheim and Green, 1992, Durrheim and Mooney, 1991, Durrheim, 1998, Green and Durrheim, 1990). The NNB region is characterised by a significant intermediate velocity lower crust (6.6 – 6.9 km/s, Green and Durrheim, 1990) and even higher velocity mantle transition zone in the southern Cape (7.0 - 7.8 km/s; Stankiewicz *et al.*, 2008). While lower crustal velocities of between 6.4 and 6.7 km/s are recorded on-craton (12-18 km), along with a thin transition zone of 1-3

km (Durrheim and Green, 1992). These velocities are confirmed by xenolith studies with garnet granulites identified in the lower crust of the NNB, and amphibolite and pyroxene granulites in the cratonic lower crust (Schmitz and Bowring, 2004).

Table 5-2. Crustal density (kg/m^3) and velocity (km/s) values from: the Council for Geoscience Physical Properties Atlas (1 - Maré, 2012), refraction seismic studies (2 - Green and Durrheim, 1990, Durrheim and Green, 1992, Durrheim, 1998) (3 - Stankiewicz *et al.*, 2007), xenolith studies (4 - Schmitz and Bowring, 2004) and teleseismic studies (5 - James *et al.*, 2003). Upper crustal rocks units (SG - Supergroups) are divided into on- and off-craton units. Rock types are listed in brackets (sst – sandstone, qtzite – quartzite). Refraction velocities are converted to densities using the velocity-depth curve from Zoback and Mooney (2003) and Ludwig *et al.* (1970).

	On Craton			Off Craton		
Depth	**Geological units**	**Velocity**	**Density**	**Units**	**Velocity**	**Density**
Upper crust	Karoo SG *(sediments)*	3.5[2]	2550[1]-2650[2]	Karoo SG	5.0[3]	2550[3]
	Cape SG *(sediments)*		2540[1]	Cape SG	5.5 - 5.75[3]	2650-2700[3]
	Transvaal SG *(shale, lava, qtzite)*	5.5-6.3[2]	2770[1] - 2850[2]			
	(dolomite)	6.8[2]	2770[1] - 2880[2]			
	Ventersdorp SG (*lavas and sediments)*	6.4[2]	2760[1] - 2850[2]			
	Wits SG (*qtzite)*	5.7[2]	2650[2] - 2740[1]			
	(shale & qtzite)	5.7-6.1[2]	2740[1] - 2800[2]			
Middle crust	Cratonic rocks *(granite-greenstone - gg)*	6.0 - 6.4[2]	3000[1] 2800 - 2850[2]	NNB *(gg)*	6.0[3]	2800[3]
Lower crust		6.4-6.7[2]	2800-2900[2]		6.6-6.9[2] 6.5 – 7.0[3]	2850-2950[2] 2900 - 3000[3]
High velocity zone/ mantle transition zone (MTZ)		1-5 km transition[2] 6.5 – 6.8, thin 8.1[2, 4]	2900 – 2950 (>3300)[2]		7.0-7.8[3] 7.0 - > 8.0[4]	3000-3250[3] 3000 - > 3300[4]
Mantle					7.8-8.4 [3]	3300-3500[3]

5.6.2 Teleseismic Data

The crustal thickness is further constrained using teleseismic data collected during the South African Seismic Experiment (SASE). The experiment consisted of 82 broad-band stations that were deployed throughout South Africa between 1997 and 1999 (Carlson *et al.*, 1996, James *et al.*, 2003). Later studies also made use of the AfricaArray network (10 stations), the South Africa National Seismic Network (1 station) and the Global Seismic Network (3 stations) (Kgaswane *et al.*, 2009). Youssof *et al.* (2013) provides a detailed description of several teleseismic studies and their different processing methods (including RF analysis and tomography studies) and compares their crustal thickness models (Yang *et al.*, 2008, Nair *et al.*, 2006, Nguuri *et al.*, 2001, Kgaswane *et al.*, 2009, Niu and James, 2002). These studies show that the NNB region is characterised by a gradual Moho and Vp/Vs ratios in general >1.74 (Youssof *et al.*, 2013). The southern portion of the Kheis belt is characterized by a high Vp/Vs ratio (1.91) and more gradual Moho transition, suggesting more mafic material in the lower crust. On-craton the Moho signal is sharper/flat and Vp/Vs ratios are lower (Youssof *et al.*, 2013), supporting the idea that the lower crust below the mobile belts is more mafic, and more felsic below the craton (Durrheim, 1998). Youssof *et al.* (2013) also uses these Vp/Vs ratios, Moho depths and characteristics to divide the craton into several different blocks that have been modified by tectonic and magmatic processes. These Moho depths and Vp/Vs ratios show little variation within the central craton.

5.6.3 Lithosphere-Asthenosphere Boundary (LAB)

We use the LAB depths calculated by Fishwick (2010), who converted surface wave tomography to temperature and lithospheric thickness using the depth at which the isentrope (constant entropy) is reached for a potential temperature of 1315°C. Depths decrease from 200 km below craton to around 130 km offshore. The asthenosphere density for this study is assumed to be 3200 kg/m^3, in line with previous studies in other regions (Jiménez-Munt *et al.*, 2012). This simplified density is based on the assumption of decreasing density with

increasing temperature within the lithospheric mantle and constant density within the asthenosphere.

5.6.4 Satellite Gravity and Gradient Fields

The satellite data were collected as part of the GOCE mission with a gravity gradiometer orbiting at ~255 km. These satellite data allow the regional gravity field in an area to be constrained at a uniform resolution compared to previous models (Ebbing *et al.*, 2013). The GOCE satellite data has a resolution of down to ~80 km, while previous satellite gravity surveys (e.g., GRACE mission) can resolve down to ~160 km (Ebbing *et al.*, 2013).

Gravity data were prepared using Lithoflex software (Braitenberg *et al.*, 2007) at satellite altitude to allow for the best signal-to-noise ratio (Ebbing *et al.*, 2013). The GOCE TIM R3 gravity and gradient field model was used including spherical harmonic degrees 2 to 250, and the data was gridded at 0.5˚ (i.e., spatial resolution associated with the gridding of ~45 – 55 km). The effect of topography was removed using tesseroids (Uieda, 2013) inside LithoFlex, which handles spherical calculations. The final Gz and Gzz maps show a broad low over southern Africa (Figure 5-3a and b).

5.6.5 Gravity Data

The Bouguer gravity data used in this study form part of the Council for Geoscience (CGS) regional dataset (Venter *et al.*, 1999) (Figure 5-3c). The gravity data were processed using standard techniques, i.e., drift corrections, latitude corrections (theoretical gravity based IGSN71 and IGF67), free air and Bouguer corrections with a reduction density of 2670 kg/m^3. A plot of Bouguer gravity versus elevation by Webb (2009) shows scatter around an approximate straight line that is relatively well fit using this reduction density. Density values for geological units are determined from hand samples (Table 5-2, Maré, 2012). The densities used in this study are oversimplified as, for example, Cape

Supergroup sediments are assigned the same density at surface and at depth. The ETOPO1 topographic model with a resolution of 1 arc-min (Amante and Eakins, 2009) was used during modelling (Figure 5-1), with a vertical uncertainty of approximately 10 m.

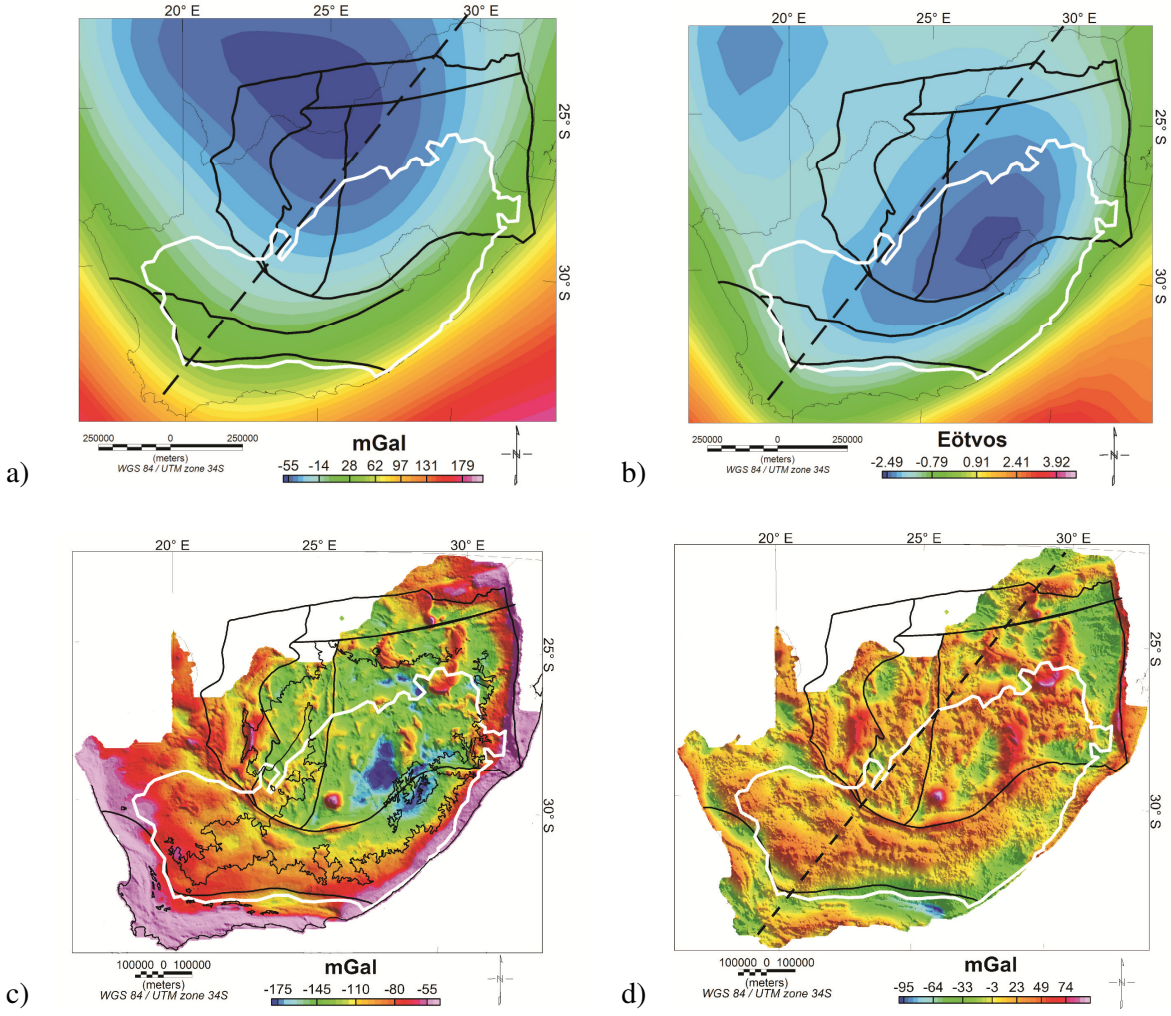
a)
20° E
25° E
30° E
25° S
30° S
250000 0 250000
(meters)
WGS 84 / UTM zone 34S
mGal
-55 -14 28 62 97 131 179
b)
20° E
25° E
30° E
25° S
30° S
250000 0 250000
(meters)
WGS 84 / UTM zone 34S
Eötvos
-2.49 -0.79 0.91 2.41 3.92
c)
20° E
25° E
30° E
25° S
30° S
100000 0 100000
(meters)
WGS 84 / UTM zone 34S
mGal
-175 -145 -110 -80 -55
d)
20° E
25° E
30° E
25° S
30° S
100000 0 100000
(meters)
WGS 84 / UTM zone 34S
mGal
-95 -64 -33 -3 23 49 74

Figure 5-3. (a) GOCE satellite Bouguer gravity (Gz) and (b) gravity gradient (Gzz) data at 255 km height across South Africa. The effect of topography has been removed using tesseroids (Uieda, 2013). (c) Ground Bouguer anomaly (BA) and (d) isostatic anomaly map of South Africa (Venter *et al.*, 1999). The 1200 m topographic contour is marked in (c, black contour) and roughly coincides with a low of -120 mGal. The isostatic map was calculated using a density contrast between the crust and mantle of 400 kg/m^3, an elastic thickness (Te) of 5 km and a reference depth of 35 km. Tectonic terranes are outlined (see Figure 5-1 and Figure 5-2. for details). The Karoo basin is outlined in white. The dashed line marks a profile from the southwest to northeast that is compared across several figures.

The long-wavelength features (>100 km) seen on the Bouguer anomaly map in Figure 5-3a correlate with structures such as the edge of the KVC. Plotting of average Bouguer anomaly versus elevation data for sites across South Africa show that for different geological terranes, different isostatic balance is reached (Webb, 2009). This could be due to differences in weathering between terranes or variations in rebound depending on different lower crustal densities (Webb, 2009). The isostatic anomaly map (Figure 5-3d) is calculated assuming an elastic thickness (Te) of 5 km, a density contrast of 400 kg/m^3 between the crust and the mantle, and a reference depth of 35 km. The main features are the edge of the extensive plateau that covers a large part of the study area (Figure 5-1), and the strongly negative Cape Isostatic Anomaly in the south (-60 to -100 mGal; Hales and Gough, 1960, Scheiber-Enslin *et al.*, 2015b). Webb (2009), however, shows that the calculated isostatic Moho depths (Figure 5-4a) do not reflect true crustal thickness variations determined from teleseismic data (Figure 5-4b; Nguuri *et al.*, 2001; Figure 5-4c; Youssof et al., 2009).

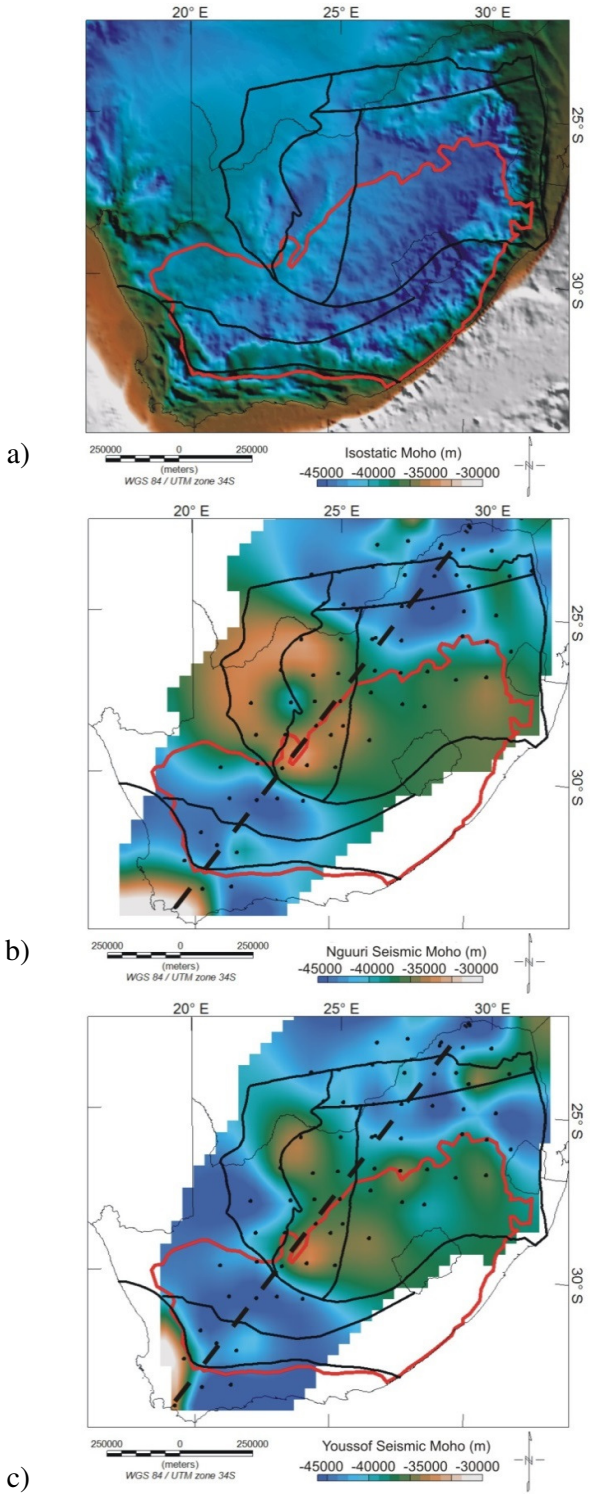

Figure 5-4. (a) Isostatic Moho calculated assuming an elastic thickness (Te) of 5 km and density contrast of 400 kg/m^3 between the crust and the mantle, and a reference depth of 35 km. These depths do not correlate well with teleseismic

crustal thickness estimates from (b) Nguuri *et al.* (2001) and (c) Youssof *et al.* (2013). The dashed line marks a profile from the southwest to northeast that is compared across several figures. Tectonic terranes are outlined (see Figure 5-1 and Figure 5-2. for details).

5.7 Isostatic State and Moho Gravity Effect

We investigate the isostatic state of different terrains by plotting Bouguer anomaly versus elevation data for SASE and additional seismic sites throughout South Africa. We also compare isostatic and seismic Moho estimates for these sites to determine the extent of compensation by crustal thickness. In general, on-craton the isostatic Moho depths are deeper than the seismic Moho depths, however, many of the sites are still in isostatic equilibrium and therefore must be compensated at greater depths. High elevations sites at the edge of the escarpment on-craton are not compensated, with Bouguer anomaly values that are higher than expected for the sites elevation. The mobile belt and Cape region, in general, appears to be accommodated by deepening of the Moho, except for sites at the highest points on the escarpment that are also undercompensated, with shallower than expected seismic Moho estimates. SASE sites are, however, limited in the southwestern Cape and show significantly different values across depth models. As southern Africa is not experiencing rapid subsidence, this would suggest that these high elevations are compensated by other structures and ultimately in equilibrium. Possible structures include lower density crust, lithospheric or asthenospheric mantle (i.e., Pratt isostasy) and/or crustal strength.

The 3D gravity effects of the different Moho models (Figure 5-5a; Nguuri *et al.*, 2001, Yang *et al.*, 2008, Nair *et al.*, 2006, Youssof *et al.*, 2013) are calculated along a profile from the Cape region in the southwest to the KVC in the northeast, using a density contrast of 400 kg/m^3 at the Moho. The modelling package IGMAS+ is used and is based on the algorithms by Götze and Lahmeyer (1988). The responses vary by up to 75 mGal, and none fit the broad signal of the regional Bouguer anomaly (Webb, 2009) (Figure 5-5b). In the case of the satellite gravity response, the models vary by up to 90 mGal (Figure 5-5c) and >2.0 Eötvös

for the gradient data (Figure 5-5d). These different crustal thickness models were therefore used to define a range within which the Moho was constrained during modelling.

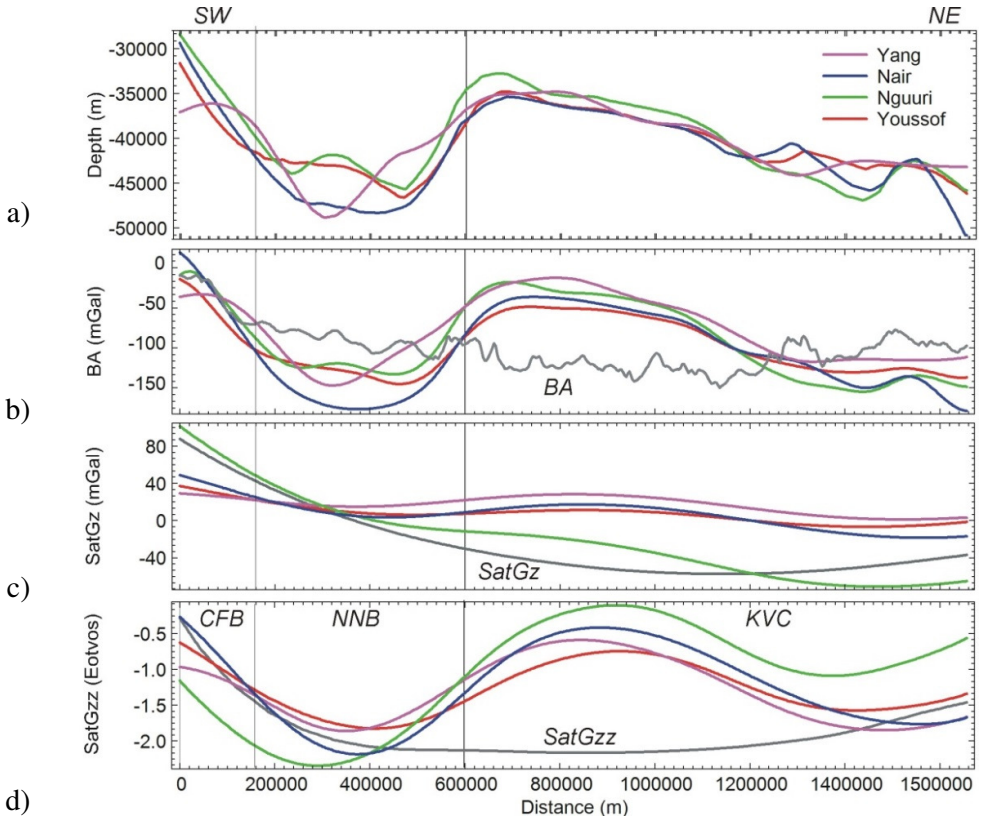

Figure 5-5. (a) Moho depths from southwest to northeast across South Africa, from the Cape Fold Belt (CFB) and Namaqua-Natal Belt (NNB) to the Kaapvaal craton. These depths are determined from teleseismic data (Nguuri *et al.*, 2001), from which several depth models have been generated (Yang *et al.*, 2008, Nair *et al.*, 2006, Youssof *et al.*, 2013). The gravitational responses of these models are calculated (b) at ground-level (BA) and (c) at 255 km (SatGz) using a density contrast of 400 kg/m^3 at the Moho. The gravity gradient response (d) is also calculated at satellite height (SatGzz). The responses show variations of up to 75 mGal, 90 mGal and 1.0 Eötvös respectively, though none fit the broad signal of the observed gravity field (grey). See Figure 5-3 and Figure 5-4 for profile location.

5.8 3D Model of the Lithosphere

In order to investigate lithospheric mantle variations below the Karoo Basin using satellite gravity data, a well constrained model was needed. A 3D crustal model was constrained interactively in IGMAS+. The model was constructed using triangulated polyhedra between parallel vertical sections to which constant densities were assigned. The gravity effect of the model was calculated at the ground surface and 255 km for satellite measurements. The parallel vertical sections run northwest to southeast, approximately parallel to several on-craton seismic profiles, and are 50 to 100 km apart. The model was continued out to approximately 2000 km on either side to reduce edge effects, though the calculated region is cropped to the main Karoo Basin as defined by outcrop. In order to focus on the longer wavelength signal the observed data were smoothed using a 20 km low-pass filter, therefore assuming the short wavelength features are due to shallower crustal sources. The starting model is described in Table 5-3. Relative densities were calculated by removing a constant background density of 3200 kg/m^3.

Table 5-3. Starting model densities (kg/m^3) and depths (km). The geological units are divided into on- and off-craton units. SG – Supergroup.

	Geological unit		**Density (kg/m^3)**		**Depths (km)**	
	on	**off**	**on**	**off**	**on**	**off**
Upper crust (UC)	Karoo SG		2550		0-10	
	Transvaal SG	Cape SG	2750	2650		
	Wits SG	UC	2750			
	Ventersdorp SG	UC	2750			
Middle crust (MC)			2800		10-20	
Lower crust (LC)			2900		20-30	
Lowest crust (LLC)			2950	3000	30-35	30-40
Mantle transition zone (MTZ)			3000	3200	~2-5 km thick	~5 km thick
Lithospheric mantle			3300		~35	~45
Asthenospheric mantle			3200		~130-200	

The lithospheric mantle of the model was divided into oceanic (OC), Namaqua (NM), Natal (NT), Cape (C), Kheis (KH) and cratonic blocks. Based on the subdivisions of Youssof *et al.* (2013), the cratonic block west of the Colesburg lineament (Kimberley) was divided into a southern (K) and northern terranes (K2). East of this lineament the cratonic block was divided into a Wits (W), southeastern (SE) and south-central (SC) terrane. North of the Thabazimbi-Murchison lineament the model was divided into the Pietersburg (P) terrane. Moho depths and Vp/Vs ratios for the lower crust from Youssof *et al.* (2013) do, however, show little variation across the Kimberley, Wits, south-central and southeastern teleseismic blocks. The craton edge was modelled based on an interpreted 16 TWT reflection seismic profile over the craton edge that shows it sloping down over ~50 km and near vertical near the surface (De Wit and Tinker, 2004). The suture zones between cratonic blocks were assumed to be vertical.

The isostatic Moho interface was used to constrain Moho depths in regions where there are no teleseismic sites, particularly below Lesotho. A reference depth of 35 km was used, in line with on- and off-shore seismic Moho depths (Parsiegla *et al.*, 2008, Parsiegla *et al.*, 2009, Hirsch *et al.*, 2009, Stankiewicz *et al.*, 2008, Nguuri *et al.*, 2001). This introduces some error to the model as in regions covered by SASE sites, the isostatic Moho and seismic Moho do not always correlate well (Figure 5-4).

Within the upper crust in the Cape region the Cape Isostatic Anomaly is assumed to be due to uplifted low density Karoo Supergroup sediments and a low density fault zone (Scheiber-Enslin *et al.*, 2015b). Due to the low-resolution of our regional model, this complex geological setting was simplified as thickening of low-density sedimentary layers in the region. Outcropping basement was taken into account within the Natal regions.

A linear inversion of mantle densities was carried out in IGMAS+ using satellite data and the crustal model. The software uses a minimum mean-square error method (Sæther, 1997, Haase, 2008). The model was inverted using Gz and/or Gzz data, and a comparison was made of the results. The “best-fit” densities were then used for modelling the ground gravity data, with the model

being adjusted using a method of trial-and-error to improve the fit. The residual and P-correlation factor provide a measure of how well the observed and calculated curves correlate, with a lower residual and a P-correlation factor closer to one being favoured.

5.9 Modelling Results

Mantle density inversion results obtained in IGMAS+ are listed in Table 5-4 and Figure 5-6. Inverting for Gz (Model 1) and Gzz (Model 2) separately led to similar density differences across the terranes, except with a shift between the two of ~90 kg/m^3 (except over the Wits and south-central cratonic block). The inversion for Gzz gives more realistic densities >3330 kg/m^3 below the Proterozoic belt as predicted by Carlson *et al.* (2005) and Griffin *et al.* (2009). The combined inversion (Gz and Gzz, Model 3) yields a worse fit for both Gz and Gzz than if these parameters are inverted separately. This is most likely due to poor crustal constraints in areas with low data coverage, e.g. over the Kheis belt and northwestern part of model.

The gravity effect of these densities/models are also computed at ground level and fit to ground gravity data (forward modelling). The residual and P-correlation factor for these ground models is lowest for the Gzz mantle inversion densities (residual of 18.4 and P-correlation factor of 0.9).

For comparison, an inversion was also carried out using ground gravity data (Model 4). While a better fit to the data is obtained (residual of 12.8 and P-correlation factor of 0.9) this is mainly due to a better fit of shorter wavelength features, resulting in a poorer fit of the longer wavelengths that are of interest to this study. Model 2 (Gzz inversion) and Model 4 (ground inversion) closely mimic each other, though there is an ~70 mGal shift between the two (Figure 5-6).

The Gzz mantle inversion densities were therefore chosen as the best-fit inversion results. The densities were therefore inserted back into the ground gravity model, and forward modelled in order to better fit the long wavelength features of the signal (Model 5). Changes to density values are evident in Figure

5-6 and Table 5-4, with the new model having a residual of 15.0 and P- factor of 0.9. Two-dimensional maps of the calculated and residual anomalies for this model are shown in Figure 5-7. The residual shows a poor fit to the short wavelength anomalies on-craton.

Table 5-4. Lithospheric mantle density results (kg/m^3) for: Model 1 – satellite Gz inversion (SatInv_Gz), 2 – Gzz inversion (SatInv_Gzz), 3 – Gz and Gzz inversion (SatInv_Gz_Gzz), 4 – ground gravity inversion (GrdInv), 5 – Forward modelling of density values from Model 2 to fit the long-wavelengths of the ground data (SatInv_Gzz_GrdFM). The different on- and off-craton tectonic terranes are listed including the various cratonic blocks from Youssof *et al.* (2013) (shaded grey). Residuals (Res) and P-correlation factors (Pf) measuring the fit of calculated data to observed satellite (Sat) and ground data (Grd) are given.

Terranes	**Model 1 SatInv_Gz**		**Model 2 SatInv_Gzz**		**Model 3 SatInv_ Gz_Gzz**		**Model 4 GrdInv**		**Model 5 SatInv_Gzz_ GrdFM**	
Pietersburg (P)	3207		3275		3273		3230		3285	
Kimberley (K)	3196		3270		3274		3222		3275	
Kimberley2 (K2)	3181		3266		3278		3224		3277	
South-central (SC)	3160		3264		3278		3214		3270	
Southeast (SE)	3184		3267		3256		3210		3265	
Wits (W)	3223		3279		3264		3223		3270	
Kheis (Kh)	3211		3278		3226		3232		3286	
Natal (NT)	3228		3324		3305		3259		3323	
Namaqua (NM)	3233		3329		3345		3263		3328	
CFB (C)	3245		3342		3335		3272		3333	
Ocean (Oc)	3201		3292		3282		3223		3289	
	Res	Pf	Res	Pf	Res	Pf	Res	Pf	Res	Pf
Grd - Gz	21.4	0.8	18.4	0.9	21.8	0.8	12.8	0.9	15.0	0.9
Sat - Gz	0.8	1	7.1	1	2.4	1				
Sat - Gzz	0.2	1	0.1	1	0.2	0.9				

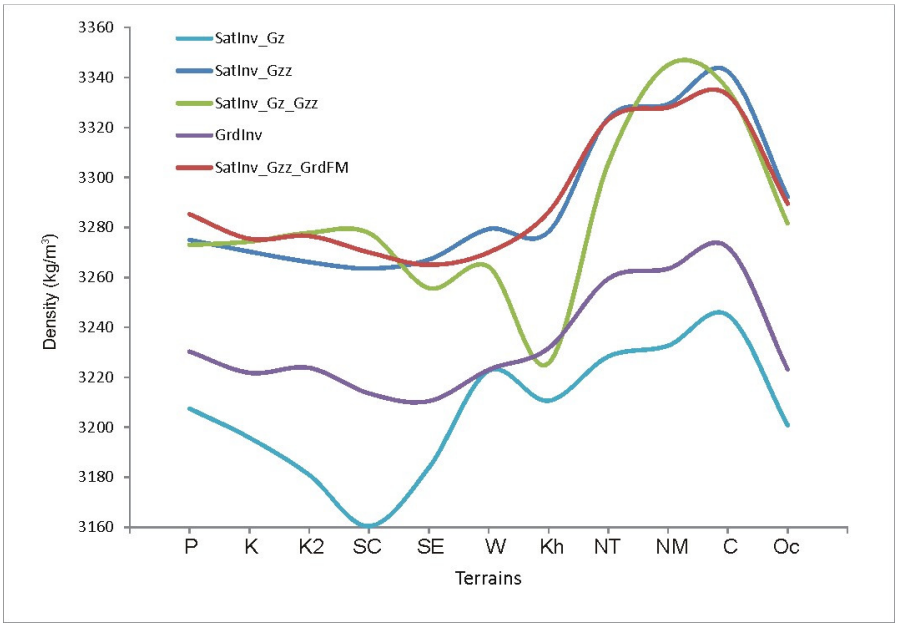

Figure 5-6. Lithospheric mantle densities (kg/m^3) for satellite Gz inversion (Model 1, SatInv_Gz); Gzz inversion (Model 2, SatInv_Gzz); Gz and Gzz inversion (Model 3, SatInv_Gz_Gzz); ground gravity inversion (Model 4, GrdInv); forward modelling of satellite Gzz inversion density values to fit the long-wavelengths of the ground data (Model 5, SatInv_Gz_FM). Terranes include: Pietersburg (P, cratonic); Kimberley (K, cratonic); Kimberley2 (K2, cratonic); south-central (SC, cratonic); southeastern (SE, cratonic); Wits (W, cratonic); Kheis (Kh); Natal (NT); Namaqua (NM); CFB (C) and Ocean (Oc).

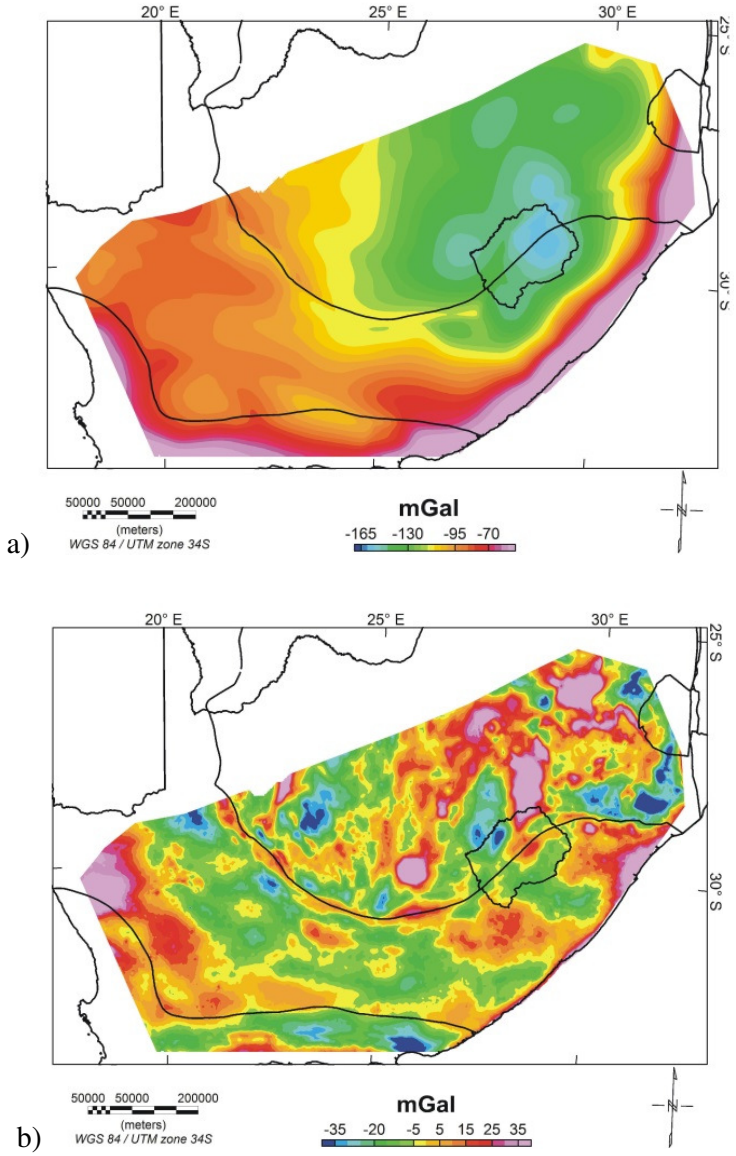

Figure 5-7. (a) Calculated Bouguer maps for the region covered by the Karoo basin for Model 5 (Table 5-4). The residual gravity map is shown in (b). The overall residual and P-correlation factor for the IGMAS+ model are listed in Table 5-4.

On-craton (Figure 5-8) and off-craton profiles (Figure 5-9) reveal lower mantle densities of 3265-3285 kg/m^3 over the craton and ~3320-3330 kg/m^3 over the surrounding Proterozoic belts (Table 5-4). This is in line with density contrasts

estimated from xenolith data (Carlson *et al.*, 2005, Griffin *et al.*, 2009). The lithospheric mantle below the Kheis belt is modelled with densities similar to on-craton (3286 kg/m^3; Table 5-4). Higher mantle densities below the Cape region (3333 kg/m^3) are in line with tomography velocity perturbations for this region that show lower velocities than the NNB (-0.2 to -0.5%, with -0.9% at one site compared to -0.5 to 0.5%). There are, however, fewer teleseismic sites in the Cape region and a large scatter in the existing data, so Moho depths are largely based on the assumption of shallowing at the continent-ocean interface.

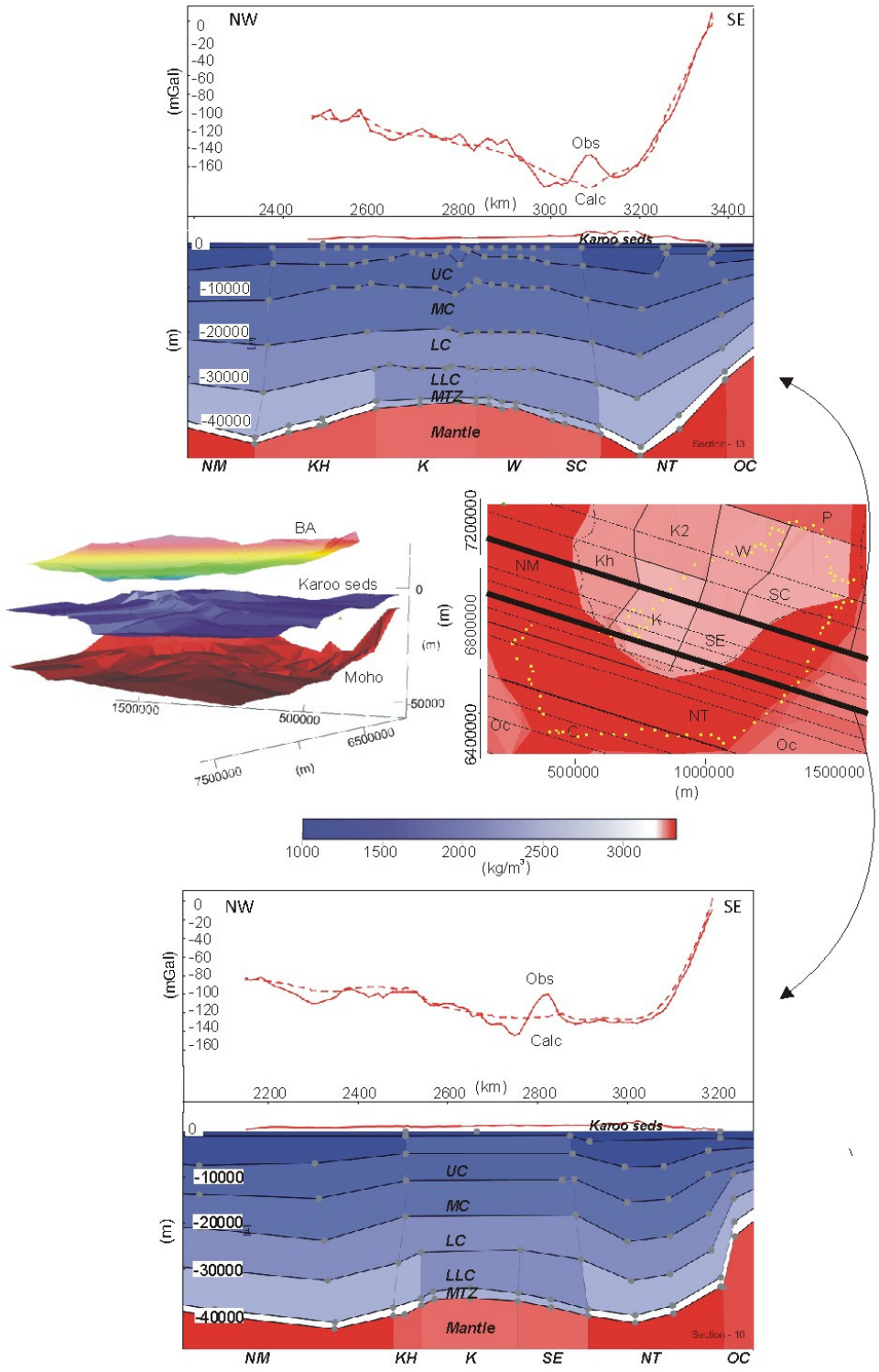

Figure 5-8. Northwest to southeast on-craton density profiles from the main Karoo Basin three-dimensional (3D) model (top and bottom). The inset maps (centre)

show: the 3D Moho and Karoo Supergroup interfaces and Bouguer anomaly (centre-left); and a two-dimensional map of the model upper mantle densities (centre-right). The northwest to southeast sections are marked on this map (dashed black lines), and the different mantle blocks are outlined (solid black lines) and labelled (see Figure 5-6 for details). The locations of the two profiles are also indicated on the map (black arrows and thick black lines). The northern profile (top, Section 13) passes over the Namaqua (NM), Kheis (KH), Kimberley (K), Wits (W), south-central (SC), Natal (NT) and ocean (OC) mantle blocks (the back view of the section). The southern profile (bottom, Section 10) passes over the NM, KH, K, southeast (SE), NT and OC mantle blocks. For the profiles, the calculated (dashed) and observed (solid red) curves are fit to each other. The model is divided into the upper (UC, including Karoo Supergroup sediments), middle (MC), lower (LC) and lowest crust (LLC), mantle transition zone (MTZ) and mantle. Densities are in kg/m^3 (listed in Table 5-4) and coordinates are in UTM34S.

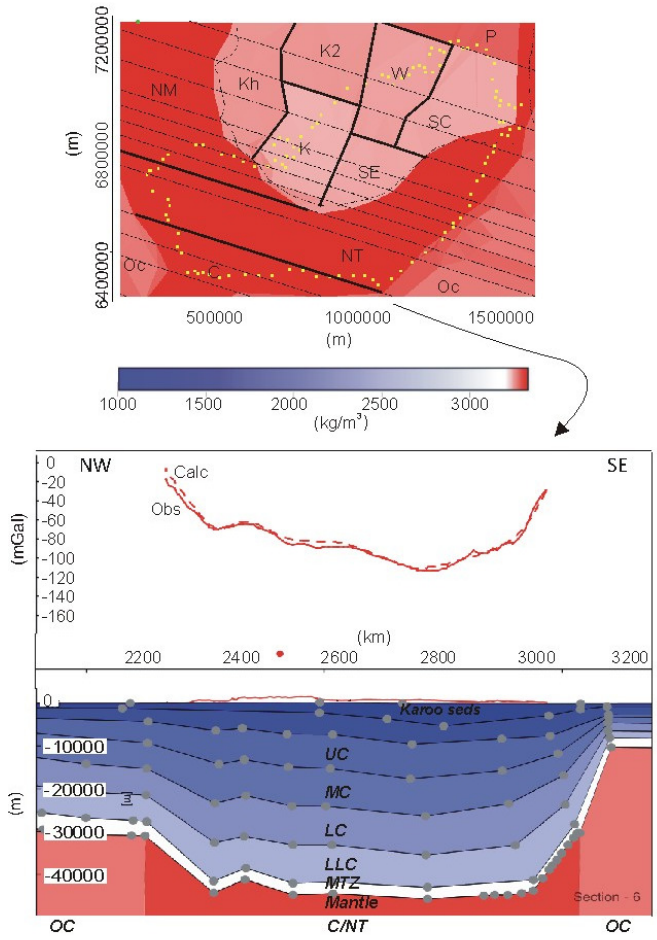

Figure 5-9. Northwest to southeast off-craton density profile from the main Karoo Basin 3D model. The inset map (top) shows a 2D map of upper mantle densities. The profile (bottom, Section 6) marks the divide between the Natal (NT, back of the section) and Cape blocks (C, front of the section), and Ocean (OC) blocks to the northwest and southeast. See Figure 5-8 for details

The crustal thickness map for Model 5 is shown in Figure 5-10. The largest depth differences compared to teleseismic data (Figure 5-4) are seen over Lesotho where teleseismic data coverage is poor and the isostatic Moho reflects the high topography.

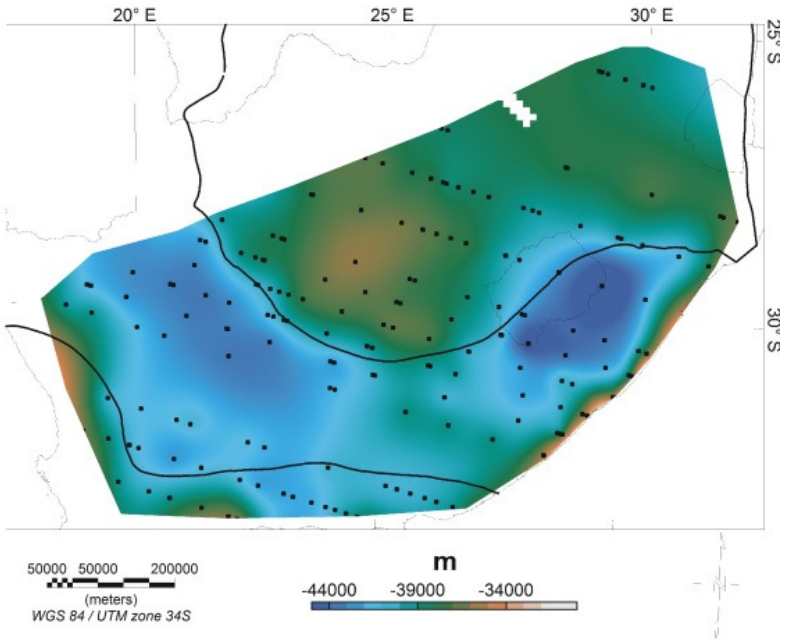

Figure 5-10. Crustal thickness map determined from the main Karoo Basin 3D gravity model (Model 5). Mantle vertices from the 3D model are marked (black dots). See Figure 5-1 and Figure 5-2. for details.

5.10 Test for Loading at the Base of the Model

Surface and subsurface loads are accommodated by either lateral variations in lithospheric densities (in the crust or mantle, known as Pratt isostasy); changes in the depth of compensation which is usually the Moho (known as Airy isostasy); or by the changes in the strength of the crust itself (known as Vening Meinesz/flexural isostasy) (Watts, 2001). As Moho undulations below South Africa have been preserved for longer than the expected relaxation time for flexure of approximately 45 000 years (Watts, 2001), this would suggest higher crustal strength (Webb, 2009).

Several events in South Africa's recent geological past have affected the isostatic balance of the crust, including thickening of the crust below the NNB belt during formation (Thomas *et al.*, 1993); the failed Cape rift and deposition of the Cape basin (Thamm and Johnson, 2006); loading of the Cape region by the

fold and thrust belt and loading of the craton by glaciers at the start of Karoo deposition; deposition of the Karoo basin (Johnson *et al.*, 2006); loading of the crust during the emplacement of the Karoo dolerite network and the extrusion of lavas (Duncan and Marsh, 2006); and major uplift in South Africa followed by erosion (2 - 7 km; De Wit, 2007). As South Africa is expected to be in relative equilibrium since it is not currently experiencing rapid current subsidence or uplift, we would expect the combined effect of all of these processes to be accommodated by Airy and/or Pratt and/or flexural isostasy. Therefore calculating the isostatic balance (or loading) at the base of our model provides validation for the model, as we would expect loading at the base of the model to be equal. The load at the base of the model is a calculation of the gravitational potential energy per unit area, with the units of kN/m.

5.11 Isostatic Implications of 3D model

The load at the base of Model 5 (300 km, Figure 5-11) shows that a large portion of the topography is compensated by changes in Moho depths and lithospheric mantle densities. However, loading is still evident along the edge of the escarpment across the NNB. These features cannot be accommodated by changes in Moho depths or lithospheric mantle densities as there is no significant change in either across the escarpment (Fouch *et al.*, 2004, Nguuri *et al.*, 2001). We therefore investigated whether a change in density in the asthenosphere mantle could accommodate the topography.

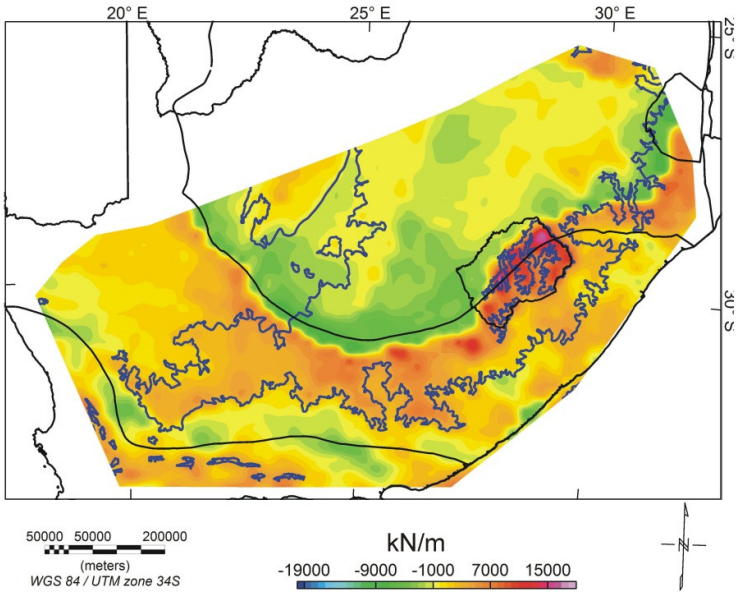

Figure 5-11. Loading (kN/m) at the base of the model (300km depth) calculated for Model 5. The 1200 m topographic contour representing the edge of the escarpment is marked (blue line). Some of the greatest uncompensated loading occurs below the escarpment and Lesotho. See Figure 5-1 for details.

Buoyancy in the asthenospheric mantle, extending both on- and off-craton below the escarpment was modelled and then lithospheric mantle densities again inverted for using the satellite gravity gradient Gzz. This region of asthenospheric buoyancy, in general, correlates with the 1200 m topographic contour (Figure 5-1), as well a broad Bouguer low of approximately -120 mGal that extends from on- to off-craton in the southeastern Karoo (Figure 5-3c). Here we record asthenospheric density contrasts instead of absolute values.

An unrealistically low asthenospheric mantle (AM) density contrast of 100 kg/m^3 is needed below southeastern Lesotho with the current craton boundary and Moho depths in order to reduce the loading at the base of the model in this region. The craton boundary was therefore extended so that the whole of Lesotho is underlain by cratonic lower density lithospheric mantle. This is a reasonable assumption as diamondiferous kimberlite pipes are found in Lesotho (Irvine *et al.*, 2001), and this new boundary is consistent with the assumption that the craton

extends below the Tugela terrane of the Natal Belt towards the east (for a distance of 40 to 85 km; Eglington, 2006).

This altered boundary allows for smaller, more realistic AM density contrasts to be modelled and therefore reduce loading at the base of the model. An AM anomaly with a density contrast of 40 kg/m^3 allows the Bouguer gravity anomaly to be modelled (particularly the low in the southeastern Karoo) and loading at the base of the model to be balanced. The contrast can be stretched to 20 or 60 kg/m^3, but past these values the load can only be balanced and gravity anomalies fit with unreasonable lithospheric mantle densities. A comparison of lithospheric mantle density values for the original Model 5 (no AM anomaly) and a buoyancy model (with an AM anomaly) is shown in Table 5-5. Only small variations in lithospheric mantle density values (≤30 kg/m^3) and residual (1.2) are evident, however, the buoyancy model is closer to equilibrium. Short-wavelength features not in isostatic equilibrium still remain and require further attention.

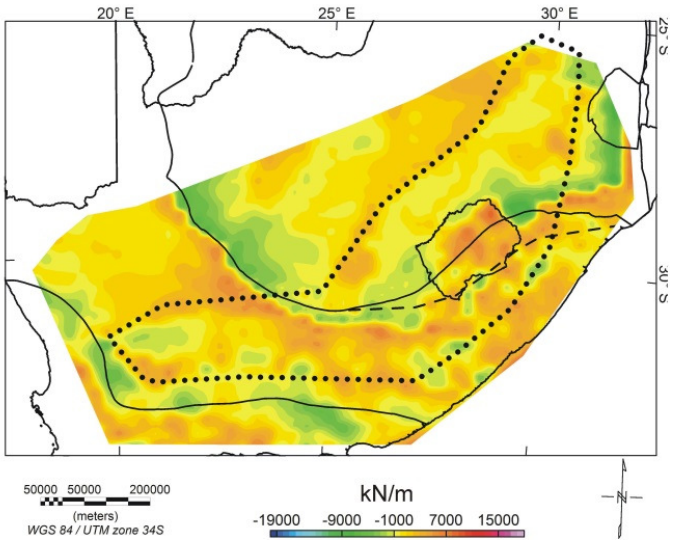

a)

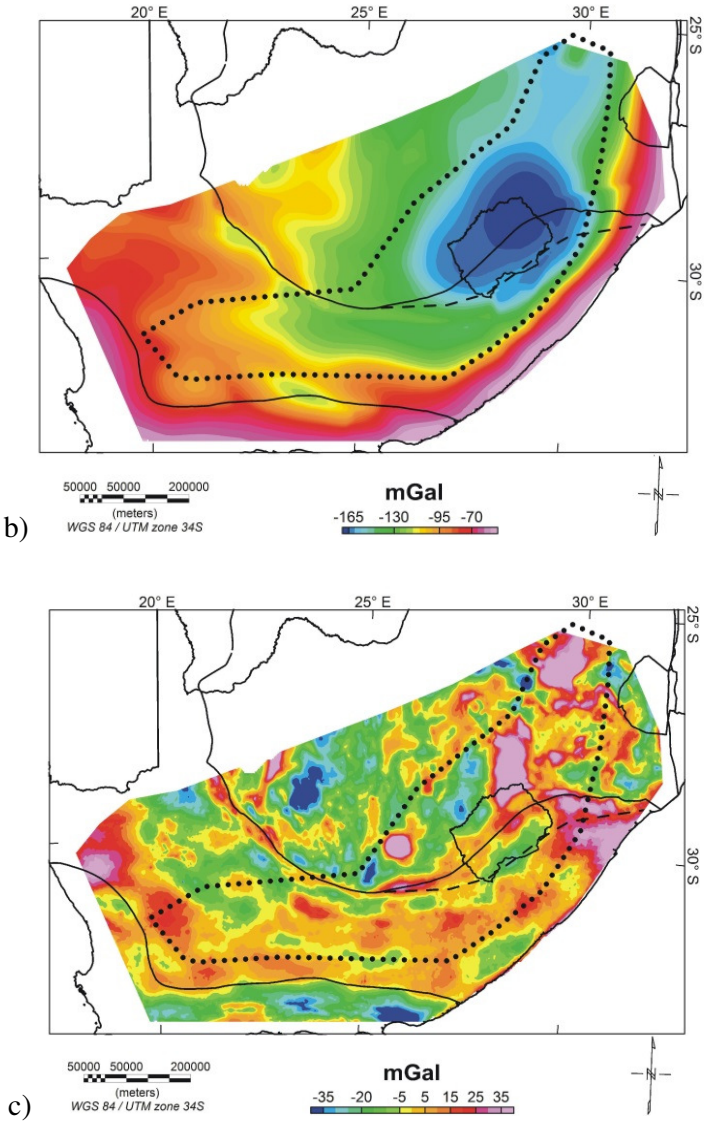

Figure 5-12. (a) Loading at the base of the model (kN/m), (b) gravity and (c) gravity residual (mGal) map for the buoyancy model. A 40 kg/m^3 density contrast exists between the region of asthenospheric buoyancy below the edge of the escarpment (dotted line) and the surrounding asthenosphere. While the gravity effect is similar to Model 5, this model is closer to isostatic equilibrium compared to Figure 5-11. The outline of the extended craton is shown (dashed line). See Figure 5-1 for details.

Table 5-5. Lithospheric mantle density results (kg/m^3) for Model 5 and the buoyancy model (40 kg/m^3 density contrast). See Table 5-4 for details.

Terranes	**Model 5**		**Buoyancy Model**	
Pietersburg (P)	3285		3283	
Kimberley (K)	3275		3283	
Kimberley2 (K2)	3277		3280	
South-central (SC)	3270		3287	
Southeast (SE)	3265		3291	
Wits (W)	3270		3287	
Kheis (Kh)	3286		3287	
Natal (NT)	3323		3330	
Namaqua (NM)	3328		3330	
CFB (C)	3333		3333	
Ocean (Oc)	3289		3305	
	Res	**Pf**	**Res**	**Pf**
Grd - Gz	15.9	0.9	14.7	0.9

A crustal thickness map for the buoyancy model is shown in Figure 5-13, with shallower, more realistic depths below Lesotho than for Model 5 (Figure 5-10). These depths are more in-line with surrounding NNB crustal thicknesses. Shallower depths can be modelled below Lesotho due to the lower lithospheric mantle densities below Lesotho resulting from the craton boundary being extended below the country, and due to the asthenospheric mantle anomaly below Lesotho. The long-wavelength, Bouguer gravity effect of the plume is shown in Figure 5-14, with a 60 mGal low centred on Lesotho. Density depth slices showing the variations in lithospheric and asthenospheric densities at 100 km and 200 km depth are shown in Figure 5-15.

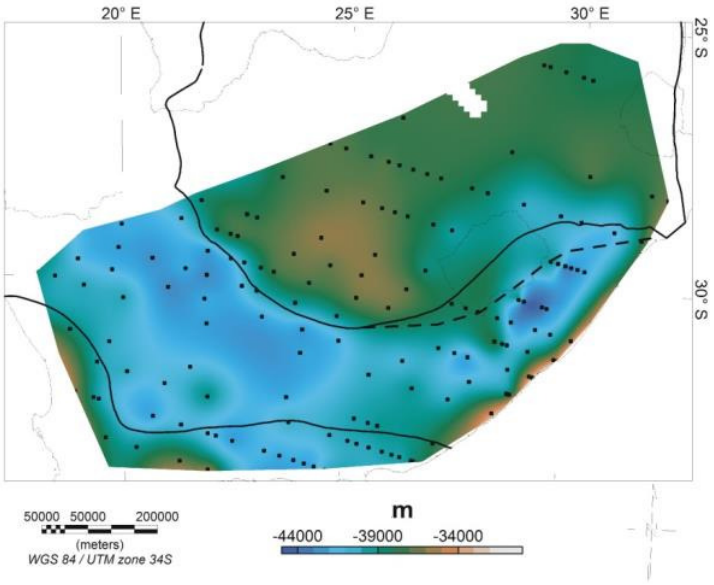

Figure 5-13. Crustal thickness map for the buoyancy model. See Figure 5-10 for details.

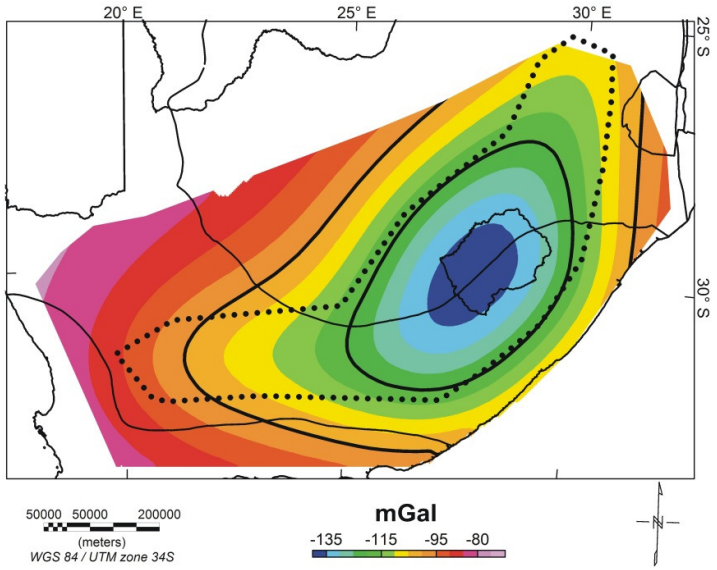

Figure 5-14. The long-wavelength gravity effect of the region of asthenospheric buoyancy outlined in Figure 5-12, with a 40 kg/m^3 density contrast. The thick black lines mark the -120 and -100 mGal isolines.

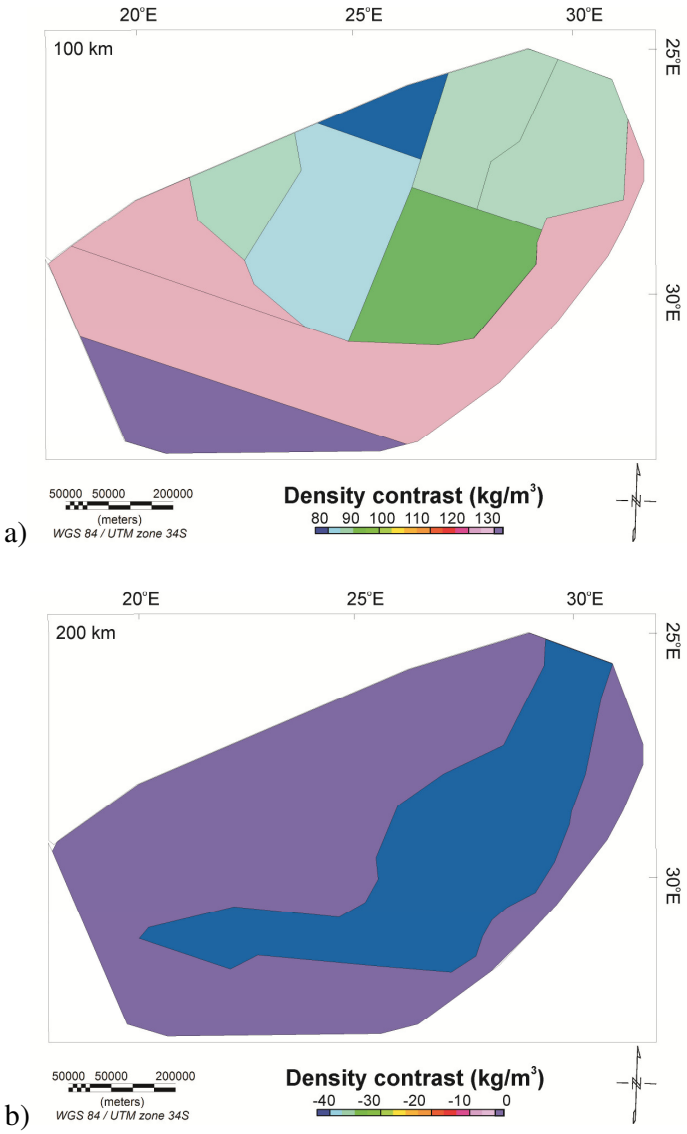

Figure 5-15. Density depth slices at (a) 100 km and (b) 200 km depth showing density contrasts relative to 3200 kg/m^3. In (a) an approximately 50 kg/m^3 change in lithospheric mantle densities from on to off-craton is evident. In (b) the extent of the region of asthenospheric buoyancy below the escarpment is evident, with a 40 kg/m^3 density contrast.

5.12 Discussion

In this study, the Bouguer anomaly low over the craton is accounted for with lower mantle densities (3270 – 3290 kg/m^3), as has been suggested by previous studies. An attempt to model density variations across the different cratonic blocks defined by Youssof *et al.* (2013)'s, however, shows little variation (≤20 kg/m^3). These density variations also do not coincide with mantle velocity perturbations (James *et al.*, 2001, Fouch *et al.*, 2004), i.e. the fastest velocities below the Kimberley and Wits blocks do not coincide with the lowest density mantle. These variations are most likely beyond the resolution of the density model. In addition, these mantle densities will differ if crustal structure and crustal densities are varied in the model. These teleseismic boudaries determined by Youssof *et al.* (2013) do, however, coincide with mantle velocity variations, with the Kimberley (K) and Wits (W) blocks coinciding with the highest percentage velocity perturbations and fastest velocities.

As the broad plateau extends over both the KVC and the Namaqua belt, the majority of the high elevations (up to 1200 m) appears to be accommodated by the lithosphere, with a combination of greater Moho depths off-craton (Nguuri *et al.*, 2001), and lower crustal and mantle densities on-craton (Durrheim, 1998, James *et al.*, 2003). This lower density keel has most likely kept the craton intact and buoyant (Carlson *et al.*, 2005, Griffin *et al.*, 2003, Durrheim and Mooney, 1994, Jordan, 1988, Jordan, 1978, Jordan, 1979).

Asthenospheric buoyancy is, however, needed to accommodate the high topography (>1200 m) at the edge of the escarpment. At crustal levels the asthenospheric buoyancy anomaly coincides with the Natal-Namaqua boundary from magnetic and borehole data (Figure 5-16), and on-craton with the southeastern and south-central block defined by Youssof et al. (2011). These blocks are characterized by 35 to 41 km Moho depths and sharp Moho transitions with Vp/Vs ratios of around 1.74. LAB depths above this anomaly are around 180 km (Figure 5-16). It is unclear whether these crustal features have been impacted by this buoyant asthenospheric region, and it does not appear that this region has resulted in current thinning of lithosphere. This buoyant region could be linked to

a deeper Large Low Shear Velocity Province (LLSVP) (Steinberger and Torsvik, 2012). Plume-like upwelling from it could have been linked to episodes of lithospheric mantle refertilisation and volcanism in the past.

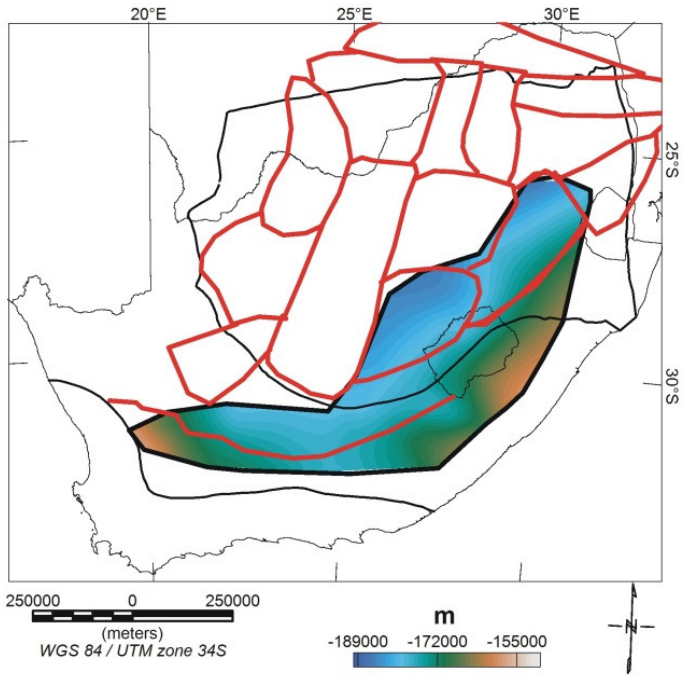

Figure 5-16. Lithosphere-Asthenosphere boundary (LAB) depths (Fishwick, 2010) above the region of asthenospheric buoyancy (thick black line). The Namaqua and Natal boundary and cratonic blocks defined by Youssof *et al.* (2013) are outlined (red lines), with the region of buoyancy correlating with the southeast and south-central blocks and Namaqua-Natal boundary. See Figure 5-1 for details.

5.13 Conclusions

- The Bouguer anomaly low over the Archean craton and higher values over the surrounding Proterozoic mobile belt are accounted for in the 3D model by assuming:

  - A thicker Karoo basin (1-5 km); younger sediments & basement; mafic material in lower crust, i.e. thicker mantle transition zone; deeper Moho (>45 km) and higher density mantle (~3315-3320 kg/m^3) below the NNB; and
  - A thinner Karoo basin (~ 1 km); older sediments and basement with higher densities at shallower depths; felsic material in lower crust; shallower Moho (35-40 km) and lower density mantle (3270-3290 kg/m^3) below the KVC.
- Inversion of the vertical satellite gravity gradient component (Gzz) data provides the most reasonable lithospheric mantle density values below South Africa.
- The high topography of the inland plateau (<1200 m) is largely isostatically compensated by variations in Moho depths and lithospheric mantle densities.
- The highest topography on the edge of the escarpment (>1200 m) is shown to be isostatically compensated by an asthenospheric buoyancy anomaly with a density contrast of around 40 kg/m^3.

5.14 Acknowledgments

This project was funded by the National Research Foundation (NRF), Council for Geoscience (CGS), University of the Witwatersrand and the Society of Exploration Geophysicists (SEG), with software support from IHS Kingdom and Geosoft. We thank Falcon Oil and Gas and the Council for Geoscience for data access.

Chapter 6

Flexure

The contents of this chapter have been submitted to the journal of Basin Research (1 August 2015). I conceived this study in discussion with my supervisors. Work for this manuscript and write-up was completed by me, with the remaining authors helping to improve the manuscript.

Flexure Modelling of the Whitehill Formation, a Key to Unlocking Basin Formation

STEPHANIE E. SCHEIBER-ENSLIN
Geophysics Unit, Council for Geoscience, Pretoria, 0184, South Africa
School of Geosciences, University of the Witwatersrand,
Private Bag 3, WITS 2050, South Africa
email: steph.scheiber@gmail.com

JÖRG EBBING
Department of Geosciences, Christian-Albrechts University,
Kiel, 24118, Germany
email: jebbing@geophysik.uni-kiel.de

SUSAN J. WEBB
School of Geosciences, University of the Witwatersrand,
Private Bag 3, WITS 2050, South Africa
email: susan.webb@wits.ac.za

6.1 Abstract

The Whitehill Formation is the current focus of shale gas interests in the Karoo Basin, South Africa. Here, we present two-dimensional flexure models of the lithosphere that are constrained using Whitehill Formation depth profiles. These profiles are taken from the southwest and southeast of the basin, and are constrained by seismic and borehole data. These models show that the depth profile of the Whitehill Formation can be explained by flexure of the crust due to loading by the Cape Fold Belt in the south. The models show an increase in effective elastic thickness (Te) from 50 km in the southwest to 80 km in the southeast of the basin. There is also an increase in the load size from 4 to 8 km. These increases correlate with broad deepening of the formation to the southeast,

from ~3000 m to ~4000 m. This increase in the load size is linked to locking of the subduction zone further south, while increased crustal strength is linked to lithospheric and asthenospheric buoyancy. This model breaks down in the far southeast of the basin. These values are similar to present day Te estimates, showing limited change over the past approximately 260 m.y.

Keywords: foreland basins, modelling, flexure

6.2 Introduction

The main Karoo Basin covers a large portion of South Africa, and therefore covers several crustal and mantle terranes. The basin stretches from the Archean Kaapvaal craton (KVC) in the northeast to the surrounding Proterozoic Namaqua-Natal Belt (NNB, Figure 6-1). Previous studies have suggested that the strength of the underlying tectonic blocks affected basin formation. It was suggested that the basin deepens over the supposed weaker mobile belts and Cape Supergroup sediments that underlie the southern portion of the basin (Catuneanu *et al.*, 1998, Cloetingh *et al.*, 1992). Here we investigate using 2D flexure profiles whether the effective elastic thickness (Te) of tectonic terranes have impacted the shape of the Karoo basin.

6.3 The Main Karoo Basin

The Karoo Supergroup was deposited from the Late Carboniferous (~300 Ma) to Middle Jurassic (~180 Ma) (Cole, 1992), forming after a 30 Ma hiatus following the deposition of Cape Supergroup (Thamm and Johnson, 2006). These Cape Supergroup sediments were deposited in a failed rift and later deformed (~250 Ma; Hälbich *et al.*, 1983) resulting in the Cape Fold Belt (CFB) along the southern and southwestern margins of South Africa (Figure 6-1). Sediments within the later main Karoo Basin range from glacial to aeolian (Cole, 1992, Catuneanu *et al.*, 1998), with the marine shales of the Whitehill Formation in the

southern part of the basin currently being explored for shale gas (Cole et al., 2011; Decker and Marot, 2012). The Whitehill Formation only occurs in the deeper part of the basin in the south and pinches out north of Hertzogville and Coffee Bay (Cole and McLachlan, 1994; Figure 6-1). The formation has been correlated with the Vryheid Formation in the distal part of the basin (on-craton) that hosts coal deposits (Catuneanu *et al.*, 1998).

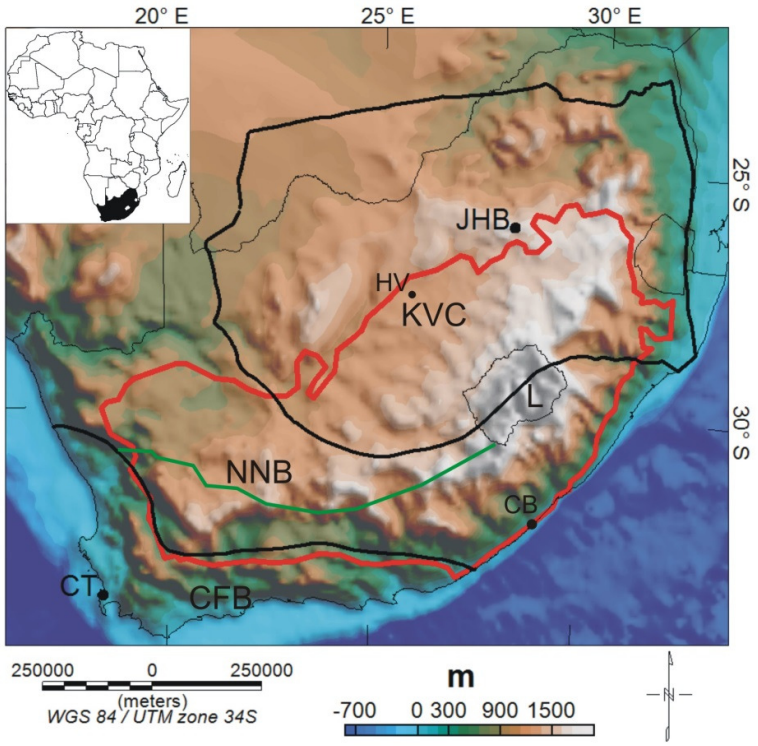

Figure 6-1. Topographic map of South Africa with the main tectonic terranes marked: KVC – Kaapvaal Craton; NNB – Namaqua-Natal Proterozoic Belt and CFB – Cape Fold Belt. The divide between the Namaqua (west) and Natal (east) terranes as determined from borehole (Eglington, 2006) and magnetic data (Scheiber-Enslin *et al.*, 2014a) is shown (green line). The Karoo basin stretches over the inland plateau and lower-lying coastal regions (red line). The country of Lesotho (L) is indicated as well as the cities of Johannesburg (JHB), Cape Town (CT), Hertzogville (HV) and Coffee Bay (CB) that mark the northeastern extent of the Whitehill Formation.

6.4 Basin Formation

The tectonic evolution of the main Karoo Basin is poorly understood. Originally, it was suggested that the basin was a thick-skinned retroarc foreland basin resulting from periods of loading and unloading by the Cape Fold Belt (CFB) in the south (Cole, 1992, Hälbich, 1992, Catuneanu *et al.*, 1998, Johnson, 1991). This loading resulted in the formation of a wedge-shaped foredeep just north of the CFB, followed by a region of uplift called the forebulge, and a shallower back-bulge subsidence region to the north (Figure 6-2a). The weight of sediments and water in the foredeep, as well as horizontal compression and slab pull also could have contributed towards subsidence (Catuneanu *et al.*, 2005).

This loading was a result of subduction of the palaeo-Pacific plate below Gondwana ~1500 km further to the south. During this period older Cape Supergroup sediments (~500 to 330 Ma) and lower sequences in the Karoo Basin were folded and thrusted during several compressional events between 300 Ma and 215 Ma, as determined from $^{40}Ar/^{39}Ar$ dating (Gresse *et al.*, 1992, Hälbich *et al.*, 1983, Catuneanu *et al.*, 1998). This CFB stretches across the southern extent of the country, and has been shown to connect up with belts in neighbouring Gondwana countries (Johnston, 2000).

Recent seismic studies, however, suggest that the basement rocks were unaffected by Cape deformation and therefore suggest the Karoo Basin resulted from thin-skinned folding and thrusting. (Figure 6-2b; Lindeque *et al.*, 2011). In this scenario subduction was to the south, culminating in a continent-continent, arc collision or suturing. This loading resulted in the formation of a foredeep region. Both the collisional and foredeep regions are yet to be identified, and the authors call for seismic studies along the Aghullas Fracture Zone off the south coast of South Africa. The CFB then formed as a thin-skinned Jura-type fold belt behind the foredeep, with the Karoo basin forming behind it due to the loading on the crust by this belt.

A combination of both thin- and thick-skinned deformation has also been suggested from geological and structural mapping and seismic studies (Paton *et al.*, 2006). Other models suggest that the basin can, in part, be linked to mantle

flow due to subduction occurring south of the continent at this time (Pysklywec and Mitrovica, 1999), combined with movement along crustal-scale faults (Tankard *et al.*, 2009). Further south, within the deepest part of the basin, Cloetingh *et al.* (1992) use backstripping to suggest that the unconventional shape of the Karoo basin can be linked to "lithospheric buckling" due to previous Cape rifting rather than just to fold and thrust loading (Cloetingh *et al.*, 1992). This extension is linked to the Cape being an Atlantic-type passive margin basin (Tankard *et al.*, 1982, Johnson, 1991, Winter, 1984, Winter, 1989, Thamm and Johnson, 2006, Shone and Booth, 2005).

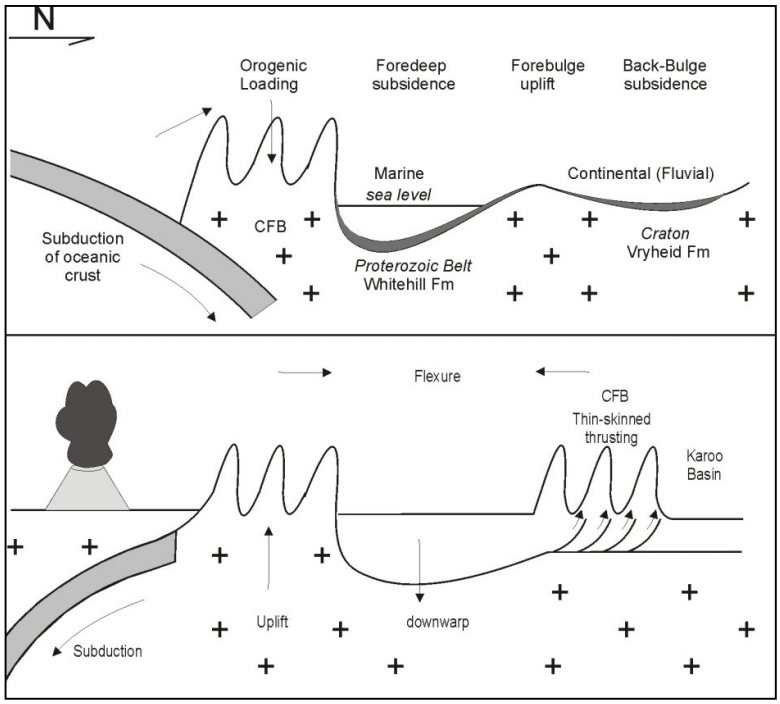

Figure 6-2. (a) The Karoo basin forming as a retroarc foreland basin. Accommodation space was created for the basin due to loading of the crust in the south by the Cape Fold Belt. This load was the result of subduction of oceanic crust below the belt further to the south. This thick-skinned folding and thrusting resulted in deformation of basement rocks. (b) The Karoo forming due to thin-skinned thrusting linked to subduction to the south and continent-continent collision.

6.5 Cretaceous Uplift

Following the formation of the Karoo basin, De Wit (2007) estimated from thermo-chronology and stratigraphy studies that 2 to 7 km of rock was eroded from southern Africa during two periods of uplift in the early-Cretaceous and mid-Cretaceous, while less than 1 km of erosion has occurred up to present times. This has resulted in a high inland plateau covering a large portion of South Africa, consisting of mainly Karoo rocks (Figure 6-1). The edge of the plateau's escarpment is >1200 m high, with the highest regions over Lesotho (>2000 m). Isostatic studies have suggested that this high topography is compensated by an area of low density asthenosphere (Scheiber-Enslin *et al.*, 2015a - Chapter 5).

6.6 Data

6.6.1 Karoo Depth Maps

Depth maps of the basin and Whitehill Formation are taken from Scheiber-Enslin *et al.* (2015b). These maps were created using published and unpublished borehole (Rowsell and De Swardt, 1976) and published seismic data (Lindeque *et al.*, 2011, Loots, 2013), including Soekor seismic data (Fatti, 1987) (Figure 6-3). The ETOPO1 topographic model with a resolution of 1 arc-min (Amante and Eakins, 2009) was also used to determine the thickness of the Whitehill Formation (Figure 6-4). Thickness values range from approximately 40 m in the deepest part to 5 m on-craton. There is some localized thickening, must likely due to structures. The ETOPO1 data have a vertical uncertainty of approximately 10 m.

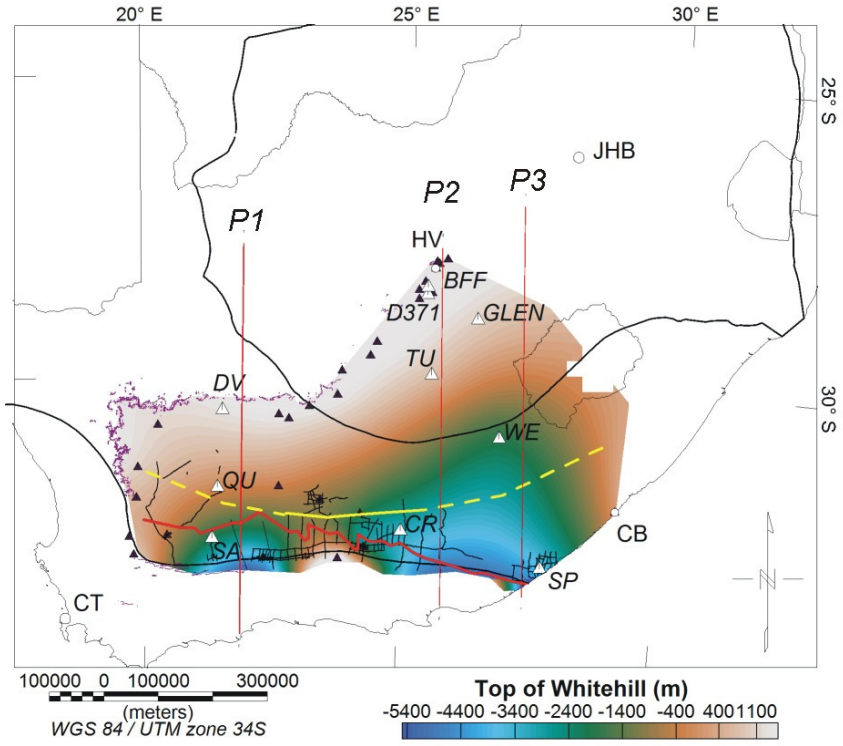

Figure 6-3. Depth map of the Whitehill Formation relative to WGS84 with three flexure profiles marked (red north-south lines) (modified from Scheiber-Enslin *et al.*, 2015b). Data used to constrain the map are marked (seismic – black lines; boreholes – black circles and white triangles). The western flexure profile (P1) includes Lindeque *et al.* (2011) seismic profile and borehole data further north (white triangles, SA1/66, QU1/65, DV - Dubbelde Vlei). The profile in the east (P2) is constrained using Soekor seismic line BV06 in the south and boreholes in the north (white triangles: CR1/68. WE1/66, TU1/50, GLEN1/67, D731/1 and BBF1). The profile in the far-east (P3) is constrained only by borehole data (white triangles: SP1/69, WE1/66 and GLEN1/67). Dolerites intruded the basin following formation around ~180 Ma. The dolerite-line, south of which no dolerite intrusions occur is marked (red line). The northern extent of Cape Supergroup is shown (yellow line; solid - definite and dashed – approximate location). The cities of Johannesburg (JHB), Cape Town (CT), Hertzogville (HV) and Coffee Bay (CB) are marked. Outcropping Whitehill Formation is shown in purple. See Figure 6-1 for details.

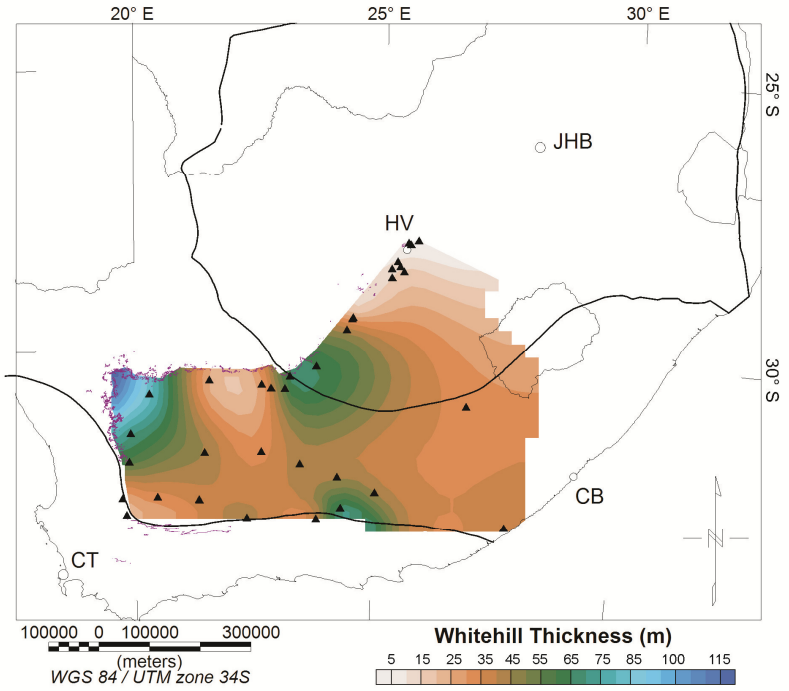

Figure 6-4. Map of Whitehill Formation thickness values (in metres), with the boreholes used shown (black triangles). In general, the layer thickens from around 40 m in the south to 5 m in the northeast on craton. Regions in the north-central, northwest and south showing local thickening, most likely due to structural features. See Figure 6-1 for details.

6.6.2 Teleseismic Data

The crustal thickness of South Africa is constrained using teleseismic data collected during the South African Seismic Experiment (SASE). Youssof *et al.* (2013) provides a detailed description of several teleseismic studies and their different processing methods (including receiver function analysis and tomography studies) and compares their crustal thickness models (Yang *et al.*, 2008, Nair *et al.*, 2006, Nguuri *et al.*, 2001, Kgaswane *et al.*, 2009, Niu and James, 2002). These studies reveal depths of ~35 km below the KVC compared to ~45 km below the mobile belts (James *et al.*, 2001, Nguuri *et al.*, 2001).

6.7 Two-Dimensional Flexure Profiles

The Whitehill Formation was deposited in a wedge-shaped depression during a period of loading (Catuneanu *et al.*, 1998). This deposition was then followed by several other periods of unloading and loading (Gresse *et al.*, 1992, Hälbich *et al.*, 1983, Catuneanu *et al.*, 1998). The depth profiles used in this study therefore reflect the culmination of these events. The two-dimensional flexure models are used to investigate the strength of the underlying lithosphere during this time-period.

In the case of flexural isostasy, the lithosphere is considered to respond to loading as an "elastic" beam floating in a weaker, fluid-like elastic base (i.e., asthenosphere; Turcotte and Schubert, 2002, Watts, 2001). It has been shown that if the period of loading extends over tens of millions of years or more, this type of model provides realistic results for the lithosphere (Watts, 2001). The "strength" of this beam (elastic lithosphere) is measured by its flexural rigidity (Equation 1; Hetenyi, 1946):

$$D = \frac{ETe^3}{12(1-v^2)} \qquad (6\text{-}1)$$

where E is Young's modulus (10^{11} N/m^2), v is Poisson's ratio (0.25) and Te is the effective elastic thickness of the beam. Te is the beam thickness that best fits the flexure of the lithosphere and represents the strength of the lithosphere.

The Whitehill Formation is modelled using an infinite elastic beam, with the deflection (u) along the x-axis at any point (c) due to a load column (CFB) equal to (Equations 2 to 4; Hetenyi, 1946):

If (c) is under the load column: $$u = \left(\frac{h\rho}{2\rho_f}\right)(2 - F(a) - F(b)) \qquad (6\text{-}2)$$

If (c) is to the left of the load column: $$u = \left(\frac{h\rho}{2\rho_f}\right)(F(a) - F(b)) \qquad (6\text{-}3)$$

If (c) is to the right of the load column: $$u = \left(\frac{-h\rho}{2\rho_f}\right)(F(a) - F(b)) \qquad (6\text{-}4)$$

where:

$$F(x) = e^{-x/\propto} cos\left(\frac{x}{\propto}\right)$$

$$\propto = \left(\frac{4D}{\rho_f g}\right)^{1/4}$$

and x is the distance along the x-axis; ρ_f is the density difference between the mantle and the material infilling the resultant depression; g is the gravitational acceleration; h is the load height; ρ the load density; and *(a)* and *(b)* are the distances from point *(c)* to the left and right borders of the load column respectively. The deflections of the beam are assumed to be small compared to the beam thickness, which in turn is small compared to the lateral extent of the beam. These formula were used in MATLAB in a program adapted from the software SlabFlexX_V2 (Whitehead, 2012; Appendix 1), as well as in the shareware software Flex2D (Cardozo, 2014) to determine *Te*.

Three profiles are investigated, with the western profile (P1) being made up of Whitehill Formation depth estimates from Lindeque *et al.* (2011)'s seismic profile and depth grids further to the north from Scheiber-Enslin *et al.* (2015b) based on borehole data (Figure 6-3). This profile crosses from the CFB over the Natal and Namaqua terranes. The eastern profile (P2) is constrained by Soekor seismic line BV06 in the southeast and similar depth grids (Figure 6-3). This profile crosses from the CFB over the Natal and onto the KVC. The Namaqua terrane, in general, is poorly constrained by borehole data and therefore Te estimates in this region have a higher error. Profile 3 (P3) is in the far-east, starting at the CFB boundary and passing over the Natal terrane and onto the KVC. It is constrained by only borehole data.

The Whitehill Formation is easily modelled as it has been unaffected by significant tilting since formation. The Karoo and Cape Supergroup sediments have, however, been subjected to burial, uplift and erosion, making exact load determination difficult. We therefore use several combinations of load widths and heights, as well as varying Te, with the solution limits of 100-200 km, 2-8 km and 5-100 km respectively. Each parameter was varied individually while the other two are held constant. This was done for every combination of parameters. The

solution space was fully explored within the geologically plausible parameters (within the limits of width, height and Te) and a brute force forward modelling method was used to obtain a minimum value. The residuals in Table 6-1 were calculated using the method of least-squares to provide a unique, best-fit solution. It is important to vary these parameters in order to simulate a geologically realistic scenario. The CFB stretches across the entire southern coast of South Africa (~800 km), and therefore the height of the belt is not expected to be uniform across the entire extent. The load also extended horizontally into other parts of Gondwana, and therefore a range of widths are investigated. In addition, Te is expected to vary across geological terrains depending on age, and from location to location depending on lithospheric and sublithospheric properties. These parameters will therefore have affected the depth and wavelength of the Whitehill Formation horizon.

These width and height end-members are constrained by the extent of the current CFB on geological maps and depth estimates from seismic data (Lindeque *et al.*, 2011). The mantle density is taken as 3300 kg/m^3, and the infill and column/load densities are simplified and assumed to be 2550 and 2650 kg/m^3 respectively. These values are in-line with densities for Karoo and Cape Supergroup sediments (Maré, 2012). The models are shifted upward to fit the observed data. As it is difficult to model the burial and uplift that the Whitehill Formation has experienced (De Wit, 2007), this shift can be taken as a minimum measure of uplift that the base of the formation has experienced since deposition (*x* in Figure 6-5).

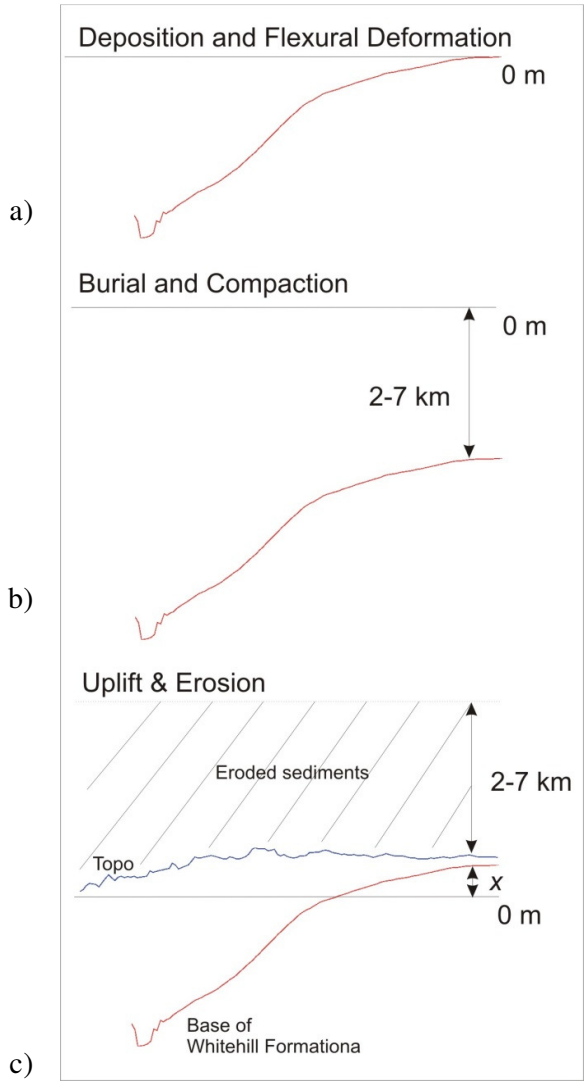

Figure 6-5. Simplified sketch of the (a) deposition and several stages of deformation, (b) burial and compaction, and (c) uplift and erosion of the Whitehill Formation. Flexure modelling provides an estimate of the difference in height (x) between the Whitehill Formation at deposition and deformation (in a), and its current location after uplift and erosion (in c).

6.8 Whitehill Formation Flexure Profiles

The best-fit models for various load width and height combinations are listed in Table 6-1 and shown in Figure 6-6. The overall best-fit along the western profile (P1) is for a load height of 4km and width of 100 km (Figure 6-7a). A load

height of 6 km and with of 100 km, or a load height of 4 km and width of 200 km provide reasonable fits to the data. Along the eastern profile (P2) an overall best-fit is provided by a load height of 8 km and width of 100 km (Figure 6-7b). While the height of the load increases from west to east, the Te of the lithosphere also appears to increase from 50 to 85 km. The shift along both profiles is between 1000 and 1100 km.

Table 6-1. Basic 2D best-fit flexure models of the lithosphere, constrained using two north-south top of the Whitehill Formation depth profiles (see Figure 6-3 for locations). The width and height of the Cape Fold Belt load, as well as the elastic thickness (Te) and shift of the modelled plate are listed. The minimum model residual (Resid) for each combination is recorded (10^3).

Western profile (P1)					**Eastern profile (P2)**				
Load		**Plate**		**Model**	**Load**		**Plate**		**Model**
Width	**Height**	**Te**	**Shift**	**Resid**	**Width**	**Height**	**Te**	**Shift**	**Resid**
100	4	50	1170	11	100	4	50	-506	68
	6	70	2135	13		6	65	229	34
	8	80	2906	18		8	85	1097	13
200	4	80	2264	13	200	4	80	464	30
	6	80	3260	47		6	100	1671	18
	8	5	278	85		8	100	2560	78

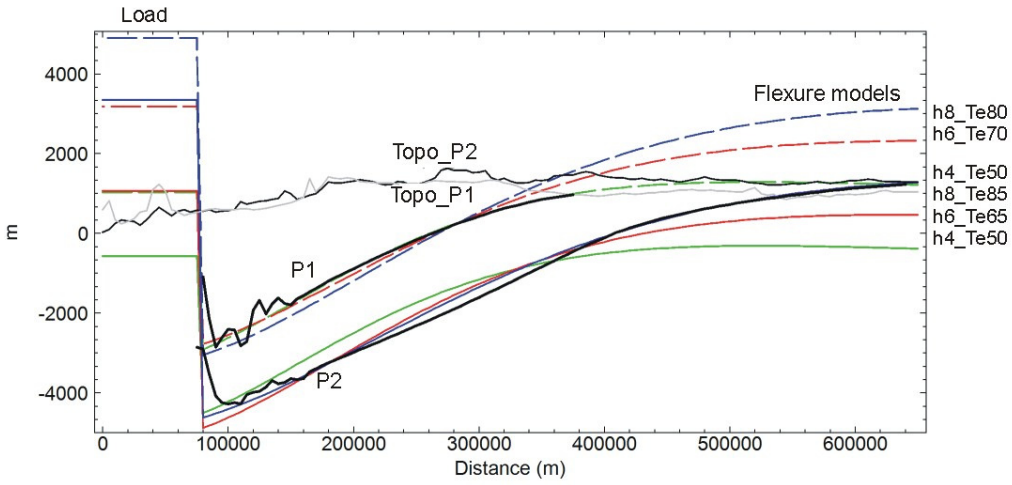

Figure 6-6. Best-fit flexure models of the lithosphere constrained by top of the Whitehill Formation depth profiles (thick black line) along the western (P1) and eastern profile (P2) for a load width of 100 km (see Figure 6-3 for locations). The load height for the flexure models is varied: 4 km (green line), 6 km (red line) and 8 km (blue line). The basin deepens towards the southeast resulting in a change in the best-fit model parameters across the two profiles. The load heights (h) and model elastic thickness (Te) values are listed (see Table 6-1 for model parameters). The topography (Topo) along each profile is shown (grey line for the western profile, black line for the eastern profile).

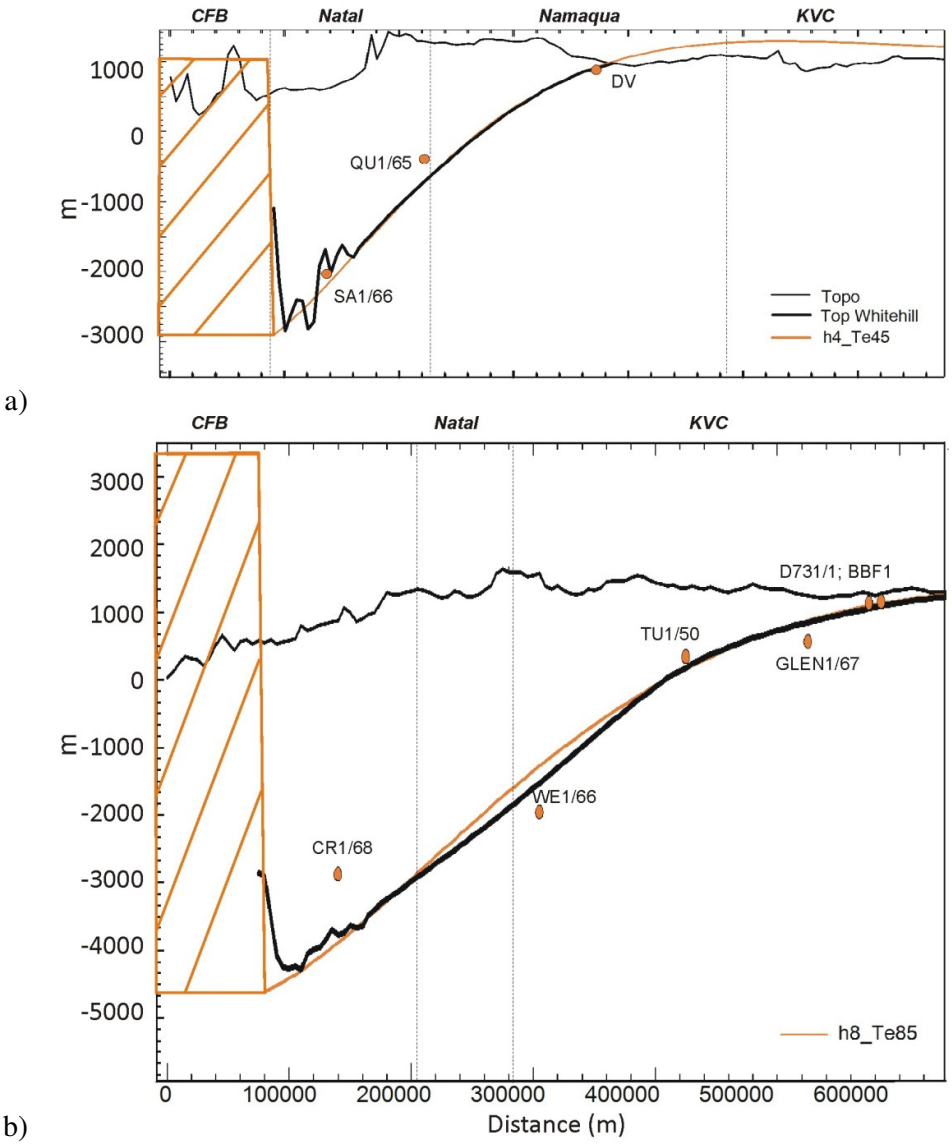

Figure 6-7. Best-fit flexure models (orange line) of the lithosphere constrained by top of the Whitehill Formation depth profiles (thick black line) along (a) the western (P1; load: 100 km wide and 4 km; Te 50 km) and (b) eastern profile (P2; load: 100 km wide and 8 km high; Te 85 km). Borehole data used to constrain the depth profile are shown (red dots with labels, see Figure 6-3 for locations). Divisions between terranes are marked (thin vertical black line): KVC - Kaapvaal craton, Namaqua and Natal terranes and CFB - Cape Fold Belt. The load representing the CFB is shown with dashed orange lines. See Figure 6-6 for details.

Further to the east there are no seismic data, but there is sparse borehole data. We investigate a Whitehill Formation profile (P3) stretching north from borehole SP1/69 near East London (Figure 6-8, see Figure 6-3 for location). In this region the Whitehill extends onto the craton as the Vryheid Formation due to a facies change (Catuneanu *et al.*, 1998). Only a model with a very high Te value (~100 km) is able to fit the two boreholes in the southern part of the profile.

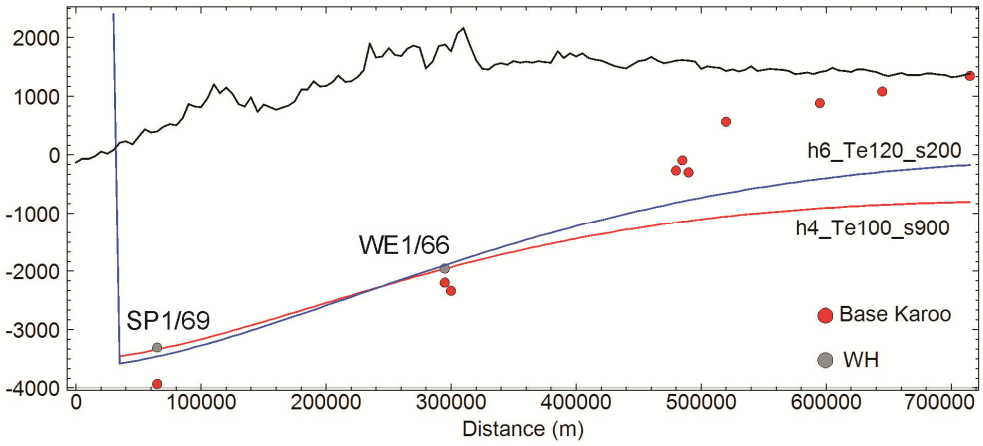

Figure 6-8. Best-fit flexure models of the lithosphere constrained by depths to the top of the Whitehill Formation as determined from borehole data (grey circles) along a profile extending north of borehole SP1/69 (P3; see Figure 6-3 for location). The Whitehill Formation only stretches along the southern portion of the profile. Borehole intercepts for the base of the Karoo Basin on-craton are therefore also plotted (red circles) (Scheiber-Enslin *et al.*, 2015b). An accurate flexure profile of the Whitehill Formation cannot easily be modelled. However, a high Te value is needed to fit the broad deepening of the Karoo Basin in this region (load height (h), model elastic thickness (Te) values and shift (s) are listed). The best-fit model for Profile 2 from Figure 6-7b is plotted for reference (h8_Te85_s1200). See Figure 6-6 and Figure 6-7 for details.

Models with laterally varying Te values along the profile (Bodine, 1981) were tested in Flex2D. These models did not improve the fit to the data.

Therefore, there appears to be no change in Te across tectonic regions along each profile.

6.9 Flexural Isostasy by Comparing Topographic Load and Seismic Moho

Studies using the coherence between gravity and elevation data estimate a current Te on-craton of ~70 km, and 38 – 48 km for the surrounding mobile belts (Doucouré *et al.*, 1996). We use a different technique here using topographic and crustal thicknesses estimates to investigate the current strength of the lithosphere, and compare it to coherence estimates and the strength during the formation of the Karoo. This is done by determining what Te values would allow the current seismic Moho to accommodate the current topographic load. Lithoflex software does this by convolving the load with the response functions of the elastic plate model to a point load in order to calculate the model flexure (Braitenberg *et al.*, 2002). This flexure is compared to the seismic Moho, and Te is calculated on a sliding window. Intracrustal bodies such as the Karoo Basin are not taken into account in this method. A crustal density of 2800 kg/m^3 and mantle density of 3200 kg/m^3 were used as the density contrast between the crust and mantle controls the inversion and therefore cannot be too high. This method is also dependent on the reference depth used, with values of 30 km and 35 km investigated here.

Inversion results for a reference depth of 30 km show high Te values (>50 km) that are restricted to the craton, and extremely low Te values (5 to 30 km) over the surrounding mobile belts (Figure 6-9.a-c). The residual is higher for sites off-craton. For a reference depth of 35 km the Te values increase to >60 km on-craton and 10 to 40 km off-craton (with 50 to 60 km Te at five sites; Figure 6-9d-f). In this case the residual is higher for sites on-craton, due to the fact that the reference depth of 35 km is very close to the average crustal thickness on-craton. No data exist over Lesotho and the southeastern Karoo, and therefore there are no Te estimates for this region.

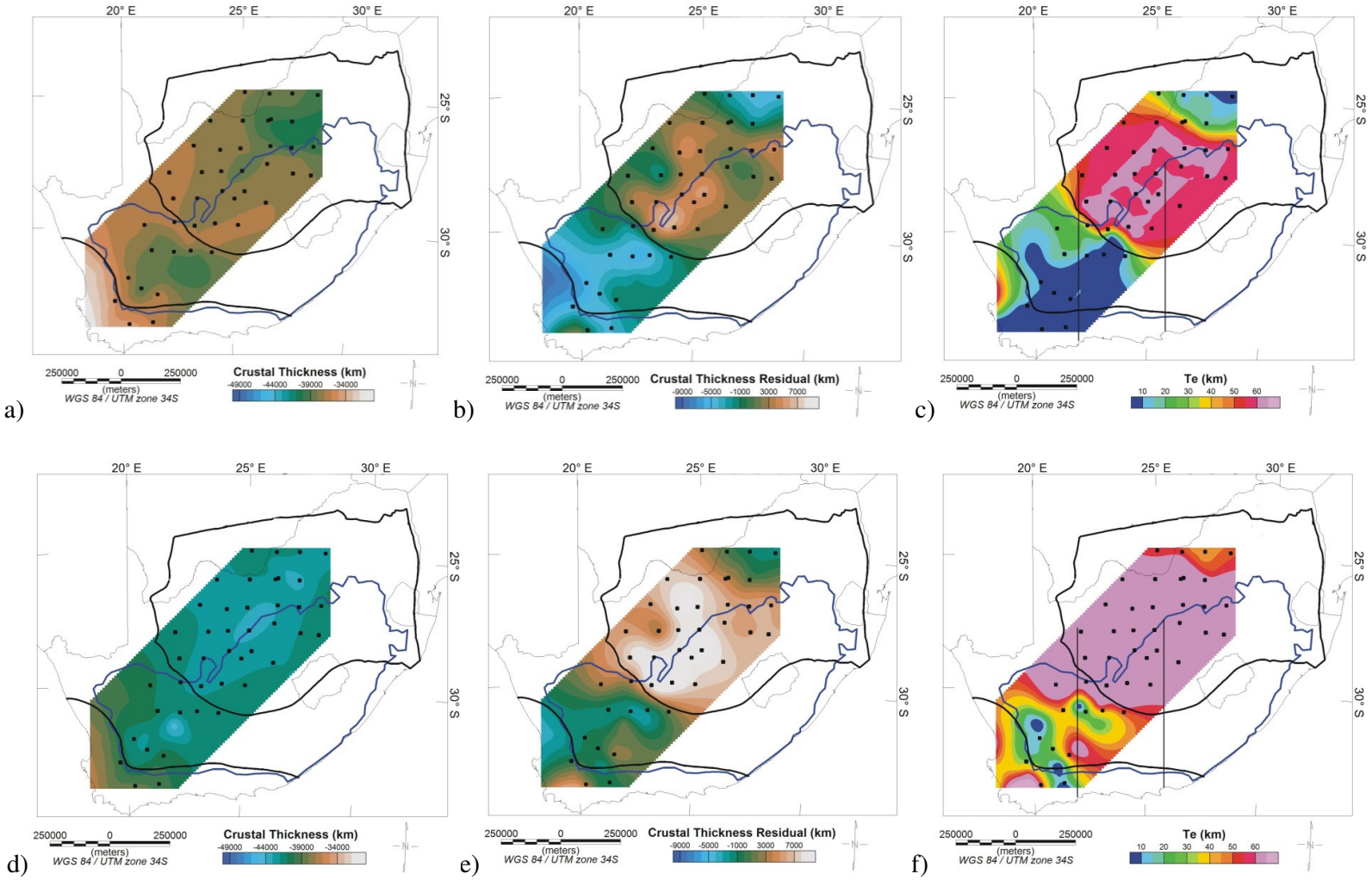
20° E
25° E
30° E
25° S
30° S
250000 0 250000
(meters)
WGS 84 / UTM zone 34S
Crustal Thickness (km)
-49000 -44000 -39000 -34000
Crustal Thickness Residual (km)
-9000 -5000 -1000 3000 7000
Te (km)
10 20 30 40 50 60
a)
b)
c)
d)
e)
f)

Figure 6-9. (a) Inverted Moho calculated using the topographic load and Moho depths from Nguuri *et al.* (2001) in Lithoflex. SASE sites are indicated (black dots). A reference depth of 30 km and density contrast of 400 kg/m^3 were used; (b) Residual when comparing (a) and Moho depths from Nguuri *et al.* (2001); (c) Te values needed to accommodate the topographic load with the Moho depths in (a). A reference depth of 35 km and density contrast of 400 kg/m^3 is used in (d), with the residual shown in (e) and calculated Te values in (f). The two north-south 2D flexure profiles are marked. See Figure 6-1 for details.

6.10 Discussion

It appears that deeper asthenospheric processes have impacted the formation of the Karoo basin rather than variations in the rheology of lithospheric terranes. If rheological variations had a major impact on basin formation then one would expect to see changes in Te along the profiles from north to south (from on- to off-craton or into the Cape region), but this is not evident. Instead a west to east change in Te is evident. Two-dimensional flexure profiles using reasonable load heights and widths show that the majority of the basin could have formed by lithospheric flexure, except along the southeastern coast near East London. We cannot, however, further expand on what caused the formation of the Cape Fold Belt (CFB), whether due to subduction of oceanic crust or due to a continent-continent collision, and what direction subduction occurred. The fact that Te values as high as 100 km are needed to model borehole depths extending from borehole SP1/69 near East London could be the reason why plate break and not bending occurred later in this region during the breakup of Gondwana (Johnston, 2000).

For the flexure profiles, the increase in load height and Te towards the southeastern Karoo can be linked to a broad deepening of the basin from ~3000 m in the southwest to ~4000 m in the southeast (Figure 6-3). This increase in the CFB load height could be due to "locking" along the subduction zone further to the south. Marshall et al., (1997) showed how "rough" segments of subducting crust, due to numerous seamounts off of Costa Rica's Nicoya Peninsula, caused

greater uplift landward of the trench as these segments became "locked". Uplift is predicted at 20 to 30 m/ka, however, rates are closer to 1 to 2 m/ka in this region due to interseismic subsidence. Surrounding “smooth” regions on the other hand display only a tenth of this uplift.

The increase in Te values towards the southeastern Karoo basin to 80 km, compared to 50 km in the southwestern Karoo, could be linked to the buoyancy due to the asthenospheric mantle density anomaly discussed by Scheiber-Enslin *et al.* (2015a) [Chapter 5]. Scheiber-Enslin *et al.* (2015a) model a 20 to 60 kg/m^3 asthenospheric mantle contrast in order to compensate the high topography around Lesotho and the edge of the inland plateau (>1200 m). The anomaly stretches from the northeastern to southeastern Karoo, and then along the escarpment into the southwestern Karoo (Figure 6-10). The lower density lithospheric mantle below the craton will also contribute towards this buoyancy (Webb, 2009, Griffin *et al.*, 2003, Griffin *et al.*, 2009).

It can be argued that this asthenospheric buoyancy started before Karoo times as the northern edge of the Cape basin coincides approximately with the edge of the escarpment (Figure 6-10). If this buoyancy is linked to a deeper Large Low Seismic Velocity Province (LLSVP), then Torsvik *et al.* (2010) suggest these LLSVPs could have been stable for up to 200 m.y., if not 540 m.y. The African LLSVP and plume-like upwellings from it could therefore also be linked to the multiple stages of volcanic activity in southern Africa, such as the failed Cape rift, the Karoo Large Igneous Province (Torsvik *et al.*, 2010), the breakup of Gondwana; and the rapid uplift of southern Africa. This activity is interspersed with “quiet” periods like that of the present day, where the buoyant asthenosphere support elevated topography.

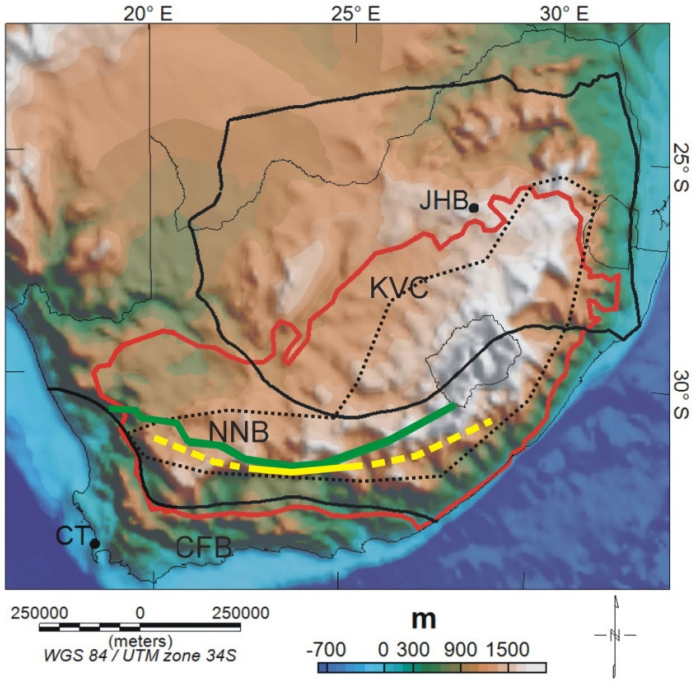

Figure 6-10. Topographic map of South Africa. The edge of the extensive inland plateau in the south (>1200 m) correlates closely with the northern extent of Cape Supergroup (yellow line; solid - definite and dashed – approximate location), as well as the divide between the Namaqua and Natal mobile belts (green line). The extent of the asthenospheric buoyancy anomaly along the edge of the escarpment is shown (dotted line). See Figure 6-1 and for details.

Contributions by a dynamic load such as mantle flow cannot, however, be ruled out, though it is no longer needed to account for the size and depth of the basin (Pysklywec and Mitrovica, 1999). Mantle flow in the form of slab-detachment and lithospheric buckling (Catuneanu *et al.*, 2005) could have contribute towards the formation of accommodation space in the basin, reducing the size of the topographic load needed. High Te values (>100 km) close to the southeastern coast of South Africa that led to the deposition of the Whitehill Formation only in the off-craton area, could support Tankard *et al.* (2009) theory of accommodation space being created due to movement along crustal blocks, but only in this region of the basin.

The broad deepening of the basin could also have influenced the dolerite line, south of which no or few dolerites occur. Dolerites stop ~60 to 80 km north of the CFB in the southwestern Karoo, but stretch to the CFB boundary in the southeast (Figure 6-3). This could be due to the basin deepening more steeply in the southwest (i.e., just north of the deepest part of the basin there is ~700 m of deepening over 5 km distance; 8^0 dip) compared to the southeast (i.e., ~200 m of deepening over 5 km; 2^0 dip) (Figure 6-6). Previous studies have shown the effect of sediment dip on dolerite emplacement (Scheiber-Enslin *et al.*, 2014b). The magma source location, namely offshore the northwest Karoo and southeast Karoo (Chevallier *et al.*, 2001, Scheiber-Enslin *et al.*, 2014b), would have a further impacted the dolerite line.

Calculated current Te estimates using topography and seismic Moho estimates are in-line with previous coherence and admittance studies (Doucouré *et al.*, 1996, Pérez-Gussinyé *et al.*, 2009, Doucouré and De Wit, 1998, Roberts and Zhong, 2004), though appear to be better constrained to geological terranes. It must, however, be noted that for coherence studies the isostatic Moho and the inverted Moho from gravity are used. These Moho estimates do not follow similar trends and neither compare well with the seismic Moho. This method therefore is not ideal for South Africa (Webb, 2009).

Current Te estimates (Figure 6-9) follow a similar pattern, though different values, to the Te values determined from the 2D flexure profiles. This difference was expected as different time frames are being investigated, i.e., current day compared to flexure around the time of Whitehill deposition. Tinker *et al.* (2004) similarly showed how the strength of the lithosphere over the western craton changed through geological time. Current Te estimates for the NNB show the lowest residual using a reference depth of 35 km, resulting in Te values from 10 to 40 km. These values explain the Moho deepening over the mobile belt. High Te values (>50 km) exist on-craton for both reference depth calculations. However, estimates on-craton have a lower residual for a reference depth of 30 km. When compared with the flexure Te estimates, both show an increase in Te from the southwest to the northeast part of the basin (i.e., 10 to 40 km in the southwest compared to 50 km for the 2D profile; >50 km on-craton in the northeast

compared to 85 km for the 2D profile). No further conclusions can be drawn due to a lack of teleseismic data in the southeastern basin. These observations would suggest that Te values have not changed significantly in the past 200 m.y.

6.11 Conclusions

The large extent and shape of the Karoo basin can, in general, be explained by flexure of the crust due to loading by the CFB in the south. This model breaks down in the southeast of the basin.

Deepening of the Whitehill Formation from ~3000 m in the southwest to ~4000 m in the southeast can be explained by an increase in the load height from 4 to 8 km, as well as a west to east increase in the elastic thickness of the lithosphere. Te values increase from around 50 km over the Namaqua and Natal Belts in the west to ≥80 km over the craton and Natal Belt in the east.

Current Te estimates are in-line with, though more constrained to tectonic terranes than previous coherence estimates (10 to 40 km off-craton and > 50 km on-craton). These current Te estimates are also similar to those determined for the Whitehill Formation depth profiles, suggesting that over the past ~260 m.y. the elastic thickness has not changed significantly.

6.12 Acknowledgments

This project was funded by the National Research Foundation (NRF), Council for Geoscience (CGS), University of the Witwatersrand and the Society of Exploration Geophysicists (SEG), with software support from IHS Kingdom and Geosoft. We thank Falcon Oil and Gas and the Council for Geoscience for data access

Chapter 7

Concluding Remarks

7.1 Conclusions

Here the focus is on how this study has advanced the understanding of the main Karoo Basin and its formation. New depth maps presented here show broad deepening of the main Karoo Basin to the southeast (from ~4000 m to ~5000m). Flexure modelling of these depths show that the effective elastic thickness values (Te) for the basin increases from west to east, instead of the expected north to south following changing tectonic terranes. It is therefore apparent that it is not the rheology of terranes that impacted the basin shape. Instead I suggest that a buoyant asthenosphere below the "Great Escarpment" can be linked to the increased Te to the southeast. This along with an increased load from the Cape Fold Belt towards the southeast resulted in the broad deepening of the basin. This increased load could be due to "locking" on the subduction zone further south during basin formation. This asthenospheric anomaly has been long-lived (>300 Ma) and provides compensation for the current high topography (>1200 m) that resulted from uplift after the breakup of Gondwana (early-Cretaceous and mid-Cretaceous). This anomaly could also be associated with plume activity linked to the Karoo LIP and ultimate continent breakup.

This study has helped shed light on the shape of the main Karoo Basin, which is important for future shale gas exploration. Existing borehole and seismic data have revealed basin architecture, which will provide a reference for future exploration projects. In addition, these data have highlighted the extensive network of dolerite sills and dykes that are pervasive throughout the basin. This has drawn attention to the fact that fracking operations cannot go ahead without the collection of new seismic and borehole data to better constrain these bodies. These historic datasets therefore provide a foundation on which knowledge can be built, highlighting the importance of data preservation.

7.2 Future Studies

In order to clearly understand the formation of the Karoo Basin, accurate dating of deformation in the CFB is needed. Existing dates are questionable, and hence it is not clear when loading from the CFB began (pre or post Dwyka

sediment deposition). The load of the glaciers resulting in the formation of the Dwyka Group glaciers has also not been closely studied. These glaciers would have helped create accommodation space for sediments to be deposited in, hence impacting basin formation. In addition, dynamic modelling of the subduction to the south is needed to understand the formation of the Karoo basin. This would allow a better understand of the role played by mantle flow and CFB loading in the creation of accommodation space (i.e., an extension of the work by Pysklywec and Mitrovica, 1999). In addition, in my study only the eastern branch of the CFB was taken into account. To fully understand the impact of the CFB on basin formation the western branch of the belt should also be included in future models.

The next step to better understanding the upper mantle structure below South Africa would be a study using Litmod (LIThospheric MODelling) software (Fullea *et al.*, 2009, Afonso *et al.*, 2008). This would allow for the creation a 3D geophysical-petrological upper mantle model. This model could allow us to validate different tectonic scenarios (e.g., plume or extended cratonic keel). In addition, dynamic modelling of the effect of the plume or buoyancy anomaly (both present or ancient) is needed to better understand how South Africa's high topography is compensated (i.e., an extension of the work by Nyblade and Sleep, 2003).

In terms of better understanding the basement below the basin, new SWARM satellite magnetic data (Stettler *et al.*, 1989) could be used to determine whether the Beattie Magnetic Anomaly (BMA) has a mantle component or whether it is restricted to the crust.

As with any study, more data is always appreciated. The region with the largest lack of data is the southeastern Karoo. Seismic and borehole data in this region (particularly along the coast) would shed light on the source of the BMA as it is at its shallowest here. This is also the deepest part of the Karoo basin and is only covered by a handful of boreholes. More data would allow for better constraining of the shape of the basin and understanding of how the flexure model breaks down here.

Reference

Aarnes, I., Fristad, K., Planke, S. & Svensen, H., 2011a. The impact of host-rock composition on devolatilization of sedimentary rocks during contact metamorphism around mafic sheet intrusions, *Geochemistry Geophysics Geosystems,* 12**,** Q10019.

Aarnes, I., Svensen, H., Polteau, S. & Planke, S., 2011b. Contact metamorphic devolitilization of shales in the Main Karoo Basin, South Africa and the effects of multiple sill intrusions, *Chemical Geology,* 281**,** 181-194.

Adie, R.J., 1952. The position of the Falkland Islands in a reconstruction of Gondwanaland, *Geological Magazine,* 89**,** 401–410.

Afonso, J.C., Fernàndez, M., Ranalli, G., Griffin, W.L. & Connolly, J.A.D., 2008. Integrated geophysical-petrological modeling of the lithosphere and sublithospheric upper mantle: Methodology and applications, *Geochemistry Geophysics Geosystems,* 9.

Airo, M.L. & Loukola-Ruskeeniemi, K., 2004. Characterization of sulfide deposits by airborne magnetic and gamma-ray responses in eastern Finland, *Ore Geology Reviews,* 24**,** 67-84.

Amante, C. & Eakins, B.W., 2009. ETOPO1 1 arc-minute global relief model: procedures, data sources and analysis. *in NOAA Technical Memorandum NESDIS NGDC-24*, pp. 19.

Bailie, R., Armstrong, R. & Reid, D., 2007. The Bushmanland Group supracrustal succession, Aggeneys, Bushmanland, South Africa: Provenance, age of deposition and metamorphism, *South African Journal of Geology,* 110**,** 59-86.

Baranov, V., 1957. A new method for interpretation of aeromagnetics maps: pseudogravimetric anomalies, *Geophysics,* 29**,** 359-383.

Barnett, W., Armstrong, R. & De Wit, M., 1997. Stratigraphy of the upper Neoproterozoic Kango and lower Paleozoic Table Mountain Group of the Cape Fold Belt revisited, *South African Journal of Geology,* 100**,** 237–250.

Bate, K.J. & Malan, J.A., 1992. Tectonostratigraphic evolution of the Algoa, Gamtoos and Pletmos Basins, offshore South Africa. *in Inversion Tectonics of the Cape Fold Belt, Karoo ad Cretaceous Basins of Southern Africa*, pp. 61-73, eds. De Wit, M. J. & Ransome, I. G. D. Balkema, Rotterdam.

Beattie, J., 1909. Report of the Magnetic Survey of South AfricaCambridge Univ. Press, New York.

Behn, M.D., Conrad, C.P. & Silver, P.G., 2004. Detection of upper mantle flow associated with the African Superplume, *Earth and Planetary Science Letters,* 224**,** 259– 274.

Blakely, R., Brocher, T.M. & Wells, R.E., 2005. Subduction-zone magnetic anomalies and implications for hydrated forearc mantle, *Geology,* 33**,** 445-448.

Bodine, J.H., 1981. Numerical computation of plate flexure in marine geophysics, pp. 153Lamont Doherty Geological Observatory of Columbia University.

Booth, P., 2011. Stratigraphic, Structural and Tectonic Enigmas associated with the Cape Fold Belt: Challenges for future research, *South African Journal of Geology,* 114**,** 235-248.

Booth, P.W.K., 1996. The relationship between folding and thrusting in the Floriskraal Formation (upper Witteberg Group), Steytlerville, Eastern Cape, *South African Journal of Geology,* 99**,** 235-243.

Booth, P.W.K., Brunsdon, G. & Shone, R.W., 2004. A Duplex Model for the Eastern Cape Fold Belt? Evidence from the Palaeozoic Witteberg and Bokkeveld Groups (Cape Supergroup), near Steytlerville, South Africa, *Gondwana Research,* 7**,** 211-222.

Booth, P.W.K. & Shone, R.W., 1999. Complex thrusting at Uniondale, eastern sector of the Cape Fold Belt, Republic of South Africa: structural evidence for the need to revise the lithostratigraphy, *Journal of African Earth Sciences,* 29**,** 125-133.

Booth, P.W.K. & Shone, R.W., 2002. A review of thrust faulting in the Eastern Cape Fold Belt, South Africa, and the implications for current lithostratigraphic interpretation of the Cape Supergroup, *Journal of African Earth Sciences,* 34**,** 179-190.

Bordy, E., Hancox, P.J. & Rubidge, B.S., 2005. Turner, B.R. and Thomson, K., Discussion on 'Basin development during deposition of the Elliot Formation (Late Triassic – Early Jurassic), Karoo Supergroup, South Africa' (South African Journal of Geology, 107, 397-412) – A Reply, *South African Journal of Geology,* 108**,** 454-461.

Braitenberg, C., Ebbing, J. & Götze, H.-J., 2002. Inverse modelling of elastic thickness by convolution method - the Eastern Alps as a case example, *Earth and Planetary Science Letters,* 202**,** 387-404.

Braitenberg, C., Wienecke, S., Ebbing, J., Born, W. & Redfield, T., 2007. Joint Gravity And Isostatic Analysis For Basement Studies - A Novel Tool. *in Extendended Abstracts, EGM 2007 International Workshop, Innovation in EM, Grav and Mag Methods: A New Perspective for Exploration*, Villa Orlandi, Capri - Italy, 15-18 April 2007.

Branch, T., Ritter, O., Weckmann, U., Sachsenhofer, R.F. & Schilling, F., 2007. The Whitehill Formation - a high conductivity marker horizon in the Karoo Basin, *South African Journal of Geology,* 110**,** 465-476.

Brunsdon, G. & Booth, P.W.K., 2009. Faulting of the Witteberg Group Rocks, Steytlerville, Eastern Cape. *in 11th SAS Biennial Tenchical Meeting and Exhibition*, pp. 500-505, Swaziland.

Burchardt, S., 2008. New insights into the mechanics of sill emplacement provided by field observations of the Njardvik Sill, Northest Iceland, *Journal of Volcanology and Geothermal Research,* 173**,** 280-288.

Burke, K., 1996. The African Plate, 24th du Toit Memorial lecture, *South African Journal of Geology,* 99**,** 339-409.

Burke, K. & Dewey, J.F., 1973. Plume generated triple junctions: key indicators in applying plate tectonics to old rocks, *Journal of Geology,* 81**,** 406-433.

Burke, K. & Gunnell, Y., 2008. The African Erosion Surface: A Continental-Scale Synthesis of Geomorphology, Tectonics, and Environmental Change over the Past 180 Million Years, *GSA Memoirs,* 201**,** 1-66.

Cardozo, N., 2014. Flex2D. *in Version 3.8, Novermber 1, 2014*.

Carlson, R.L. & Miller, D.J., 2003. Mantle wedge water contents estimated from seismic velocities in partially serpentinized peridotites, *Geophysical Research Letters,* 30**,** 1250.

Carlson, R.W., Grove, T.L., De Wit, M.J. & Gurney, J.J., 1996. Anatomy of an Archean Craton: a program for interdisciplinary studies of the Kaapvaal Craton, southern Africa, *EOS Transactions American Geophysical Union,* 77**,** 273-277.

Carlson, R.W., Pearson, D.G. & James, D.E., 2005. Physical, Chemical, And Chronological Characteristics Of Continental Mantle, *Reviews of Geophysics,* 43**,** RG1001.

Catuneanu, O., Hancox, P.J. & Rubidge, B.S., 1998. Reciprocal flexural behaviour and contrasting stratigraphies: a new basin development model for the Karoo retroarc foreland system, South Africa, *Basin Research,* 10**,** 417-439.

Catuneanu, O., Wopfner, H., Eriksson, P.G., Cairncross, B., Rubidge, B.S., Smith, R.M.H. & Hancox, P.J., 2005. The Karoo basins of south-central Africa, *Journal of African Earth Sciences,* 43**,** 211–253.

Cawthorn, R.G., 2012. Distribution of Dolerite Sills in the Karoo Supergroup. *in LASI 5 Conference*, pp. 28-29, Port Elizabeth, South Africa.

Cawthorn, R.G. & Walraven, F., 1998. Emplacement and Crystallization Time for the Bushveld Complex, *Journal of Petrology,* 39**,** 1669-1687.

Chevallier, L., Gibson, L.A., Nhleko, L.O., Woodford, A.C., Nomquphu, W. & Kippie, I., 2004. Hydrogeology of fractured-rock aquifers and related ecosystems within the Qoqodala dolerite ring and sill complex, Great Kei Catchment, Eastern Cape, pp. 134Water Research Commission.

Chevallier, L., Goedhart, M. & Woodford, A., 2001. The Influence of Dolerite Sill and Ring Complexes on the Occurrence of Groundwater in Karoo Fractured Aquifers: A Morpho-Tectonic Approach. *in Water Research Commission Report*.

Chevallier, L. & Woodford, A., 1999. Morpho-Tectonics And Mechanism Of Emplacement Of The Dolerite Rings And Sills Of The Western Karoo, South Africa, *South African Journal of Geology,* 102**,** 43-56.

Christensen, N.I. & Mooney, W.D., 1995. Seismic velocity structure and composition of the continental crust: a global view, *Journal of Geophysical Research,* 100**,** 9761-9788.

Cloetingh, S., Lankreijer, A., De Wit, M.J. & Martinez, I., 1992. Subsidence history analysis and forward modelling of the Cape and Karoo Supergroups. *in Inversion Tectonics of the Cape Fold Belt, Karoo and Cretaceous Basins of Southern Africa*, pp. 239-248, eds. De Wit, M. J. & Rowsell, D. M. Balkema, Rotterdam.

Cole, D.I., 1992. Evolution and development of the Karoo Basin. *in Inversion Tectonics of the Cape Fold Belt, Karoo ad Cretaceous Basins of Southern Africa*, pp. 87-99, eds. De Wit, M. J. & Ransome, I. G. D. Balkema, Rotterdam.

Cole, D.I., 2011. Shale gas targets in the Ecca group of the main Karoo basin, South Africa. *in Geosynthesis Conference*, pp. 79, Cape Town.

Cole, D.I. & McLachlan, I.R., 1994. Oil shale potential and depositional environment of the Whitehill Formation in the main Karoo basin, *Publication (unedited), Geological Survey of South Africa, Library book no. 553.283COL (Volume I Text; Volume II Tables and Appendixes). Also Report No. 1994-0213.*

Cole, D.I., Robey, K., Chevallier, L. & Viljoen, J., 2011. The geology of shales with a gas potential in the Main Karoo Basin of South Africa and impact of hydraulic fracturing on groundwater. *in Council for Geoscience Report 2011-0142*, pp. 43p.Council for Geoscience Western Cape Regional Office (Bellville).

Cornell, D.H., Hawkesworth, C.J., van Calstersen, P. & Scott, W.D., 1986. Sm–Nd study of Precambrian crustal development in the Prieska-Copperton region, Cape Province, *Transactions Geological Society of South Africa,* 89**,** 17–28.

Cornell, D.H., Thomas, R.J., Moen, H.F.G., Reid, D.L., Moore, J.M. & Gibson, R.L., 2006. The Namaqua-Natal Province. *in The Geology of South Africa*, pp. 325-379, eds. Johnson, M. R., Anhaeusser, C. R. & Thomas, R. J. Geological Society of South Africa and Council for Geoscience.

Corner, B., 1989. The Beattie anomaly and its significance for crustal evolution within the Gondwana framework. *in Extended Abstracts, South African Geophysical Association, First Technical Meeting*, pp. 15-17.

Coward, M.P., 1983. Thrust tectonics, thin skinned or thick skinned, and the continuation of thrusts to deep in the crust, *Journal of Structural Geology,* 5**,** 113-123.

de Beer, J., van Zijl, J. & Gough, D., 1982. The Southern Cape Conductive Belt (South Africa): Its Composition, Origin and Tectonic Significance, *Tectonophysics,* 83**,** 205-225.

de Beer, J.H. & Gough, D.I., 1980. Conductive structures in southernmost Africa: A magnetometer array study, *Geophysical Journal of the Royal Astronomical Society,* 63**,** 479-495.

de Beer, J.H. & Meyer, R., 1983. Geoelectrical and gravitational characteristics of the Namaqua-Natal Mobile Belt and its boundaries, *Special Publication of Geology Society of South Africa,* 10**,** 91-100.

de Beer, J.H. & Meyer, R., 1984. Geophysical characteristics of the Namaqua-Natal Belt and its boundaries, South Africa, *Journal of Geodynamics,* 1**,** 473-494.

de Beer, J.H., Van Zyl, J.S.V. & Bahnemann, F.K., 1974. Plate tectonic origin for the Cape Fold Belt, *Nature,* 252**,** 675-676.

De Wit, M.J., 2007. The Kalahari Epeirogeny and climate change; differentiating cause and effect from core to space, *South African Journal of Geology,* 110**,** 367-392 (Spec Inkaba yeAfrica).

De Wit, M.J., 2011. The great shale debate in the Karoo, *South African Journal of Science,* 107**,** 1-9.

De Wit, M.J. & Ransome, I.G.D., 1992. Regional inversion tectonics along the southern margin of Gondwana. *in Inversion Tectonics of the Cape Fold*

Belt, Karoo ad Cretaceous Basins of Southern Africa, pp. 15-21, eds. Wit, M. J. d. & Ransome, I. G. D. Balkema, Rotterdam.

De Wit, M.J., Roering, C., Hart, R.J., Armstrong, R.A., de Ronde, C.E.J., Green, R.W.E., Tredoux, m.M., Peberdy, E. & Hart, R.A., 1992. Formation of an Archaean continent, *Nature* 357**,** 553–562.

De Wit, M.J. & Tinker, J., 2004. Crustal structures across the central Kaapvaal craton from deep-seismic reflection data. , *South African Journal of Geology,* 107**,** 185–206.

Decker, J.E., 2013. The shale gas potential of the main Karoo Basin, South Africa. *in South African Geophysical Association 13th Biennial Conference*, pp. 84, Skukuza.

Decker, J.E., 2014. Geological evaluation of the Karoo Basin's shale gas resource. *in 4th Shale Gas Southern Africa Summit, 24-26 March 2014*, Cape Town.

Decker, J.E. & Marot, J., 2012. Annexure A: Resource Assessment. *in In: Department of Mineral Resources, 2012. Report on Investigation of Hydraulic Fracturing in the Karoo Basin of South Africa*, pp. 81 p., 15 annexures.

Doucouré, C.M. & De Wit, M.J., 1998. Mapping thickness variations of the elastic lithosphere in South Africa, *Southern African Geophysical Review,* 2**,** 11-18.

Doucouré, C.M., De Wit, M.J. & Mushayandebvu, M.F., 1996. Effective elastic thickness of the continental lithosphere in South Africa, *Journal Geophysical Research,* 101**,** 11291-11303.

Du Toit, A.I., 1920. The Karoo Dolerites, *Transactions, Geological Society of South Africa,* 33**,** 1-42.

Duncan, A.R. & Marsh, J.S., 2006. The Karoo Igneous Province. *in The Geology of South Africa*, pp. 461-499, eds. Johnson, M. R., Anhaeusser, C. R. & Thomas, R. J. Geological Society of South Africa and Council for Geoscience.

Durrheim, R.J., 1987. Seismic reflection and refraction studies of the deep structure of the Agulhas bank, *Geophysical Journal of the Royal Astronomical Society,* 89**,** 395-398.

Durrheim, R.J., 1998. Seismic Refraction Investigations of the Kaapvaal Craton, *Southern African Geophysical Review,* 2**,** 29-35.

Durrheim, R.J. & Green, R.W.E., 1992. A seismic refraction investigation of the Archean Kaapvaal Craton, South Africa, using mine tremors as the energy source, *Geophysical Journal International,* 108**,** 812-832.

Durrheim, R.J. & Mooney, W.D., 1991. Archean and Proterozoic crustal evolution: Evidence from crustal seismology, *Geology,* 19**,** 606-609.

Durrheim, R.J. & Mooney, W.D., 1994. Evolution of the Precambrian lithosphere: Seismological and geochemical constraints, *Journal of Geophysical Research,* 99**,** 15359-15374.

Ebbing, J., Bouman, J., Lieb, V., Haagmans, R., Meekes, J.A.C. & Fattah, R.A., 2013. Advancements in satellite gravity gradient data for crustal studies, *The Leading Edge,* 32**,** 900-906.

Eglington, B.M., 2006. Evolution of the Namaqua-Natal Belt, southern Africa – A geochronological and isotope geochemical review, *Journal of African Earth Science,* 46**,** 93-111.

Eglington, B.M. & Armstrong, R.A., 2003. Geochronological and isotopic constraints on the Mesoproterozoic Namaqua-Natal Belt: evidence from deep borehole intersection in South Africa, *Precambrian Research,* 125**,** 179-189.

Eglington, B.M., Harmer, R.E. & Kerr, A., 1989. Isotope and geochemical constraints on Proterozoic crustal evolution in South-eastern Africa, *Precambrian Research,* 45**,** 159-174.

Encarnación, J., Fleming, T.H., Elliot, D.H. & Eales, H.V., 1996. Synchronous emplacement of Ferrar and Karoo dolerites and the early breakup of Gondwana, *Geology,* 24**,** 535-538.

Fatti, L., 1970. The use of seismic reflection techniques in the Karoo basin, MSc, University of the Witwatersrand, South Africa, Johannesburg.

Fatti, L., 1987. Reflection Seismic Surveys in the Karoo Basin by Soekor, *SAGA Yearbook***,** 22-30.

Fatti, L. & Du Toit, J.J.L., 1970. A regional reflection-seismic line in the Karoo basin near Beaufort West, *Geological Society of South Africa - Transactions and Proceedings,* 73**,** 17-28.

Fishwick, S., 2010. Surface wave tomography: Imaging of the lithosphere–asthenosphere boundary beneath central and southern Africa?, *Lithos,* 120**,** 63-73.

Fouch, M.J., James, D.E., VanDecar, J.C., Lee, S.v.d. & Group, K.S., 2004. Mantle seismic structure beneath the Kaapvaal and Zimbabwe Cratons, *South African Journal of Geology,* 107**,** 33-44.

Frimmel, H.E., 2004. Formation of a late Mesoproterozoic supercontinent: the South Africa–East Antarctica connection. *in The Precambrian Earth: Tempos and Events*, pp. 240–255, eds. Eriksson, P. G., Altermann, W., Nelson, D. R., Mueller, W. U. & Catuneanu, O. Elsevier Science BV, Amsterdam.

Fullea, J., Afonso, J.C., Connolly, J.A.D., Fernàndez, M., García-Castellanos, D. & Zeyen, H., 2009. LitMod3D: An interactive 3-D software to model the thermal, compositional, density, seismological, and rheological structure of the lithosphere and sublithospheric upper mantle, *Geochemistry Geophysics Geosystems,* 10.

Galerne, C.Y., Galland, O., Neumann, E.-R. & Planke, S., 2011. 3D relationships between sills and their feeders: evidence from the Golden Valley Sill Complex (Karoo Basin) and experimental modelling, *Journal of Volcanology and Geothermal Research,* 202**,** 189-199.

Galland, O., Cobbold, P.R., de Bremond d'Ars, J. & Hallot, E., 2007. Rise and emplacement of magma during horizontal shortening of the brittle crust: Insights from experimental modeling, *Journal of Geophysical Research,* 112**,** B06402.

Galland, O., Cobbold, P.R., Hallot, E., de Bremond d'Ars, J. & Delavaud, G., 2006. Use of vegetable oil and silica powder for scale modelling of magmatic intrusion in a deforming brittle crust, *Earth and Planetary Science Letters,* 243**,** 786-804.

Galland, O., de Bremond d'Ars, J., Cobbold, P.R. & Hallot, E., 2003. Physical models of magmatic intrusion during thrusting, *Terra Nova,* 15**,** 405–409.

Geel, C., Schulz, H.-M., Booth, P., De Wit, M. & Horsfield, B., 2013. Shale gas characteristics of Permian black shales in South Africa: results from recent drilling in the Ecca Group (Eastern Cape), *Energy Procedia,* 40**,** 256 – 265.

Geringer, G.J., Humphreys, H.C. & Scheepers, D.J., 1994. Lithostratigraphy, protolithology and tectonic setting of the Areachap Group along the eastern margin of the Namaqua Mobile Belt, South Africa, *South African Journal of Geology,* 97**,** 78-100.

Gilchrist, A.R., Kooi, H. & Beaumont, C., 1994. Post-Gondwana geomorphic evolution of southwestern Africa: Implications for the controls on landscape development from observations and numerical experiments, *Journal of Geophysical Research,* 99**,** 12,211-212,228.

Goedhart, M.L., Combrinck, W.L. & Booth, P.W.K., 2011. A new geodetic station near Willowmore, to monitor neotectonic crustal movement over the Cape Isostatic Anomaly, Cape Fold Belt, South Africa. *in Inkaba yeAfrica Workshop*, pp. Poster, Cape Town.

Golynsky, A., Chiappini, M., Damaske, D., Ferraccioli, F., Finn, C.A., Ishihara, T., Kim, H.R., Kovacs, L., Masolov, V.N., Morris, P. & von Frese, R., 2006. ADMAP — A Digital Magnetic Anomaly Map of the Antarctic. *in Antarctica*, pp. 109-116, eds. Fütterer, D. K., Damaske, D., Kleinschmidt, G., Miller, H. & Tessensohn, F. Springer, Berlin Heidelberg.

Gose, W.A., Helper, M.A., Connelly, J.N., Hutson, F.E. & Dalziel, I.W.D., 1997. Paleomagnetic data and U-Pb isotopic age determinations from Coats Land, Antarctica: implications for late Proterozoic plate reconstructions, *Journal Geophysical Research,* 102.

Götze, H. & Lahmeyer, B., 1988. Application of three-dimensional interactive modeling in gravity and magnetics, *Geophysics,* 53**,** 1096–1108.

Gough, D., de Beer, J. & van Zijl, J., 1973. A magnetometer array study in southern Africa, *Geophys. J. R. Astron. Soc.,* 34**,** 421– 433.

Graham, K.W.T. & Hales, A.L., 1965. Surface-ship gravity measurements in the Agulhas Bank area, south of South Africa, *Journal of Geophysical Research,* 70**,** 4005-4011.

Grantham, G.H., Eglington, B.M., Thomas, R.J. & Mendonidis, P., 2001. The nature of the Grenville-age Charnockitic A-type magmatism from the Natal, Namaqua and Maud Belts of southern Africa and western Dronning Maud Land, Antarctica, *Memoir, National Institute of Polar Research, Tokyo, Japan, Special Issue,* 55**,** 59-86.

Green, R.W.E. & Durrheim, R.J., 1990. A Seismic Refraction Investigation of the Namaqualand Metamorphic Complex, South Africa, *Journal of Geophysical Research,* 95**,** 19927-19932.

Gresse, P.G., Theron, J.N., Fitch, F.J. & Miller, J.A., 1992. Tectonic inversion and radiometric resetting of the basement in the Cape Fold Belt. *in Inversion Tectonics of the Cape Fold Belt, Karoo ad Cretaceous Basins of Southern Africa*, pp. 217-228, eds. De Wit, M. J. & Ransome, I. G. D. Balkema, Rotterdam.

Gressier, J.-B., Mourgues, R., Bodet, L., Matthieu, J.-Y., Galland, O. & Cobbold, P., 2010. Control of pore fluid pressure on depth of emplacement of magmatic sills: An experimental approach, *Tectonophysics,* 489**,** 1-13.

Griffin, W.L., O'Reilly, S.Y. & Ryan, C.G., 1999. The composition and origin of subcontinental lithospheric mantle. *in Mantle Petrology: Field Observations and High-pressure Experimentation: A Tribute to Francis R. (Joe) Boyd*, pp. 13-45, eds. Fei, Y., Bertka, C. M. & Mysen, B. O. The Geochemical Society, Hous-ton, TX.

Griffin, W.L., O'Reilly, S.Y., Ryan, C.G., Gaul, O. & Ionov, D., 1998. Secular variation in the composition of subcontinental lithospheric mantle. *in Structure and Evolution of the Australian Continent, Geodynamics Series*, pp. 1-25, eds. Braun, J., Dooley, J., Goleby, B., Hilst, R. v. d. & Klootwijk, C., American Geophysical Union.

Griffin, W.L., O'Reillly, S.Y., Afonso, C. & Begg, G.C., 2009. The Composition and Evolution of Lithospheric Mantle: a Re-evaluation and its Tectonic Implications, *Journal of Petrology,* 50**,** 1185-1204.

Griffin, W.L., O'Reilly, S.Y., Natapova, L.M. & Ryan, C.G., 2003. The evolution of lithospheric mantle beneath the Kalahari Craton and its margins, *Lithos,* 71**,** 215-241.

Haase, C., 2008. Inversion of gravity, gravity gradient, and magnetic data with application to subsalt imaging, Diploma thesis, Christian-Albrechts-Universität zu Kiel.

Hälbich, I.W., 1992. The Cape Fold Belt orogeny; State of the art 1970–1980s. *in Inversion Tectonics of the Cape Fold Belt, Karoo and Cretaceous Basins of Southern Africa*, pp. 141-158, eds. De Wit, M. J. & Ransome, I. G. D. Balkema, Rotterdam.

Hälbich, I.W., 1993. Cape Fold Belt - Agulhas Bank Transect across Gondwana suture, southern Africa, *American Geophysical Union Special Publication,* 202**,** 18pp.

Hälbich, I.W., Fitch, F.J. & Miller, J.A., 1983. Dating the Cape orogeny. *in Geodynamics of the Cape Fold Belt*, pp. 149-164, eds. Söhnge, A. P. G. & Hälbich, I. Geological Society of South Africa Special Publication.

Hales, A.L. & Gough, D.I., 1960. Isostatic Anomalies and crustal structure in the Southern Cape, *Geophysical Journal of the Royal Astronomical Society,* 3**,** 225-236.

Hales, A.L. & Gough, D.I., 1961. Correction to paper: Isostatic anomalies and crustal structure in the southern Cape, *Geophysical Journal of the Royal Astronomical Society,* 5**,** 263.

Hansen, D.M., Cartwright, J.A. & Thomas, D., 2004. 3D Seismic Analysis of the Geometry of Igneous Sills and Sill Junction Relationships, *Geological society, London, Memoirs,* 29**,** 199-209.

Hargraves, R.B. & Rehacek, J., 1997. Palaeomagnetism of the Karoo igneous rocks in southern Africa, *South African Journal of Geology,* 100**,** 195-213.

Harvey, J.D., De Wit, M.J., Stankiewicz, J. & Doucouré, C.M., 2001. Structural variations of the crust in the south-western Cape deduced from seismic received-functions, *South African Journal of Geology,* 104**,** 231-242.

Hastie, W.W., Watkeys, M.K. & Aubourg, C., 2014. Magma flow in dyke swarms of the Karoo LIP: Implications for the mantle plume hypothesis, *Gondwana Research,* 25**,** 736-755.

Hattingh, P.J. & de Wet, J.A.J., 1996. A palaeomagnetic investigation of the Insizwa intrusives, *South African Journal of Geology,* 99**,** 221-229.

Hetenyi, M., 1946. *Beams on Elastic Foundations,* edn, Vol., pp. Pages, The University of Michigan Press.

Hirsch, K.K., Bauer, K. & Scheck-Wenderoth, M., 2009. Deep structure of the western South African passive margin - Results of a combined approach of seismic, gravity and isostatic investigations., *Tectonophysics,* 470**,** 57-70.

Hobday, D.K. & Mathew, D., 1974. Depositional environment of the Cape Supergoup in Transkei, *Transactions Geological Society South Africa,* 77**,** 223-227.

Hunt, J.M., 1996. *Petroleum Geochemistry and Geology,* edn, Vol., pp. Pages, W.H. Freeman, San Francisco.

Hyndman, R.D. & Peacock, S.M., 2003. Serpentinization of the forearc mantle, *Earth and Planetary Science Letters,* 212**,** 417–432.

Irvine, G.J., Pearson, D.G. & Carlson, R.W., 2001. Lithospheric mantle evolution of the Kaapvaal Craton: A Re-Os isotope study of peridotite zenoliths from Lesotho kimberlites, *Geophysical Research Letters,* 28**,** 2505-2508.

Jacobs, J., Bauer, W. & Schmidt, R., 2004. Magnetic Susceptibilities of the different Teetone-Stratigraphie Terranes of Heimefrontfjella, Western Dronning Maud Land, East Antarctica *Polarforschung,* 72**,** 41-48.

Jacobs, J., Bauer, W., Spaeth, G., Thomas, R.J. & Weber, K., 1996. Lithology and structure of the Grenville-aged (»1.1 Ga) basement of Heimefrontfjella (East Antarctica), *Geologische Rundschlag,* 85**,** 800–821.

Jacobs, J., Falter, M., Thomas, R.J., Kunz, J. & Jessberger, E.K., 1997. $^{40}Ar/^{39}Ar$ thermochronological constraints on the structural evolution of the Mesoproterozoic Natal Metamorphic Province, SE Africa, *Precambrian Research,* 86**,** 71-92.

Jacobs, J., Fanning, C.M., Henjes-Kunst, F., Olesch, M. & Paech, H.-J., 1998. Continuation of the Mozambique Belt into East Antarctica: Grenville-age metamorphism and polyphase Pan-African high-grade events in central Dronning Maud Land, *Journal of Geology,* 106**,** 385–406.

Jacobs, J. & Thomas, R.J., 1994. Oblique collision at about 1.1 Ga along the southern margin of the Kaapvaal continent, south-east Africa, *Geologische Rundschlag,* 83**,** 322–333.

Jacobs, J., Thomas, R.J. & Weber, K., 1993. Accretion and indentation tectonics at the southern edge of the Kaapvaal craton during the Kibaran (Grenville) orogeny., *Geology* 21**,** 203–206.

James, D.E., Boyd, F.R., Schutt, D., Bell, D.R. & Carlson, R.W., 2004. Xenolith constraints on seismic velocities in the upper mantle beneath southern Africa, *Geochemistry Geophysics Geosystems,* 5**,** Q01002.

James, D.E., Fouch, M.J., VanDecar, J.C., van der Lee, S. & Group, K.S., 2001. Tectospheric structure beneath southern Africa, *Geophysical Research Letters,* 28**,** 2485-2488.

James, D.E., Niu, F. & Rokosky, J., 2003. Crustal structure of the Kaapvaal craton and its significance for early crustal evolution, *Lithos,* 71**,** 413–429.

Jiménez-Munt, I., Fernàndez, M., Saura, E., Vergés, J. & Garcia-Castellanos, D., 2012. 3-D lithospheric structure and regional/residual Bouguer anomalies in the Arabia–Eurasia collision (Iran), *Geophysical Journal International,* 190**,** 1311-1324.

Johnson, M.R., 1991. Sandstone petrography, provenance and plate tectonic setting in Gondwana context of the southeastern Cape-Karoo basin, *South African Journal of Geology,* 94**,** 137–154.

Johnson, M.R., van Vuuren, C.J., Visser, J.N.J., Cole, D.I., Wickens, H.d.V., Christie, A.D.M., Roberts, D.L. & Brandl, G., 2006. Sedimentary rocks of the Karoo Supergroup. *in The Geology of South Africa*, pp. 461-499, eds. Johnson, M. R., Anhaeusser, C. R. & Thomas, R. J. Geological Society of South Africa and Council for Geoscience.

Johnston, S.T., 2000. The Cape Fold Belt and Syntaxis and the rotated Falkland Islands: dextral transpressional tectonics along the southwest margin of Gondwana, *Journal of African Earth Science,* 31**,** 51-63.

Jones, M.Q.W., 1988. Heat flow in the Witwatersrand basin and environs and its significance for the south African shield geotherm and lithosphere thickness, *Journal of Geophysical Research,* 93**,** 3243-3260.

Jones, M.Q.W., 1992. Heat flow anomaly in Lesotho: Implications for the Southen boundary of the Kaapvaal Craton, *Geophysical Research Letters,* 19**,** 2031-2034.

Jordan, T.H., 1978. Composition and development of the continental tectosphere, *Nature,* 274**,** 544-548.

Jordan, T.H., 1979. The deep structure of the continents, *Scientific American,* 240**,** 70-82.

Jordan, T.H., 1988. Structure and Formation of the Continental Tectosphere. *in Journal of Petrology, Special Lithosphere Issue*, pp. 11-37, eds. Menzies, M. A. & Cox, K. G. Transactions of the Royal Society of London, London, United Kingdom.

Jourdan, F., Féraud, G., Bertrand, H., Watkeys, M.K. & Renne, P.R., 2008. The 40Ar/39Ar ages of the sill complex of the Karoo large igneous province: Implications for the Pliensbachian-Toarcian climate change, *Geochemistry Geophysics Geosystems,* 9**,** Q06009.

Karpeta, W.P. & Johnson, M.R., 1979. The geology of the Umtata area, *Explanation Sheet 3128, Geological Survey of South Africa***,** 16pp.

Kawano, S., Yoshino, T. & Katayama, I., 2012. Electrical conductivity of magnetite-bearing serpentinite during shear deformation, *Geophysical Research Letters,* 39**,** L20313.

Kgaswane, E.M., Nyblade, A.A., Julia, J., Dirks, P.H.G.M., Durrheim, R.J. & Pasyanos, M.E., 2009. Shear wave velocity structure of the lower crust in southern Africa: Evidence for compositional heterogeneity within Archaean and Proterozoic terrains, *Journal Geophysical Research,* 114**,** 1-19.

Kingsley, C.S., 1975. A new stratigraphic classification implying a lithofacies change in the Table Mountain Sandstone in southern Natal, *Transactions Geological Society South Africa,* 78**,** 43-55.

Leaman, D.E., 1984. Notes on microbarometer elevation determinations, *Exploration Geophysics,* 15**,** 53-59.

Leith, M.J., 1970. Well completion report of SP1/69. *in Internal Soekor Report* pp. 37.

Lindeque, A.S., de Wit, M.J., Ryberg, T., Weber, M. & Chevallier, L., 2011. Deep crustal profile across the Southern Karoo basin and Beattie magnetic

anomaly, South Africa: An integrated interpretation with tectonic implications, *South African Journal of Geology,* 114**,** 265-292.

Lindeque, A.S., Ryberg, T., Stankiewicz, J., Weber, M.H. & De Wit, M.J., 2007. Deep Crustal Seismic Reflection Experiment across the Southern Karoo Basin, South Africa, *South African Journal of Geology,* 110**,** 419-438.

Lithgow-Bertelloni, C. & Silver, P., 1998. Dynamic topography, plate driving forces and the African superswell, *Nature,* 395**,** 269 - 272.

Loots, L., 2013. Investigation of the crust in the southern Karoo using the seismic reflection technique, MSc, University of the Witwatersrand, South Africa.

Ludwig, W.J., Nafe, J.E. & Drake, C.L., 1970. Seismic refraction. *in The Sea*, pp. 53-84, ed. Maxwell, A. E. Wiley-Interscience, New York.

MacKay, S., 2013. The Interpreter's Guide to Depth Imaging**,** 604.

Malthe-Sørenssen, A., Planke, S., Svensen, H. & Jamtveit, B., 2004. Formation of saucer-shaped sills. *in Physical geology of High-Level Magmatic Systems*, pp. 215-227, eds. Breitkreuz, C. & Petford, N. Geological Society, London, Special Publication, London.

Maré, L., de Kock, M., Cairncross, B. & Mouri, H., 2014. Application of magnetic geothermometers in sedimentary basins: an example from the western Karoo Basin, South Africa, *South African Journal of Geology,* 117**,** 1-14.

Maré, L.P., 2012. Council for Geoscience Petrophysical Properties Atlas, Silverton, Pretoria.

Maré, L.P., de Kock, M.O., Cairncross, B. & Mouri, H., 2013. What rock magnetism reveals of the Karoo Basin. *in South African Geophysical Association 13th Biennial Conference*, pp. 70, Skukuza.

Maré, L.P. & Thomas, R.J., 1998. Palaeomagnetism and aeromagnetic modelling of the Mesoproterozoic Ntimbankulu Pluton, KwaZulu-Natal, South Africa: mushroom-shaped diapir?, *Journal of African Earth Science,* 25**,** 519-537.

Marsh, J.S. & Mindaweni, M.J., 1998. Geochemical variations in a long Karoo dyke, Eastern Cape., *South African Journal of Geology,* 101**,** 119-123.

Martelat, J.-E., Randrianasolo, B., Schulmann, K., Lardeaux, J.-M. & Devidal, J.-L., 2014. Airborne magnetic data compared to petrology of crustal scale shear zones from southern Madagascar: A tool for deciphering magma and fluid transfer in orogenic crust, *Journal of African Earth Science,* 94**,** 74–85.

McCarthy, T. & Rubidge, B.S., 2005. *The story of earth and life: A southern African perspective on a 4.6-billion-year journey,* edn, Vol., pp. Pages, Struik Publishers, Cape Town.

McCourt, S., Armstrong, R.A., Grantam, G.H. & Thomas, R.J., 2006. Geology and evolution of the Natal belt, South Africa, *Journal of African Earth Sciences,* 46**,** 71-92.

McEnroe, S., Harrison, R., Robinson, P., Golla, U. & Jercinovic, M., 2001. Effect of fine-scale microstructures in titanohematite on the acquisition and stability of natural remanent magnetization in granulite facies metamorphic rocks, southwest Sweden: implications for crustal magnetism, *Journal of Geophysical Research,* 106**,** 30523-30546.

McEnroe, S., Harrison, R., Robinson, P. & Langenhorst, F., 2002. Nanoscale haematite–ilmenite lamellae in massive ilmenite rock: an example of 'lamellar magnetism' with implications for planetary magnetic anomalies, *Geophysical Journal International,* 151**,** 890-912.

McEnroe, S.A., Fabian, K., Robinson, P., Gaina, C. & Brown, L.L., 2009. Crustal Magnetism, Lamellar Magnetism and Rocks That Remember, *Elements,* 5.

Miller, H.G. & Singh, V., 1994. Potential field tilt a new concept for location of potential field sources, *Applied Geophysics* 32**,** 213–217.

Mowzer, Z., 2013. Seismic interpretation of legacy data from the Main Karoo Basin for the evaluation of shale gas potential. *in South African Geophysical Association 13th Biennial Conference (poster presentation)*, Skukuza.

Muller, M.R., 1991. Lithospheric structure for the Kaapvaal craton and its margins from the analysis of long-period and broad-band teleseismic P-waves, MSc, University of the Witwatersrand, Johannesburg, South Africa.

Nair, S.K., Gao, S.S., Liu, K.H. & Silver, P.G., 2006. Southern African crustal evolution and composition: Constraints from receiver function studies, *Journal of Geophysical Research,* 111**,** B02304.

Neumann, E.R., Svensen, H., Galerne, C.Y. & Planke, S., 2011. Multistage Evolution of Dolerites in the Karoo Large Igneous Province, Central South Africa, *Journal of Petrology,* 52**,** 959-984.

Nguuri, T.K., Gore, J., James, D.E., Webb, S.J., Wright, C., Zengeni, T.G., Gwavava, O., Snoke, J.A. & Group, K.S., 2001. Crustal structure beneath southern Africa and its implications for the formation and evolution of the Kaapvaal and Zimbabwe cratons, *Geophysical Research Letters,* 28**,** 2501–2504.

Niu, F. & James, D.E., 2002. Fine structure of the lowermost crust beneath the Kaapvaal craton and its implications for crustal formation and evolution, *Earth Planet. Sci. Lett.,* 200**,** 121–130.

Nyblade, A.A. & Sleep, N.H., 2003. Long lasting epeirogenic uplift from mantle plumes and the origin of the Southern African Plateau, *Geochemistry Geophysics Geosystems,* 4**,** 1105.

Odgers, A.T.R., Hinds, R.C. & von Gruenewaldt, G., 1993. Interpretation of a seismic reflection survey across the southern Bushveld Complex, *South African Journal of Geology,* 96**,** 205-212.

Parsiegla, N., Gohl, K. & Uenzelmann-Neben, G., 2007. Deep crustal structure of the sheared South African continental margin: first results of the Agulhas-Karoo Geoscience Transect, *South African Journal of Geology,* 110**,** 393-406.

Parsiegla, N., Gohl, K. & Uenzelmann-Neben, G., 2008. The Agulhas Plateau: structure and evolution of a Large Igneous Province, *Geophysical Journal International,* 174**,** 336-350.

Parsiegla, N., Stankiewicz, J., Gohl, K., Ryberg, T. & Uenzelmann-Neben, G., 2009. Southern African continental margin: Dynamic processes of a transform margin, *Geochemistry Geophysics Geosystems,* G3**,** Q03007.

Partridge, T.C. & Maud, R.R., 1987. Geomorphic evolution of southern Africa since the Mesozoic, *South African Journal of Geology,* 90**,** 179–208.

Paton, D.A., Macdonald, D.I.M. & Underhill, J.R., 2006. Applicability of thin or thick skinned structural models in a region of multiple inversion episodes; southern South Africa, *Journal of Structural Geology,* 28**,** 1933-1947.

Pérez-Gussinyé, M., Metois, M., Fernández, M., Vergés, J., Fullea, J. & Lowry, A.R., 2009. Effective elastic thickness of Africa and its relationship to other proxies for lithospheric structure and surface tectonics, *Earth and Planetary Science Letters,* 287**,** 152–167.

Pitts, B., Mahler, M., Beer, J.d. & Gough, D., 1992. Interpretation of magnetic, gravity and magnetotelluric data across the Cape Fold Belt and Karoo Basin. *in Inversion Tectonics of the Cape Fold Belt, Karoo and Cretaceous Basins of Southern Africa*, pp. 27–32, eds. De Wit, M. J. & Ransome, I. G. D. Balkema, Rotterdam.

Planke, S. & Svensen, H., 2012. Field Guide - Karoo Basin, pp. p.24LASI IV: Physical geology of subvolcanic systems: Laccoliths, Sills, and Dykes

Polteau, S., Mazzini, A., Galland, O., Planke, S. & Malthe-Sørenssen, A., 2008. Saucer-shaped intrusions: Occurrences, emplacement and implications, *Earth and Planetary Science Letters,* 266**,** 195-204.

Pysklywec, R.N. & Mitrovica, J.X., 1999. The role of subduction-induced subsidence in the evolution of the Karoo basin, *Journal of Geology,* 107**,** 155–164.

Quesnel, Y., Weckmann, U., Ritter, O., Stankiewicz, J., Lesur, V., Mandea, M., Langlais, B., Sotin, C. & Galdéano, A., 2009. Simple models for the Beattie Magnetic Anomaly in South Africa, *Tectonophysics,* 478**,** 111-118.

Raith, J.G., Cornell, D.H., Frimmel, H.E. & De Beer, C.H., 2003. New insights into the geology of the Namaqua tectonic province South Africa, from ion probe dating of detrital and metamorphic zircon., *Journal of Geology* 111**,** 347–366.

Reynard, B., Mibe, K. & Van de Moortele, B., 2011. Electrical conductivity of the serpentinised mantle and fluid flow in subduction zones, *Earth and Planetary Science Letters,* 307**,** 387-394.

Riley, T.R. & Knight, K.B., 2001. Age of pre-break-up Gondwana magmatism, *Antarctic Science,* 13**,** 99-110.

Riley, T.R., Leat, P.T., Curtis, M.L., Millar, I.L. & Fazel, A., 2005. Early-Middle Jurassic dolerite dykes from western Dronning Maud land (Antarctica): identifying mantle sources in the Karoo large igneous province, *Journal of Petrology,* 46**,** 1489-1524.

Robb, L.J., Armstrong, R.A. & Waters, D.J., 1999. The history of granulitefacies metamorphism and crustal growth from single zircon U–Pb geochronology: Namaqualand, South Africa, *Journal Petrology* 40**,** 1747–1770.

Roberts, J.H. & Zhong, S., 2004. Plume-induced topography and geoid anomalies and their implications for the Tharsis rise on Mars, *Journal of Geophysical Research,* 109**,** E03009.

Robinson, P., Harrison, R., McEnroe, S. & Hargraves, R., 2002. Lamellar magnetism in the haematite–ilmenite series as an explanation for strong remanent magnetization., *Nature,* 418**,** 517–520.

Roby, D.J., Johnson, M.R. & le Roux, F.G., 1995. Geological map of the Grahamstown Area, Sheet 3326, *Geological Survey of South Africa, 1:250 000 Series*.

Rowsell, D.M. & De Swardt, A.M.J., 1976. Diagenesis in Cape and Karroo sediments, South Africa, and its bearing on their hydrocarbon potential, *Transactions, Geological Society of South Africa,* 79**,** 81-145.

Rutherford, A.B., 2009. The Sedimentology and Stratigraphy of the Beaufort Group of the Karoo Supergroup in the Vicinity of Thaba Nchu, Central Free State Province., MSc, University of the Witwatersrand, Johannesburg.

Sæther, B., 1997. Improved estimation of subsurface magnetic properties using minimum mean-square error methods., PhD, Norwegian University of Science and Technology.

Scheiber-Enslin, S.E., Ebbing, J., Eberle, D.G. & Webb, S.J., 2012. Geophysical 3D Modelling of the Karoo Basin, South Africa - Preliminary Results. *in LASI 5 Conference*, Port Elizabeth, South Africa.

Scheiber-Enslin, S.E., Ebbing, J. & Webb, S.J., 2014a. An integrated geophysical study of the Beattie Magnetic Anomaly, South Africa, *Tectonophysics,* 636**,** 228-243.

Scheiber-Enslin, S.E., Ebbing, J. & Webb, S.J., 2015a. An Integrated 3D Geophysical Study Of The Karoo Basin And Underlying Lithosphere, *In press*.

Scheiber-Enslin, S.E., Ebbing, J. & Webb, S.J., 2015b. New Depth Maps Of The Main Karoo Basin, Used To Explore The Cape Isostatic Anomaly *South African Journal of Geology,* 118**,** 261-284.

Scheiber-Enslin, S.E., Webb, S.J. & Ebbing, J., 2014b. Geophysically Plumbing the Main Karoo Basin, South Africa, *South African Journal of Geology,* 117**,** 275-300.

Schmitz, M.D. & Bowring, S.A., 2004. Lower crustal granulite formation during Mesoproterozoic Namaqua-Natal collisional orogenesis, southern Africa, *South African Journal of Geology,* 107**,** 261-284.

Scogings, A.J., Mkaza, J. & Mngomezulu, M.A., 1984. Final report on the Mvoti scheelite project, pp. 12SA Dev. Trust Int. Rep.

Shone, R.W., 2006. Onshore post-Karoo Mesozoic deposits. *in The Geology of South Africa*, pp. 541–552, eds. Johnson, M. R., Thomas, R. J. & Anhaeusser, C. R. Geological Society of South Africa and Council for Geoscience.

Shone, R.W. & Booth, P.W.K., 2005. The Cape Basin, South Africa: A review, *Journal of African Earth Science,* 43**,** 196-210.

Smith, C.B., 1983. Pb, Sr and Nd isotopic evidence for sources of southern African Cretaceous kimberlites, *Nature,* 304.

Smithard, T., Bordy, E. & Reid, D.L., 2013. The effect of igneous intrusions on the hydrocarbon potential of the Whitehill Formation in the Karasburg Basin, Southern Namibia and the Main Karoo Basin (Northern Cape), South Africa. *in South African Geophysical Association 13th Biennial Conference*, Skukuza.

Söhnge, A. & Hälbich, I.W., 1983. Geodynamics of the Cape Fold Belt, Special Publication, *Geological Society of South Africa,* 12**,** 165-175.

Stankiewicz, J., Ryberg, T., Parsiegla, N., Gohl, K., Trumbull, R. & Weber, M., 2008. Crustal structure of the Southern Margin of the African Plate: Results from Geophysical Experiments, *Journal Geophysical Research,* 113**,** B10313.

Stankiewicz, J., Ryberg, T., Schulze, A., Lindeque, A.S., Weber, M.H. & De Wit, M.J., 2007. Initial results from wide-angle seismic refraction lines in the southern Cape, *South African Journal of Geology,* 110**,** 407-418.

Steinberger, B. & Torsvik, T.H., 2012. A geodynamic models of plumes from the margins of Large Low Shear Velocity Provinces, *Geochemistry Geophysics Geosystems (G3),* 13**,** Q01W09.

Stettler, E.H., de Beer, J. & Blom, M.P., 1989. Crustal domains in the northern Kaapvaal craton as defined by magnetic lineaments, *Precambrian Research,* 45**,** 263-276.

Stettler, E.H., Fourie, C.J.S., Bühmann, J.R., Hattingh, E., Cole, P., Kleywegt, R.J., Wolmarans, L.G. & Cloete, A.J., 1999. Magnetics. *in South African Geophysical Atlas. Volume 2 (CD Rom).*Council for Geoscience, South Africa.

Stettler, E.H., Fourie, C.J.S. & Cole, P., 2000. Total magnetic field intensity map of the Republic of South Africa (in 4 panels), *Council for Geoscience, Pretoria.*

Stratigraphy), S.S.A.C.f., 1980. Stratigraphy of South Africa. Part 1 (Compiled by L.E. Kent). Lithostratigraphy of the Republic of South Africa, South West Africa/Namibia, and the Republics of Bophuthatswana, Transkei and Venda, *Handbook 8, Geological Survey, South Africa***,** 690.

Svensen, H., Corfu, F., Polteau, S., Hammer, Ø. & Planke, S., 2012. Rapid magma emplacement in the Karoo Large Igneous Province, *Earth and Planetary Science Letters,* 325-326**,** 1-9.

Svensen, H., Planke, S., Chevallier, L., Malthe-Sörensen, A., Corfu, F. & Jamtveit, B., 2007. Hydrothermal venting of green-house gases triggering Early Jurassic global warming, *Earth and Planetary Science Letters,* 256**,** 554-566.

Talwani, M. & Heirtzler, J.R., 1964. Computation of magnetic anomalies caused by two-dimensional bodies of arbitrary shape. *in Computers in the mineral industries, Part 1*, pp. 464-480, ed. Parks, G. A. Stanford Univ. Publ., Geological Sciences.

Talwani, M., Worzel, J.L. & Landisman, M., 1959. Rapid gravity computations for two-dimensional bodies with application to the Mendocino submarine fracture zone, *Journal Geophysical Research,* 64**,** 49-59.

Tankard, A., Welsink, H., Aukes, P., Newton, R. & Stettler, E.H., 2009. Tectonic evolution of the Cape and Karoo Basins of South Africa, *Marine and Petroleum Geology,* 26**,** 1379-1412.

Tankard, A.J., Jackson, M.P.A., Eriksson, K.A., Hobday, D.K., Hunter, D.R. & Minter, W.E.L., 1982. *3,5 Billion years of Crustal Evolution in Southern Africa,* edn, Vol., pp. Pages, Springer-Verlag, New York.

Ten Brink, U. & Stern, T., 1992. Rift flank uplifts and hinterland basins: Comparison of the Transantarctic mountains with the Great Escarpment of Southern Africa. *in Rockbursts and Seismicity in Mines*, ed. Fairhurst, C. Balkema, Rotterdam.

Thamm, A.G. & Johnson, M.R., 2006. The Cape Supergroup. *in The Geology of South Africa*, pp. 461-499, eds. Johnson, M. R., Anhaeusser, C. R. & Thomas, R. J. Geological Society of South Africa and Council for Geoscience.

Thomas, R.J., 1989. A tale of two tectonic terranes, *South African Journal of Geology,* 92**,** 306-321.

Thomas, R.J., 1992. Mapumulo Group. *in Catalogue of South Africa Lithostratigraphic Units*, ed. Johnson, M. R. SA Committee for Stratigraphy.

Thomas, R.J., Cornell, D.H. & Grantam, G.H., 1992a. Protolithology of the Quha Formation in the type area, Natal Metamorphic Province. *in Geocongress*, pp. 396-398Geological Society of South Africa, Bloemfontein.

Thomas, R.J., Du Plessis, A.J., Fitch, F., Marshall, C.G.A., Miller, J.A., Von Brunn, V. & Watkeys, M.K., 1992b. Geological studies in southern Natal and Transkei: implications for the Cape Oroogen. *in Inversion Tectonics of the Cape Fold Belt, Karoo and Cretaceous Basins of Southern Africa*, pp. 229-236, eds. De Wit, M. J. & Ransome, I. G. D. Balkema, Rotterdam.

Thomas, R.J. & Eglington, B.M., 1990. A Rb–Sr, Sm–Nd and U–Pb zircon isotopic study of the Mzumbe suite, the oldest intrusive granitoid in southern Natal, South Africa, *South African Journal of Geology,* 93**,** 761-765.

Thomas, R.J., Von Veh, M.W. & McCourt, S., 1993. The tectonic evolution of southern Africa: an overview, *Journal of African Earth Science,* 16**,** 5-24.

Tinker, J., De Wit, M. & Grotzinger, J., 2002. Seismic Stratigraphic Constraints on Neoarchean - Paleoproterozoic Evolution of the Western Margin of the Kaapvaal Craton, South Africa, *South African Journal of Geology,* 105**,** 107-134.

Tinker, J.H., De Wit, M.J. & Royden, L.H., 2004. Old, strong continental lithosphere with weak Archaean margin at ~1.8 Ga, Kaapvaal Craton, South Africa, *South African Journal of Geology,* 107**,** 255-260.

Toerien, D.K., 1986. Geological map of the Port Elizabeth Area, Sheet 3324., *Geological Survey of South Africa, 1:250 000 Series.*

Toerien, D.K., 1991. Geological map of the Port Elizabeth Area, Sheet 3324, *Geological Survey of South Africa, 1:250 000 Series.*

Toerien, D.K. & Roby, D.J., 1979. Geological map of the Oudtshoorn Area, Sheet 3322, *Geological Survey of South Africa, 1:250 000 Series.*

Torsvik, T.H., Burke, K., Steinberger, B., Webb, S.J. & Ashwal, L.D., 2010. Diamonds sampled by plumes from the core–mantle boundary, *Nature,* 466.

Turcotte, D.L. & Schubert, G., 2002. *Geodynamics,* Second edn, Vol., pp. Pages, Cambridge University Press.

Turner, B.R., 1999. Tectonostratigraphical development of the Upper Karoo foreland basin: orogenic unloading versus thermally-induced Gondwana rifting, *Journal of African Earth Science,* 28**,** 215-238.

Turner, B.R. & Thomson, K., 2005. Discussion on 'Basin development during deposition of the Elliot Formation (Late Triassic – Early Jurassic), Karoo Supergroup, South Africa' (South African Journal of Geology, 107, 397-412), *South African Journal of Geology,* 108**,** 448-453.

Uieda, L., 2013. Source code and compiled binaries for software Tesseroids, *figshare,* http://dx.doi.org/10.6084/m9.figshare.786514.

van Zijl, J.S.V., 2006a. Physical characteristics of the Karoo sediments and mode of emplacement of the dolerites, *South African Journal of Geology,* 109**,** 329-334.

van Zijl, J.S.V., 2006b. A review of the resistivity structure of the Karoo Supergroup, South Africa, with emphasis on the dolerites: A study in anisotropy, *South African Journal of Geology,* 109**,** 315-328.

van Zijl, J.S.V., Graham, K.W.T. & Hales, A.L., 1962. The palaeomagnetism of the Stormberg lavas of South Africa, *Geophysical Journal of the Royal Astronomical Society,* 7**,** 23-29.

Venter, C.P., du Plessis, J.G., Stettler, R.H., Potgieter, T.D., Kleywegt, R.J., Hattingh, E., Fourie, C.J.S., Wolmarans, L.G., Cloete, A.J. & Maré , L.P., 1999. Gravity. *in South African Geophysical Atlas*, pp. 77Council for Geoscience, South Africa.

Verduzco, B., Fairhead, J.D., Green, C.M. & MacKenzie, C., 2004. New Insights into Magnetic Derivatives for Structural Mapping, *The Leading Edge,* 23**,** 116-119.

Vinnik, L., Kiselev, S., Weber, M., Oreshin, S. & Makeyeva, L., 2012. Frozen and active seismic anisotropy beneath southern Africa, *Geophysical Research Letters,* 39**,** L08301.

Voordouw, R.J., 2010. A D3 Shear Zone In The Margate Terrane And Its Implications For Regional Deformation In The Natal Metamorphic Province (South Africa), *South African Journal of Geology,* 113**,** 183-194.

Wall, M., Cartwright, J., Daviesw, R. & McGrandlez, A., 2009. 3D seismic imaging of a Tertiary Dyke Swarm in the Southern North Sea, UK, *Basin Research,* 22**,** 181-194.

Watts, A.B., 2001. *Isostasy and flexure of the lithosphere,* edn, Vol., pp. Pages, Cambridge University Press.

Webb, S.J., 2009. The use of potential field and seismological data to analyze the structure of the lithosphere beneath southern Africa, University of the Witwatersrand, Johannesburg.

Weckmann, U., Jung, A., Branch, T. & Ritter, O., 2007a. Comparison of electrical conductivity structures and 2D magnetic modelling along two profiles crossing the Beattie Magnetic Anomaly, South Africa, *South African Journal of Geology,* 110**,** 449–464.

Weckmann, U., Ritter, O., Jung, A., Branch, T. & De Wit, M., 2007b. Magnetotelluric measurements across the Beattie magnetic anomaly and the Southern Cape Conductive Belt, South Africa, *Journal Geophysical Research,* 112**,** doi:10.1029/2005JB0039755.

Welford, J.K. & Clowes, R.M., 2006. Three-dimensional seismic reflection investigation of the upper crustal Winagami sill complex of northwestern Alberta, Canada, *Geophysical Journal International,* 166**,** 155-169.

Whitehead, R., 2012. Modelling the Initiation of a Subduction Zone, BSc Honours thesis, University of the Witwatersrand.

Winter, H.d.l.R., 1984. Tectonostratigraphy, as applied to analysis of South African Phanerozoic basins, *Transactions of the Geological Society of South Africa,* 87**,** 169-179.

Winter, H.d.l.R., 1989. Tectonic classification of certain South African depositional basins and criteria for recognition of major unconformitybounded sequences, *South African Journal of Geology,* 92**,** 167–182.

Winter, H.d.l.R. & Venter, J.J., 1970. Lithostratigraphic correlation of recent deep boreholes in the Karoo-Cape sequence. *in Proc & Papers, 2nd IUGS symposium*, pp. 395-408, ed Haughton, S. H. CSIR, Pretoria.

Won, I.J. & Bevis, M., 1987. Computing the gravitational and magnetic anomalies due to a polygon: Algorithms and Fortran subroutines, *Geophysics,* 52**,** 232-238.

Woodford, A. & Chevallier, L., 2002. Regional Characterization and Mapping of Karoo Fractured Rock Aquifer Systems - an integrated approach using a geographical information system and digital processing. *in Water Research Commission Report*, pp. 192.

Yang, Y., Li, A. & Ritzwoller, M.H., 2008. Crustal and uppermost mantle structure in southern Africa revealed from ambient noise and teleseismic tomography, *Geophysical Journal International,* 174**,** 235-248.

Youssof, M., Thybo, H., Artemieva, I.M. & Levander, A., 2013. Moho depth and crustal composition in Southern Africa, *Tectonophysics,* 609**,** 267-287.

Zoback, M.L. & Mooney, W.D., 2003. Lithospheric buoyancy and continental intraplate stresses, *International Geologic Review,* 45**,** 95-118.

Appendix

Appendix 1 – Matlab Best-fit Program for Eastern Flexure Profile

```
function [minALL]=SlabFleX_V2_Eastern_BestFit;

% Input: Width of load and densities

clear

%Import observed Whitehill Fm depth data
load 4_Geosoft5_Flex2D_Models_BV06_2_Noheading_WH.csv;

% Assign variables to data
x1=X4_Geosoft5_Flex2D_Models_BV06_2_Noheading_WH(1:132,1)';
y1=X4_Geosoft5_Flex2D_Models_BV06_2_Noheading_WH(1:132,5)';

% Tectonic regions the profile passes over
Capex=150000; % Edge of Cape Supergroup sediments (Distance)
NAMx=340000; % Edge of Kaapvaal Craton (Distance)
ENDx=630000;% End of obs profile

% Parameters
    % Beginning position, end position and height of load
stop = 85*10^3; % Edge of load to correlate with northern edge of
CFB (m)
width=100*10^3; % Load width (m)
start = stop-width;
    % Density
rho1 = 2550; % Infill (kg/m3);
rho3 = 2550; % Beam (kg/m3);
rho4 = 3300; % Mantle (kg/m3);
    % Young's modulus
E = 100*10^9;
    % Thickness
```

```
Tstart=5; % Beginning elastic thickness (km)
Tend=100; % End elastic thickness (km)
Tdiv1=5; % Divisions
Tdiv=Tend/Tdiv1;
for T1=Tstart:Tdiv1:Tend;
T = T1*10^3;
    % Poisson's ratio
v = 0.25;
    % Height
for Height1 = 2:1:8;
Height = Height1*10^3;
    % Acceleration due to gravity
g = 9.81;
rho = [rho1,rho3,rho4];
    % Total load
pb = rho(1)*Height*(stop-start);
    % Linear load density
q = pb/(stop-start);
    %length of the profile (m)
x = 0:5000: ENDx;

% Tectonic regions the profile passes over (cont.)
[rSTOP,cSTOP]=find(x==stop);
[rCape,cCape]=find(x==Capex);
[rNAM,cNAM]=find(x==NAMx);
[rEND,cEND]=find(x==ENDx);

cSTOP2=cSTOP+1;
cCape2=cCape+1;
cEND5=cNAM;

%%%%%%%%%%%%%%%%%%%%%%%%%%%%%%%%%%%%%%%%%%%%%%%%%%%%%%%%%%%%%%%%%%%%%%%%%%%%
%%%%%%%%%

%%%%%%%%%%%%%%%%%% - Properties of the beams -
%%%%%%%%%%%%%%%%%%%%%%%%%%%%%

D = zeros(1,1);
```

```
for k = 1 : length(E);
D(k) = (E(k)*T(k)^3)/(12*(1-v(k)));
end
    % Lambda
if (rho(3)-rho(1))>0
la(1) = (((rho(3)-rho(1))*g)/(4*D(1)))^0.25;
else
    la(1) = (((rho(4)-rho(1))*g)/(4*D(1)))^0.25;
end
    % Winkler foundation
if (rho(3)-rho(1))>0
k = (rho(3)-rho(1));
else
   k = (rho(4)-rho(1));
end

%%%%%%%%%%%%%%%%%%%%%%%%%%%%%%%%%%%%%%%%%%%%%%%%%%%%%%%%%%%%%%%%%%%%%%%%%%%%%%%%
%%%%%%%%%

%%%%%%%%%%%%%%%%%%% - Flexure of first beam -
%%%%%%%%%%%%%%%%%%%%%%%%%%%%%

y = zeros(1,1);
for i = 1 : length(x);
if x(i) < start;                                % To the left of the
load
   a = start - x(i);
   b = stop - x(i);
   y(i) = (q/(2*(k)*g)) * (exp(-la(1)*a)*cos(la(1)*a)-exp(-
la(1)*b)...
       *cos(la(1)*b));
end
if x(i) == start;
    x(i) = x(i) + 0.001;
end
if x(i) > start && x(i) < stop;                 % Under the load
    a = x(i)-start;
    b = stop - x(i);
```

```
    y(i) = (q/(2*(k)*g)) * (2 -exp(-la(1)*a)*cos(la(1)*a)-exp(-
la(1)*b)...
        *cos(la(1)*b));
end
if x(i) == stop;
    x(i) = stop + 0.001;
end
if x(i) > stop;                                % To the right of
the load
    a = x(i) - start;
    b = x(i) - stop;
    y(i) = (-q/(2*(k)*g)) * (exp(-la(1)*a)*cos(la(1)*a)-exp(-
la(1)*b)...
        *cos(la(1)*b));
end
end


%%%%%%%%%%%%%%%%%%%%%%%%%%%%%%%%%%%%%%%%%%%%%%%%%%%%%%%%%%%%%%%%%%%%%%%%
%%%%%%%%%

%%%%%%%%%%%%%%%%%%%%%%%%%%%%%%%%%% - Shift -
%%%%%%%%%%%%%%%%%%%%%%%%%%%%%%%%

y=(-10*y); % why 10?
if y(1,cEND5)>y1(1,cEND5); % Match two curves at end of profile
(END)
    ydiff200(T1./5,Height1) = y(1,cEND5)-y1(1,cEND5);
    ydiff2 = y(1,cEND5)-y1(1,cEND5);
    y=y-ydiff2;
elseif  y(1,cEND5)<y1(1,cEND5);
    ydiff200(T1./5,Height1) = y1(1,cEND5)-y(1,cEND5);
    ydiff2 = y1(1,cEND5)-y(1,cEND5);
    y=y+ydiff2;
end;

%%%%%%%%%%%%%%%%%%%%%%%%%%%%%%%%%%%%%%%%%%%%%%%%%%%%%%%%%%%%%%%%%%%%%%%%
%%%%%%%%%
```

```
%%%%%%%%%%%%%%%%%%%%%%%%%%%%%%%% - Best-fit  -
%%%%%%%%%%%%%%%%%%%%%%%%%%%%%%%%


% Difference between observed and calculated data - KVC
ydiff(1,cSTOP2:cEND)=y1(1,cSTOP2:cEND)-y(1,cSTOP2:cEND);
ydiffT(T1./5,Height1)=sum(abs(ydiff(1,cSTOP2:cEND)));
ydiffTN(T1./5,Height1)=sum(abs(ydiff(1,cSTOP2:cEND)));

Height2(1,Height1)=Height1;
T2(1,T1./5)=T1;

end;
end;

% Minimum difference for profile (best-fit)
min4TN=min(ydiffTN(1:Tdiv,4));% Height of 4 km
min6TN=min(ydiffTN(1:Tdiv,6));% Height of 6 km
min8TN=min(ydiffTN(1:Tdiv,8));% Height of 8 km

% Determine the parameters that give that minimum difference
[r4TN,c4TN]=find(ydiffTN==min4TN);% Height of 4 km
r4TN2=r4TN*5;
[r6TN,c6TN]=find(ydiffTN==min6TN);% Height of 6 km
r6TN2=r6TN*5;
[r8TN,c8TN]=find(ydiffTN==min8TN);% Height of 8 km
r8TN2=r8TN*5;

diff4TN=ydiff200(r4TN,c4TN); % Height of 4 km
diff6TN=ydiff200(r6TN,c6TN); % Height of 6 km
diff8TN=ydiff200(r8TN,c8TN); % Height of 8 km

minALL=[4 r4TN2 min4TN diff4TN; 6 r6TN2 min6TN diff6TN; 8 r8TN2
min8TN diff8TN];
```

```
%%%
```

"If we knew what it was we were doing, it would not be called research, would it?"

~ Albert Einstein ~

